

High-strength steels and innovative design approaches for sustainable steel structures

A thesis submitted in partial fulfilment of the requirements for the degree of Doctor of Philosophy (PhD) in Engineering Science

by

Loris SAUFNAY



© Sweden Arena Management

© Ian Jolipa via CTBUH

© Motomag, T. Leconte

Supervisor: Jean-François DEMONCEAU

DOCTORAL COLLEGE IN ARCHITECTURE, ENGINEERING AND GEOLOGY

OCTOBER 2024

Members of the jury

Prof. Dr. Boyan Mihaylov (President)

University of Liège

Prof. Dr. Jean-François Démonceau (Supervisor)

University of Liège

Prof. Dr. Laurent Duchêne

University of Liège

Prof. Dr. Markus Knobloch

Universität Stuttgart

Prof. Dr. Milan Veljkovic

TU Delft

Dr. Ir. François Hanus

ArcelorMittal

"It always seems impossible until it's done."

Nelson Mandela

Abstract

Greenhouse gas emissions from industry are a major contributor to climate change and the catastrophic consequences the world has been facing for several years. The construction sector has a significant responsibility since it represents about 42% of global CO₂ emissions. The recent communication from the IPCC (Intergovernmental Panel on Climate Change) is unambiguous: significant measures must be taken without delay to achieve the objective of limiting global warming to 1.5°C, as set out in the Paris Agreement. Faced with this situation, construction stakeholders must reinvent themselves to meet the growing demand for solutions that will reduce the carbon footprint of buildings while keeping the same level of comfort and safety.

Among the existing solutions, the steel market is continuously witnessing the emergence of new, ever-stronger steels. This is driven by improvements in the operational capabilities of the steelmaking process, which have enabled the production of much heavier and thicker sections with improved material properties. Indeed, it is now feasible to manufacture wide flange sections without any significant reduction in the yield strength, with good toughness and weldability performance. The development of high-strength steels, which exhibit the highest strength-to-weight ratio among existing steel grades, contributes to the optimisation of structural designs with the potential for substantial weight, cost and carbon savings. Hot-rolled steel sections with a yield strength of up to 500 MPa in Europe and 80 ksi (550 MPa) in the United States already exist and comply with the product standards for civil engineering applications. Nevertheless, the use of high-strength steels remains quite marginal. This can be explained by a lack of information on existing high-performance products and the advantages they offer, as well as a lack of availability resulting from the current low demand for these grades. Furthermore, the use of a higher steel grade is frequently associated with an increase in the unit material cost, accompanied by a larger carbon footprint and an increased risk of local and global buckling instabilities. Consequently, the designer is frequently reluctant to employ such materials, lacking recommendations to assess their economic and environmental benefit in specific designs.

The objective of this thesis is to provide insights that may contribute to the reduction of material use and thus contribute to the optimisation of future structures. The sustainability of high-strength steels is initially addressed to establish reliable trends for relative prices and carbon emissions as a function of the yield strength. Based on these trends, a comparative study is conducted on the use of the right steel at the right place for individual members, and reference member slendernesses are established allowing the identification of the relevant field of application for the different considered steel grades. In addition, the establishment of appropriate design rules for flexural buckling and the consideration of intrinsic sources of structural stabilisation are also addressed, as they also contribute to the achievement of efficient designs. This doctoral thesis demonstrates the necessity for collaboration between the various stakeholders in the construction sector (designers, researchers and manufacturers) in order to develop the optimal structural solution for each application, thereby collectively contributing to a more sustainable future.

Résumé

Les émissions de gaz à effet de serre provenant de l'industrie contribuent largement au changement climatique et aux conséquences catastrophiques auxquelles le monde est confronté depuis plusieurs années. Le secteur de la construction a une responsabilité importante dans cette situation, puisqu'il représente environ 42% des émissions mondiales de CO₂. La récente communication du GIEC (Groupe d'experts Intergouvernemental sur l'Evolution du Climat) a été sans ambiguïté ; des mesures significatives doivent être prises sans délai afin de limiter le réchauffement climatique à 1.5°C, tel que prévu dans l'accord de Paris. Face à cette situation, les acteurs de la construction doivent se réinventer pour répondre à la demande croissante de solutions permettant de réduire l'empreinte carbone des bâtiments tout en conservant le même niveau de confort et de sécurité.

Parmi les solutions existantes, le marché de l'acier assiste continuellement à l'émergence de nouveaux aciers, toujours plus résistants. Cette évolution est due à l'amélioration des capacités opérationnelles du processus de production de l'acier, qui a permis de produire des sections plus épaisses et donc plus massives avec des propriétés matérielles améliorées. En effet, il est désormais possible de fabriquer des profilés à larges ailes sans réduction significative de la limite d'élasticité, tout en conservant de bonnes performances en termes de ténacité et de soudabilité. Le développement d'aciers à haute limite d'élasticité, présentant le rapport résistance – poids le plus élevé parmi les nuances d'acier existantes, contribue à l'optimisation des dimensionnements structuraux, ce qui peut conduire à des économies substantielles en termes de poids, de coûts et d'empreinte carbone. Des profilés laminés à chaud présentant une limite d'élasticité allant jusqu'à 500 MPa en Europe et 80 ksi (550 MPa) aux Etats-Unis, existent d'ores-et-déjà et sont conformes aux normes produit relatives aux applications du génie civil. Cependant, l'utilisation de ce type de nuance reste assez marginale. Cela peut s'expliquer par un manque d'information sur les produits à haute limite d'élasticité existants et sur les avantages qu'ils offrent, ainsi qu'au manque de disponibilité résultant de la faible demande actuelle pour ce type de nuances. En outre, l'utilisation d'une nuance d'acier plus élevée est souvent associée à une augmentation du coût unitaire du matériau, à une augmentation de l'empreinte carbone ainsi qu'à un risque accru par rapport aux différentes instabilités (locales ou globales). Par conséquent, le concepteur est souvent réticent à utiliser de tels matériaux, car il ne dispose pas de recommandations permettant de déterminer si ces aciers présentent un avantage économique et environnemental pour une application donnée.

L'objectif de cette thèse est donc de fournir des informations susceptibles de contribuer à la réduction de matière utilisée et d'ainsi contribuer à l'optimisation de futures structures. La durabilité des aciers à haute limite d'élasticité est premièrement abordée afin d'établir des tendances fiables en matière de prix relatifs et d'émissions relatives en fonction de la limite d'élasticité. Sur base de ces tendances, une étude comparative est menée sur l'utilisation du bon acier au bon endroit pour des éléments isolés, et des élancements limites de référence sont établis permettant d'identifier les domaines d'application adéquats en fonction de la nuance d'acier. De plus, l'établissement de règles de dimensionnement appropriées pour le flambement par flexion et la prise en compte de sources intrinsèques de stabilisation sont également abordées, car elles contribuent également à la réalisation de dimensionnements optimisés. Cette thèse de doctorat démontre la nécessité de synergies entre les différents acteurs du monde de la construction (concepteurs, chercheurs et producteurs) afin de développer la solution structurale optimale pour chaque application, et d'ainsi contribuer collectivement à la création d'un avenir plus durable.

Acknowledgements - Remerciements

This thesis would not have been possible without the guidance, the technical and the emotional support of several individuals who have contributed in one way or another to this achievement. I would like to take the time to express my gratitude to those persons.

First of all, I would like to thank the jury members, Markus Knobloch, Milan Veljkovic and François Hanus for agreeing to be part of this jury and for dedicating their time to the evaluation of my thesis.

Merci à mes promoteurs, Jean-Pierre Jaspert et Jean-François Demonceau pour la confiance qu'ils m'ont témoignée depuis mon travail de fin d'étude jusqu'à l'accomplissement de cette thèse de doctorat tant pour la recherche que pour l'enseignement. Merci de m'avoir guidé et conseillé tout au long de ce parcours. Votre rigueur, votre ouverture d'esprit et votre humilité sont les principales valeurs que je retiens des années passées avec vous. Celles-ci m'ont permis de grandir à la fois professionnellement mais aussi personnellement.

Merci à Laurent Duchêne, d'avoir fait partie de mon comité de thèse annuel ainsi que de prendre part à l'évaluation de cette thèse de doctorat.

Je tiens à remercier les nombreux contacts industriels, l'aboutissement de cette thèse est en grande partie le fruit de ces nombreux échanges qui ont jalonné mes réflexions. Je remercie le département de recherche et développement d'Astron, et ce en particulier René Oly et Etienne Lesuisse, pour leurs conseils avisés et toujours bienveillants. Je remercie Louis-Guy Cajot, Mike Tibolt, Liudmila Webber et Marina D'Antimo d'ArcelorMittal qui m'ont octroyé quelques heures de leur temps pour discuter de mes développements et pour les informations techniques qu'ils ont pu me faire parvenir. Merci à Vincent de Ville de Goyet, Yves Duchêne et Raphaël Ludwig du Bureau Greisch pour les réunions de travail et les nombreux conseils qui m'ont été prodigués pour le calcul numérique et le dimensionnement de racks de stockage. Un grand merci également à Julian Flock du Bureau Greisch pour son aide apportée sur le logiciel Finelg.

Merci à mes collègues pour l'ambiance de travail positive et saine qui m'a permis d'évoluer au sein de l'équipe et pour m'avoir soulagé de nombreuses tâches d'assistantat au cours de cette dernière année.

"Thank you, Zois, for being the first and the so-called "best colleague". You have been a reference, and I would like to thank you for all the kind advice you gave me throughout the journey of this thesis."

Merci, Adrien, d'avoir partagé mon bureau pendant 3 années et d'avoir été mon « pacer », ton ouverture d'esprit et ta réussite ont été un point de repère pour terminer cette thèse dans de bonnes conditions. Au-delà de l'aspect professionnel, nos sorties à vélo ces dernières semaines ont contribué à garder un esprit sain dans la dernière ligne droite.

Merci, Maxime, pour ta bonne humeur constante et ta joie de vivre communicative qui rendent les journées au bureau si agréables. Je te souhaite bon courage pour ta fin de thèse et te promets que tu pourras compter sur moi dans cette dernière ligne droite.

"Thank you, Tudor, for all the good times we spent together at conferences and in the office. As I write these lines, you are also in the final stages of your thesis. I'm looking forward to our last conference together in Barcelona to celebrate our achievements with the team!"

Merci, Arnaud, d'avoir partagé mon bureau durant cette dernière année de thèse et de m'avoir déchargé de nombreuses tâches d'assistantat à des moments clés. Je te souhaite bon courage dans ton aventure doctorale.

D'une façon générale, je remercie l'ensemble des doctorants et collègues du couloir MS²F – SE, Vincent, Clément, Damien, Anass, Julien, Kevin, Les discussions du temps de midi, les pauses d'anniversaire, la traditionnelle « grande-cafet » du vendredi midi ou encore les nombreuses activités extra-thèses telles que les célèbres Goodminton que nous avons faites ont été un parfait exutoire aux périodes de découragement qui peuvent apparaître au cours d'une thèse de doctorat. La génération dorée porte bien son nom !

Merci à tous les « vélotaffeurs » du plateau, Adrien, Gilles, Renaud, Florent, Romain et Clément avec qui j'ai passé de nombreuses heures à papoter sur le trajet du travail. Il m'a fallu du temps pour emboîter votre pas, ou plutôt votre roue, mais je suis désormais pleinement convaincu des bienfaits de concilier les trajets quotidiens à la pratique sportive.

Enfin, je vais conclure ces remerciements par les personnes sans qui cet accomplissement n'aurait pas été possible.

Merci à ma belle-famille, Bernard, Laurence et Nicolas pour le soutien, pour l'hospitalité que vous m'avez réservée et pour tous les bons moments que nous avons passés ensemble, qui m'ont fait quelque peu oublier l'échéance finale de cette thèse. Danke für alles !

Mes parents, merci d'avoir toujours été là pour moi, la réussite des études et de cette thèse est en grande partie grâce à votre soutien émotionnel indéfectible. Vous avez toujours su me relever et me supporter à chaque moment de doutes, merci infiniment. Merci également à Naomi, d'avoir passé la majeure partie de mes années d'étude à mes pieds, sur mes genoux ou dans mes bras à ne pas comprendre pourquoi je travaillais encore. Il n'est peut-être pas courant de mettre un animal dans les remerciements mais j'estime que tu y as ta place au même titre que quiconque.

Mes derniers mots vont à ma compagne, Caroline, pour ta présence au quotidien et ton soutien inébranlable depuis maintenant plus de 5 années. De nombreux dictons lient la réussite d'un homme à la femme à ses côtés, la confiance et la fierté que tu éprouves à mon égard en lisant cette thèse font que j'en suis désormais persuadé. La thèse terminée, nous pouvons désormais nous atteler à concevoir nos nombreux projets communs, l'esprit maintenant libéré de cette échéance.

Loris Saufnay

Octobre, 2024

Symbols and Abbreviations

Latin lower-case symbols

a	Design throat thickness or distance between two horizontal displacements
b	Profile width
b_{min}	Minimum flange width for profiles with different flange dimensions
c	Appropriate width to be taken for local buckling classification
c_f	Coefficient in the deflection formula for a beam subjected to a uniform loading ($c_f = 5$ for pinned end beams and $c_f = 1$ for fixed end beams)
c_{grade}	Unitary cost for a given steel grade
c_{HSS}	Unitary cost of a high-strength steel grade
c_M	Coefficient in the bending moment expression for a beam subjected to a uniform loading ($c_M = 8$ for pinned end beams and $c_M = 12$ for fixed end beams)
c_{RS}	Unitary cost of a regular steel grade
d	Depth of straight portion of web or diameter of fastener
d_{M16}	Nominal diameter of a M16 bolt
e	Initial loading eccentricity
e_0	Equivalent bow imperfection
f_y	Yield strength
f_y^*	Reference yield strength for residual stress model ($f_y^* = 235$ MPa)
f_{yb}	Yield strength of the bolt or the basic yield strength according to EN1993-1-3
$f_{y,exp}$	Measured yield strength obtained by coupon tests
$f_{y,HSS}$	Yield strength of a high-strength steel grade
$f_{y,RS}$	Yield strength of a regular steel grade
f_u	Ultimate tensile strength
f_{ub}	Ultimate tensile strength of bolt
h	Depth of a cross-section
h_1, h_2	Transversal displacements taken at two locations on the web of C-shaped sections during the Ghent experimental campaign
h_w	Depth of a web measured between the inner surfaces of the flanges
i_y, i_z	Radius of gyration about y-axis and z-axis, respectively
k	Stiffness coefficient or thermal conductivity
k_1	Stiffness of bolts in shear
k_2	Stiffness of bolts in bearing in the web of the supporting beam
k_3	Stiffness of bolts in bearing in the support of the supporting beam
k_4	Stiffness of bolts in tension
k_b	Stiffness coefficient of bolts in bearing
k_t	Stiffness coefficient of bolts in tension, for a single bolt row
k_w	Effective length factor for warping
k_y, k_z	Buckling length factors about y-axis and z-axis, respectively
m	Slope parameter of the fatigue resistance curve, number of cost extras or number of alloying elements
m_1	First slope parameter of the fatigue resistance curve
m_3	Second slope parameter of the fatigue resistance curve
n	Exponent in the modified imperfection factor for flexural buckling or the straightening coefficient of a Ramberg-Osgood material law
n_b	Number of bolts (with 2 bolts per row)
q_{Ed}	Design value of a uniform load
$q_{Ed,SLS}$	Maximum allowable design uniform load to respect the SLS requirements

$q_{Ed,ULS}$	Maximum allowable design uniform load to respect the ULS requirements
q_{Ek}	Characteristic value of a uniform load
r	Radius of root fillet
s	Standard deviation
t	Wall thickness of a hollow section or plate thickness
t_f	Flange thickness
t_w	Web thickness
v	Vertical deflection
v_{max}	Maximum vertical deflection
v_1, v_3	Vertical deflections at midspan of spans 1 and 3
w_i	Measured member out-of-straightness
x	Longitudinal axis or displacement along the member
\bar{x}	Mean value of a statistical evaluation
y	Major axis (parallel to flange)
z	Minor axis (parallel to web)
z_g	Coordinate of the point of load application related to the shear centre
z_j	Parameter to account for the non-symmetry effect against lateral-torsional buckling

Latin upper-case symbols

A	Cross-sectional area
$A_{c,eff}$	Effective cross-sectional area of the compression zone
A_{eff}	Effective area of a cross-section
A_{exp}	Measured cross-sectional area during an experimental test
A_{FEM}	Cross-sectional area used in finite element simulations
A_{HSS}	Optimum area for the high-strength steel grade
A_{net}	Net area of a cross-section
A_{opt}	Optimum area (lighter section to support a defined load)
A_{RS}	Optimum area for the regular steel grade
A_S	Tensile stress area of the bolt
A_{vy}, A_{vz}	Shear area with load parallel to flanges and parallel to web, respectively
A_w	Area of web
C	Constant
$C1, C2, C3$	Coefficients which depend on the loading and the end conditions, used for computing the critical moment for lateral-torsional buckling
C_B	Blasting cost
C_C	Cutting cost
C_E	Erection cost
C_M	Material cost
C_P	Painting cost
C_S	Sawing cost
C_T	Transport cost
C_W	Welding cost
C_{rel}	Relative cost
D	Outer diameter
D_x, D_y, D_z	Translational degree of freedom in the x-, y- and z-direction, respectively
E	Modulus of elasticity (Young's modulus)
E_{sh}	Strain hardening slope
F_f	Friction force
F_x, F_y, F_z	Concentrated load in the x-, y- and z- direction, respectively
G	Shear modulus (Coulomb's modulus)

I	Second moment of area
I_t	Torsion constant
I_w	Warping constant
I_y, I_z	Second moment of area (moment of inertia) about y-axis and z-axis, respectively
$K_{eq, shear}$	Resulting shear stiffness at a bolt node
$K_{eq, tension}$	Resulting tension stiffness at a bolt node
L	Member length
L_b	Bolt elongation length
L_{cr}	Buckling length
M	Bending moment
$M_{b, Rd}$	Design value of the buckling resistance of a member in bending
M_{cr}	Elastic critical moment for lateral torsional buckling
M_{Ed}	Design value of the bending moment
$M_{eff, Rd}$	Design value of the effective elastic bending moment resistance
$M_{el, Rd}$	Design value of the elastic bending moment resistance
M_{max}^+	Maximum positive bending moment
M_{max}^-	Maximum negative bending moment
M_{max}	Maximum bending moment in absolute value
$M_{pl, Rd}$	Design value of the plastic bending moment resistance
M_{Rd}	Design value of the bending moment resistance
M_{Rk}	Characteristic value of the bending moment resistance
N	Number of cycles in the fatigue design or axial load
$N_{b, Rd}$	Design member buckling resistance to compression
N_{cr}	Euler buckling load
N_D	Stress cycles in the fatigue design
N_{EC3}	Axial resistance according to the design recommendations of EN1993-1-1:2005
N_{Ed}	Design axial force
$N_{eff, Rd}$	Design value of the effective elastic axial resistance
N_{FprEN}	Axial resistance according to the design recommendations of FprEN1993-1-1:2022
$N_{pl, Rd}$	Design value of the plastic load capacity
N_{prop}	Axial resistance according to the design proposal made in Chapter 5
N_{Rd}	Design value of endurance in the fatigue design or design value of axial resistance
N_{Rk}	Characteristic value of the axial resistance
$N_{u, Rd}$	Design value of the ultimate resistance to axial force of the net cross-section at holes for fasteners
$N_{u, FEM}$	Ultimate axial resistance obtained through finite element simulations
$N_{u, exp}$	Ultimate axial resistance obtained in a buckling test
P	Concentrated load
P_{base}	Base price of steel
P_{Ed}	Design value of a concentrated load
P_{Ek}	Characteristic value of a concentrated load
P_{rel}	Relative price
R_x, R_y, R_z	Rotational degree of freedom about x-x, y-y and z-z axis, respectively
T	Temperature
$V_{b, Rd}$	Design value of the shear resistance (accounting for shear buckling)
V_{Ed}	Design value of the shear force
$V_{pl, Rd}$	Design value of plastic resistance to shear force
V_{Rd}	Design value of the shear resistance
W	Section modulus or warping (degree of freedom)
W_{eff}	Effective section modulus

W_{el}	Elastic section modulus
$W_{el,y}, W_{el,z}$	Elastic section modulus for bending about y-y axis and z-z axis, respectively
W_{pl}	Plastic section modulus
$W_{pl,y}, W_{pl,z}$	Plastic section modulus for bending about y-y axis and z-z axis, respectively

Greek letters and symbols

α	Imperfection factor for flexural buckling, the coefficient of dilatation or the rotation angle
α^*	Modified imperfection factor (with residual stresses)
α_0	Reference imperfection factor
α_1, α_3	Rotation angles in spans 1 and 3 in the Ghent experimental tests
α_2^*	Modified imperfection factor (without residual stresses)
α_{ref}	Reference imperfection factor for S235, without residual stresses
β	Local buckling reduction factor (pure compression)
β_{EC3}	Local buckling reduction factor (complying with Eurocode 3)
β_{num}	Local buckling reduction factor (obtained numerically)
β_{LT}	Coefficient to compute the equivalent geometrical imperfection for a lateral torsional buckling mode
β_w	Local buckling reduction factor (pure bending)
γ_{M0}	Partial safety factor for resistance of cross-sections
γ_{M1}	Partial safety factor for resistance of members to instability assessed by member checks
γ_{M2}	Partial safety factor for resistance of cross-sections in tension to fracture
γ_{Mf}	Partial safety factor for fatigue resistance
δ	Imposed displacement in the roller-straightening process
$\Delta\sigma$	Nominal stress range for the fatigue design
$\Delta\sigma_C$	Reference stress value at $2 \cdot 10^6$ stress cycles for the fatigue design
$\Delta\sigma_{Ed}$	Design stress value of the applied stress range for the fatigue design
ε	Engineering strain or material parameter depending on f_y
ε_f	Eurocode 3 material parameter for flanges
ε_{sh}	Strain hardening strain
ε_u	Strain at ultimate stress
ε_y	Yield strain
ζ	Part of the general formulation of the elastic critical moment - see Eq. (2-6)
η	Imperfection parameter for flexural buckling or factor accounting for the yield strength in the shear buckling check
λ	Slenderness
λ_1	Reference slenderness to determine the relative slenderness
λ_{FB}	Flexural buckling slenderness
$\lambda_{FB,y}, \lambda_{FB,z}$	Flexural buckling slenderness about strong axis and weak axis, respectively
λ_{lim,α^*}	Limit of slenderness for an economic advantage (considering the modified imperfection factor α^*)
λ_{lim,α_2^*}	Limit of slenderness for an economic advantage (considering the modified imperfection factor α_2^*)
$\lambda_{lim,EC3}$	Limit of slenderness for an economic advantage (considering EC3 design rules)
$\lambda_{lim,H}$	Limit of slenderness for an economic advantage (considering a high-cost level)
$\lambda_{lim,L}$	Limit of slenderness for an economic advantage (considering a low-cost level)
$\lambda_{lim,M}$	Limit of slenderness for an economic advantage (considering a medium cost level)
λ_{LTB}	Lateral torsional buckling slenderness
$\bar{\lambda}$	Relative slenderness for flexural buckling
$\bar{\lambda}_{LT}$	Relative slenderness for lateral torsional buckling

μ	Static friction coefficient
$\mu_{num,x}$	Ratio between concentrated forces F_x and F_z at contact nodes in numerical simulations
$\mu_{num,y}$	Ratio between concentrated forces F_y and F_z at contact nodes in numerical simulations
ν	Poisson's ratio in the elastic range
π	Pi number
ρ	Density or reduction factor for local buckling
σ	Engineering stress
σ_{app}	Applied stress
σ_c	Compressive residual stress
σ_{cf}	Compressive residual stress in the flanges
σ_{cw}	Compressive residual stress in the web
$\sigma_{cr,d}$	Elastic critical distortional buckling stress according to EN1993-1-3
σ_{res}	Residual stress
σ_t	Tensile residual stress
σ_{tot}	Resulting stress
χ	Reduction factor for relevant buckling mode
χ_{exp}	Reduction factor due to flexural buckling obtained by buckling test
χ_{EC3}	Reduction factor due to flexural buckling according to EN1993-1-1:2005
χ_{FEM}	Reduction factor due to flexural buckling obtained by finite element simulations
χ_{FprEN}	Reduction factor due to flexural buckling according to FprEN1993-1-1:2022
$\chi_{Jönsson}$	Reduction factor due to flexural buckling according to the research of Jönsson
χ_{LT}	Reduction factor for lateral torsional buckling
χ_{Maquoi}	Reduction factor due to flexural buckling according to the research of Maquoi
χ_{Meng}	Reduction factor due to flexural buckling according to the research of Meng
χ_w	Contribution of the web to shear buckling resistance
χ_y, χ_z	Reduction factor due to flexural buckling about y-y axis and z-z axis, respectively

Abbreviations

<i>AISC</i>	American Institute of Steel Construction
<i>AP</i>	Acidification Potential
<i>AR</i>	As-Rolled steels
<i>BOF</i>	Basic Oxygen Furnace
<i>CCS</i>	Carbon Capture and Storage
<i>CED</i>	Cumulative Energy Demand
<i>CEV</i>	Carbon Equivalent Value
<i>CHS</i>	Circular Hollow Section
<i>COP21</i>	Conference of the Parties 21
<i>COV</i>	Coefficient of Variation
<i>D</i>	Distortional buckling
<i>DP</i>	Dual-Phase steel
<i>DRI</i>	Direct Reduced Iron
<i>EAF</i>	Electric Arc Furnace
<i>EC3</i>	Eurocode 3
<i>ECCS</i>	European Convention for Constructional Steelwork
<i>EPD</i>	Environmental Product Declaration
<i>ESDEP</i>	European Steel Design Education Programme
<i>EU</i>	European Union
<i>FB</i>	Flexural Buckling
<i>FE</i>	Finite Element
<i>FEM</i>	Finite Element Model

<i>GMNIA</i>	Geometrically and Materially Nonlinear Analysis with Imperfections
<i>GWP</i>	Global Warming Potential
<i>HSLA</i>	High Strength Low Alloy
<i>HSS</i>	High Strength Steels
<i>IEA</i>	International Energy Agency
<i>IPCC</i>	Intergovernmental Panel on Climate Change
<i>LB</i>	Local Buckling
<i>LBA</i>	Linear Buckling Analysis
<i>LCA</i>	Life cycle assessment
<i>LCC</i>	Life cycle cost assessment
<i>LETI</i>	London Energy Transformation Initiative
<i>LTB</i>	Lateral Torsional Buckling
<i>N</i>	Normalised steel
<i>Q/QT</i>	Quenched and Tempered steel
<i>QST</i>	Quenched and Self-Tempered steel
<i>RE2020</i>	Réglementation Environnementale 2020
<i>RFCS</i>	Research Fund for Coal and Steel
<i>RHS</i>	Rectangular Hollow Section
<i>RS</i>	Regular Steel grade
<i>SHS</i>	Square Hollow Section
<i>SLS</i>	Serviceability Limit States
<i>TM/M</i>	Thermomechanical steel
<i>UHSS</i>	Ultra-High Strength Steel
<i>UK</i>	the United Kingdoms
<i>ULS</i>	Ultimate Limit States
<i>US/USA</i>	the United States of America

Alloying elements

<i>Al</i>	Aluminium
<i>B</i>	Boron
<i>C</i>	Carbon
<i>Cr</i>	Chromium
<i>Cu</i>	Copper
<i>Fe</i>	Iron
<i>FeCr</i>	Ferrochrome
<i>FeMn</i>	Ferromanganese
<i>FeMo</i>	Ferromolybdenum
<i>FeNi</i>	Ferronickel
<i>FeSi</i>	Ferrosilicon
<i>FeV</i>	Ferrovandium
<i>Mn</i>	Manganese
<i>Mo</i>	Molybdenum
<i>Ni</i>	Nickel
<i>Nb</i>	Niobium
<i>N</i>	Nitrogen
<i>P</i>	Phosphorus
<i>Si</i>	Silicon
<i>S</i>	Sulphur
<i>Ti</i>	Titanium
<i>V</i>	Vanadium

Table of Content

Abstract	I
Résumé.....	III
Acknowledgements - Remerciements.....	V
Symbols and Abbreviations	VII
Table of Content.....	XIII
Chapter 1 Introduction.....	1
1.1. Contextualisation	1
1.1.1. Steel industry CO ₂ emissions	1
1.1.2. Net-zero CO ₂ emissions by 2050	2
1.1.3. Decarbonisation pathways by 2030 and 2050	3
1.1.4. Building better with less.....	4
1.2. Research objectives.....	7
1.3. Personal motivations.....	7
1.4. Thesis outline.....	8
Chapter 2 Research Context.....	11
2.1. Introduction.....	11
2.2. High-strength steels	12
2.2.1. Production processes, specifications and availability	13
2.2.2. Mechanical properties.....	15
2.2.3. Higher temperature performance.....	18
2.2.4. Fatigue performance	18
2.2.5. Relative price and carbon footprint	20
2.3. Design provisions for members in Eurocode 3.....	22
2.3.1. Scope	22
2.3.2. Resistance of cross-section	23
2.3.3. Member slenderness.....	23
2.3.4. Flexural buckling.....	25
2.3.5. Lateral torsional buckling	27
2.3.6. Serviceability limit states.....	28
2.3.7. Reference papers highlighting the benefits of HSS grades	29
2.4. Influence of residual stresses on column resistance.....	30
2.4.1. Development of residual stresses	31
2.4.2. Residual stress distributions.....	31

2.4.3. Influence of the yield stress and modified imperfection factors	33
2.4.4. Influence of the straightening process.....	35
2.5. Overview of project examples.....	38
2.6. Research questions.....	40
Chapter 3 Sustainability of High-Strength Steels	43
3.1. Introduction.....	43
3.2. The three pillars of sustainability	44
3.3. Establishment of reliable relative prices	45
3.3.1. Background on cost breakdowns	45
3.3.2. Cost components.....	47
3.3.3. Methodology	49
3.3.4. Validation	49
3.3.5. Results	56
3.4. Establishment of reliable relative carbon emissions.....	60
3.4.1. Background on production emissions	60
3.4.2. Methodology	64
3.4.3. Validation	65
3.4.4. Results	67
3.5. Discussions and conclusions.....	69
Chapter 4 The Right Steel at The Right Place.....	71
4.1. Introduction.....	71
4.2. Methodology	72
4.2.1. General structure	72
4.2.2. Assumptions and case studies.....	73
4.2.3. Optimisation procedure and benefit criterion	75
4.2.4. Establishment of continuous quantities.....	76
4.3. Validation	77
4.4. Results for hot-rolled sections.....	80
4.4.1. Members in tension	80
4.4.2. Members in pure compression	83
4.4.3. Members in simple bending.....	92
4.4.4. Members subjected to combined compression and bending.....	101
4.5. Results for hollow sections.....	103
4.5.1. Members in tension	103
4.5.2. Members in pure compression	103
4.5.3. Members subjected to combined compression and bending.....	107

4.6. Case studies for compression members	109
4.6.1. Mapfre Tower in Barcelona.....	109
4.6.2. NRG Stadium in Houston.....	111
4.7. Discussions and conclusions.....	113
Chapter 5 Improvement of the Existing Design Rules for Flexural Buckling.....	115
5.1. Introduction.....	115
5.2. Establishment of a modified imperfection factor	116
5.2.1. Methodology	116
5.2.2. Description of the numerical model.....	118
5.2.3. Validation of the numerical model.....	119
5.2.4. Assessment of current recommendations for S235 and S460 grades	122
5.2.5. Considerations for intermediary S355 and S420 grades	125
5.2.6. Modified imperfection factor for hot-rolled sections	126
5.2.7. Validity of the proposal for slender sections.....	129
5.2.8. Confrontation with other existing expressions from literature	133
5.2.9. Benefit in terms of buckling resistance	136
5.2.10. Summary and conclusions.....	137
5.3. Beneficial influence of the roller-straightening process	138
5.3.1. The reference machine setting and the model description	138
5.3.2. Validation on experimental measurements.....	142
5.3.3. Straightened residual stress patterns for selected profiles	145
5.3.4. Optimisation of machine setting.....	147
5.3.5. Influence of roller-straightening on column buckling resistance.....	152
5.3.6. Discussions and conclusions.....	154
5.4. Modified imperfection factor for columns without residual stresses	155
5.5. Discussions on the right choice of steel grade	157
5.5.1. Resistance to flexural buckling	157
5.5.2. Results of the optimisation routine.....	158
5.5.3. Case studies for compression members	159
5.6. Conclusions.....	160
Chapter 6 Consideration of Inherent Sources of Stabilisation in Storage Racks	161
6.1. Introduction.....	161
6.2. Methodology and research assumptions	162
6.3. State-of-the-art regarding the stabilising effect of wooden pallets.....	162
6.4. Description of the experimental campaign of Ghent.....	164
6.4.1. Experimental set-up description	164

6.4.2. Measurements performed during the tests.....	165
6.4.3. Experimental results and coupon tests.....	167
6.4.4. Selection of relevant tests for validation	168
6.5. Description of the numerical model.....	170
6.5.1. Mesh sensitivity study and finite element choice.....	170
6.5.2. Stress-strain relationship and loading configuration	172
6.5.3. Modelling of joints and contact regions.....	173
6.5.4. Modelling of pallets and loading simplification	174
6.5.5. Modelling of the coupling system between rack beams.....	175
6.5.6. Computation of numerical displacements for comparison with experimental tests	175
6.6. Validation of the numerical model based on an experimental campaign	176
6.6.1. Numerical model assumptions.....	176
6.6.2. Linear bifurcation analyses.....	177
6.6.3. Results for Test 2	178
6.6.4. Results for Test 3a	182
6.6.5. Necessity of the coupling element.....	185
6.7. Numerical results for the case study.....	186
6.7.1. Case study description.....	186
6.7.2. Description of the numerical models	187
6.7.3. Mesh sensitivity study	188
6.7.4. Numerical results.....	191
6.8. Beneficial advantage of a higher yield strength.....	197
6.9. Conclusions.....	199
Chapter 7 General Conclusions.....	201
7.1. The challenges of sustainable construction	201
7.2. Summary of contributions.....	202
7.3. Limitations and perspectives.....	205
7.4. Thoughts about tomorrow's practice.....	209
7.4.1. Closing the loop	209
7.4.2. Collaboration for a sustainable future	210
List of Publications.....	213
References.....	215
Appendices	233
List of Figures.....	265
List of Tables.....	271

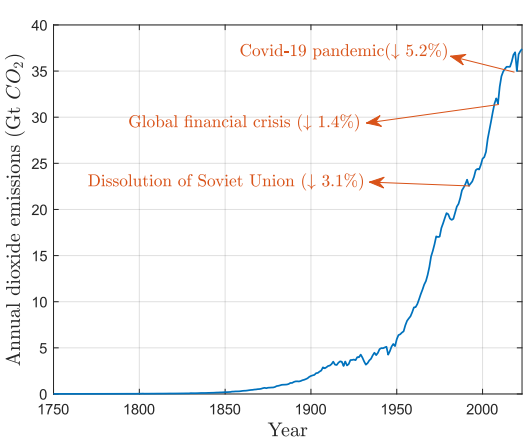
Chapter 1

Introduction

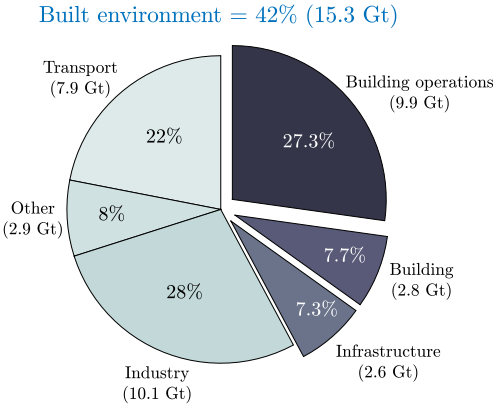
1.1. Contextualisation

1.1.1. Steel industry CO₂ emissions

Climate change can be defined as the long-term alteration of global average weather patterns, which has a profound impact on all forms of life on Earth. Since the Industrial Revolution, human activities have been a major contributing factor to the release of carbon dioxide and other greenhouse gases into the atmosphere. This results in an increase in global temperatures, leading to long-term climate change. A review of the scientific evidence reveals that 97% of climate scientists have concluded that the world is undergoing extraordinary and traumatic climatic changes which are widely human-induced [1], [2], [3]. Notwithstanding the recent disturbances, including the global financial crisis and the pandemic caused by the SARS-CoV-2 virus, the annual emissions continue to increase following an exponential trend that has been observed since the 19th century, as illustrated in Fig. 1-1a. It is widely acknowledged that the construction sector plays a significant role in this regard. Indeed, the building and construction sector is currently responsible for 42% of global energy-related CO₂ emissions – see Fig. 1-1b. It is expected that the global building stock will double in size by 2060 [4], with the construction of more than 230 billion m² of new buildings. This corresponds to the construction of one city as large as Paris every week or the current floor area of Japan every year until 2060 [4]. It is therefore imperative to implement radical changes across the entire spectrum of construction sector activity.



(a) Global CO₂ emissions [5]



(b) Global emission share [6]

Fig. 1-1. Global CO₂ emissions and responsibility of the building sector.

The steel industry is responsible for approximately 2.8 Gt of CO₂ emissions per year, representing 8% of total energy system emissions and up to 10% when indirect emissions from electricity generation are included [7], [8]. In 2023, the global production of crude steel reached 1,850 Mt and by 2050, steel use is projected to increase by 20% to meet the needs of a growing global population and the corresponding building expansion. In the absence of intervention, these emissions are therefore forecasted to a continuous increase.

1.1.2. Net-zero CO₂ emissions by 2050

In response to the climate emergency, the Paris Agreement was concluded at the 21st Conference of Parties (COP21) on December 12, 2015, with 196 parties signing the document [9]. The goal is to achieve carbon neutrality by 2050, although significant reductions must be made in a relatively short time to limit global warming. Indeed, it is required to limit global warming to a maximum of 2°C, with an optimal target of 1.5°C above pre-industrial levels. Therefore, there is a defined “carbon budget”, representing the net amount of CO₂ that humans can still emit while limiting global warming to the level fixed by the Paris Agreement. The remaining carbon budget from the beginning of 2020 is 500 GtCO₂, with a 50% likelihood of limiting global warming to 1.5°C (400 GtCO₂, with a 67% certainty) and 1150 GtCO₂, with a 50% likelihood of limiting global warming to 2°C, according to the IPCC Sixth Assessment Report (AR6) [10]. The estimated carbon budget for the steel sector associated with a 1.5°C limit is thought to be between 19 GtCO₂ [11] and 56 GtCO₂ [12]. There is therefore some uncertainty regarding the remaining carbon budget for the steel industry. Nevertheless, an immediate reduction in emissions from the sector is imperative.

Today, steel producers are investing in new production methods to reduce the carbon footprint of steel. The reference CO₂ intensities for the various production technologies [13] are reported in Table 1-1.

Production technology	CO₂ intensity (t CO₂eq/t)
Basic Oxygen Furnace (BOF)	2.3
BOF + biofuels	1.1
Direct Reduced Iron (DRI)	1.1
BOF + Carbon Capture and Storage (CCS)	0.9
Electric Arc Furnace (EAF)	0.4
EAF + zero-carbon electricity	0.1

Table 1-1. CO₂ intensity of steel production.

According to the WorldSteel Association [14], the current predominant routes of steel production can be divided into two main categories: the Basic Oxygen Furnace (BOF), which accounts for 71% of crude steel production, and the Electric Arc Furnace (EAF), which accounts for 29%. The latter can be charged with 100% steel scrap, which explains its lower carbon intensity in Table 1-1. This share of production routes explains the current high carbon intensity of steel, but it is however expected to change significantly by 2050. This will have a direct impact on the associated carbon factors, which will also be reduced by the forthcoming further breakthroughs in the steelmaking process. It is therefore crucial to decarbonise the steel production process through the implementation of innovative production technologies and efficient material usage [15].

1.1.3. Decarbonisation pathways by 2030 and 2050

When speaking about the carbon emissions in a built environment, i.e. man-made structures in which people live and work, it is essential to differentiate between embodied and operational carbon emissions. Embodied carbon can be defined as the carbon footprint of a building before it becomes operational. In contrast, operational emissions are those associated with the used energy to operate the building, which can be activated or deactivated (heating/cooling, ventilation, lighting, ...).

The objective of achieving net zero emissions by 2050 is insufficient to maintain carbon budgets below the desired limit as it does not provide any milestones that should be reached before this deadline to limit carbon emissions. Indeed, the pace of progress must accelerate significantly before 2030 [16]. In accordance with the estimates made by the International Panel on Climate Change (IPCC), greenhouse gas emissions should peak before 2025, be reduced by 43% by 2030 and by 60% by 2035 in comparison to 2019 [17] but all energy-emitting sectors should rather at least halve emissions by 2030. To achieve the same objective, different proposals may be found. According to the World Green Building Council [21], the objective for buildings is to achieve net zero carbon in operation and a 40% reduction in embodied carbon by 2030, with also the goal of reaching net zero for the latter by 2050 [18]). The European Union's Green Deal has set a global target of reducing CO₂ emissions by 30% by 2030 compared to the 2018 level and achieving carbon neutrality by 2050. The "LETI Climate Emergency Design Guide" [24] gives some recommendations for the UK's building sector by establishing a maximum steel intensity by building, i.e. for domestic building, the embodied carbon should be reduced from 800 kgCO₂/m² (the baseline) to a value below 300 kgCO₂/m² by 2030. In France, equivalent regulations are set out in the RE2020 [25], this document establishes ambitious limits on embodied carbon for new construction and promotes the systematic use of life cycle assessments.

A recent publication on the greenhouse gas emission reduction targets set by the 60 largest steel producers in the world [26] reveals that only 30 of them have their own targets and 14 out of the 30 steel producers did not provide an emission reduction plan. The most frequently cited technology is the hydrogen-based direct reduced iron. For instance, steel manufacturers, like ArcelorMittal, Tata Steel UK or US Steel [22], [23] have presented ambitious emission reduction plans with the stated objective of reducing by 2030 greenhouse gas emissions by 20%-30%, which is clearly below the recommendations of IPCC. Fig. 1-2 reflects the two different pathways to achieve the same objective of net-zero emissions by 2050: the first pathway depicts the IPCC-aligned curve considering a reduction of 55% in 2030, whereas the second pathway is derived by fixing a reduction of 25% in 2030 according to the fixed goal of world-leading steel companies.

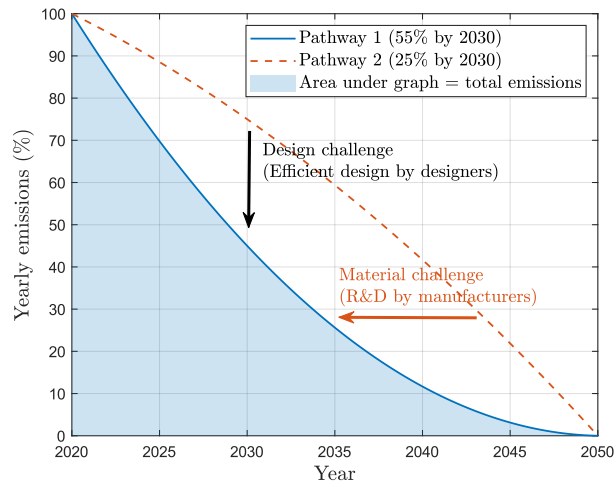


Fig. 1-2. Toward net-zero emissions by 2050 – importance of the pathway (Adapted from istructe.org [24], [25], [26]).

To ensure that global warming will remain below 2°C, it is essential to ensure that the area below the pathway to net zero remains below the carbon budget fixed by the Paris Agreement. Despite both pathways achieving net zero by 2050, they exhibit disparate concavity, resulting in a significant discrepancy in carbon emissions. The second pathway generates emissions that are approximately twice those of the first pathway, thereby exceeding the carbon budget. In light of the IPCC recommendations, the steel industry must pursue two primary objectives: the achievement of net-zero emissions by 2050 and a quicker reduction of emissions associated with embodied carbon to avoid exceeding the carbon budget by that year. The formula for embodied carbon is provided in Eq. (1-1).

$$\text{Embodied carbon (kgCO}_2\text{e)} = \sum_{\text{all materials}} [\text{Quantity (kg)} \cdot (\text{Carbon factor (kgCO}_2\text{eq/kg)})] \quad (1-1)$$

Accordingly, to reduce the embodied carbon of buildings, there are two levers for action: (i) reduction of the carbon factor through the production of low-carbon materials via novel and innovative production processes, and (ii) the reduction of the quantity of material used by the realisation of more efficient designs. The development and the launching of innovative technologies to reduce the carbon factor requires time and significant economic investment (from 25 to 65% surge in investment [13]), so influencing the future price trajectory of steel. However, the optimisation of the design process through the use of the appropriate steel grade has the potential to result in savings of 19% to 46% in embodied carbon, with cost impacts of less than 1% [27]. In general, it is cost-effective to reduce a project’s embodied carbon through the use of less material. However, the cost savings could be sometimes less than the environmental savings [28], [29]. Consequently, at each stage of the design and construction processes, all parties involved (architects, engineers, construction professionals and others) have a responsibility to contribute to the creation of a more sustainable built environment. This requires the establishment of synergies and collaborations since the early phase of any project.

1.1.4. Building better with less

In civil engineering design, safety is often seen as an overriding concern compared to material optimisation. But, as highlighted in the previous section, in the forthcoming years, things will have to change with a serious concern to build more efficiently with less material to respect the Paris Agreement in terms of carbon emissions. For design engineers, the various strategies for reducing material usage and thus the embodied carbon emissions in the building sector are presented in Fig. 1-3 and summarised hereafter.

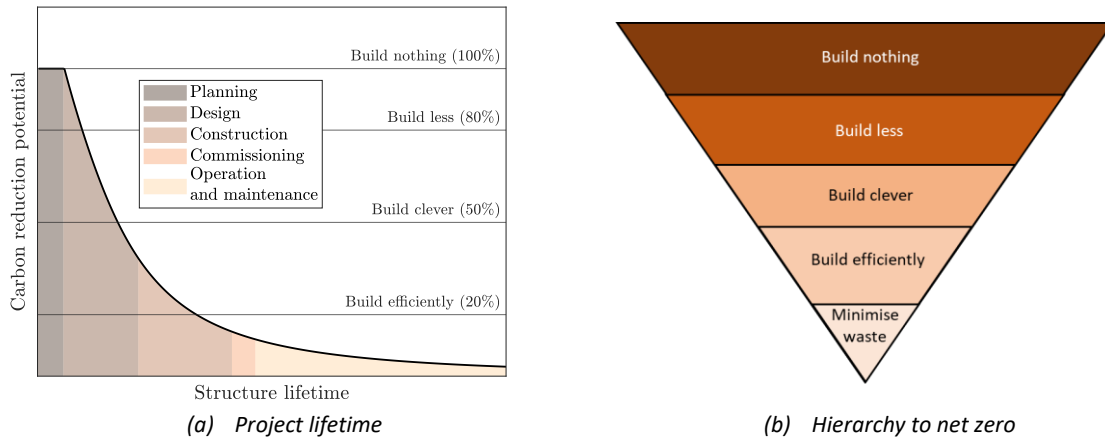


Fig. 1-3. Tackle carbon early in the structure's lifetime and hierarchy to net zero [24], [30], [31].

➤ **Build nothing**

This represents the most radical perspective, which is a paradox for the construction sector. Even for structural engineers, the construction of a new building is not always the optimal solution, particularly in countries and regions with a significant existing building stock, including some that are currently unoccupied. In the case of buildings with low occupancy, such as hospitals or schools, there is a significant opportunity to repurpose these existing structures for alternative uses. In this critical context, it is somewhat illogical to demolish buildings that could serve for alternative purposes. This necessitates that designers need to consider whether the project can be accomplished without the construction of a new building. They must persuade the client and the design team by demonstrating the achievable potential carbon and cost savings. Several articles published by the Institution of Structural Engineers provide guidance for practitioners [32], [33], [34], [35].

➤ **Build less**

If the concept of building nothing is not achievable, it has been previously demonstrated the necessity of reducing the amount of new material used in the construction process. The concept of a circular economy [13] represents the next trend in the field of structural engineering to achieve zero waste in the building sector. The R-strategies of the circular economy are composed of the following concepts: Rethink, Refuse, Repair, Repurpose, Refurbish, Reduce, Reuse and Recycle.

Due to its ferromagnetic properties, steel is one of the most straightforward materials to recycle. At present, the steel demand exceeds the amount of steel that can be recycled. Approximately 83% of end-of-life steel is collected for recycling, which corresponds to almost 150 Mt losses each year. This amount is comparable to the EU's annual production. Consequently, while there is still a necessity to manufacture new steel, there is an economic (approximately 70 billion euros) and an environmental (320 Mt CO₂ per year) advantage in reducing the loss of steel [13].

Nevertheless, new structures should be designed with standardised, modularised building elements to facilitate the reusability of steel elements. For instance, it is essential to have straightforward dismantlable connections on site. Therefore, the use of bolted joints instead of welded connections is recommended to facilitate the reuse of each element in other structures. The objective of the RFCS project, entitled "REDUCE", was to develop practical tools and steel-based technologies to facilitate the design of structures that can be dismantled and reused [36]. The fundamental principles may be summarised as follows: design for disassembly, reuse of structural elements, reuse of buildings and design for adaptability.

Several pioneering projects have already been initiated, including “La Petite Maison” in Luxembourg, which has been designed to be disassembled, the “Mundo Louvain-la-Neuve” in Belgium for structural element reuse and the “New Zealand International Convention Centre” in New Zealand for building reuse [37]. These projects constitute benchmark examples for future constructions.

➤ **Build clever**

The objective of clever building is to avoid overdesign by employing, for example, efficient materials, efficient structural forms, low-carbon materials, reduced spans and refined loading criteria. The use of higher grades for strength-governed members may result in substantial weight savings. For instance, using a steel with a yield strength of 460 MPa instead of 355 MPa results in a weight saving of 30% for strength-controlled members. Indeed, for such members, the weight saving is equal to the yield-strength ratio. Therefore, an effective approach is to employ a thoughtful design approach that incorporates the right material at the right place in the structure, thereby further reducing the carbon footprint of the project. Indeed, optimising the steel elements that constitute a structure results in weight savings that imply a reduction in the supporting elements (e.g. columns and foundations). Consequently, a minor improvement at a local level can result in a significant overall saving and appropriate design criteria should be available to take benefit of the material resistance.

➤ **Build efficiently**

It is recommended that utilisation ratios be maximised by optimising the designs. A publication [38] analysed in 2014 the average utilisation of steel beams in 23 steel-framed buildings. The analysis of over 10000 beams revealed that the average utilisation is below 50% of their capacity. The reason behind this observation is twofold: firstly, to facilitate the construction process and reduce labour costs; secondly, to mitigate the risk of construction errors. For the detailed designs, utilisation ratios should be adjusted to reach a maximum utilisation, close to 1.0 [28]. In other words, it means that the designers should consider material efficiency at the same level as safety. Indeed, a design strategy that prioritises minimising material usage over minimising labour costs could result in a significant reduction in embodied carbon emissions.

All these actions contribute to a more sustainable future for the building sector. The term sustainable, in the context of this thesis, primarily refers to the economic and environmental branches of sustainability, whereas sustainability often refers to a balance between social, economic and environmental priorities. It will be highlighted throughout the thesis that, while there may not necessarily be a definitive sustainable building model, there are a lot of actions that can be made for realising weight savings thus moving towards a more sustainable building model. Striving for sustainability is a complex matter. Sometimes reaching a modifiable construction targeting reusability is not the lightest structural solution. Furthermore, the most environmentally sustainable option is not necessarily the most economically or socially sustainable option. Anyway, more and more projects aspiring to ambitious embodied carbon targets arise nowadays and this sustainability criterion starts to be a relevant criterion for the design selection process. Accordingly, design solutions must be proposed to realise more sustainable structures which are environmentally and economically viable. In particular, it means realising material savings to reduce the price and the carbon footprint of a structure, which can be achieved by using the right material at the right place, developing new design processes and adopting appropriate design rules. The present thesis intends to contribute to this achievement as reflected in the following section.

1.2. Research objectives

In this context of structural optimisation, high-strength steels represent the highest strength-to-weight ratio of existing steel materials. Their use could contribute to the optimisation of steel structures by reaching the same level of resistance for a reduced material quantity, thereby resulting in lighter buildings requiring less extensive and costly foundations. Therefore, it is more and more important to position the right material at the right place but also the right steel at the right place to realise weight savings and hence, to reduce drastically the carbon footprint and the material cost of steel structures. These materials are, in addition, reusable and recyclable which represent further reductions in a long-term scenario. In the existing literature, most research generally focuses on welded sections or cold-formed tubular sections for which high-strength steel grades already exist for several years. Steel manufacturers have not yet invested in production lines for high-strength hot-rolled sections because the demand for such profiles is still very low [39]. But this fact may change in the future as the steel industry continuously improves the production processes to answer to the challenges of the future.

The general objective of this thesis is therefore to develop and validate methodologies to investigate the weight savings that can be achieved by choosing appropriate steel grades for hot-rolled sections, having appropriate design rules as well as using innovative solutions that permit to benefit entirely from the increase of yield strength. The impact of high-strength steels on structural performance by focusing on their applications, their resulting benefits and the challenges and concerns they raise are also analysed. To achieve the objective, a multidisciplinary approach is adopted and sequenced in three main steps:

1. Empirical investigations of prices and carbon footprints of such grades;
2. Realisation of extensive numerical campaigns to adapt existing design rules to take full advantage of the increased yield strength;
3. Identification of fields of application for which high-strength steels are economically and environmentally justified through comparative studies.

1.3. Personal motivations

Of course, realising scientific research that results in a contribution to more sustainable steel structures cannot save the planet in itself, but it can at least serve to empower the structural engineer who will design future construction projects. The sum of collective individual and professional actions can facilitate the attainment of a critical threshold needed for measurable change. But maybe more importantly, it can help reduce a feeling of helplessness, and sometimes guilt, that many young people experience face to the climate crisis [40]. As a young structural engineer belonging to Generation Z (persons born between 1995 and 2010), I believe that our generation has a pivotal role to play in addressing climate change as this generation is particularly affected by this global issue [41], [42]. In light of these considerations, I sought to ascertain the extent to which the professional research might lead to significant environmentally conscious change relative to the impact of other actions in daily life. These actions include reducing travel emissions by using rail and ceasing air travel, optimising the daily working journey from home to office, reducing heating usage and eliminating beef and lamb consumption. The implementation of these actions, whether at home or in the workplace, has the potential to create a positive ripple effect [43]. The reference values are compared in Fig. 1-4.

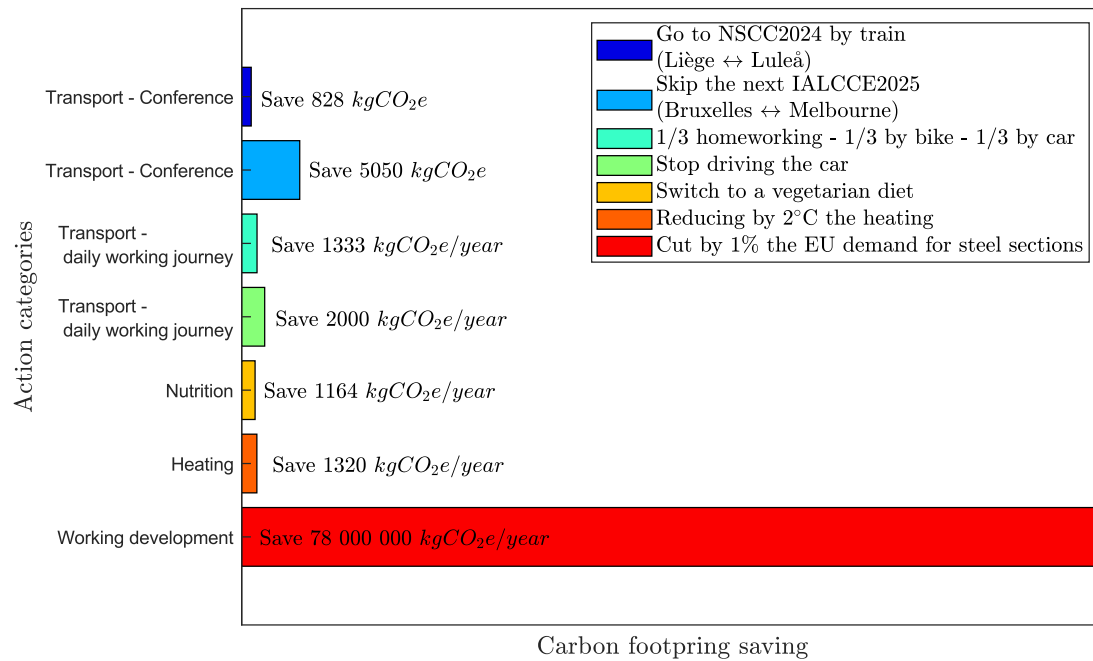


Fig. 1-4. Contextualising the potential impact of the researcher's actions [adapted from [44]]¹.

As illustrated in Fig. 1-4, a reduction in European steel demand for heavy sections by 1% through the utilisation of innovative materials and solutions can result in an emissions reduction that is almost equivalent to that achieved by removing the emissions from forty thousand cars over the year or eliminating sixteen thousand personal trips to Australia each year of production. This demonstrates the necessity in developing scientific research in the field of structural optimisation. This infographic can be seen as the starting point of my PhD thesis.

1.4. Thesis outline

Apart from this introduction, the thesis is divided into six main chapters, which are briefly detailed hereafter.

- **Research context** – In the opening chapter, the research background about high-strength steels is presented. Faced to the climate crisis and the importance of optimising the building sector to build less, using appropriate steel specifications and appropriate design rules is becoming a necessity to offer the possibility for designers to realise significant savings in their designs. This chapter presents the existing design rules and a deep literature review of the reference publications and projects highlighting the beneficial effect of using an appropriate steel grade. Finally, it highlights the research questions that guided the scientific developments made in this thesis.

¹ **Assumptions:** the emissions for transport to conferences were evaluated using the data website Impact CO₂ [45]. An average distance of 25 kms has been assumed between the worker's home and his office (corresponding to 50 kms/day), the emission per km of a thermal car is assumed to 0.2kg CO₂eq/km and the number of working days is estimated to 200 over a year. The reductions resulting from a change in our alimentation and in the heating are extracted from the recommendations given on the Neo & Nea website [46]. Finally, according to Eurofer [47], the EU total finished production of heavy sections was 6.897 Mt in 2023. The impact of a reduction of 1% may thus be computed based an average emission of 1.13kgCO₂eq/t according to the Bauforumstahl EPD [48].

- **Sustainability of high-strength steels** – This second chapter is devoted to explaining the importance of considering high-strength steels to realise sustainable steel structures and establishing reference values to enable a comparative study to determine the economic and environmental benefits of using high-strength steel grades.
- **The right steel at the right place** – Based on the relationships established in the previous chapter, this part consists of a comparative study to identify the challenges limiting the benefit of high-strength steels as well as to define the fields of application for which they are justified.
- **Improvement of the existing design rules for flexural buckling** – The fourth part aims at adapting the design rules to account for the beneficial effect of the high yield stress on the impact of residual stress and thereby, on the stability of steel columns. The consideration of innovative design approaches is investigated, and conclusions are drawn regarding the benefit of increasing the yield stress in the specific case of steel columns.
- **Consideration of inherent source of stabilisation in storage racks** – This last chapter results from an industrial project on storage rack structures. These specific structures are particularly well optimised given the tonnage of steel. They are already composed of high-strength steel grades because innovative construction techniques have been used to reduce the prevalence of instabilities in the design, which are particularly detrimental to the use of high-yield strength steels. Nevertheless, these techniques may increase material and labour costs. So, investigations were conducted to study the possibility of limiting these stabilising techniques through the activation of inherent sources of stabilisation.
- **Conclusions** – The closing chapter gathers the contributions of the present dissertation; it provides some recommendations for future research works as well as some thoughts about the tomorrow's practice in the construction sector.

Chapter 2

Research Context

2.1. Introduction

The development of new steel production techniques has led to a notable advancement of steel products, facilitating the fabrication of steels with enhanced mechanical and chemical properties [45], [46], [47]. In 2022, according to the WorldSteel Association [14], the steel industry invested 6.3% of its revenue in research and process improvement, so the development of new production technologies is in constant evolution. Indeed, about 75% of the 3500 steel grades in use today did not exist 20 years ago. Thanks to these ongoing process innovations, only 1/3 of the steel used to build the Eiffel Tower and ½ for the Golden Gate Bridge would be required today. New production technologies are already available to produce hot-rolled steel sections up to 500 MPa that meet the construction requirements and the consideration of the right material at the right place may lead to further investments by manufacturers in the future to develop the best material solution for each application. Nevertheless, the use of mild steel is still often preferred for heavy hot-rolled sections in steel structures. This may result from a lack of information on existing high-performance products and their resulting benefits as well as a lack of availability. Furthermore, using a higher steel grade is often associated with an increase in the unitary cost of steel as well as a carbon factor increase, so the designer is sometimes reluctant to use them as he does not know in which cases they are economically and environmentally justified.

With regard to the reinforcing steel grades, B235 and B355 grades have been superseded by the B500 grade which has become the basis grade for this application [48], [49]. It may therefore be anticipated that, in the future, S460 will compete with S355 or even become the basis grade for structural steels. Table 2-1 presents an overview of the current utilisation of steel grades for hot-rolled sections on the steel market, extracted from a previous status [48].

Grade designation	Status, 2024		
	"Yesterday"	"Today"	"Tomorrow"
"Low strength"	-	-	S235/S275
"Standard"	S235	S235 / S275	S355 / Gr. 50
"Higher strength"	S275	S355 / Gr. 50	S460 / Gr. 65 S500 / Gr. 70
"High strength"	S355 / Gr. 50	S460 / Gr. 65 S500 / Gr. 70	S550 / Gr. 80

Table 2-1. Steel grade transitioning for hot-rolled sections: history and evolution outlook.

In the United States, the transition from S235 to S355 as the standard steel grade was completed in the early 2000s. Nevertheless, in most European countries, the S235 grade continues to be the reference grade. However, in Germany, the S355J2 grade has emerged as the most prevalent steel grade [48], [49]. A slight trend towards S355 as the basis grade can be observed in most of the European steel market, which indicates that the construction industry is gradually adopting higher steel grades. In the United Kingdom, twenty-five years ago, S275 was the preferred steel choice of structural engineers. Today, the prevailing preference is for S355 as the default structural grade. The S275 grade is no longer a standard product and it is even reserved for special orders. The market share of S420/S460 is relatively modest but is nevertheless experiencing growth, particularly in the context of applications such as columns in high-rise buildings and/or bridges. The global steel market is witnessing an expansion in the availability of high-strength steel products. The pace of change is slow in lengthy supply chains, such as those associated with the construction industry, due to a lack of confidence in welding and fabrication techniques. However, contemporary challenges emerge when designing steel structures, including considerations of resilience, sustainability, robustness and material efficiency. It seems reasonable to assume that interest in high-strength steel grades will increase in the coming years.

Chapter 2 addresses several important themes intending to adequately account for high-strength steels in the optimisation process of steel structures. Based on this research context, this chapter will conclude with an overview of the objectives and contributions of this thesis.

2.2. High-strength steels

High-strength steels are advanced structural steels with a nominal yield strength of 460 MPa or greater [50]. This classification is the most prevalent and adopted in this thesis; however, there is no universal definition in the literature, as a grade can be classified as regular or high-strength, depending on the intended steel application [51]. The forthcoming version of EN1993-1-1 [52] for the design of structural steels, encompasses steel grades up to and including S700. The structural steel grades are thus classified in Table 2-2.

Steel category	Grade	$t \leq 40 \text{ mm}$		$40 \text{ mm} < t \leq 80 \text{ mm}$	
		$f_y \text{ (MPa)}$	$f_u \text{ (MPa)}$	$f_y \text{ (MPa)}$	$f_u \text{ (MPa)}$
<i>Regular / Mild steels (RS)</i>	S235	235	360	215	360
	S275	275	490	245	370
	S355	355	510	325	470
	S420	420	540	390	490
<i>High-Strength Steels (HSS)</i>	S460	460	580	410	510
	S500	500	600	450	580
<i>Ultra-High-Strength-Steels (UHSS)</i>	S550	550	650	500	600
	S600	600	650	550	650
	S620	620	700	560	660
	S650	650	700	-	-
<i>Not yet available for rolled sections</i>	S690	690	770	630	710
	S700	700	750	-	-

Table 2-2. Steel categories according to FprEN1993-1-1:2022 (for a thickness below 80 mm).

Accordingly, all steel grades reported in Table 2-2 will be considered in the framework of this thesis. The use of these high-strength steel grades offers a multitude of advantages, primarily due to the reduction in thickness when compared to the use of standard steel:

- A reduction in the self-weight of the element and the supporting structure;
- The construction of smaller foundations thanks to the reduction in self-weight;
- The improvement of the space utilisation through the reduction of column and beam sizes;
- The use of less material may lead to lower production costs and CO₂ emissions;
- The ease of fabrication, processing, assembly and transport, leads to a reduction in fabrication and erection costs.

However, there are also many challenges associated with the use of high-strength steels:

- Greater tendency to failure modes associated with instability issues such as global buckling and local buckling;
- Deflection and vibration criteria are more likely to be critical as less material often means less stiffness in addition to a lower mass;
- The market availability is often limited due to the low demand, requiring longer lead times;
- There is no benefit when fatigue problems are critical as the fatigue resistance is not influenced by the yield strength according to the European normative documents.

Finally, design codes are often unnecessarily conservative and prevent the realisation of efficient designs that could take advantage of the benefits of these materials in many circumstances. Other barriers include their higher price, a lack of experience in execution and fewer available profiles leading to a general reluctance within the steel construction industry. The present section provides an overview of the existing grades, their mechanical and physical properties as well as the increase in material price and carbon footprint resulting from the use of high-strength steels.

2.2.1. Production processes, specifications and availability

Steelmakers use a variety of different approaches to achieve the required balance of steel properties. In particular, achieving high-strength properties requires a careful balance between chemistry and process conditions. Indeed, adding more carbon can increase strength, but this reduces ductility, toughness and weldability. One solution is to use microalloying elements such as niobium, vanadium, titanium or molybdenum in small quantities. This is a cost-effective way of achieving a balanced combination of properties. The other way is to achieve a higher yield strength through heat treatment (normalising, quenching and tempering or thermomechanical rolling). Each steel grade in each quality therefore has different microstructural elements and mechanical properties. The various European product standards, for hot-rolled H-shaped or I-shaped sections and hollow sections, as well as the corresponding steel grades and qualities, are listed in Table 2-3 [53], [54], [55], [56], [57], [58], [59], [60], [61], [62].

European Product Standards		Steel grades	Steel qualities
EN10025-2:2019	Non-alloyed structural steels ("As rolled")	S235, S275, S355, S420, S460, S500	JR, J0, J2 and K2
EN10025-3:2019	Normalised rolled weldable fine-grain structural steels	S275, S355, S420, S460	N, NL
EN10025-4:2019	Thermomechanically rolled weldable fine-grain structural steel	S275, S355, S420, S460, S500	M, ML
EN10025-5:2019	Weathering steels – improved atmospheric corrosion resistance	S235, S355, S420, S460	J0W, J2W, K2W, J4W, J5W

EN10025-6:2019	Flat products of high-yield strength structural steels in the quenched and tempered condition	S460, S500, S550, S620, S690, S890, S960	Q, QL, QL1
EN10210-1:2006	Hot-finished hollow sections – non-alloy	S235, S275, S355	JRH, JOH, J2H, K2H
	Hot-finished hollow sections – fine grain steels	S275, S355, S420, S460	NH, NLH
EN10210-3:2020	Hot-finished hollow sections – Thermomechanical formed	S275, S355, S420, S460, S500, S550, S600, S650, S700	MH/MLH
EN10219-1:2006	Cold-formed hollow sections – non-alloy	S235, S275, S355	JRH, JOH, J2H, K2H
	Cold-formed hollow sections – fine grain steels	S275, S355, S420, S460	NH, NLH MH, MLH
EN10219-3:2020	Cold-formed hollow sections – Thermomechanical formed	S500, S550, S600, S650, S700, S900	MH/MLH
EN10149-2:2013	Hot-rolled flat products made of high-yield strength steels for cold-forming	S315, S355, S420, S460, S500, S550, S600, S650, S700, S900, S960	MC

Table 2-3. Product standards compatible with EN1993-1-1 and the related steel grades and qualities.

The harmonised standard EN10025 is the reference standard for most structural steelwork and the new version, available from 2019, includes the requirements for a new steel grade, S500, in Parts 2 and 4 [53], [54]. In parallel, for hollow sections, a new Part 3 has been added to standards EN10210 [59] and EN10219 [60] in 2020 to cover grades between S460 and S900. The recently added steels are written in bold in Table 2-3, illustrating the ongoing developments of new grades. The steels complying with EN10149-2:2013 [57] are for cold-forming applications.

Table 2-3 shows that there are different routes to achieve higher strength in steel up to S500. Thermomechanical steels are low carbon equivalent as they provide the same strength as an equivalent normalised steel but with lower carbon and alloy content, giving better weldability and toughness performance. Quenched and tempered (Q) steels are most commonly used to produce high-strength steels, but mainly in non-structural applications, with higher carbon content which requires controls for welding. However, long products can also be produced using the quenched and self-tempered process (QST). In this process, the beam undergoes two successive treatments: (i) a thermomechanical rolling is applied during forming, at a temperature of around 850°C and (ii) the beam then immediately passes through a ramp to be cooled by spraying water over its entire surface. Accelerated cooling of a thick beam creates a temperature gradient similar to that obtained by quenching. In this way, the thermomechanical rolling technique combined with accelerated cooling allows the production of high-strength members with improved mechanical properties, with reduced amounts of alloying elements such as vanadium (V) and niobium (Nb), and improved weldability due to reduced amounts of carbon (C) and other alloying elements. This process has been specifically developed to produce fine-grained high-strength steels for thick flange sections without the need for costly alloy additions [63], [64], [65]. The grades available for hot-rolled sections according to the European standard EN10025 for structural steels [53], [54] and other internationally used standards such as ASTM A913-19 (USA) [66] or GB/T 33968-2017 (China) [67] are listed in Table 2-4. Products with even stricter specifications are also available under the trade name HISTAR®; such products are specified in European Technical Approval ETA 10-0156 [68].

Grade	Europe			USA			China
Yield strength (MPa)	HISTAR®	EN10025-2 (2019)	EN10025-4 (2019)	ASTM A913(2019)	ASTM A992	ASTM A572	GB/T 33968 (2017)
355	355	S355 JO/JR/J2/K2	S355 M/ML	Gr. 50	Gr. 50	Gr. 50	Q345 QST
460	460	S450 JO/JR/J2/K2	S460 M/ML	Gr. 65	/	Gr. 60	Q460 QST
500	/	S500 JO/J2	S500 M/ML	Gr. 70	/	/	Q485 QST
550	/	/	/	Gr. 80	/	/	/

Table 2-4. Normative situation for hot-rolled sections depending on the region.

Nevertheless, it is noteworthy that the presence of a particular steel grade in product standards does not necessarily guarantee its availability from stockholders or steel producers.

2.2.2. Mechanical properties

The key mechanical properties of a structural material are strength, stiffness, ductility, fracture toughness and weldability. As mentioned above, these material properties are influenced by the chemical composition and the manufacturing processes (controlled heat treatment, rolling temperatures, cooling rate).

2.2.2.1. Strength

Strength is a measure of the stress that a material can withstand. Two values are typically used to define the strength of a material; the ultimate strength, which is the maximum stress achieved in a tensile test, and the yield strength, which is the stress at which the material begins to deform plastically. Structures are often designed to deform only elastically, so yield strength is a commonly used criterion for defining failure in engineering design codes. Traditionally, the guaranteed yield strength of a steel grade decreases with increasing thickness, as shown in Fig. 2-1 for hot-rolled sections and hot-finished hollow sections.

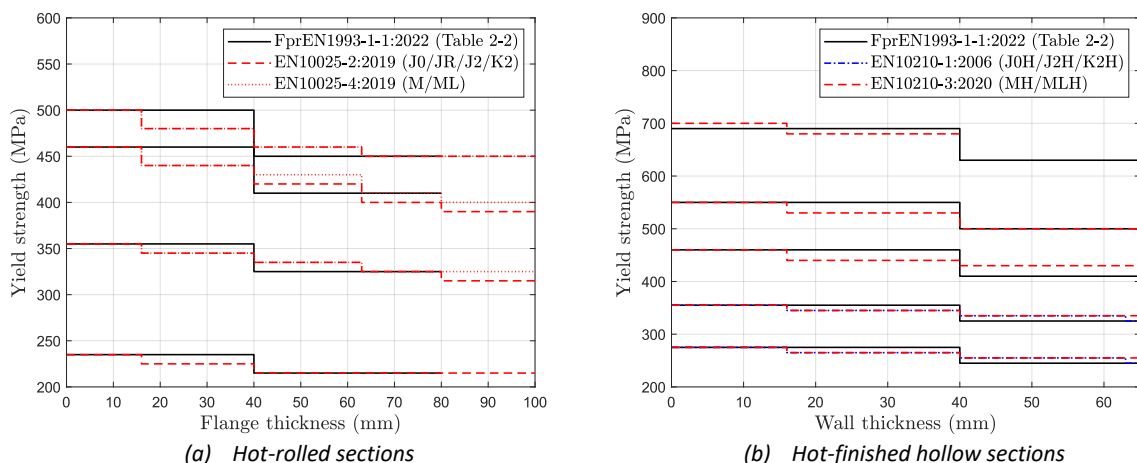


Fig. 2-1. Evolution of the yield strength depending on the thickness.

However, it is possible to offer sections with stable yield strength over the entire thickness range by taking advantage of the accelerated cooling technique at the exit of the rolling hotplate. The HISTAR® trademark steels of ArcelorMittal offer enhanced yield strength up to higher flange thicknesses. For example, the nominal yield strength of HISTAR® 460 hot-rolled sections is maintained up to 100 mm [69]. Thus, the yield strength of a S500JO or S500M grade drops to 460 MPa from 40 mm and to 450

MPa from 63 mm, while a HSTAR® 460 grade conserves its nominal yield strength of 460 MPa up to 100 mm. Therefore, considering a “higher” grade does not systematically lead to a higher yield strength for higher thicknesses.

2.2.2.2. Ductility

Ductility is a measure of the material’s ability to deform plastically before fracture. Steel must be sufficiently ductile to guarantee appropriate rotational capacity to form plastic hinges. As strength increases, the ratio of ultimate strength to yield strength decreases. Ductility also decreases but with a limited impact on the design process for most structures. The main restriction is for the realisation of plastic global analysis which is limited to steel grades up to and including S460 as stated in FprEN1993-1-1:2022 [52]. The ductility requirements that are given in the current and forthcoming version of Eurocode 3 [52], [70], [71], are reported in Table 2-5.

Applicability	Current version [70], [71]		Next version FprEN1993-1-1:2022 [52]	
	S235-S460 EN 1993-1-1:2005	S500-S700 EN 1993-1-12:2007	Elastic	Plastic
f_u/f_y	≥ 1.10	≥ 1.05	≥ 1.05	≥ 1.10
<i>Elongation at fracture</i>	$\geq 15\%$	$\geq 10\%$	$\geq 12\%$	$\geq 15\%$
ε_u	$\geq 15 \cdot f_y/E$	$\geq 15 \cdot f_y/E$	/	/

Table 2-5. Ductility requirements in design recommendations.

The current version of Eurocode 3 allows a relaxation of the requirements on the minimum tensile-to-yield strength ratio and the elongation at fracture for grades above S460 but maintains the requirement for ultimate strain [71]. These recommendations were assessed as conservative and unjustified, and they have been revised in the forthcoming standard [52]. In this new version, all steel grades are subject to the same ductility requirements, but the latter are now a function of the type of analysis. Furthermore, the requirement in terms of ultimate strength has been removed as it is not included in the product standards. Based on tensile tests, some researchers [72], [73] have established the relationship between yield strength and ultimate strength as shown in Eq. (2-1) and Fig. 2-2.

$$\frac{f_y}{f_u} = 1 - 0.72 \cdot e^{-0.0027 \cdot f_y} \quad (2-1)$$

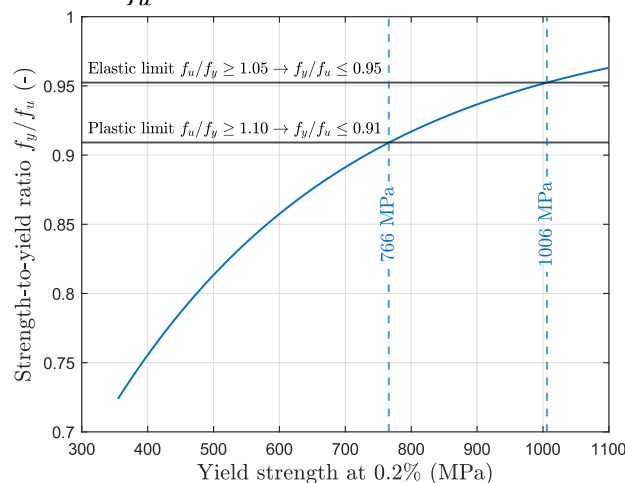


Fig. 2-2. Strength-to-yield strength ratio for different steel grades from tensile tests.

As shown in Fig. 2-2, the f_y/f_u ratio increases with the yield strength but the grades below 700 MPa meet the ductility requirements expressed in Table 2-5. The limit for plastic design is around 766 MPa and the limit for elastic design is around 1006 MPa. Concerning elongation, defined as the percentage of extension up to failure showing how ductile the steel is, it appears that the elongation can be very close to 20%, even for grades above 690 MPa. It means that it is possible to produce high-strength steels that meet the ductility requirements [50].

2.2.2.3. Physical properties

The physical properties of steel are: the density $\rho = 7850 \text{ kg/m}^3$, the Poisson's ratio $\nu = 0.3$, the Young's modulus $E = 210000 \text{ MPa}$ (at 20°C), the shear modulus $G = \frac{E}{2 \cdot (1 + \nu)} = 80769.2 \text{ MPa}$, the coefficient of linear thermal expansion $\alpha = 12 \cdot 10^{-6} \text{ }^\circ\text{C}^{-1}$ (at $T \leq 100^\circ\text{C}$) and the thermal conductivity $k = 54 \text{ W/mK}$ (at 20°C). The physical properties are not affected by the material yield stress.

2.2.2.4. Toughness

Toughness is the ability of a material to absorb energy up to failure. This corresponds to the area below the stress-strain curves and can therefore be seen as the ability to resist brittle fracture, for example during welding or loading. The greater the area below the stress-strain curve, the greater the toughness, as the material will absorb a lot of energy before failure. Steels contain imperfections in the form of very small cracks. If the steel is not tough enough, the cracks can propagate rapidly without plastic deformation, leading to a brittle failure. Consequently, to achieve good toughness performance, a material should have a good balance between ductility and strength.

The Charpy V-notch impact test is used to measure the impact energy required to break a small, notched specimen at a specified temperature as the temperature affects the stress-strain behaviour of steel. The temperature is important when characterising the toughness performance of a material as a material is more brittle at low temperatures than at high temperatures.

EN1993-1-10 [75] gives guidance on the selection of a suitable subgrade or the allowable value for the member thickness. For instance, normalised steels induce a higher brittle failure tendency. For steels requiring improved low-temperature toughness performance, a much finer-grained microstructure is required, which can be achieved by thermomechanical rolling [76] and thus also by the QST process. With regard to the toughness performance of high-strength steels and based on Charpy test results on S460, S690 and S890, it appears that the ductile-brittle transition temperatures are generally lower for high-strength steels [77], meaning that their toughness performance is higher. This can be attributed to the fact that most high-strength steels are fine-grained steels, i.e. they result from the thermomechanical process [50]. It is worth noting that most steel producers can agree with customers on improved toughness requirements at extra cost.

2.2.2.5. Weldability

Weldability is the ability of a material to be welded. This is an important consideration in the steel selection process, as the addition of alloying elements to produce certain qualities generally reduces weldability performance. The Carbon Equivalent Value (CEV) is the reference parameter for assessing the weldability of steels, which is determined by the chemical composition – see Eq. (2-2).

$$CEV = C + \frac{Mn}{6} + \frac{Cr + Mo + V}{5} + \frac{Cu + Ni}{15} \quad (2-2)$$

A high CEV value has a negative effect on weldability. In general, the higher the CEV, the greater the risk of hydrogen cracking in the welded joint. Weldability also generally decreases with thickness

because more alloying elements are required to achieve the required mechanical properties in the thicker sections. Therefore, some of these alloying elements must be limited at the expense of a slight reduction in strength because their addition reduces weldability. The relationship between the yield strength and the weldability, i.e. the carbon equivalent CEV (%), depending on the production process is shown in Fig. 2-3.

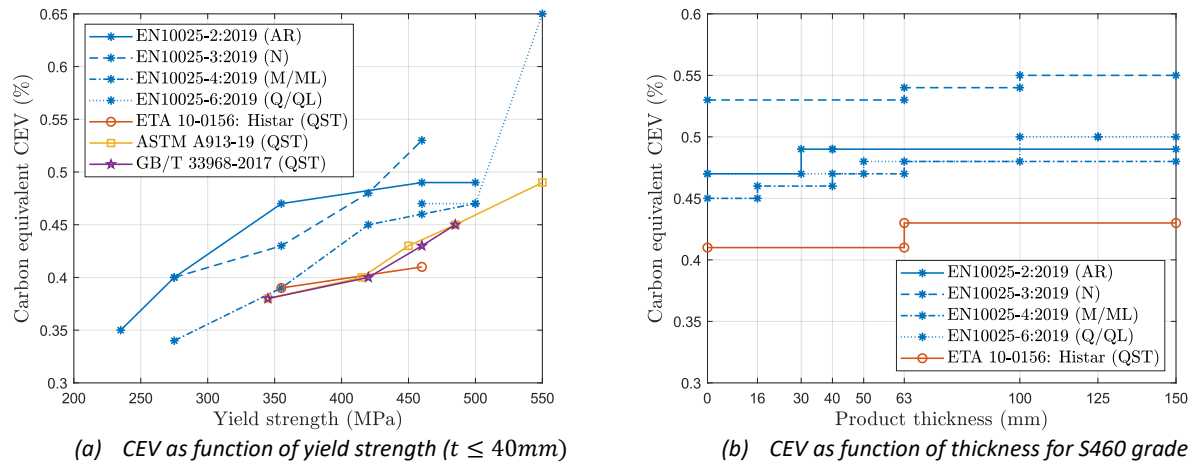


Fig. 2-3. Weldability of high-strength steel grades.

As can be deduced from Fig. 2-3, the normalised steels (N) are more highly alloyed, so they have a higher CEV than the equivalent thermomechanical steels (M). The use of micro-alloying elements, temperature-controlled rolling techniques and subsequent accelerated cooling (QST process) to produce higher strengths has made it possible to limit the equivalent carbon content, thereby improving weldability.

2.2.3. Higher temperature performance

The chemical composition and manufacturing process affect the rate of degradation of mechanical properties under high temperatures. High-strength steel members are likely to have thinner plates, so the temperature may rise more rapidly than for mild steels [76]. According to the current Eurocode recommendations in EN1993-1-12 [71] for grades up to S700, the rules of EN1993-1-2 [78] apply to steels above S460 up to S700 without further additional rules. Based on scientific results, some references [76], [79], [80] confirm that the strength reduction factors for conventional strength steels given in EN1993-1-2 [78] can be safely applied to high-strength steels up to and including S700 based on the existing research on the topic [81], [82], [83]. On the contrary, for the reduction factor for the Young's modulus, all the papers tend towards the same conclusion that the Eurocode underestimates the performance of high-strength steels at high temperatures. An assessment of the validity of Eurocode recommendations has been carried out in a master's thesis at the University of Liège [84]. Despite the number of experiments existing in the literature, further experiments and statistical analyses should be carried out to assess the reliability of reduction factors for more steel grades and products [50].

2.2.4. Fatigue performance

Fatigue is a damage mechanism resulting from the cumulative action of repeated and cyclic stresses. The fatigue failure can be either ductile if cyclic stresses exceed the yield strength of the material, or brittle if the stress intensity at the crack tip exceeds the fracture toughness of the material. The fatigue life is largely determined by the crack initiation stage and its duration generally increases as the yield

strain of the steel increases, but in most cases, the fatigue does not govern the design. The fatigue resistance is determined by the number of cycles that a design detail can withstand, as shown in Fig. 2-4.

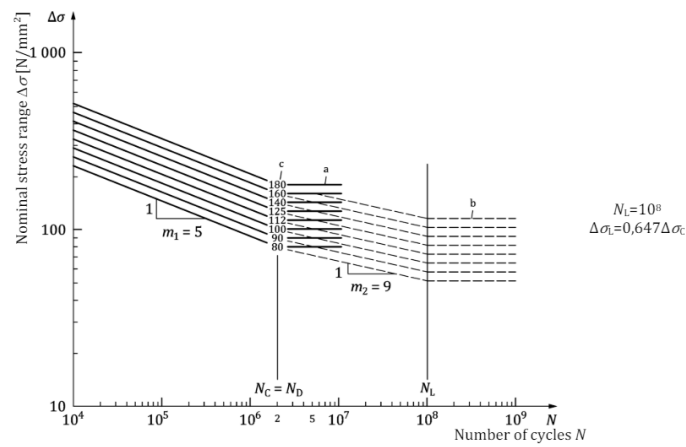


Fig. 2-4. Characteristic fatigue resistance curves for non-welded details subject to nominal normal stress ranges.

According to the forthcoming version of prEN1993-1-9:2023 [85], for constant amplitude loading with normal stress ranges $\Delta\sigma_{Ed}$, the design value of fatigue strength should be computed according to Eq. (2-3).

$$N_{Rd} = (2 \times 10^6) \cdot \left(\frac{\Delta\sigma_c/\gamma_{Mf}}{\Delta\sigma_{Ed}}\right)^{m_1} \text{ for } \Delta\sigma_{Ed} \leq \Delta\sigma_D/\gamma_{Mf}$$

$$\rightarrow N_{Rd} = \frac{(2 \times 10^6) \cdot (\Delta\sigma_c/\gamma_{Mf})^{m_1}}{\Delta\sigma_{Ed}^{m_1}} = C \cdot \frac{1}{\Delta\sigma_{Ed}^{m_1}} \quad (2-3)$$

Where: N_{Rd} is the design value of endurance, $\Delta\sigma_c$ the reference value at 2×10^6 stress cycles, γ_{Mf} the partial factor for fatigue resistance, $\Delta\sigma_{Ed}$ is the design value of the applied stress range, m_1 the first slope parameter of the fatigue resistance curve and $\Delta\sigma_D$ the constant amplitude fatigue limit at N_D stress cycles and C a constant value.

Several design details were selected to investigate the effect of yield strength on fatigue performance and are listed in Table 2-6.

Detail category	Construction detail	Description
160 $m_1 = 5$		Rolled or extruded products subject to normal stress - Rolled sections with as rolled edges
125 $m_1 = 5$		Rolled or extruded products subject to normal stress - Seamless hollow sections, either rectangular or circular
100 $m_1 = 5$		Rolled or extruded products subject to shear stress

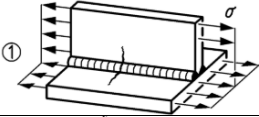
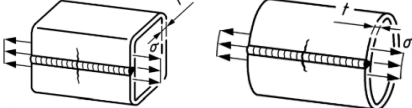
125 / 112 $m_1 = 5$		Welded built-up sections with automatic or fully mechanised butt welds, welded from both sides
140/125 $m_1 = 5$		Cold-formed hollow sections with fully mechanised longitudinal welds ($t \leq 12.5\text{mm}$ / $t > 12.5\text{mm}$)

Table 2-6. Selection of constructional details directly affected by an increased yield stress.

In terms of fatigue resistance, there is a difference between designing a steel member made from mild steel or high-strength steel. As reflected in the above-mentioned design procedure, the fatigue resistance is not affected by the steel strength. But, in reality, the advantage of high-strength steels is the reduction in section size. By reducing the size of the member proportionately to the yield strength increase, the stresses in the cross-section (and the associated stress variation $\Delta\sigma_{Ed}$) increase for the same applied load. The application of Eq. (2-4) makes it possible to represent the evolution of the fatigue life of a given construction detail as a function of the yield strength for the above-mentioned assumptions – see Fig. 2-5.

$$N_{Rd,HSS} = C \cdot \frac{1}{\left(\frac{f_{y,HSS}}{355} \cdot \Delta\sigma_{Ed,S355}\right)^m} \quad (2-4)$$

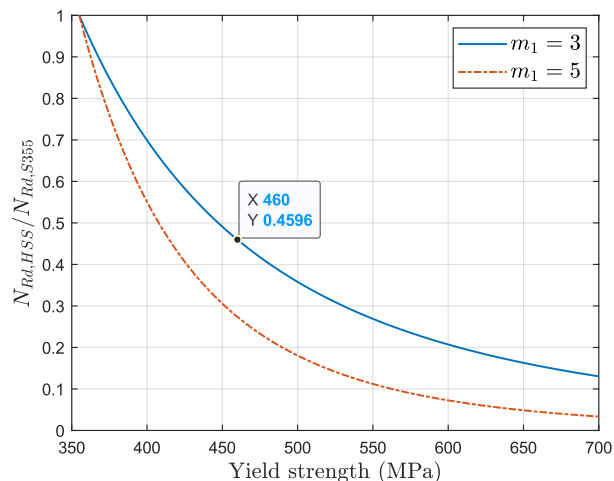


Fig. 2-5. Fatigue life as function of the yield strength.

As observed in Fig. 2-5, if the increase in strength by using S460 instead of S355 (i.e. $460/355=1.3$) is equal to the increase in stress range resulting from the reduction of section size, then the fatigue life for S460 section is less than half the one for S355 section as calculated in Eq. (2-4). Since fatigue is likely to govern the design of high-strength steel members, some fabrication practice guidelines must be followed, such as: avoiding the construction details with poor fatigue strength (see EN1993-1-9 [85]), to locate welded joints in areas of low stress given the poor fatigue performance of welded joints and to specify all the quality requirements that are needed to achieve the desired fatigue performance [76].

2.2.5. Relative price and carbon footprint

In the report of the European RFCS project RUOSTE [80], the authors compare two papers published by Johansson [86] and Stroetmann [87] which derive relative material prices for high-strength steel heavy plates. Although these two references are regularly cited when analysing the economic benefits

of using high-strength steels ([51], [88], [89], [90], [91], [92]), the two trends are significantly different. Indeed, in 2005, Johansson [86] proposed that the relative price trend follows the square root of the yield strength, while in 2011, Stroetmann [87] provided lower relative values based on the average prices of several producers on the German market, as shown in Fig. 2-6.

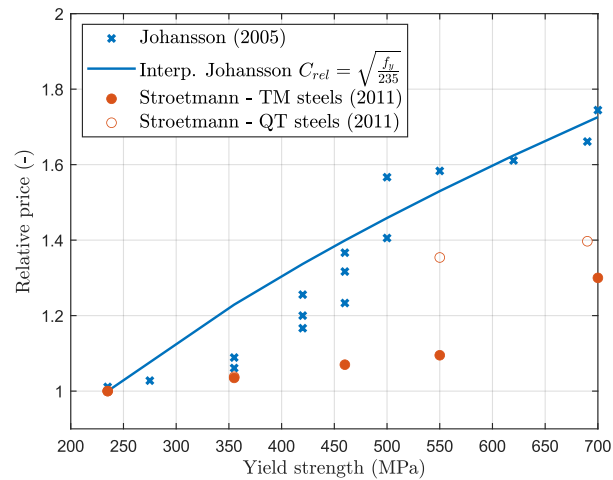


Fig. 2-6. Material relative prices as a function of yield strength according to literature references.

Fig. 2-6 illustrates that there is a significant scatter in the literature data for heavy plates and that the interpolation proposed by Johansson in 2005 is not representative of the recent values provided by Stroetmann for the German steel market. As stated in [80], [86], [93], the price is highly dependent on changes in the production process, e.g. a change from a quenched and tempered (QT) to a thermomechanical (TM) production process, which may explain the discrepancy between the two references. For hot-rolled sections, ArcelorMittal stated that the S355 grade is about 5% and S460 about 15% more expensive than the basic S235 grade [48], [49], [51]. Therefore, it is likely that the reality, for hot-rolled sections, falls somewhere in between. Because of this discrepancy for heavy plates and as the research focuses on hot-rolled sections, there is a need to carry out a cost investigation to establish realistic relative price trends that may allow to draw conclusions about the cost efficiency of high-strength steels.

In terms of relative CO₂ emissions, specific information on building materials or products is disseminated in Environmental Product Declarations (EPDs). Currently, the EPDs available on the market do not provide GWP values depending on the yield strength. For instance, the Bauforumstahl EPD ([94]) mentions the following: "This EPD is valid for structural sections and merchant bars of various steel grades and different forms of delivery". Nevertheless, a project entitled "The environmental value of HSS structures" has already been conducted as part of the Steel Eco-Cycle project (2004-2012) [95], [96], [97], [98]. In this project, the Swedish steel industry in collaboration with the Swedish Environmental Research Institute, carried out a series of cradle-to-gate analyses and provided carbon emission trends as a function of yield strength and steel typology (Fig. 2-7). A cradle-to-gate analysis assesses the environmental footprint of a product from the raw materials extraction until it leaves the factory.

The differences between steel qualities are mainly explained by the composition of the steel [95]. In fact, the higher the alloy content, the higher the carbon footprint of the steel, as the emissions associated with the extraction of rare alloying elements are likely to have a detrimental effect on the steel footprint.

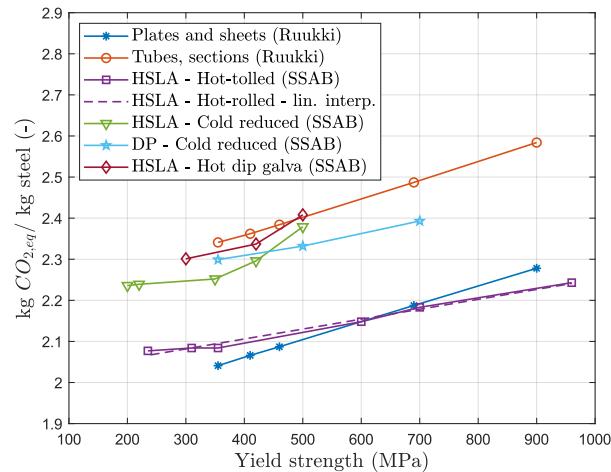


Fig. 2-7. GWP evolutions provided by Swedish researchers in the Steel Eco-Cycle project.

High-strength steels produced by the QST process are more sustainable than standard steels because the process requires no external energy supply and significantly reduces the use of alloying elements to increase strength [99]. The weight savings achieved by using a higher yield strength are therefore likely to offset the increase in material cost and carbon footprint, but this requires a reliable relationship between relative price and yield strength as well as a similar relationship between relative carbon footprint and yield strength to conduct comparative studies.

2.3. Design provisions for members in Eurocode 3

2.3.1. Scope

The technical knowledge on the design of high-strength steel members is greatly increased by many contributions in the literature, thanks to national and international initiatives such as the European RFCS projects [2–6]. The behaviour of these members under different loading conditions has been evaluated through several scientific studies and new recommendations for standards have been derived. The upcoming version FprEN1993-1-1:2022 [52] covers steel grades up to S700, whereas the current EN1993-1-1 [70] only covers grades up to S460, with a limited extension to higher steel grades in EN1993-1-12 [71]. In the future, a new version of EN1993-1-12 is expected to cover grades up to S960 as summarised in Table 2-7.

Existing	New
EN1993-1-1:2005 (grades up to S460)	FprEN1993-1-1:2022 (grades up to S700)
EN1993-1-12:2007 (extension up to S700)	FprEN1993-1-12 (extension up to S960)

Table 2-7. Normative situation in terms of covered steel grades.

The design of steel structures follows the limit state design approach:

- Ultimate Limit States - ULS (yielding, instabilities, fatigue, ...);
- Serviceability Limit States - SLS (deflections, vibrations).

The use of a high-strength steel grade only improves resistance to yielding failure modes. If an element is prone to instabilities, the resistance of the member will not increase to the same extent as the

increase in yield strength. The use of a high-strength steel grade is likely to result in the selection of members with a smaller cross-section, the associated reduced inertia undeniably leading to an increase in deflection. Therefore, it should be considered that, when using a higher yield strength, deflections under service loads are likely to become the governing design criterion. Dynamic response is also likely to govern some design configurations, and therefore limit the benefit of using high-strength steels. The focus is made on hot-rolled sections in this thesis, so the instability phenomena presented in this section are those typically encountered by members with such sections. Finally, the scope is limited to the structural behaviour of the members, so the resistance of the joints will not be addressed.

2.3.2. Resistance of cross-section

The cross-section resistance increases proportionally to the yield strength. However, in cases where the member is subjected to compressive stresses, there is a risk of local buckling. To account for this risk, the Eurocodes rely on the concept of classification of the cross-section. There are four classes which reflect the extent to which the resistance and rotational capacity of the cross-section is limited by local buckling. The cross-section resistances related to the different classes for members subjected to (i) compression (columns) and (ii) bending (beams) are reported in Table 2-8.

This classification depends on the width-to-thickness ratio of the different constitutive parts of the cross-section subjected to compression, the stress distribution, the plate support conditions (outstand or internal elements) and the yield strength of the steel. In particular, each classification limit depends on the ε coefficient, which takes into account the yield stress. Consequently, the recommendations imply that as the yield strength of the steel increases, the classification limits become more restrictive.

Classification	Columns	Beams
Class 1	$N_{Rd} = N_{pl,Rd} = \frac{A \cdot f_y}{\gamma_{M0}}$	$M_{Rd} = M_{pl,Rd} = \frac{W_{pl} \cdot f_y}{\gamma_{M0}}$
Class 2		$M_{Rd} = M_{el,Rd} = \frac{W_{el} \cdot f_y}{\gamma_{M0}}$
Class 3		
Class 4	$N_{Rd} = N_{eff,Rd} = \frac{A_{eff} \cdot f_y}{\gamma_{M0}}$	$M_{Rd} = M_{eff,Rd} = \frac{W_{eff} \cdot f_y}{\gamma_{M0}}$

Table 2-8. Cross-sectional resistances depending on the section class.

In the presence of local buckling (class 4 cross-sections), the design recommendations require a fictive reduction of the gross section area. The effective properties (A_{eff} or W_{eff}) are calculated based on the effective width of the constitutive parts of the section, which decreases as the plate slenderness increases. Therefore, although the cross-sectional resistance generally increases with the steel strength, this increase can be counterbalanced by the reduction in effective area, as justified in [51], [73]. Indeed, in the case of class 4 cross-sections, it is not possible to take full advantage of the high-strength steel because the local buckling limits the maximum resistance that can be achieved.

2.3.3. Member slenderness

The cross-sectional resistance is decreased by a reduction factor, noted χ for columns and χ_{LT} for beams in design rules. This reduction factor allows to account for the risk of flexural or flexural-torsional buckling for columns and the risk of lateral-torsional buckling for beams. The value of this reduction factor is a function of the relative slenderness, and it is determined by the corresponding

European buckling curve. The format consisting of having a reduction factor which is a function of the relative slenderness is adopted by the Eurocode 3 for the different instability phenomena as shown in Fig. 2-8 (adapted from B. Johansson [93]).

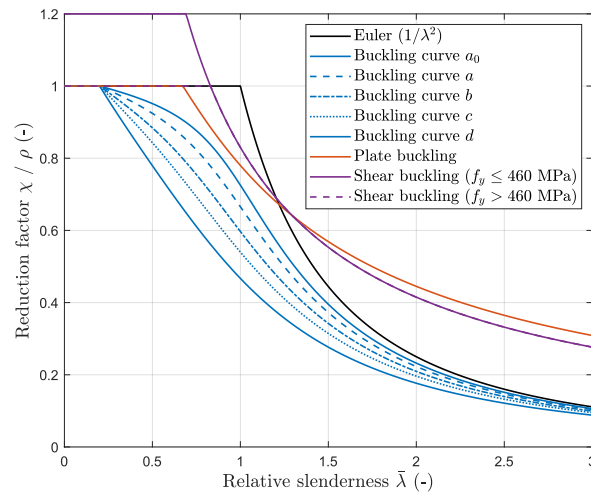


Fig. 2-8. Buckling curves in Eurocode provisions.

The relative slenderness characterises the behaviour of a cross-section against instabilities. It gives an indication of how much the resistance is affected by instability as opposed to yielding – see Eq. (2-5).

$$Relative\ Slenderness = \sqrt{\frac{Characteristic\ resistance}{Resistance\ to\ elastic\ buckling}} \quad (2-5)$$

As the elastic buckling resistance is independent of the steel strength, the relative slenderness increases with the yield strength. This means that high-strength steel members are more susceptible to being affected by buckling instability if the cross-sectional geometry of the member is the same as that of a member made from a lower steel grade. In addition, for the same cross-sectional resistance, the member made of a high-strength steel grade will exhibit a smaller cross-section, generally associated with smaller inertia, so to a smaller value of critical loads and finally to higher relative slenderness. So, in conclusion, high-strength steel members will be more prone to member instabilities than members made of a lower steel grade. This observation could compromise the benefit of high-strength steels for stability-governed members as the higher the slenderness, the closer to the Euler’s resistance (see Fig. 2-8) and the less the advantage in using high-strength steels. Column and beam slenderness ratios are established in Table 2-9 by comparing the two related member instabilities, i.e. flexural buckling for columns and lateral-torsional buckling for beams.

	Flexural Buckling (FB)	Lateral torsional buckling (LTB)
<i>Characteristic cross-sectional resistance</i>	$N_{Rk} = \beta \cdot A \cdot f_y$ With: $\beta = 1$ for class 1,2 & 3 $\beta = A_{eff}/A$ for class 4	$M_{Rk} = \beta_w \cdot W_{pl,y} \cdot f_y$ With: $\beta_w = 1$ for class 1 & 2 $\beta_w = W_{el,y}/W_{pl,y}$ for class 3 $\beta_w = W_{eff,y}/W_{pl,y}$ for class 4
<i>Critical resistance to the instability</i>	$N_{cr} = \frac{\pi^2 E I}{L_{cr}^2}$	$M_{cr} = \frac{\pi^2 E I_z}{L_{cr}^2} \cdot \zeta$

<i>Relative slenderness</i>	$\bar{\lambda} = \sqrt{\frac{N_{Rk}}{N_{cr}}} = \frac{\lambda_{FB}}{\lambda_1} \cdot \sqrt{\beta}$	$\bar{\lambda}_{LT} = \sqrt{\frac{M_{Rk}}{M_{cr}}} = \frac{\lambda_{LTB}}{\lambda_1} \cdot \sqrt{\beta_w}$
<i>Slenderness ratio</i>	<p style="text-align: center;">$\lambda_{FB} = \frac{L_{cr}}{i}$</p> <p>Where:</p> <ul style="list-style-type: none"> - L_{cr} is the buckling length in the buckling plane considered - i is the radius of gyration about the relevant axis, determined using the properties of the gross cross-section - $\lambda_1 = \pi \cdot \sqrt{\frac{E}{f_y}}$ 	<p style="text-align: center;">$\lambda_{LTB} = L_{cr} \cdot \sqrt{\frac{W_{pl,y}}{\zeta \cdot I_z}}$</p> <p>Where:</p> <ul style="list-style-type: none"> - L_{cr} is the buckling length in the minor axis of the beam - $W_{pl,y}$ is the plastic section modulus for bending about the y-y axis - ζ – see Eq. (2-6); - $\lambda_1 = \pi \cdot \sqrt{\frac{E}{f_y}}$

Table 2-9. Comparison between reference slenderness for both global instability modes (FB and LTB).

According to the general formulation of the elastic critical moment for lateral-torsional buckling provided in the national annexe EN 1993-1-1 ANB [104], the term ζ from Table 2-9 can be estimated using Eq. (2-6).

$$\zeta = C_1 \cdot \left[\sqrt{\left(\frac{k_z}{k_w}\right)^2 \cdot \frac{I_w}{I_z} + \frac{(k_z \cdot L)^2 \cdot G \cdot I_t}{\pi^2 \cdot E \cdot I_z} + (C_2 z_g - C_3 z_j)^2} - (C_2 z_g - C_3 z_j) \right] \quad (2-6)$$

2.3.4. Flexural buckling

According to the design recommendations of Eurocode 3 [70], the resistance of an element subjected to compression is checked using Eq. (2-7):

$$N_{b,Rd} = \frac{\chi \cdot \beta \cdot A \cdot f_y}{\gamma_{M1}} \geq N_{Ed} \quad (2-7)$$

where $N_{b,Rd}$ is the design buckling resistance, N_{Ed} the design value of the compression force, χ the reduction factor to account for the risk of flexural buckling, β the reduction factor to account for the risk of local plate buckling, A the cross-sectional area, f_y the yield strength and γ_{M1} the partial safety coefficient for stability problems.

Both initial geometrical imperfections and residual stresses negatively affect the behaviour of compressed columns. A correct characterisation of the column buckling phenomenon therefore requires considering these geometrical and material imperfections. For this purpose, the European buckling curves $\chi = f(\bar{\lambda})$ were introduced as a practical design tool. These curves provide characteristic resistance values based on more than 1000 experimental tests carried out under the auspices of the European Convention for Constructional Steelwork (ECCS) in various European countries in the 1960s [105] and on a theoretical study on which the curves are based [106]. These experimental and numerical campaigns led to a proposal of buckling curves for which the safety was assessed by Monte-Carlo simulations [107]. Finally, Maquoi and Rondal derived the current Ayrton-Perry format of the buckling curves [108], which is still used for designs nowadays. This formulation is given below.

$$\chi = \frac{1}{\phi - \sqrt{\phi^2 - \lambda^2}} \text{ with } \phi = 0.5 \cdot (1 + \eta + \bar{\lambda}^2) \text{ where } \eta = \alpha \cdot (\bar{\lambda} - 0.2) \quad (2-8)$$

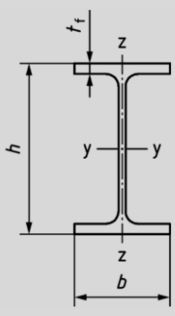
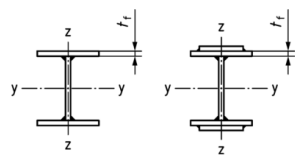
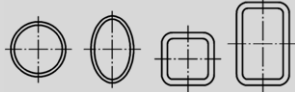
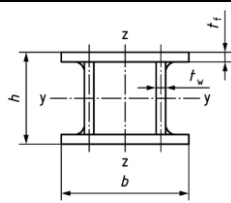
with η the imperfection parameter, α the imperfection factor and $\bar{\lambda}$ the relative slenderness.

A half-sinusoidal out-of-straightness of $L/1000$ as well as residual stresses according to the section typology are accounted for through an imperfection parameter α . The geometrical imperfection of $L/1000$ was already proposed in 1894 [109] and was confirmed by several measurements during the extensive experimental campaign in the 1960s. This parameter α can take different values according to EN1993-1-1 [70] as listed in Table 2-10.

Buckling curve	a ₀	a	b	c	d
Imperfection factor	0.13	0.21	0.34	0.49	0.76

Table 2-10. Buckling curve specification according to EN1993-1-1 [70].

The selection of the buckling curve depends on the cross-section shape, the buckling axis, the cross-section height-to-width ratio h/b , the flange thickness t_f and the production process which influences the residual stress pattern, and therefore the buckling resistance of the member. A comparison of the buckling curve selection tables for flexural buckling between the current and the forthcoming version of EN1993-1-1 [52], [70] is given in Table 2-11.

Cross-section	Limits	Buckling about axis	EN1993-1-1:2005		FprEN1993-1-1:2022		
			S235-S420	S460	S235-S420	S460 up to S700 inclusive	
Rolled I- or H-sections 	$h/b > 1.2$	$t_f \leq 40 \text{ mm}$	y-y	a	a ₀	a	a ₀
			z-z	b	a ₀	b	a
	$h/b \leq 1.2$	$t_f > 40 \text{ mm}$	y-y	b	a	b	a
			z-z	c	a	c	b
		$t_f \leq 100 \text{ mm}$	y-y	b	a	b	a
			z-z	c	a	c	b
$t_f > 100 \text{ mm}$	y-y	d	c	d	c		
	z-z	d	c	d	c		
Welded I-sections 	$t_f \leq 40 \text{ mm}$	y-y	b	b	b	b	
		z-z	c	c	c	c	
	$t_f > 40 \text{ mm}$	y-y	c	c	c	c	
		z-z	d	d	d	d	
Hollow sections 	Hot-finished	any	a	a ₀	a	a ₀	
	Cold-formed	any	c	c	c	c	
Welded box sections 	Generally (except as below)	any	b	b	b	b	
	Thick welds $a > 0.5t_f$ and $b/t_f < 30$ and $h/t_w < 30$	any	c	c	c	c	

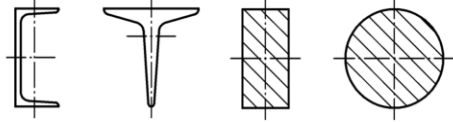


U-, T- and solid sections			any	c	c	c	c
L-sections		Rolled sections	any	b	b	b	a
		Welded sections ($t_f \leq 40 \text{ mm}$)	any	b	b	c	c

Table 2-11. Selection of buckling curve for flexural buckling according to the current and forthcoming version of EN1993-1-1.

Table 2-11 shows that, in the next version of EN1993-1-1 [52], the column buckling curves specified for S460 have been slightly modified for minor axis buckling. Indeed, for hot-rolled sections prone to minor axis buckling, the buckling curve specified for grades equal to or greater than S460 is two curves higher than the curve specified for grades lower than S460 in the current EN1993-1-1 [70]. This difference will be reduced to one buckling curve in the forthcoming version [52], as highlighted in grey in Table 2-11. Therefore, the forthcoming recommendations are consistent with those set forth in the ECCS recommendations [110], i.e. a gap of one buckling curve is once again contemplated between mild and high-strength steel grades for hot-rolled sections. The sole discrepancy is that the high-strength grade previously considered was S430, whereas the current is S460. Furthermore, EN1993-1-12 [71] and the forthcoming FprEN1993-1-1:2022 [52] recommend the same buckling curve as for S460 for grades up to S700. Nevertheless, this stepwise evolution of this imperfection as a function of yield strength by only distinguishing grades below and higher S460 is questionable as expressed in Section 2.4.3.

2.3.5. Lateral torsional buckling

According to the design recommendations of Eurocode 3 [70], the resistance of an element subjected to bending is evaluated according to Eq. (2-9).

$$M_{b,Rd} = \frac{\chi_{LT} \cdot \beta_w \cdot W_{pl,y} \cdot f_y}{\gamma_{M1}} \geq M_{Ed} \quad (2-9)$$

where $M_{b,Rd}$ is the design resistance to lateral torsional buckling, M_{Ed} the design value of the bending moment, χ_{LT} the reduction factor to account for the risk of lateral torsional buckling, β_w the reduction factor to account for the risk of local plate buckling, $W_{pl,y}$ the plastic section modulus, f_y the yield strength and γ_{M1} the partial safety coefficient for stability problems.

Similarly to members subjected to pure compression, and to account for the risk of flexural buckling, the reduction factor is a function of the relative slenderness of the beam, so $\chi_{LT} = f(\bar{\lambda}_{LT})$, which defines the equivalent lateral torsional curves. The analytical expression of these curves follows the same Ayrton-Perry formulation as expressed in Eq. (2-8). However, the coefficient of imperfection is different – see Table 2-12.

Recent research has shown a significant margin of improvement in the design rules for lateral-torsional buckling and a recent European project STROBE even prescribed a gain of one buckling curve between mild steels (S235 to S420) and high-strength steels (S460 to S700) [92], [111], [112], [113]. Despite such evidence and in contrast to the buckling curve selection for flexural buckling (Table 2-11), the current design rules and the ones in the forthcoming version of the Eurocode 3 remain independent of the yield stress as shown in Table 2-12.

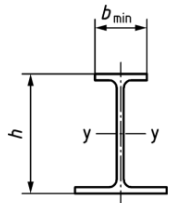
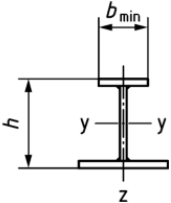

Cross-section		Limits	Buckling curve
Rolled I-sections		$h/b_{min} \leq 2.0$	a
		$h/b_{min} > 2.0$	b
Welded I-sections		$h/b_{min} \leq 2.0$	c
		$h/b_{min} > 2.0$	d
Other sections		-	d

Table 2-12. Selection of buckling curve for lateral-torsional buckling in current and forthcoming version of EN1993-1-1.

The literature review and the current design provisions highlight the necessity to investigate the beneficial effect of the yield stress on the prescribed buckling curve for lateral torsional buckling.

2.3.6. Serviceability limit states

In most designs, it is necessary to check the serviceability limit states (SLS) in addition to the ultimate limit states (ULS). These checks correspond to conditions that result in limited damage to the structure or, alternatively, to circumstances that render the serviceability requirements specified for the structure (or an element) no longer applicable. The most common check is to ensure that elastic deflections remain below a defined deflection limit. This limit is expressed as a fraction of the span of the element and depends on the application of this element (conventional floor, roof, etc). The calculated deflections are a function of the geometrical properties of the beams and the Young's modulus but do not depend on the yield strength of the material.

In addition to controlling excessive deflections, structures must be protected against the effects of vibration and dynamic amplification due to resonance phenomena. These problems are generally related to the global dynamic behaviour of the structure, and not to an isolated member. The dynamic response of a floor system or an entire structure is a function of its mass and stiffness. The use of high-strength steels generally results in lighter structures for the same load than other traditional materials. Therefore, this reduction in mass makes these structures more sensitive to vibration and dynamic loading. The natural frequency of the system must be outside the frequency range of the applied dynamic load, to avoid a possible resonance phenomenon that greatly amplifies the displacements. As part of a European RFCS project called STROBE, a floor vibration analysis tool has been developed to predict the dynamic response of a floor system with conventional and high-strength steel beams [92]. Consequently, Serviceability Limit States (SLS) considerably limit the benefit of high-strength steels when they are dominant in the design.

2.3.7. Reference papers highlighting the benefits of HSS grades

The increase in relative material cost of high-strength steels is generally offset by the reduction in self-weight. For instance, for weight-sensitive members, the use of S460 instead of S355 represents a 30% increase in strength, while the relative material cost is approximately 10-15% higher, assuming that the fabrication costs are not unduly affected by the material yield strength. The advantage of using high-strength steels may be found in various structural applications such as: in compression members with low to medium slenderness, for lower-storey columns in multi-storey frames as these members are often highly loaded, in tension members in trusses, such as the bottom chord and the members loaded in tension.

The paper of Griffis et al. in 2003 illustrates, on a practical case study, the applicability of Grade 65 (450 MPa) steel in the long-span retractable roof of the Reliant Stadium [114] and provides guidelines for the economic use of such a steel grade in long-span roofs. They raised the issue of availability, as only specific rolled shapes and sizes were available in Grade 65 (450 MPa) at that time, particularly larger sizes. So, the first conclusion was that Grade 65 (450 MPa) should only be specified for large, heavily loaded structures. If the number of large, required shapes is not significant, it is likely that it is not economical to specify Grade 65 (450 MPa) for those members. For longer unbraced lengths, the benefit of higher strength is reduced as the load-bearing capacity approaches the critical Euler resistance. As the compression members used in the Reliant Stadium were mostly in slenderness ratios between 35 and 60, the typical weight saving in this range was around 25%. For tension members, resistance is controlled by fracture at the effective net area, and the ratio of ultimate-to-yield strength (f_u/f_y) decreases with yield strength, i.e. $f_u/f_y = 1.23$ for Grade 65 (450 MPa) while $f_u/f_y = 1.30$ for Grade 50 (345 MPa). Finally, the average weight saving with Grade 65 (450 MPa) tension members was about 20 to 25%.

In 2005, Johansson [86], [93] provided some insight into the economic benefits of using high-strength steels as shown in Fig. 2-9. These graphs have been produced using an approximate material cost normalised to S235 (shown in Fig. 2-6) and by assuming full strength utilisation. The relative material cost in Fig. 2-9 is defined as the relative material cost between a given yield strength and the reference S235 grade.

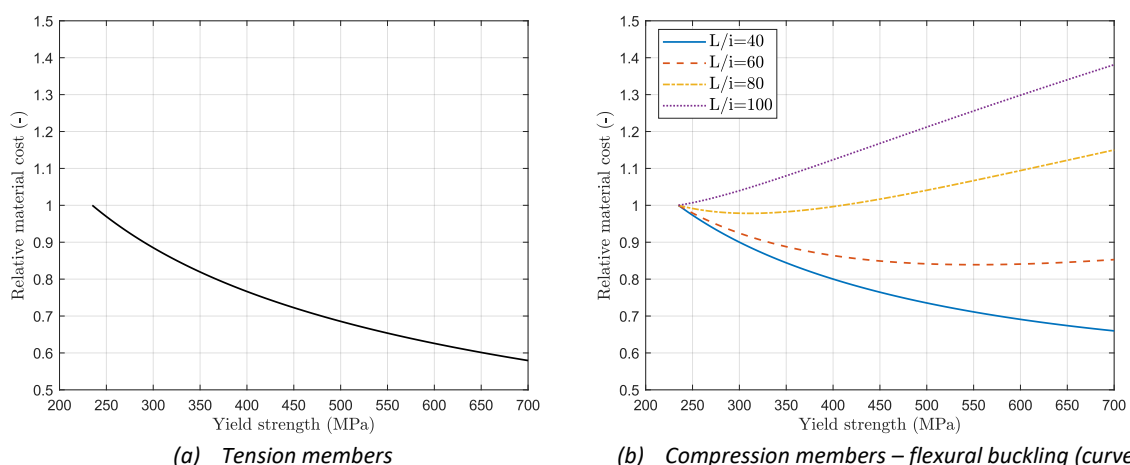


Fig. 2-9. Relative material costs for tension members (a) and for compression members (b) considering a curve “a” and that the material can be fully utilised [86], [93].

The results presented in Fig. 2-9, demonstrate that, for compression members, the economic benefit depends on the column slenderness. Johansson [86], [93] reported that for stocky columns ($L/i =$

40), which are typically used in high-rise buildings, there is a large economic potential to increase the yield strength. On the contrary, for slender columns ($L/i = 100$), there is even an increase in material cost of considering a grade above S235. For intermediate slenderness ratios, the minimum of the cost functions is obtained at 550 MPa and 300 MPa for slenderness ratios of 60 and 80 respectively. However, the curves plotted in Fig. 2-9 assume that one curve "a" should be adopted for all steel grades. In reality, there is a step of one curve gain for S460 in current recommendations (Table 2-11), so the benefit for grades above S460 is likely to be over a wider column slenderness range.

In 2009, Hechler et al. [115] presented a high-rise case study investigating the benefits of replacing the S355 grade with the HISTAR® 460 grade for the Mapfre Tower in Barcelona. For the most heavily loaded columns on the lower floor, the column weight is reduced by 28% and overall, a weight saving of 24% was achieved, thereby demonstrating that the use of such a high-strength steel grade is a cost-effective choice, particularly for the design of multi-storey buildings and heavily loaded structures.

Stroetmann [51], [73], [116], [117] confirmed the above-mentioned observations by providing the result that higher strengths have a positive influence on steel consumption when the stability sensitivity members are in the compact and medium slenderness range, i.e. between 3 and 5 m for typical column lengths in buildings. He presented some results on the detrimental impact of local buckling on the benefit of using high-strength steels for HEA profiles and square hollow sections. He also concluded that some high-strength steels have a lower or even negligible increase in GWP impact. Based on this environmental assessment, the weight savings required to offset the additional environmental impact of manufacturing high-strength steels were provided.

In addition, Cederfeld and Sperle [97] proved the cost-effectiveness of high-strength steels in another specific case study, the Friends Arena in Stockholm. The use of high-strength steels for the roof trusses resulted in a weight reduction of 17% compared to the conventional S355 design, a total cost saving of 14.5% and a reduction in global warming potential of 17%. Consequently, they also assumed that the GWP would not be affected by the yield strength.

Finally, in a guide for sustainable steel buildings [51], M. May confirms that the optimisation potential of passing from S355 to S460 is of the order of 20%-40% in the range of typical buckling lengths. Furthermore, this document illustrates the necessity of considering the appropriate cross-section to achieve such savings and presents some case studies such as the Torre Diamante in Milan (Italy) or the DoubleTree Hotel by Hilton in Istanbul (Turkey), for which the use of S460 resulted in significant weight, cost and carbon savings.

The literature review on the economic benefits shows that high-strength steels have an advantage in certain applications, but not everywhere. The high-strength steel guide [76] mentions that the weight savings can range from 10 to 40%, but regrets that there is a lack of reliable data on the environmental impact savings achievable using high-strength steels. Given the limited availability of high-strength sections and the lack of clear guidance on the selection of the appropriate steel grade, some recommendations should be written to help designers in optimising their designs [45].

2.4. Influence of residual stresses on column resistance

The initial imperfections have a significant influence on the structural behaviour of steel columns under compression. These imperfections can be of different types, i.e. geometrical (out-of-straightness) or structural (residual stresses, non-uniform yield stress, ...). While it is generally agreed that geometrical imperfections fit well with a half-sine wave amplified by $L/1000$, the situation is somewhat more complex for residual stresses.

2.4.1. Development of residual stresses

Longitudinal residual stresses can be of thermal or mechanical origin and represent a material imperfection in hot-rolled sections that significantly affects the buckling behaviour as identified in the literature [107], [110], [118], [119], [120], [121]. Thermal residual stresses arise due to the uneven solid phase change due to the uneven cooling of all parts of the section from the rolling temperature to the ambient temperature. Hot rolling takes place at substantial temperatures of 900°C or higher and the cooling process is not uniform for all the individual “fibres” in the shape. For example, in a double-T section, the flange tips, which are more exposed to the ambient air, will reach room temperature and solidify earlier than the web-flange junctions, where the thermal radiation is higher. The flange tips, which first cool down, cause a contraction of the adjacent zones which are still warm. With the fibres kept in the state of forced shortening, the effect is that they are subjected to a state of compressive stress (according to the Hooke’s law $\sigma = E \cdot \varepsilon$). On the other hand, at the web-flange junctions, cooling takes more time because the heat dissipation paths are more complex, inducing residual tensile stresses. It has been shown in the past that residual stresses have a much greater influence than the yield stress variation in the cross-section. Therefore, the yield stress dispersion is no longer explicitly considered while residual stresses are still a major concern, especially when dealing with flexural buckling. The magnitude of the residual stress is observed to be independent of the yield stress for the produced hot-rolled profiles. This explains why the residual stresses are generally more detrimental for lower steel grades. Residual stresses which are due to differential cooling between the different longitudinal fibres of a steel profile present the following characteristics:

- They are more important in welded sections than in hot-rolled sections;
- They are greater in thick-walled sections than in thin-walled sections. This feature is explained by the cooling behaviour, which is a combination of surface heat transfer and internal heat conductivity [122];
- They lead to a different yielding progression depending on whether the profile is buckling about the strong or the weak axis;
- They are distributed differently in the cross-section depending on the profile dimensions (e.g. H-sections or I-sections).

Consequently, the residual stress distribution depends on a series of factors, including the profile dimensions, cooling rate, proximity to other profiles, etc. The presence of residual stresses within a profile can lead to premature yielding and accelerate the onset of instabilities [123], [124]. Based on the above-mentioned outcomes, it was therefore agreed to a certain classification, i.e. to assign different buckling curves for flexural buckling depending on the section typology, section dimensions and the yield stress (see Table 2-11).

2.4.2. Residual stress distributions

Extensive data on residual stress distributions are available in the literature for different section typologies [120], [125], [126], [127], [128], [129], [130], [131]. The focus is made on hot-rolled sections, for which various models exist to predict residual stresses, such as: ECCS [110], Galambos and Ketter [118] and Young [132] as depicted in Fig. 2-10 and Table 2-13.

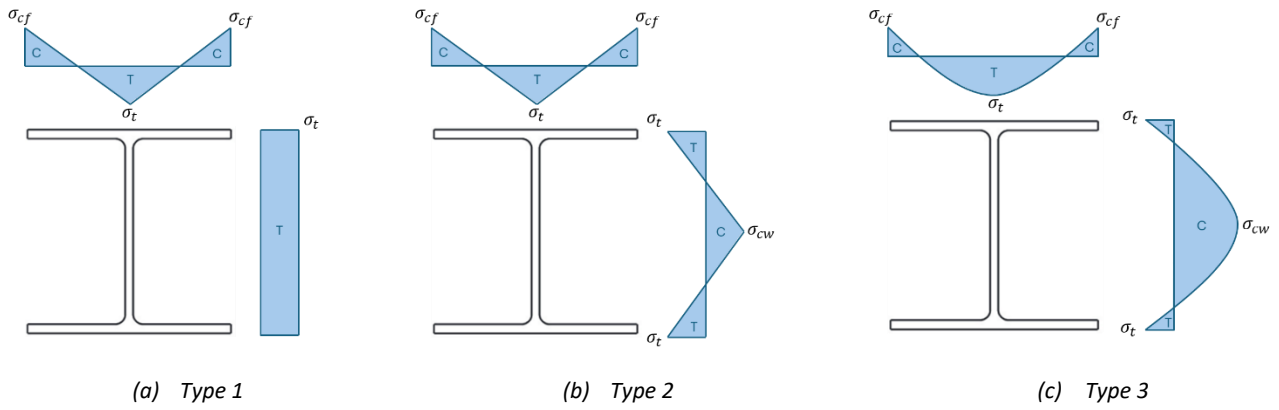


Fig. 2-10. Residual stress models for hot-rolled sections.

Model	Galambos & Ketter	ECCS	BSK 99 (Swedish's code)	Young
Type	1	2	2	3
Year	1959	1984	2003	1972
σ_{cf}	$0.3f_y$	$\frac{h}{b} \leq 1.2 \Rightarrow \sigma_c = \sigma_t = 0.5f_y$ $\frac{h}{b} > 1.2 \Rightarrow \sigma_c = \sigma_t = 0.3f_y$	$\frac{h}{b} \leq 1.2 \Rightarrow \sigma_c = \sigma_t = 120 \text{ MPa}$ $\frac{h}{b} > 1.2 \Rightarrow \sigma_c = \sigma_t = 70 \text{ MPa}$	$-165 \left(1 - \frac{h t_w}{2.4Bt}\right)$
σ_{cw}	/			$-100 \left(1 - \frac{h t_w}{2.4Bt}\right)$
σ_t	$\sigma_c \left(\frac{b_f t_f}{b_f t_f + t_w(d - 2t_f)}\right)$			$100 \left(0.7 + \frac{h t_w}{2Bt}\right)$

Table 2-13. Analytical formulations for residual stress models.

More recent model proposals have been established by Szalai and Papp [133] in 2005 or Skiadopoulou et al. [134] in 2023, but the ECCS model remains the reference model for simulating residual stresses in hot-rolled sections as recommended in FprEN1993-1-14:2024 [135]. It is noteworthy that, in current recommendations, the reference yield stress to be considered for the computation of the residual stresses is 235 MPa, whatever the actual steel grade under consideration, as the yield strength does not affect the residual stress distributions for hot-rolled sections [110], [129], [134], [136]. Since the buckling resistance of wide flange members is mainly provided by the flanges [130], residual stresses are often only shown in the flanges in this thesis.

The residual stress models prescribed in FprEN1993-1-14:2024 [135] for hot-finished hollow sections are depicted in Fig. 2-11 with $f_y^* = 235 \text{ MPa}$. The amplitude of residual stresses for hot-finished hollow sections is lower than that for cold-formed hollow sections [137], [138], [139], which explains the more detrimental buckling curve prescribed for the latter in current recommendations (see Table 2-11).

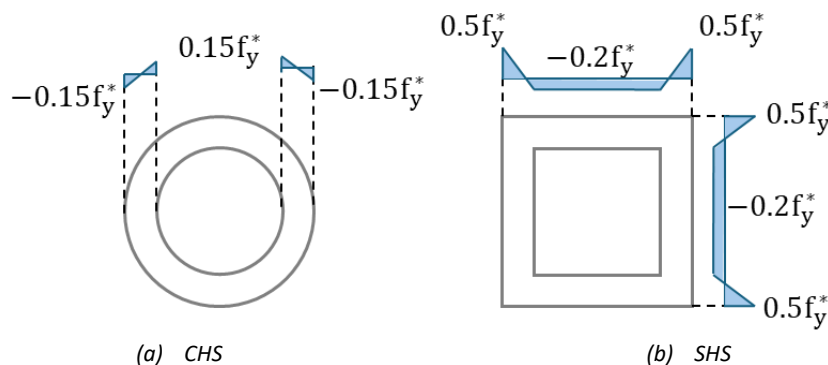


Fig. 2-11. Residual stress models for hot-finished hollow sections.

As noticed in Fig. 2-11, the residual stress amplitude is also independent of the yield stress for such hot-rolled sections. However, recent measurements made on high-strength steels [140], [141], [142] indicate that the residual stresses for hot-finished hollow sections are very low in amplitude. This has thus a beneficial effect on the flexural buckling capacity for such sections. Consequently, there is a need to reduce the detrimental effect of residual stresses to realise weight savings for stability-sensitive members.

The most common way to reduce residual stresses is to anneal the concerned member, but this process can affect the material properties and is not realistic for big-size members. Another method is the peening of various types (shot, laser or water), which reduces the amplitude of residual stresses in members. However, it is considered more economical to keep the residual stresses unmodified and increase the member size instead of investing in fabrication costs to reduce the amplitude of residual stresses [122]. As can be seen in Table 2-11, the relative importance of residual stresses decreases with the yield stress but only S460 benefits from this advantage. In addition, the hot rolled sections are regularly cold straightened after the rolling process, which implies the straightening of the profile but also a redistribution of residual stresses [122]. In the two following subsections, a literature review was therefore carried out regarding their specific potential on the load-carrying capacity of the column before investigating further.

2.4.3. Influence of the yield stress and modified imperfection factors

The buckling curves were originally established on the basis of a fictitious material characterised by an elastic limit $f_y = 255$ MPa. The experimental campaign was carried out in the 1960s on mild steels of low thickness (less than 40 mm), while only a few tests were carried out on higher steel grades, equivalent to today's S275 and S355 grades. It was concluded at that time that the yield strength had little influence on the dimensionless buckling curves, which justifies that they were established for a fixed value of 255 MPa [106].

In opposition to this statement, it was later shown that residual stress distributions do not evolve proportionally with the yield strength [120], [125], [126], [127], [128], [129], [132], leading to an increase in buckling resistance for higher grades as the local yielding is delayed. For hot-rolled sections, the residual stresses effectively depend on the geometrical properties of the section and the cooling rate during the production process and are definitely not proportional to the yield strength [143], as confirmed by experimental investigations [144]. In fact, the residual stress-to-yield strength ratio decreases as the yield strength increases. Therefore, it could have been decided to define the imperfection factor as a function of the yield strength to take into account the beneficial effect of increasing yield strength on the member buckling resistance. In 1976, the ECCS recommendations [110] allowed a jump of one buckling curve when the yield stress reaches 430 MPa as stated in Section 2.3.4. Maquoi established, in 1982, a yield strength-dependent expression of the imperfection factor [145] based on these recommendations, respecting the "jump" between mild and high-strength steel grades as expressed in Eq. (2-10).

$$\alpha^* = \alpha \cdot \left(\frac{235}{f_y} \right)^{0.8} \quad (2-10)$$

The value of 255 MPa could have been adopted instead of 235 MPa to be consistent with the value on which the buckling curves are based [146]. However, Maquoi [145] decided to consider S235 as the reference, together with an exponent of 0.8 to respect the jump of a buckling curve as specified in the ECCS recommendations. In this manner, if $\alpha = 0.34$ for S235 which corresponds to curve "b", $\alpha^* = 0.21$ for S430 which corresponds to buckling curve "a". Similarly, if $\alpha = 0.21$ for S235, $\alpha^* = 0.13$ for S430 which corresponds to buckling curve "a₀". However, when $\alpha = 0.49$ for S235 which corresponds

to curve “c”, $\alpha^* = 0.30$ for S430 which does not correspond to buckling curve “b”. This feature was not discussed at that time and considering that this proposal was based on a limited number of experimental tests, it was therefore not implemented in the design standards. The research campaign for S460 subsequently led to a beneficial adjustment of the buckling curve selection for this specific grade. So nowadays, as shown in Table 2-11, only S460 benefits from the reduced influence of the residual stresses for higher yield strength. Indeed, the curves originally established for a yield stress of 255 MPa were considered applicable without modifications for grades up to S420 while grade S460 got preferential treatment. In some cases, the buckling curve α_0 is even recommended for S460 whereas this curve was originally established for sections without any residual stresses [106], the subscript 0 meaning “zero residual stresses” [146]. Intermediate grades between S235 and S460 may deserve higher buckling resistances than those currently obtained considering the buckling curves assigned to S235.

Indeed, for several years, given the increasing number of experimental and numerical investigations on the structural behaviour of members made of high-strength steels [140], [147], [148], [149], [150], [151], [152], [153], [154], some authors [145], [148], [155], [156], [157], [158] have proposed new expressions for the imperfection parameter η , as defined in Eq. (2-8), in which the influence of the yield strength is explicitly accounted for - see Table 2-14. The proposed expressions for the imperfection parameter are listed by section typology in Table 2-14.

Type of sections	Maquoi, 1982	Jönsson & Stan, 2016	Somodi & Kövesdi, 2017	Meng & Gardner, 2020	Yun & Gardner, 2023
Hot-rolled (y-y)		$\alpha \cdot (\bar{\lambda}\varepsilon - 0.2)$ with; $\varepsilon = \sqrt{\frac{235}{f_y}}$ Class 4 neglected, only for strong axis buckling	/	/	/
Hot-rolled (z-z)	$\alpha^* \cdot (\bar{\lambda} - 0.2)$ $\alpha^* = \alpha \cdot \left(\frac{235}{f_y}\right)^n$ n=0.8, Maquoi, 1982;	/	/	/	$\alpha^* \cdot (\bar{\lambda} - 0.1)$
Welded I-sections	n=1.0, Johansson, 2005;	/	$\alpha^* \cdot (\bar{\lambda} - 0.2)$ $\alpha^* = \alpha \cdot \left(\frac{235}{f_y}\right)^{0.6}$	/	$\alpha^* = 0.45\varepsilon_f$ for major axis $\alpha^* = 0.55\varepsilon_f$ for minor axis
Hot-finished tubes		/	/	$\alpha^* \cdot (\bar{\lambda} - 0.1)$	/
Cold-formed tubes		/	$\alpha^* \cdot (\bar{\lambda} - 0.2)$ $\alpha^* = \alpha \cdot \left(\frac{235}{f_y}\right)^{0.5}$	$\alpha^* = 0.24\varepsilon$ for hot-finished $\alpha^* = 0.56\varepsilon$ for cold-formed	/

Table 2-14. Existing modified expressions of the imperfection parameter η in the literature.

According to Table 2-14, there are different approaches to consider the influence of the yield strength in the imperfection factor:

- The first approach consists of proposing a modified imperfection factor, denoted α^* in the following form: $\alpha^* = \alpha \cdot \left(\frac{235}{f_y}\right)^n$. This approach has been the most promoted one in the literature for decades as can be seen in Table 2-14. Indeed, Maquoi already proposed this format in 1982 [145] and it was later recommended in a generalised form in an IABSE report

[93]. In 2005, the exponent $n=1$ was considered more appropriate for grades up to S400, while Maquoi recommended an exponent $n=0.8$ [145]. The main advantages of this formulation for the modified imperfection factor are: (i) to keep the same historical buckling curves for S235 and (ii) to avoid proposing different specific imperfection factor values for each steel grade. The exponent could be different depending on the section typology as shown in Table 2-14.

- The second approach consists of applying a coefficient $\varepsilon = \sqrt{\frac{235}{f_y}}$ on the relative slenderness as proposed by Jönsson and Stan [155] in 2016 for hot-rolled sections subjected to strong-axis flexural buckling. This approach consists of considering this parameter ε , which is well-known in the steel construction sector for accounting the yield strength. But, in this form, it implies that the higher the yield strength, the longer the yielding plateau. The validity of this approach for weak axis flexural buckling has not been investigated.
- The third approach consists of forgetting all current buckling curves and proposing a modified imperfection factor as a function of ε . In the publication for hollow sections by Meng and Gardner [148], they also proposed to reduce the length of the yielding plateau to a relative slenderness of 0.1, instead of 0.2.

The various approaches do not comply with the current recommendations of Eurocode 3, since the first one was set to 430 MPa instead of 460 MPa, the second one modifies the length of the yielding plateau, and the third one does not respect the historical buckling curve discretisation. Consequently, further investigations should be performed on the buckling resistance with the objective of proposing a consolidated model to account for the beneficial impact of high-yield strength for all section typologies.

2.4.4. Influence of the straightening process

The concern about the effect of cold straightening on the load-carrying capacity of columns has been the subject of publications since the early 1970s. There are two main techniques to straighten a profile:

- *Gag straightening*: in this cold-treatment process, concentrated weak-axis forces are applied at discrete locations along the length of the member with the objective of bending it to approximate straightness. This process induces a yielding of flanges, but it is limited to very localised cross-sections, so the residual stress redistribution is not constant along the length;
- *Roller-straightening (or Rotarizing)*: the shape is passed through a train of rolls that bend the member back and forth, progressively reducing the out-of-straightness. This process induces a continuous yielding along the length, thereby ensuring that the effect on residual stresses is continuously distributed along the length.

The increase in strength associated with the residual stress redistribution after this post-treatment process was already contemplated by Frey in 1969 [159] and Alpsten in 1970 [160] but investigations had already started even before. Indeed, Galambos reported residual stress diagrams for both straightening processes in his guide to stability design [161]. Amongst them, one from Huber [162] already gave in 1956 a residual stress pattern of a W8x31 section after gag straightening about its weak axis. Residual stress distributions depending on the straightening method are also provided by Beedle & Tall in 1960 [125]. Furthermore, according to Tall in 1964 [163], the effect of steel grade on the residual stress patterns is not as significant as the geometry. In addition, about the potential gain resulting from the roller-straightening process, Alpsten has confirmed in some papers [164], [165] that the load-carrying capacity of the column can be increased by 20% while maintaining the same slenderness and the same out-of-straightness. As the roller straightening process is more commonly

used nowadays than the gag straightening, only the residual stress distributions available for this process are shown in Fig. 2-12 [161], [166].

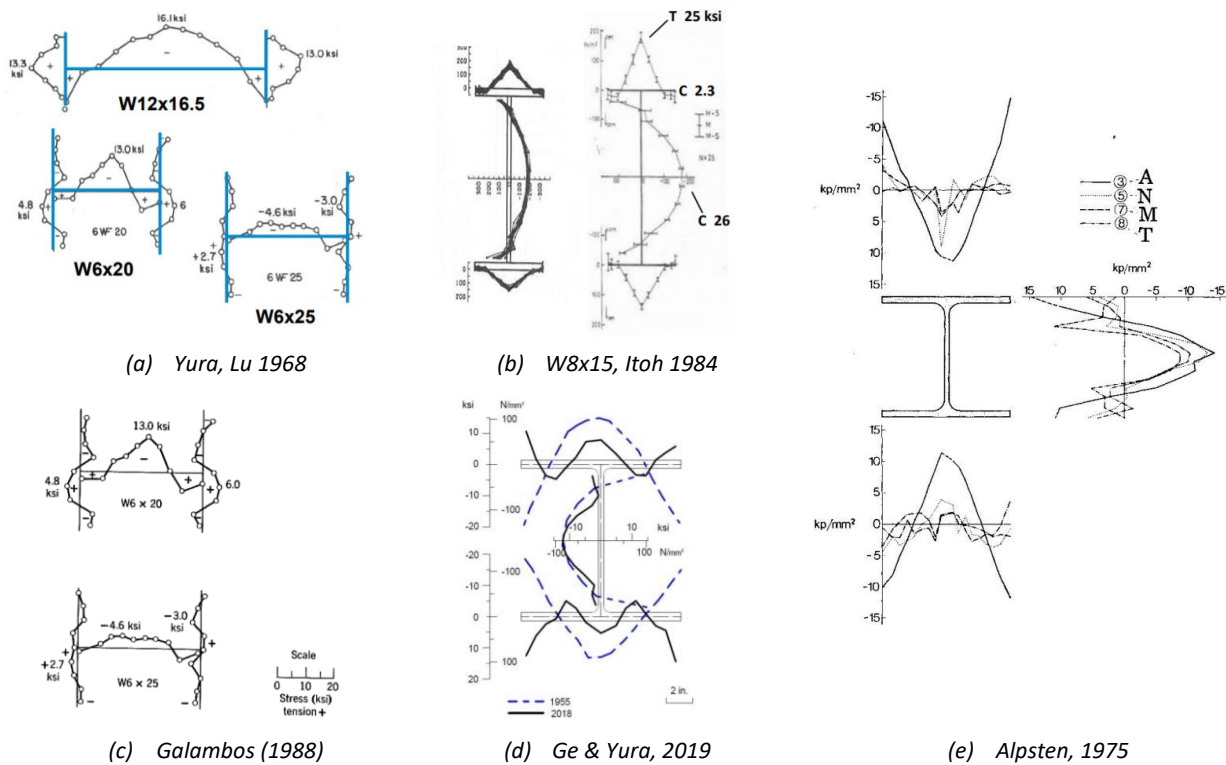


Fig. 2-12. Residual stress distributions for straightened members in the literature.

As shown in Fig. 2-12, this process entails a further redistribution of residual stresses within a structural member similar to the cold bending process that alters the residual stresses formed after welding and/or hot rolling which has been recently studied [167], [168]. However, in all this experimental data, little information is given on how the straightening was achieved, so there are some fundamental unknowns, such as the amplitude of the imposed displacements. In addition, most of these experimental tests involve American steel grades and sections, and no systematic effect resulting from the straightening can be clearly identified. Therefore, the beneficial effect of straightened residual stresses resulting from cold straightening after the rolling process has been safely neglected due to its inherent randomness. Each manufacturer has its own straightening machine, and a suitable straightening calibration should be realised for each profile in each grade to achieve greater savings.

Frey published a paper [159] in 1969 in which he analytically derived the shape and the maximum values of the residual stresses following a straightening operation. In this study, Frey considers that a pure bending moment is progressively applied to the member up to a stage at which, after releasing the applied moment, the profile is perfectly straight. The length L of the member to be straightened is fixed at 10 m and the initial out-of-straightness is also fixed at $L/100$. These values are obsolete compared to current practice. Moreover, this mathematical model does not introduce any imposed displacements, the only objective being to obtain a straight member at the end of the process, which is not in line with the current straightening practice. Despite the difficulty in deriving an analytical residual stress model, the ECCS recommendations proposed a straightened residual pattern as shown in Fig. 2-13a [110], which was considered to be representative of all rotorised small and medium I-sections, regardless of the height to width ratio.

Subsequently, research on this topic has been resumed in 2019. Indeed, a recent study by Ge & Yura published in 2019 [166] addresses the roller-straightening of columns by experimentally evaluating the residual stress patterns of a straightened W12x65 section and then, by assessing the influence of this experimental pattern on weak and strong axes column stability. Based on the experimental measurements, this research proposes an idealised residual stress model to be used in numerical simulations (Fig. 2-13b). This study expressed that, in the case where the residual stresses are negligible, it could provide up to a 45% increase in strength for this section. The margin between the classical residual stress pattern and the negligible residual stress pattern is significant, so considering a reduction in the residual stress amplitude may provide a notable strength benefit. Based on the idealised model, further studies have been carried out to evaluate the effect of this straightened residual stress pattern on the column-bearing capacity [169], [170], [171]. These studies show that the beneficial influence is particularly pronounced for minor axis buckling especially as the floor load magnitude increases. A large difference was observed in the inelastic buckling range, but everything was based on this idealised residual stress pattern proposed by Ge & Yura in 2019 while Fig. 2-13 and this literature review testify of the difficulty in proposing a standardised residual stress pattern for all straightened products and dimensions.

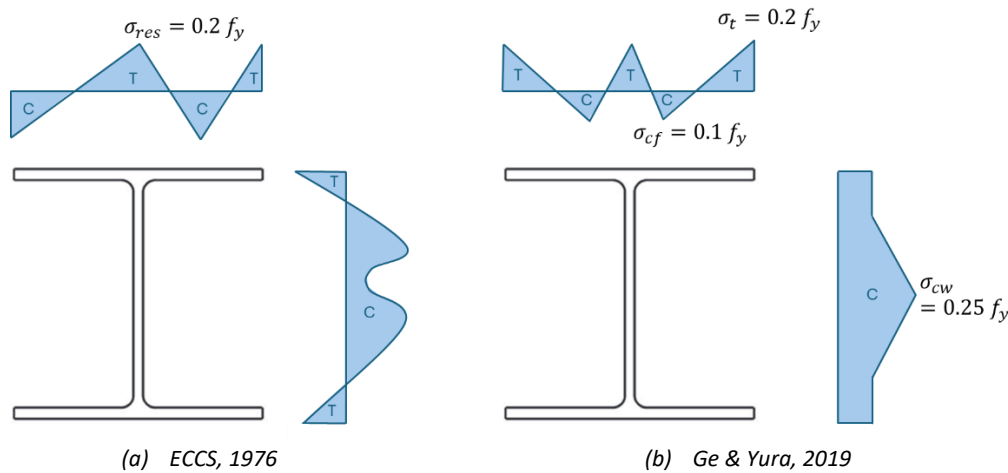






Fig. 2-13. Existing residual stress models for straightened members in the literature.







On the other hand, a paper [172] was published by Guan in 2017, in which the author studies the stress-inheriting behaviour of an H-beam during the roller-straightening process with repeated elastic-plastic bending and its effect on the section's bending properties. In addition, in this paper, the author has developed a MATLAB routine which numerically simulates the process of continuous bending of an H-beam and studies the law of sectional stress inheritance and its effect on the evolution of geometrical imperfections. This numerical model is based on several rough assumptions expressed in the paper, such as the idealised elastic-plastic material law, the linear superposition of residual stress or the uniaxial stress-strain assumption.

Finally, the new standard for design assisted by finite element analysis FprEN1993-1-14:2024 [135] reports the following note: "Positive effect of post-production treatment methods (e.g. in the case of hot-rolled sections continuously straightened by rotarization) can be considered on residual stress pattern." This review highlights the necessity for further research investigation regarding this post-treatment process, given the potential for significant weight, cost and carbon savings.

2.5. Overview of project examples

Among the reference projects that are regularly cited in the literature, the use of high-strength steels is particularly developed in several applications such as: diagonal and chord of steel trusses in long-span structures (e.g. Friends Arena in Sweden - S460M/S690QL, Airbus Hangar in Germany - S500M, Beijing National Stadium Q460 for the box cocoon, ...), in bridge decks (Millau Viaduct in France - S460M for the deck) or columns for multi-storey buildings. Indeed, high-strength steels are particularly interesting for high-rise buildings. As a structure increases in height, the vertical forces acting upon its columns and foundations also increase, thus the use of a high-strength steel grade to realise weight savings is likely to be justified. Among different high-rise buildings that have been constructed using high-strength steels, Table 2-15 presents an overview of some reference buildings over the years.

Structure	Location	Picture	Grade	Year	Description
Torre Mapfre	Barcelona Spain	 © https://www.torremapfre.com/en	HISTAR® 460	1992	24% Weight reduction by the use of HISTAR® 460 instead of S355 grade
D2 tower	Paris France	 © ConstruirAcier via constructalia	HISTAR® 460	2014	3000 tonnes of HD400 sections in HISTAR® 460
The One World Trade Center	New-York United States	 © R.A.R. de Bruijn Holding BV / Shutterstock.com	A913 Grade 65 (450 MPa)	2014	12,500 tonnes of HISTAR® beams and columns
Bay Adelaide East	Toronto Canada	 © Entuitive via Constructalia	A913 Grade 70 (485 MPa)	2016	The first high-rise building designed with Grade 70 (485 MPa) steel. It results in a weight reduction of 9%.

150 N Riverside	Chicago United States	 © TomRossiterPhotographie via Constructalia	A913 Grades 65 and 70 (450 and 485 MPa)	2017	2,530 tonnes of ASTM A913 Grades 65 and 70 column sections. The first in the United States
Lakhta tower	St. Petersburg Russia	 (CC BY-SA) ЗАО ОДЦ "Охта" via Constructalia	HISTAR® 460	2019	Europe's tallest building -18309 tonnes in HISTAR® 460
103 Colmore Row Office Building	Birmingham UK	 ©rightmove.co.uk	HISTAR® 460	2020	Reduction of 30% in weight resulting using HISTAR® 460
BMO tower (320 South canal)	Chicago United States	 © Ian Jolipa via CTBUH	A913 Grades 65,70 and 80 (450, 485 and 550 MPa)	2021	The first structure ever to use sections with a yield strength of 80ksi (550 MPa), which led to a reduction of almost 20%
425 Park Avenue	New-York United States	 © Field Condition	A913 Grade 70 (485 MPa)	2022	The first building in New York to implement ASTM A913 Grade 70
Merdeka 118	Kuala Lumpur, Malaysia	 © Fender Katsalidis via CNN	HISTAR® 460 / S460M	2023	4000 tonnes of heavy steel sections in HISTAR®460 / S460M

1900 Laurence Avenue	Denver, United States	 <p style="text-align: center; font-size: small;">© Goettsch Partners</p>	A913 Grades 50,65 and 80 (345, 450 and 550 MPa)	2024	Grade 80 for columns W14x159 and larger, Grade 50 for columns smaller than W14x90 and Grade 65 for the rest
----------------------------	--------------------------	--	--	------	--

Table 2-15. Reference high-rise buildings made of high-strength steels.

Table 2-15 shows how the use of high-strength steel sections in high-rise buildings has evolved over the years. In the early 2000s, the move towards higher-strength steels made structural shapes in ASTM A913 Grade 65 increasingly popular in the US market [65]. In parallel, S460M / HISTAR® 460, the European equivalent of Grade 65, is also becoming more widely used in European projects as can be seen in Table 2-15.

In 2016, the Bay Adelaide East was built in Toronto [173], it was the first building to use Grade 70 (485 MPa) steel sections. The use of this higher yield strength resulted in an overall weight saving of more than 9%. This building was followed by other projects in the United States using this new grade. Since 2019, the ASTM A913-19 standard [66] has allowed the use of Grade 80 (550 MPa). This grade was used for the first time at the BMO Tower in Chicago in 2021. Since 2019, according to the product standards EN10025-2 [53] and EN10025-4 [54], S500 JO and S500M grades can also be used in the European market and reference projects using this maximum grade in Europe are likely to increase in the coming years. These examples, which are representative of the development of high-strength steel sections in tall buildings, show that the continuing quest for height will continue to require the development of new materials with higher strengths to realise human dreams, as well as improving the use of materials to make construction more sustainable.

2.6. Research questions

This background chapter illustrates that, despite the current low demand for members with higher yield strengths, there are advantages in considering such steels in various applications. However, to increase their demand, it is necessary to develop appropriate guidelines and design rules to realise weight, cost and carbon savings in order to take full advantage of such innovative materials. The present thesis aims at providing the required scientific background (i) to improve the current design rules to take full advantage of new emerging steel grades and (ii) to identify the fields of application for such steel grades through a multidisciplinary approach, as expressed in Section 1.2. As a result, the thesis outcomes allow to provide guidelines for the selection of the appropriate steel for different types of structural members through the use of improved design rules. To achieve these objectives, the following research questions have been addressed:

- How can realistic cost estimations be derived for existing and future emerging steel grades? Can benchmark ranges be established for comparative studies?
- How to establish a relation between the carbon factor and the yield strength based on the steel production process and the chemical composition of the steel?
- How to assess the most appropriate steel grade for a structural member subjected to a given loading scenario?

- Based on the outcomes of the previous questions and the current design recommendations, what are the economic and environmental benefits of using high-strength steels in steel members?
- How to accurately account for the relation between the yield strength and the effect of the residual stresses on the column buckling capacity?
- How to account for the positive effect of the roller-straightening process on the residual stress distribution? How does the so-obtained residual stress distribution affect the load-bearing capacity of the column?
- Can lateral-torsional buckling be prevented through the consideration of inherent sources of stabilisation in the particular case of storage racks? What is the role of the section shape and friction forces at the beam-pallet interfaces in the optimisation of such structures using high-strength steels?

Several industrial collaborations have oriented some developments in this thesis, especially regarding the last research question, but they have always been under the same global objective, which is to reduce the material consumption in steel structures and to contribute to sustainable steel structures.

Chapter 3

Sustainability of High-Strength Steels

3.1. Introduction

Nowadays, the concepts of sustainability and resilience are becoming increasingly important from both an economic and environmental perspective, as the Earth's resources are not inexhaustible, and the climate challenges of tomorrow's world will be crucial to ensuring the best possible lifestyle for future generations. In this context, all professional sectors are trying to adapt their operating methods to reduce their emissions and waste. As stated in the general introduction of this thesis (**Chapter 1**), improvements in the construction sector are essential to achieve carbon neutrality by 2050.

Among the structural solutions for buildings, significant improvements can be observed in the field of steel structures, allowing for a progressive decarbonisation of production processes, but also for a reduction in the weight of structures through an increase in yield strength and/or improved design methods. Indeed, when the strength of the material is the dimensioning criterion, the increase in yield strength will lead to a significant gain in material use by drastically reducing the section dimensions. Less material may also mean less environmental impact, as well as indirect benefits such as savings in foundation costs, reduced transportation, faster construction and therefore reduced costs and environmental burden.

Considering some production techniques for high-strength steels, which are sometimes more energy-consuming and more demanding in terms of alloy content, the cost and global warming potential (GWP) generally increase with yield strength. However, for a circular design, it is necessary to consider a life cycle approach, including a possible comparison of all phases (from raw material extraction to end-of-life) and taking into account the design benefits already mentioned (weight reductions, cost savings, etc.). Without this way of thinking (called life cycle thinking) comparing only the production cycle would be reductive and penalising. However, the choice of high-strength steels for passive structures mainly affects the production stage, so most of the following investigations are focused on this stage of the material life cycle.

Chapter 2 illustrates that only a limited number of studies have examined the relationship between relative price or relative environmental footprint and increasing steel strength. Based on this observation, Chapter 3 addresses the various investigations initiated at the University of Liège to assess the sustainability of high-strength steels, with the ultimate aim of determining the benefits of using high-strength steels in steel structures.

3.2. The three pillars of sustainability

Sustainability can be defined as the ability of something to be sustained or to last. Ensuring sustainability means preserving the way of life on Earth and the Earth's ability to meet our needs not only today but also in the future. The Earth's resources must be used in such a way that they can be used forever; if something is used too abundantly now, it could be gone forever. Sustainability is often associated with environmental concerns, but it is more than just preventing climate change. To assess the sustainability of a new material or construction technique, it is necessary to adopt a holistic approach accounting for the scarcity of resources, the need to reduce and eliminate inequalities and the need to ensure the economic viability of this improvement. The various aspects that compose the concept of sustainability are gathered into three main areas, also known as pillars, as represented in Fig. 3-1.

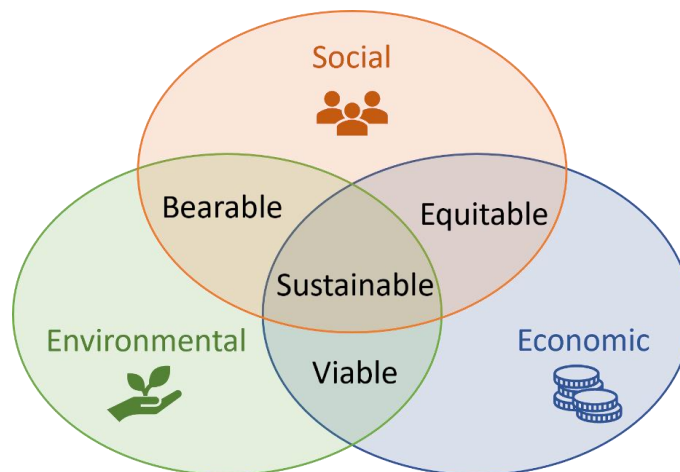


Fig. 3-1. The three pillars of sustainability.

- *Social pillar:*

Social equity, or the right of everyone to have access to basic resources and services to meet their essential needs, is a prerequisite for a development that is beneficial for everyone.

- *Environmental pillar:*

The environmental pillar seeks to regulate human activities to ensure that they are not only in harmony with ecosystems but at least maintain or restore them. It is also the most forward-looking pillar, meaning that our current activities must not compromise the ability of future generations to carry out their activities in similar conditions.

- *Economic pillar:*

The idea of sustainable development is a challenge to existing business models. Far from advocating degrowth, sustainable development seeks a balance between value creation and resource conservation.

The concept of sustainable development rests on three pillars, each of which is essential to its support. A physical pillar analogy can be used to illustrate this point. If any of the pillars is weak, the entire structure can collapse. Therefore, achieving sustainability requires a balanced approach that respects all three pillars, with each pillar shouldering an equal weight of sustainable development.

However, this concept needs to be nuanced depending on a person's attraction to one or other of these pillars. Environmental restrictions are becoming increasingly important in the construction industry. For example, although more expensive, certain construction projects are sometimes preferred if they are eco-responsible. So, the equal weighting of the 3 pillars is debatable. This thesis focuses on the sustainability assessment of high-strength steels, an economic approach is pursued while ensuring that the solutions proposed are also environmentally viable. The use of higher steel strengths allows for the use of fewer resources for the same application which results in material savings. If the material savings outweigh the increases in relative prices and carbon footprints, there are economic and environmental benefits of using such grades. Additionally, conserving material resources helps to preserve the Earth's resources and reduce the cost and carbon footprint of buildings. This approach addresses all three pillars of sustainability, ensuring that our lifestyle can be sustained for future generations.

However, it is important to note that in some cases, the weight savings achieved through the use of high-strength steels may not offset the relative price increase or the increase in carbon footprint. Therefore, the use of a high-strength steel grade does not necessarily guarantee a more sustainable construction. To assess whether the use of high-strength steel grades can contribute to more sustainable construction, it is essential to establish reference and reliable relative price-strength and carbon emission-strength relationships for both existing and future emerging steel grades.

3.3. Establishment of reliable relative prices

Based on the limited literature available presented in Section 2.2.5, it appears that the increase in relative prices as a function of yield strength is often balanced by the weight reduction achieved by using higher yield-strength materials. Nonetheless, such a conclusion cannot be pronounced without a comprehensive understanding of how prices evolve with yield strength. To conduct a comparative study and draw conclusions on the economic benefit of using high-strength steels, it is necessary to have a reliable estimate of relative prices.

3.3.1. Background on cost breakdowns

According to several cost functions [174], [175], [176], [177], [178] aiming at evaluating the manufacturing costs, the total cost can be divided into a series of cost components as written in Eq. (3-1):

$$C = C_M + C_B + C_C + C_S + C_W + C_P + C_T + C_E \quad (3-1)$$

With: C_M the material cost, C_B the blasting cost, C_C the cutting cost, C_S the sawing cost, C_W the welding cost, C_P the painting cost, C_T the transport cost and C_E the erection cost.

The use of high-strength steels enables to reduce:

1. The direct costs if the material saving allows compensating for the higher material cost of high-strength steels;
2. The indirect costs such as transport, painting, welding, erection and foundations thanks to the weight and surface reductions.

A literature review has been conducted to gain a better understanding of the breakdown of steel costs. An overview of cost breakdowns in the literature is provided in Fig. 3-2.

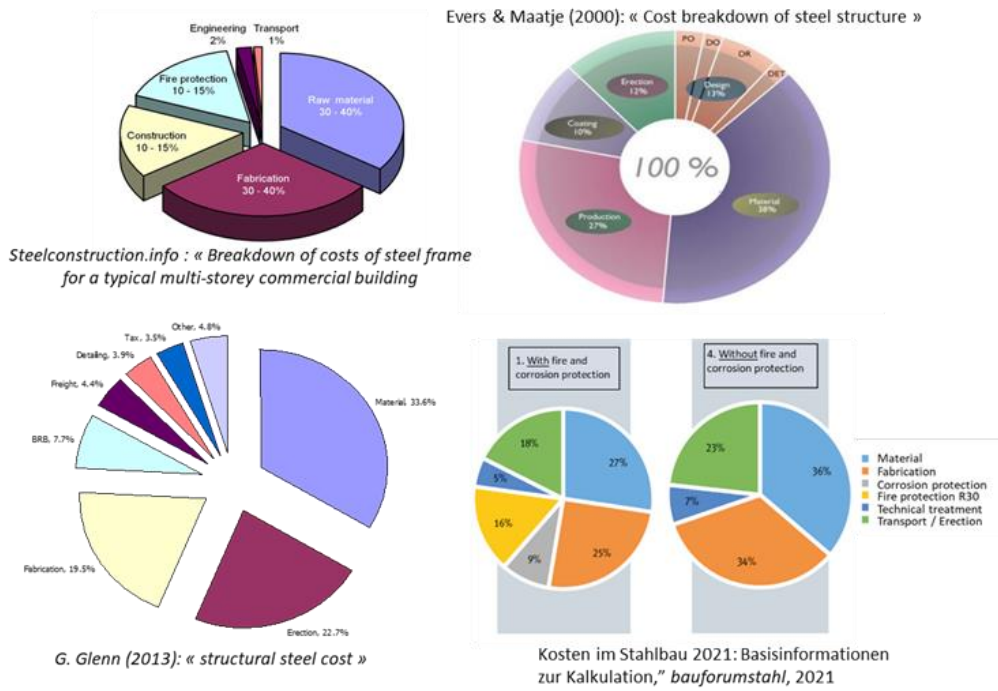


Fig. 3-2. Cost breakdowns of steel structures.

As can be seen in Fig. 3-2, the percentages of the cost breakdown related to fabrication and erection processes are approximately equal to those associated with material costs. It is widely agreed among scientists and industry professionals that each main part accounts for about 30%.

The study solely investigates the impact of high-strength steels on production costs, specifically on modules A1 to A3 of the life cycle stages as defined in EN 15084 [179] (see Table 3-1). Indeed, the higher yield strengths are achieved through a combination of alloys and production processes, which significantly affect the production stages (A1 to A3 in Table 3-1) and especially the raw material component. However, high-strength steels can result in material savings, but they also lead to a reduction of the area. This reduction affects the primer coating, fire protection and transport costs. In conclusion, although higher yield strengths may positively impact transport and erection costs, they will be neglected as they represent a lower proportion compared to material and fabrication costs.

Product stage			Construction stage		Use stage							End-of-life stage				Benefits and loads beyond the system boundary
A1	A2	A3	A4	A5	B1	B2	B3	B4	B5	B6	B7	C1	C2	C3	C4	D
Raw material	Transport	Manufacturing	Transport	Construction, installation	Use	Maintenance	Repair	Replacement	Refurbishment	Operational energy use	Operational water use	Demolition	Transport	Waste processing	Disposal	Reuse / Recovery / Recycling potential

Table 3-1. Life cycle stages according to EN15084.

3.3.2. Cost components

The manufacturing cost of steel elements is complex and fluctuating, influenced by various factors. According to producer pricelists, the price is typically composed of a base price to which various extras are added. These extras come from dimensional differences (thickness-width, thickness-length, unitary weight), differences in grades and qualities, certificates (e.g. 3.1 certificate which certifies the raw material used in the manufacturing process) and transportation (rail or road). Additional surcharges to be considered include those for quality tests (striction, coupon, ultrasonic, ...), possible shot blasting, cutting, sawing and painting.

3.3.2.1. Base prices

Base prices of steel members are highly time and space-dependent and depending on their amplitude, the relative prices between steel grades could be impacted. Fig. 3-3 illustrates the steel price evolution at the European level according to the MEPS statistical website [180] for various steel typologies.

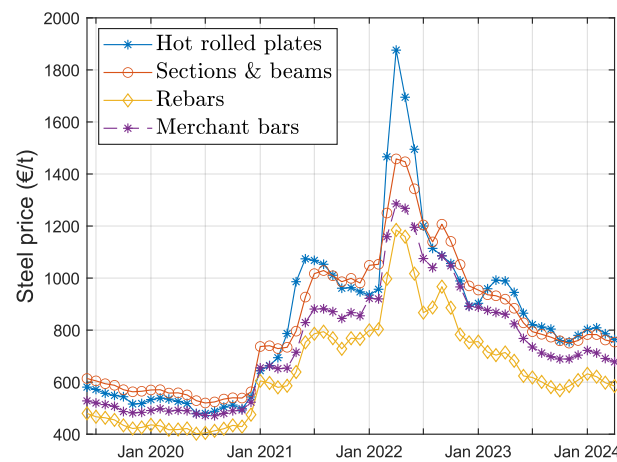


Fig. 3-3. European steel prices according to MEPS.

Between 2002 and 2021, base prices for hot-rolled plates and sections have remained relatively stable, with the exception of the financial crisis in 2008. The prices have ranged from 500€/t to 700€/t, according to data from MEPS [180] and SteelBenchMarker [181]. However, as can be seen in Fig. 3-3, certain historical events that occurred during the completion of this thesis, such as severe rises in production and energy prices, poor demand and unforeseeable war-related disruptions in Ukraine, have contributed to a very high level of steel base prices due to their impact on global supply chains. The price history demonstrates that base prices are dynamic and fluctuate depending on the geopolitical landscape.

The second key feature which impacts the base price amplitude is the provenance. The pricelists considered in this research mainly come from Europe, the UK and the USA.

Eventually, the last key feature is the ordered quantity. As for many goods, buying steel in bulk always offers a lower price per unit. An example is provided for a hollow section 50x50x5 in S235 JR from three different suppliers (in Belgium in 2021) in Fig. 3-4. It is not necessary to apply any additional charges for ordering, as these are mainly applicable to low quantities, which are relatively uncommon in steel structures.

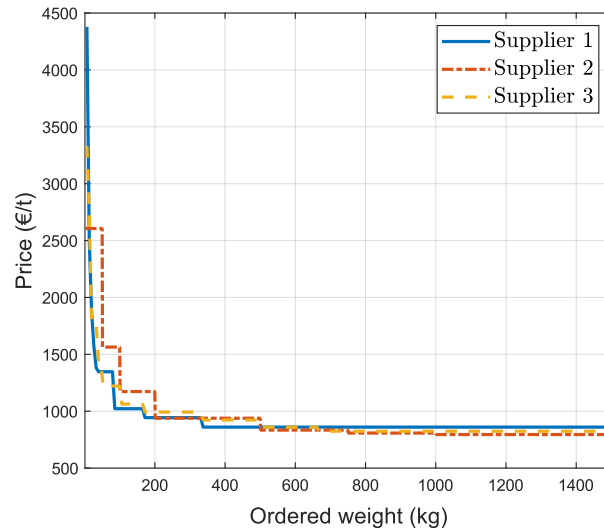


Fig. 3-4. Impact of the ordered quantity on the base price.

3.3.2.2. Extras

There are different types of extras depending on the section typology. They are listed below:

- *Size extras* (thickness – width, thickness – length, profile classification, unitary weight);
- *Grade/quality extras* (“JR/JO/J2”, “N/NL”, “M/ML”, “MC”, ...) function of the yield strength;
- *Finishing extras* (shot-blasting, primer coating, roller-straightening, flame-cutting, marking, ...);
- *Freight charges* (delivery by rail, ship or truck);
- *Mill test certificates* (e.g. EN10204-2.1, EN10204-2.2, EN10204-3.1 or EN10204-3.2) [182];
- *Quality tests* (ultrasonic test, tensile test, bending test, Charpy, chemical composition, ...);
- *Quantities and storage*.

The applicable extras are cumulative to compose the effective price. Concerning the time evolution of grade extras which are the most affected by the steel strength, it has been decided to track the daily prices of a given supplier for several months after the pandemic outbreak, when prices were highly volatile, to evaluate whether grade extras are affected by base price changes (see Table 3-2).

Steel specification	Nov. 2020	Jan. 2021	Mar. 2021	Jun. 2021	Grade extras
<i>S235 JR</i>	817	887	1083	1646	<i>Base</i>
<i>S355 MC</i>	857	927	1123	1686	<i>+40</i>
<i>S420 MC</i>	894	964	1160	1723	<i>+77</i>
<i>S500 MC</i>	922	992	1188	1751	<i>+105</i>
<i>S700 MC</i>	1134	1204	1400	1963	<i>+317</i>

Table 3-2. Evolution of grade extras (€/t) in a period of high base price fluctuations.

Based on the values reported in Table 3-2, it can be observed that grade extras remained unchanged even during periods of significant base price increases. This observation is supported by exchanges with some industrials who explain that although this is theoretically the case, manufacturers may take advantage of short steel supplies to increase both the extras and the base price.

3.3.3. Methodology

It is worth mentioning the difference between price and cost to avoid any confusion. The invoiced price includes the manufacturing cost and taxes related to the sale and delivery of the goods. Since distribution and taxes are not dependent on the material resistance, they are supposed to be included in the base price.

Only pricelist data are detailed as these are the only values that the designers have in their possession when they must choose the most appropriate steel grade. Consequently, investigations are focused on manufacturing prices from pricelists. Based on a given price breakdown example, the relative price of a given steel grade can be derived as written in Eq. (3-2).

$$P_{rel} = \frac{P_{base} + \sum_{i=1}^m Extra_{i,grade\ 2}}{P_{base} + \sum_{i=1}^m Extra_{i,grade\ 1}} \quad (3-2)$$

Where; P_{rel} is the relative price, P_{base} the base price and m the number of extra costs.

The main assumption behind these developments is to consider the same profile for both compared steel grades, to consider that only the grade extra is affected by the yield strength as well as to consider only the manufacturing prices in a conservative approach. Indeed, the relative prices tend to decrease when some size extras are applied because increasing the yield strength leads to a size reduction, which may correspond to a lower size extra category. So, to get conservative relative prices, it has been decided to focus on grade extras by keeping the same cross-section for both compared grades. As proven in Section 3.3.2.1, accounting for base price fluctuations is fundamental when computing the relative prices of high-strength steels, thus three relevant levels have been adopted according to base price history (Fig. 3-3) as reported in Table 3-3.

<i>Low</i>	<i>Medium</i>	<i>High</i>
500	750	1000

Table 3-3. Adopted base price levels for relative price establishment.

Based on this methodology, relative prices are firstly established for hot-rolled thermomechanically produced coils and heavy plates produced by quenching and tempering for which high-strength steels (above S460) exist. The computed values are compared to the literature and realistic relative price intervals are then established for hot-rolled sections to determine prospectively whether yield strengths higher than 500 MPa present an economic benefit.

3.3.4. Validation

As expressed in Chapter 2, high-strength steels, i.e. steels with a yield strength between 500 MPa and 700 MPa are already covered in EN10149-2 [57] and EN10025-6 [56]. The first product standard deals with thermomechanically (TM) hot-rolled steels for cold forming, usually delivered as coils while the second deals with quenched and tempered (QT) steel plates. Furthermore, Chapter 2 indicates that there are two main references in the literature regarding the relative prices of high-strength steels; Johansson [86], in 2005, proposed that the relative price trend follows the square root of the yield strength and Stroetmann [87], in 2011, provided lower relative values based on average prices from several producers in the German market. These relative prices are discussed in this section considering the already existing high-strength steel coils and plates.

3.3.4.1. Thermomechanically hot-rolled steels for cold forming according to EN10149-2

This first cost analysis is based on a steel sheet order realised in March 2021. The product is a black sheet (without surface treatment) 1500x6000x6mm in S355J2+N and the price breakdown is presented in Eq. (3-3).

$$\begin{array}{cccccc}
 \text{Price} = & 730\text{€/t} & + & \mathbf{50\text{€/t}} & + & 16\text{€/t} & + & 25\text{€/t} & + & 25\text{€/t} & = & 846\text{€/t} & (3-3) \\
 & \underbrace{\hspace{1.5cm}} & & \underbrace{\hspace{1.5cm}} & & \underbrace{\hspace{1.5cm}} & & \underbrace{\hspace{1.5cm}} & & \underbrace{\hspace{1.5cm}} & & \underbrace{\hspace{1.5cm}} \\
 & \text{Base} & & \text{Grade} & & \text{Width} & & \text{Length} & & \text{Extra for} & & \text{Total price} \\
 & \text{price} & & \text{extra} & & \text{extra} & & \text{extra} & & \text{certificate} & &
 \end{array}$$

The different extras expressed hereabove have been confirmed by some mill's pricelists. This research focuses on grade extras as they directly depend on the steel grade and other extras, which are assumed to be constant in a conservative approach. Accordingly, a deeper investigation has been conducted to establish a relative price-strength relationship. The online website Vosta Stahlhandel GmbH [183] and other mill pricelists (US Steel Kosice 2017 [184], Tata 2013-2015 [185]-[186], Salzgitter [187], Voestalpine [188], Arvedi [189] and SSAB [190]) contain their respective grade extras for hot-rolled sheets/coils (Table 3-4). The grade extra of +50€/t in Eq. (3-3) was found in precious pricelists as shown in bold in Table 3-4.

Steel specification	Thyssen Krupp (2010)	Salzgitter (2011-2012)	Tata (2011-2013-2015)	ArcelorMittal (2010)	Us Steel Kosice (2012-2017)	Acciaieria Arvedi	Voestalpine (2013)	SSAB (2016)
<i>S235JR</i>	16	16	10	5	5	5	10	15
<i>S235J2</i>	25	25	20	15	15	15	25	15
<i>S275JR</i>	21	21	20	15	15	20	20	20
<i>S275J2</i>	-	40	35	30	30	30	40	30
<i>S355JR</i>	-	45	40	35	35	35	40	40
<i>S355J2+N</i>	59	59	55	50	50	50	-	60
<i>S355J2</i>	59	55	50	45	45	45	50	50
<i>S315MC</i>	40	40	35	40	40	40	35	40
<i>S355MC</i>	50	50	45	45	45	45	45	50
<i>S420MC</i>	65	65	65	65	65	60	65	65
<i>S460MC</i>	75	75	75	75	75	75	75	75
<i>S500MC</i>	85	85	85	80	80	80	80	90
<i>S550MC</i>	98	98	98	100	100	95	95	105
<i>S600MC</i>	110	110	-	110	-	110	110	120
<i>S650MC</i>	-	-	160	-	-	200	170	160
<i>S700MC</i>	-	200	185	200	-	230	230	195

Table 3-4. Grade extras for TM steels for cold forming (€/t).

All these values are scattered with a linear interpolation of the mean values in Fig. 3-5.

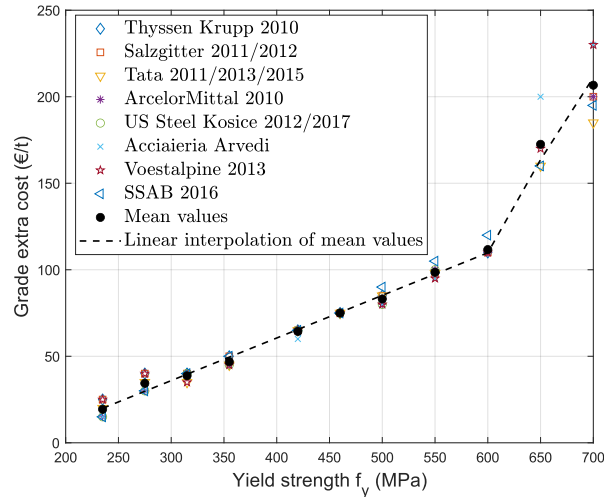


Fig. 3-5. Grade extras for TM steels for cold forming.

Referring to the United States Steel Corporation [191] and ArcelorMittal USA [192], it appears that the American pricelists for HSLA (high strength low-alloy steels) with improved formability are in line with the European linear trend as shown in Fig. 3-6.

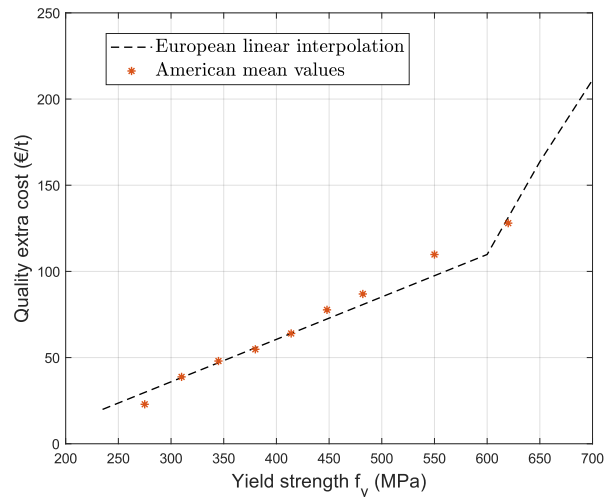


Fig. 3-6. European linear trend vs American grade extra values.

The linear interpolation is expressed in Eq. (3-4).

$$Extra_{grade}(f_y) = \begin{cases} 0.2463 \cdot f_y - 37.937, & f_y \leq 600 \text{ MPa} \\ 0.95 \cdot f_y - 453.89, & f_y > 600 \text{ MPa} \end{cases} \quad (3-4)$$

Based on this linear interpolation and considering the example treated in Eq. (3-3), relative prices between a given grade and S235J2 are computed according to Eq. (3-5).

$$\frac{c_{grade}}{c_{S235J2}} = \frac{730\text{€/t} + Extra_{grade} + 16\text{€/t} + 25\text{€/t} + 25\text{€/t}}{730\text{€/t} + Extra_{S235J2} + 16\text{€/t} + 25\text{€/t} + 25\text{€/t}} \quad (3-5)$$

For the sake of comparison, S235J2 is chosen as the reference steel because this is the grade chosen as a reference in the existing literature. The following relative prices are then obtained using the linear interpolation derived in Eq. (3-4): S235J2 = 1.000, S315MC = 1.024, S355J2/MC = 1.036, S420MC =

1.056, S460MC = 1.068, S500MC = 1.079, S550MC = 1.095, S600MC = 1.118, S650MC = 1.176 and S700MC = 1.234. Of course, these relative ratios are inherently dependent on the base price. A sensitivity study has been performed in MATLAB [193] to determine the base price influence, as shown in Fig. 3-7.

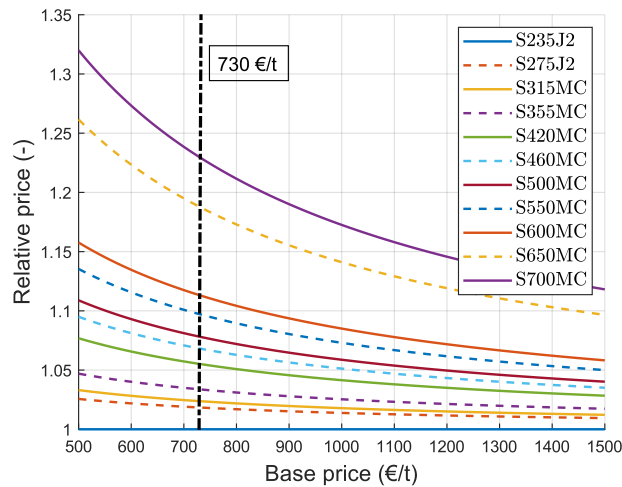


Fig. 3-7. Effect of a base price change on the relative prices.

As clearly stated in Fig. 3-7, the relative prices of high-strength steel grades are relatively lower when the base price is higher. This is due to the insensitivity of grade extras to changes in the base price, as confirmed by the literature review and industrial exchanges. The constancy of grade extras can be explained by the negligible percentage of alloying elements in the chemical composition of steels. Furthermore, the comparable values in Table 3-2 and Table 3-4 overtime confirm that competition among producers is solely based on the material base price. This confirms the assumption made in the methodology (Section 3.3.3) that only the base price is subject to fluctuations.

Fig. 3-8 reports the relative prices for both literature reference values respectively proposed by Johansson [86] and Stroetmann [116] for heavy plates, some values from Ruukki [194] and a Belgian supplier for thermomechanical hot-rolled coils. Additionally, three evolutions computed according to the developed methodology detailed in Section 3.3.3 are shown in Fig. 3-8 for the sake of validation.

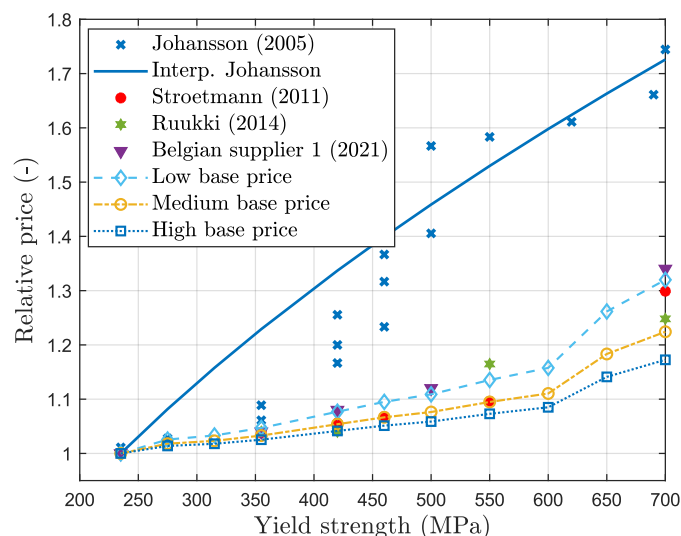


Fig. 3-8. Relative prices for TM steels for cold-forming (EN10149-2).

As can be seen in Fig. 3-8, the established relative price relationships are validated by Stroetmann and other collected values. Referring to a presentation by Stroetmann [117], the base price at the

publication period (October 2010) was 700€/t, which explains why the “Medium base price” evolution, corresponding to a base price of 750€/t, is closer to Stroetmann’s relative prices. Furthermore, as stated in [194], Stroetmann’s values are for TM steels for cold forming, which aligns with the product standard being considered herein. An example of the methodology application for estimating the relative price of the S550MC grade is provided in Example 3-1.

Example 3-1. Relative price prediction of the S550MC grade for a medium base price level

According to the linear interpolation defined in Eq. (3-4), the corresponding grade extras for both compared grades are:

$$Extra_{S235J2} = 0.2463 \cdot 235 - 37.937 = 19.94 \text{ €/t } (f_y < 600 \text{ MPa})$$

$$Extra_{S550MC} = 0.2463 \cdot 550 - 37.937 = 97.53 \text{ €/t } (f_y < 600 \text{ MPa})$$

Consequently, according to Eq. (3-5) and considering the medium base price level defined in Table 3-3, the relative price of S550MC is:

$$\frac{c_{S550MC}}{c_{S235J2}} = \frac{750 + 97.53 + 16 + 25 + 25}{750 + 19.94 + 16 + 25 + 25} = 1.093$$

Stroetmann provided in 2011 the relative price of 1.096 for S550MC.

Example 3-1 illustrates that considering only the base price and the grade extras would have led to a slightly higher relative price. Therefore, a conservative approach would be to evaluate the relative price of a grade without considering additional extras. One may notice the sudden slope change at 600 MPa; there are various possible explanations for this feature, as listed below.

- The first reason comes from the steel chemistry. Indeed, according to the chemical compositions prescribed in EN10149-2 [57], listed in Table 3-5, a Boron (“B”) alloying element is added to the steel composition for yield strengths higher than 600 MPa and the unitary price of this alloying element is relatively high [195], [196]. In addition to the Boron, Molybdenum (Mo) is also added to the chemical compositions for grades higher than 600 MPa to avoid heat-affected zone softening in weld areas [76]. Eventually, an increase in titanium (Ti) percentage is observed from 600 MPa. Thus, the sudden increase in the grade extra-yield strength relationship at 600 MPa can be explained by the use of these alloying elements.

Steel grade	Chemical composition in %. max										
	C	Mn	Si	P	S	Al (min)	Nb	V	Ti	Mo	B
S315MC	0.12	1.3	0.5	0.025	0.002	0.015	0.09	0.2	0.15	-	-
S355MC	0.12	1.5	0.5	0.025	0.002	0.015	0.09	0.2	0.15	-	-
S420MC	0.12	1.6	0.5	0.025	0.015	0.015	0.09	0.2	0.15	-	-
S460MC	0.12	1.6	0.5	0.025	0.015	0.015	0.09	0.2	0.15	-	-
S500MC	0.12	1.7	0.5	0.025	0.015	0.015	0.09	0.2	0.15	-	-
S550MC	0.12	1.8	0.5	0.025	0.015	0.015	0.09	0.2	0.15	-	-
S600MC	0.12	1.9	0.5	0.025	0.015	0.015	0.09	0.2	0.22	0.5	0.005
S650MC	0.12	2.0	0.6	0.025	0.015	0.015	0.09	0.2	0.22	0.5	0.005
S700MC	0.12	2.1	0.6	0.025	0.015	0.015	0.09	0.2	0.22	0.5	0.005
S900MC	0.20	2.2	0.6	0.025	0.001	0.015	0.09	0.2	0.25	1.0	0.005
S960MC	0.20	2.2	0.6	0.025	0.001	0.015	0.09	0.2	0.25	1.0	0.005

Table 3-5. Chemical compositions of steels complying with EN10149-2.

- The second reason for these increases may be the requirements for toughness. A higher yield strength requires a finer-grained microstructure to enhance low-temperature toughness performance [76] which may be reflected in the price through the grade extra.
- The third reason coming out from exchanges with industries is related to marketing strategies behind the selling of such high-strength steels.

3.3.4.2. Fine-grained structural steels made to EN10025-6, water quenched and tempered

A high-strength steel guide [79] expresses some price breakdowns for steel plates ordered to compose flanges and webs of welded I-beams for hybrid girders. A price breakdown is given for a 24300x1000x20 plate in S460M, and the details are reported in Eq. (3-6).

$$Price = 850 + 188 + 162 + 15 + 28 + 24 + 28.8 + 21.56 = 1317.36\text{€}/t \quad (3-6)$$

Heavy plates of yield strengths higher than 500 MPa only exist for fine-grained structural steels (QT steels - EN 10025-6). Referring to several Dillinger (2012 to 2016), Ilseburger - Salzgitter (2011) pricelists [197], [198], various grade extras are reported in Table 3-6. These extras depend on the thickness, an increase of +35€/t has to be applied to reach the second thickness domain (up to 70 mm) and +85€/t for thicknesses up to 100 mm. Indeed, the thicker the plate, the greater the alloying percentage to reach the expected yield strength resulting in a higher grade extra.

Grade typology	Steel specification	Thickness domain (mm)	Extras (€/t)	Alloy extra(€/t)
Unalloyed structural steel made to EN 10025-2	S235J2	≤195	26	-
	S355J2	≤195	59	-
High-strength, fine-grained structural steels made to EN 10025-6, water quenched and tempered	S460QL	≤40	288	36
	S500QL	≤40	298	36
	S550QL	≤40	311	39
	S620QL	≤40	328	39
	S690QL	≤40	346	39
	S890QL	≤40	446	135
	S960QL	≤40	481	135
S1100QL	≤40	551	175	

Table 3-6. Grade extras for heavy plates made of QT steels (EN10025-6).

As indicated in the consulted pricelists, additional extras for alloy content upcharges/discounts must be added when evaluating the total price as reported in Table 3-6.

Similarly to hot-rolled coils in Section 3.3.4.1, grade extras increase proportionally with the yield strength and can be calculated using Eq. (3-7).

$$Extra_{grade}(f_y) = \begin{cases} 0.2516 \cdot f_y + 172.27, & 460 \text{ MPa} \leq f_y \leq 620 \text{ MPa} \\ 0.5 \cdot f_y + 1, & f_y > 620 \text{ MPa} \end{cases} \quad (3-7)$$

Considering the given example, the relative price can be derived through Eq. (3-8).

$$\frac{c_{grade}}{c_{S235J2}} = \frac{P_{base} + Extra_{grade} + Extra_{alloy} + 15€/t + 28€/t + 24€/t + 21.56€/t}{P_{base} + 26€/t + 0€/t + 15€/t + 28€/t + 24€/t + 21.56€/t} \quad (3-8)$$

As previously stated, Johansson [86] and Stroetmann [116] provided relative values for hot-rolled heavy plates which are under concern here. Therefore, a comparison has been performed between the literature values and those based on Eq. (3-8) for the three base price levels (defined in Table 3-3) as shown in Fig. 3-9.

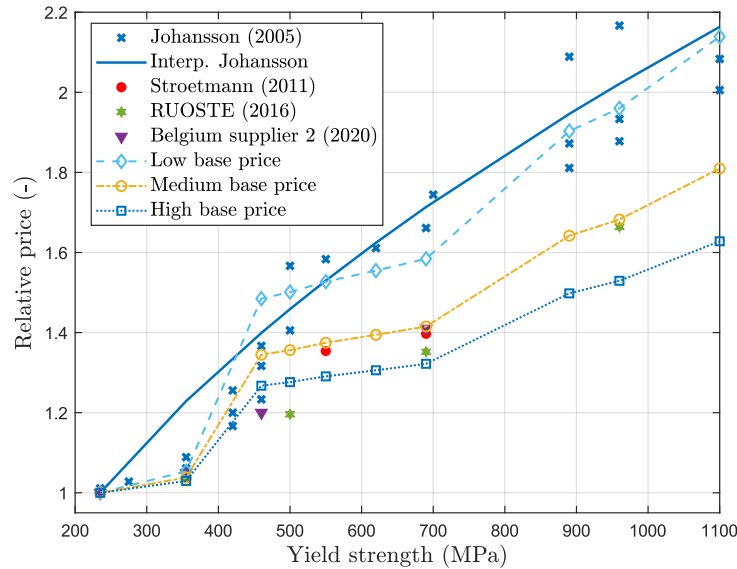


Fig. 3-9. Relative prices for QT steels (EN10025-6).

Fig. 3-9 shows that the computed values for medium base price remain close to Stroetmann even for QT steels, confirming the consistency of the computed trends. In addition, the base price was low in 2005, probably around or even below the low base price (500€/t). This explains why the “low base price” trend is closer to the interpolated values of Johansson. The scattered values of Johansson also show a change of slope at 690 MPa, confirming the computed trends. Example 3-2 and Example 3-3 provide two computation examples of relative prices to illustrate the above-mentioned conclusions.

Example 3-2. Relative price prediction for S550QL for a medium base price level

The grade extra for S550QL can be determined using the linear interpolation defined in Eq. (3-7), as follows:

$$Extra_{S550QL} = 0.2516 \cdot 550 + 172.27 = 310.65 \text{ €/t } (460 < f_y < 620 \text{ MPa})$$

Consequently, based on the values of Table 3-6, and using the medium base price level defined in Table 3-3, the relative price of S550QL is computed using Eq. (3-8):

$$\frac{c_{S550QL}}{c_{S235J2}} = \frac{750 + 310.65 + 39 + 15 + 28 + 24 + 21.56}{750 + 26 + 0 + 15 + 28 + 24 + 21.56} = 1.374$$

Stroetmann provided in 2011 the relative price of 1.354 for S550QL.

Example 3-3. Relative price prediction for S890QL and a low base price level

According to the linear interpolation expressed in Eq. (3-7), the grade extra for S890QL is:

$$Extra_{S890QL} = 0.5 \cdot 890 + 1 = 446 \text{ €/t } (f_y > 620 \text{ MPa})$$

Consequently, considering the values of Table 3-6 and the low base price level defined in Table 3-3, the relative price of S550QL is:

$$\frac{c_{S890QL}}{c_{S235J2}} = \frac{500 + 446 + 135 + 15 + 28 + 24 + 21.56}{500 + 26 + 0 + 15 + 28 + 24 + 21.56} = 1.903$$

Johansson provided in 2005 the interpolated relative price of $\sqrt{\frac{890}{235}} = 1.946$ for S890QL.

3.3.5. Results

According to the validation, both literature trends are validated but Johansson's interpolation does not provide a good correspondence for TM steels and this trend would even be over-conservative in periods of high base prices. Based on these two comparisons, this study confirms that the differences in the literature relative prices can be explained by the improvement in the production process between 2005 and 2011, as stated in the RUOSTE project [80] as well as by fluctuations in base prices which significantly affect the relative prices. Regarding the production process improvement, thermomechanical treatment is now preferred for achieving high-strength properties for structural applications due to its better welding performance and this production change has led to lower relative prices for high-performance grades.

For hot-rolled sections, the maximum yield strength available in Europe is currently 500 MPa (on special order since 2019) while 550 MPa (grade 80) is already available in the USA. The S550 is likely to appear in the medium term on the European market following the revision of EN10025 (which takes place every 3-4 years). Similarly, as for the previous section typologies, the relative price investigations are based on a selected example (see Eq. (3-9)), specifically a HEA160 profile in S355JR. The values of the various extras are extracted from an ArcelorMittal pricelist [199].

$$Price = 800 + 15 + 50 + 35 + 15 + 25 = 940 \text{ €/t} \quad (3-9)$$

As expressed in Eq. (3-9), for hot-rolled sections, there are two types of extras related to the section's geometry: extras depending on the profile range (HEA, HEB, HD, IPE, ...) and extras depending on the profile category within a range (HEA100, HEA120, HEA140, ...). The considered reference values are extracted from several ArcelorMittal pricelists of 2015, 2016 and 2017 [200] which were available online.

3.3.5.1. Estimation of grade extras for hot-rolled sections

All consulted ArcelorMittal pricelists for hot-rolled sections report the same grade extras as shown in Table 3-7. As S500M and S500J0 appeared in the last versions of corresponding product standards released in 2019, no values were available for these grades before that year.

Steel specification	ArcelorMittal pricelists 2015, 2016 & 2017
S235J0	Base
S235J2	20
S275J0	Base
S275J2	20
S355J0	40
S355J2	50
S460J0	80
S355M / Histar® 355	60
S460M / Histar® 460	100

Table 3-7. Grade extras for hot-rolled sections from recent ArcelorMittal pricelists (€/t).

As can be seen, the grade extra increases with the yield strength. This statement is correct for all the collected pricelists except for British sections (according to Corus, Tata Steel and British sections [201], [202], [203]) as reported in Table 3-8.

Steel specification	Corus Long products 2010	Tata Steel Sections 2013	British Sections 2020	British Sections 2023
S275JR	Base	30	30	/
S275J0	25	40	40	/
S275J2	30	80	80	/
S355JR	30	Base	Base	/
S355J0	40	10	10	Base
S355J2	85	40	40	30
S355K2	110	80	80	80

Table 3-8. Grade extras for British sections (£/t).

As can be seen in Table 3-8, the grade extra for S275JR is unexpectedly higher than for S355JR since 2013. This non-growing trend can be explained by the market share in the United Kingdom. According to an estimated market share presented in 2015 [48], steel is the most commonly used material in the building sector in the UK, accounting for 70% of the market share, while it only represents 20% in the Benelux, 20% in France and only 10% in Germany. Furthermore, producers tend to push for the use of S355 instead of S235. It is worth noting that while S355 is the most commonly used steel grade in the UK, S235 remains the preferred choice in other European countries [48].

Although steel grades higher than S500 do not exist in the European steel market yet, it is necessary to propose realistic values for a prospective study. Starting from Eq. (3-9), it is required to propose realistic extrapolations for the grade extras of steel grades higher than S460 (Fig. 3-10).

The area of possible values in Fig. 3-10 has been obtained by considering two different extrapolations i.e. the upper boundary by assuming a bi-linear extrapolation of the existing values for hot-rolled sections based on the slopes defined in Eq. (3-4) related to TM steels for cold-forming and the lower boundary by the linear extrapolation of the first slope up to S700 in a conservative approach.

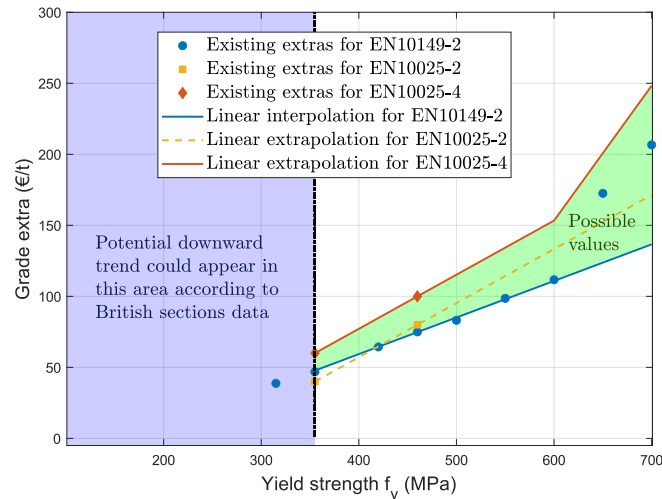


Fig. 3-10. Determination of realistic grade extras for future emerging hot-rolled section grades.

Several arguments support the consideration of similar values for sections as for hot-rolled coils, these include:

- The as-rolled steel grade extra for S355J0 is the same for both typologies (+40€/t) and it should become the basis grade for sections according to [48]. In addition, steels from EN10025-2 [53] reveal similar values for S355J0/S355MC and S460J0/S460MC (a difference of 5€/t);
- For thicker elements, the need for alloying elements increases. It is for this reason that a range has been considered but it appears that the grade extras are more sensitive to the production process than the chemical compositions. Besides, heavy plate pricelists show an identical evolution for the “MC” quality and for the “M” quality [197]. As a reminder, both are produced via a thermomechanical process that requires less carbon and alloy content for better weldability than QT steels [76]. Therefore, it makes sense to expect a similar trend for grade extras;
- According to a pricelist for hot-rolled coils, the grade extras for S355MC and S460MC were respectively 60€/t and 95€/t in 2009. These values are similar to the current ones for long products in S355M and S460M. According to Fig. 3-10, as for thermomechanical hot-rolled coils, it is reasonable to assume that the grade extras for S355M and S460M will likely decrease when the demand for new emerging steel grades such as S500M or S550M will increase in the long product steel market.

Although there are differences in chemical compositions between steel quality typologies, especially between steels from EN10149-2 [57] and EN10025-4 [54], these differences have only a slight effect on grade extras as they are determined by the competitive market. However, due to these differences and the dependence on base prices and section thickness, realistic ranges of values have been established for future emerging section grades. According to Fig. 3-10, realistic grade extra ranges for future emerging steels can be proposed such as [50; 60] €/t for S355, [75; 100] €/t for S460, [85; 115] €/t for S500, [98; 134] €/t for S550, [112; 153] €/t for S600 and [137; 248] €/t for S700.

3.3.5.2. Relevant relative price ranges

The production route for semi-finished products used in sections tends to be electrical furnaces (EAF), while basic oxygen furnaces (BOF) are more commonly used for coils. In addition to the variability of grade extras due to the chemical compositions, the production route directly affects the base price. A range of relative prices can be established based on the previous grade extra intervals, taking into

account low and high base price values to account for the production route, as well as time fluctuations according to the levels defined in Table 3-3. The lower bound is obtained by considering the high base price level with the lower bound of grade extra while the upper bound is conservatively obtained by considering the low base price level with the upper bound of grade extra.

The results are represented in Fig. 3-11 with all the collected values for all steel grades for the sake of interval validation.

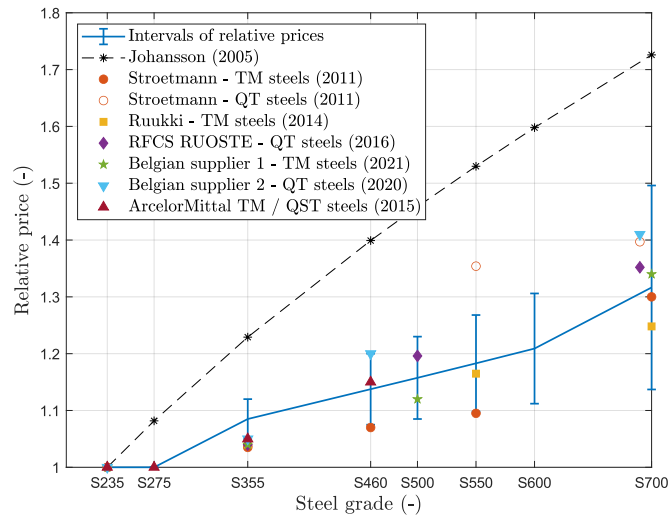


Fig. 3-11. Establishment of reliable relative price intervals for steel grades up to S700.

As can be seen in Fig. 3-11, all collected data confirm the relative price ranges and illustrate the variability due to the production process and base price fluctuations over time. Indeed, for steels according to EN10149-2 (TM steels for cold-forming) [57] with a low concentration of alloying elements, the values are positioned below the mean relative prices. Conversely, for steels according to EN10025-6 (quenched and tempered) [56], the values are positioned above the mean relative prices. However, most of the collected data falls within the determined relative price ranges, indicating the reliability of the latter in assessing the economic benefits of existing and emerging steel grades for hot-rolled sections.

The European project RUOSTE [80] suggests that cold-formed tubular sections will undergo the same evolution as plates. These values are also recommended in a handbook for the design of high-strength hollow sections by SSAB [204]. Consequently, the established relative price ranges can also be applied to hollow sections for a prospective study on the economic benefits of using high-strength steel grades for this section typology. It is even on the safe side as the base price for hollow sections is generally higher than for other sections, resulting in lower relative prices. A detail of the range boundaries computation for grade S500 is provided in Example 3-4.

It is important to note that the above relative prices were established assuming that the same profile was made of different grades of steel. However, in an actual design process, the use of steel with a higher yield strength often results in a reduction of the required cross-section and, so a reduction of one or even several profile sizes. Other aspects such as dimensions, blasting and painting may also benefit from the size reduction. In this manner, the established ranges are therefore conservative.

Although cost remains a primary driver, environmental considerations are becoming increasingly important as discussed in Chapter 1, so it is appropriate to establish a similar relationship including the carbon footprint of high-strength materials.

Example 3-4. Establishment of a relevant relative price range for S500.

According to the grade extra intervals defined in Section 3.3.5.1, the grade extra value for S500 grade ranges from 85 €/t to 115 €/t while no grade extra applies for the basis grade (S235). Considering the low and high base price levels defined in Table 3-3, the lower and upper limits of relative prices for S500 can be conservatively derived as follows.

$$\text{Lower bound: } \frac{C_{S500}}{C_{S235}} = \frac{1000 + 85}{1000 + 0} = 1.085$$

$$\text{Upper bound: } \frac{C_{S500}}{C_{S235}} = \frac{500 + 115}{500 + 0} = 1.230$$

Therefore, the relative price range for S500 is [1.085 1.230] with a mean value of 1.16. If S355 is used as the reference instead of S235, the new range is obtained by dividing the result by the lower boundary for S355, i.e. [1.085 1.230] / 1.05 = [1.033 1.17]. An industrial exchange has validated 1.17 as the upper boundary value for this maximum marketed grade for hot-rolled sections. Furthermore, the RUOSTE European project has provided a value of 1.15 for S500 for both tubular cold-formed sections and plates, which is included in the established range. As a result, the established range of relative prices is deemed suitable for conducting parametric studies.

3.4. Establishment of reliable relative carbon emissions

The introduction highlights the growing importance of considering environmental factors from a global perspective. The thesis contextualises this by emphasising the need to address the environmental impact of using high-strength steels. Despite common misconceptions, the steel sector is constantly evolving with a concern for quality, safety and economic efficiency through the development of new products. For instance, the yield strength that can be achieved by the steel production route is constantly increasing thanks to chemistry (alloying elements) and production improvements (melting, quenching, tempering, thermomechanical processing, ...). This increase in yield strength offers an opportunity to create more sustainable structures through weight and energy savings. In a similar way as for the economic investigations, evaluating the environmental impact of high-strength steels requires a clear understanding of the evolution of the environmental parameters, such as the global warming potential (GWP) in relation to yield strength. Consequently, this section aims to provide insights regarding the relative carbon footprint increases as a function of steel strength to enable comparative studies on the environmental benefit of using high-strength steels.

3.4.1. Background on production emissions

Industries are striving to reduce their carbon emissions in order to respect the objectives of energy transition and carbon neutrality. The steel industry's emissions are divided into three main scopes as defined by the Greenhouse Gas Protocol, namely:

- *Scope 1*: Direct emissions resulting from steel production;
- *Scope 2*: Indirect emissions related to energies (electricity, heat, or steam);
- *Scope 3*: Indirect emissions of the supply chain that differ from energies such as transport-related activities, waste disposal, outsourced activities, ...

Direct emissions are those that are owned and controlled by the steel producer, while indirect emissions are a consequence of the producer's activities. The decarbonisation roadmaps of various steel producers, presented in Chapter 1, mainly target the reduction of emissions from Scopes 1 and

2. Indeed, emissions from Scope 1 are under their ownership, so they focus on the production emissions of crude steel. For those of Scope 2, they are striving to sign new energy agreements for the use of more renewable energy sources. By contrast, emissions of Scope 3 which are categorised as consequential emissions resulting from production activities, such as raw material production or transport are often overlooked. According to the document of the International Energy Agency (IEA) report [205], it seems that future decarbonisation targets do not cover CO₂ emissions resulting from the use of micro alloys as these are included in Scope 3 emissions.

Firstly, it is appropriate to make the distinction between passive and active structures. Active structures include cars, trucks or trains while passive structures are more like buildings, furniture, etc. Active structures benefit from an initial weight saving during their entire lifecycle while passive structures only save on material resources during the production stage. Indeed, reducing the weight of a car not only reduces the amount of material used but also decreases fuel consumption during the use phase of the car lifecycle. This thesis only considers steel passive structures, for which no environmental savings are expected during the use stage. Therefore, the investigation focuses mainly on the production stage, as also assumed for relative price investigations (see Table 3-1). Consequently, the focus is made on the carbon emissions resulting from the production of the different steel grades, and particularly the global warming potential of the production stage (modules A1 to A3 as defined in Table 3-1).

The global warming potential (GWP) in the process of metal production is a conversion factor used to compare the impact of various greenhouse gases on the climate system. The GWP of the production stage depends on:

- *The steel production route*

All steel products can be produced by each of the steelmaking routes listed in Table 3-9. Nonetheless, flat products such as hot-rolled or cold-rolled plates and coils are mainly produced via the BOF route while long products such as sections or rebars are rather produced by a mix between BOF and EAF routes. Currently, the BOF route accounts for 71% of total steel production, while the EAF route accounts for 29%, crude steel is then rolled into finished steel products [14].

Steelmaking route	Blast furnace – basic oxygen furnace (BF-BOF)	Direct reduced iron (DRI) followed by an EAF	Electric arc furnace (EAF)	EAF with renewably produced electricity
<i>Main input</i>	Coal and iron ore	Direct reduced iron	100% scrap	100% scrap
<i>Main CO₂ source</i>	Chemical interaction between carbon and iron ore	Emissions from purchased electricity	Emissions from purchased electricity	Emissions from purchased electricity
<i>Emissions (incl. rolling mill)</i>	2.25 - 2.8 t CO ₂ eq/t	1.12 - 1.35 t CO ₂ eq/t	0.62 - 0.85 t CO ₂ eq/t	0.3 t CO ₂ eq/t

Table 3-9: CO₂ intensity of steel production depending on the production route.

In 2021, ArcelorMittal launched a new brand of steel called XCarb® for products made via the EAF route using 100% scrap steel and powered by renewable electricity to offer steels with very low levels of CO₂ emissions per tonne of finished steel (around 0.3 t CO₂ eq/t as reported in Table 3-9) [206]. However, the global steel demand exceeds the supply of scrap, this is the

reason why the BOF route is still maintained. Currently, the quantity of recycled steel can only meet approximately 30% of the total steel demand [13] given the long service life of steel in structures. Therefore, there are two simultaneous goals for decarbonising steel production, namely: decarbonising the BOF route and developing the use of EAF with renewable electricity as the primary energy source. Similarly to the effect of base prices on relative prices, it is important to account for the production route when establishing the relative carbon emissions of high-strength steels. Table 3.9 provides evidence of the significant differences in associated footprints between production routes.

- *The steel production process* - As rolled (AR), Normalised (N), Thermo-mechanically rolled (M) and quenched and tempered (Q);
- *The chemical compositions of steel* - alloys significantly affect the environmental impact of steel.

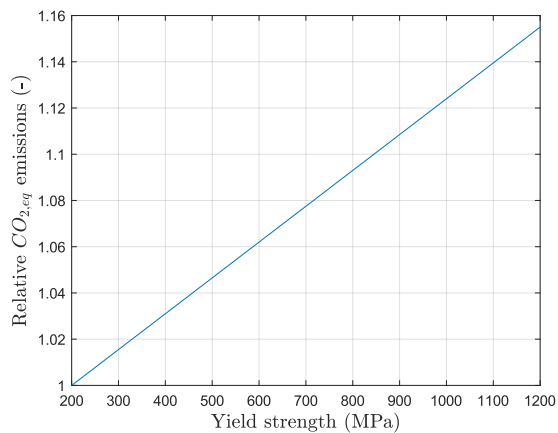
As stated in Chapter 2, specific information relating to construction materials or products is disseminated using Environmental Product Declarations (EPD). These standardised documents contain quantitative data on the environmental impact of a product throughout its entire life cycle, including global warming potential, smog creation, ozone depletion and water pollution. EPDs are produced based on Life Cycle Assessment (LCA) calculations in accordance with ISO14025 [207] and EN15804 [208] standards. These declarations are typically written by steel manufacturers or by associations, such as Bauforumstahl or Asociación Sostenibilidad Siderúrgica. It might be thought that such documents could be used to compare products with different yield strengths but currently, the available EPDs on the market do not provide, or only partially provide, GWP values depending on the yield strength. Besides, the Bauforumstahl EPD ([94]) mentions the following sentence: "This EPD is valid for structural sections and merchant bars of various steel grades and different forms of delivery". In addition, ArcelorMittal provides an EPD for their HISTAR® trademark. HISTAR® is a structural fine-grain steel grade complying with the requirements of the European Technical Approval ETA-10/0156 [68]. The producer markets two grades, HISTAR®355 and HISTAR®460, which are produced using quenching and self-tempering (QST) processes and via the EAF production route. Traditional steel grades, on the other hand, are rather produced via the classical BOF route. Therefore, it is not possible to compare the yield strength impact on the total carbon emissions between the different grades based on these documents.

As expressed in Chapter 2, a project called "The environmental value of HSS structures" has been already conducted within the framework of the Steel Eco-Cycle project (2004-2012) [95], [96], [97], [98]. In this project, the Swedish steel industry carried out a series of cradle-to-gate analyses in collaboration with the Swedish Environmental Research Institute and provided carbon emission evolutions as a function of yield strength and steel typology (Fig. 2-7). The Gabi database was used to get general data such as alloying elements as well as transportation requirements to establish the reported evolutions in Fig. 2-7. It should be noted that the term "sections" in this context refers to cold-formed hollow sections (EN10219 [60]). As can be concluded regarding Fig. 2-7, the carbon emissions are more affected by the steel quality than by the yield strength, due to significant differences in alloying content between qualities. For instance, hot-rolled steels are lower embodied CO₂ than cold-rolling steel because of the additional cold-rolling process. The explanation for the higher values given for hot-dip galvanising comes from the chemical compositions as these steels contain more alloying elements. This feature can be confirmed by examining the GWP of modules A1 to A3 (production stage) given by EPDs from two manufacturers [209], [210] as reported in Table 3-10.

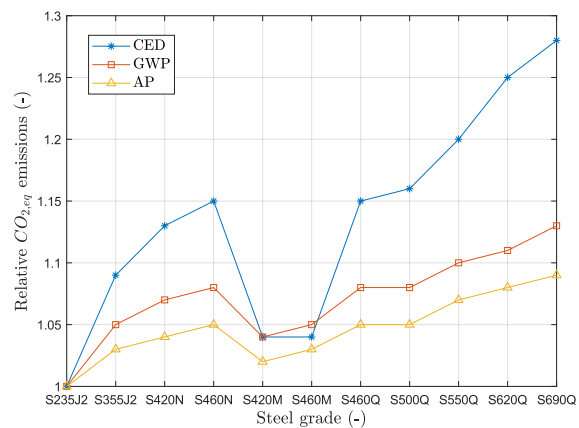
Producer	ArcelorMittal	SSAB
Hot dip galvanised steel (Zinc coating): EN10346	2.56	2.42
Hot rolled coils: EN10149-1, EN10025-1 to 4	2.23	2.16
Hollow sections: EN10210-1 & EN10219-1	2.27	2.30
Heavy plates: EN10025-1 to 6	2.60	2.71
Structural sections and bars (mix BOF and EAF)	0.84	/

Table 3-10. GWP for modules A1 to A3 depending on the typology and the producer (t CO₂ eq/t).

Some papers in literature [95], [96], [97], [98], [116], [211] also provide the relative GWP of high-strength steels as represented in Fig. 3-12. It is worth noting that Fig. 3-12a is applicable for Domex LA / MC trademarks, which corresponds to steels that comply with the product standard EN10149-2 [57]. Stroetmann [116] evaluated the evolution of other environmental parameters, i.e. the cumulative energy demand (CED) and the acidification potential (AP) for heavy plates as illustrated in Fig. 3-12b. The results demonstrate that the CED increases much more for quenched and tempered steels than for thermomechanically rolled steels, due to the presence of other alloying elements such as molybdenum, chromium and silicon, as well as the energy-consuming heat treatment process.



(a) Sperle, 2010



(b) Stroetmann, 2011

Fig. 3-12. Relative GWP of high-strength steels according to the literature.

As can be seen in Fig. 3-12, the relative CO₂ equivalent emissions are between 1.0 and 1.15 up to 1200 MPa. In other words, upgrading from regular to high-strength steel results in a carbon emission increase of less than 15%. This increase is even lower when considering S355J2 as a reference instead of a lower grade. The weight saving should be higher to offset this increase and to present an environmental benefit in considering the high-strength steel grade. As this study focuses on hot-rolled sections, which are mainly produced via the thermomechanical process, the GWP parameter is a relevant environmental parameter.

In conclusion of the literature review, it appears that the yield strength has only a minor impact on carbon emissions, it is even sometimes negligible in terms of relative GWP. However, to validate these observations, the relative GWP of high-strength steels have been evaluated based on their chemical compositions.

3.4.2. Methodology

The Steel Eco-Cycle project [95] states that alloys significantly impact the environmental impact value of steel, particularly in a specific production process. Indeed, greenhouse gases for carbon steel (cradle-to-gate) are cumulative and can be divided as expressed in Eq. (3-10).

$$\begin{aligned}
 GWP = & GWP_{steelworks, \text{ site specific}} + GWP_{Rolling \& \text{ coating, site specific}} \\
 & + GWP_{steelworks, \text{ upstream}} + GWP_{Rolling \& \text{ coating, upstream}} \\
 & + GWP_{alloys, \text{ upstream}}
 \end{aligned}
 \quad (3-10)$$

Upstream emissions refer to emissions that occur before raw materials enter in the steel production mill (production of raw materials, transport, ...). In other words, in Eq. (3-10), the first line corresponds to Scope 1 emissions, the second line to Scope 2 emissions and the third line to Scope 3 emissions, as defined in Section 3.4.1. To increase yield strength, additional alloying elements are added to enhance the yield strength, which can affect the GWP of this grade. Some examples are provided in the handbook of the Steel Eco-Cycle project [95] where it is indicated that the alloy production in the total environmental impact is higher for metal-coated steels than for classical hot-rolled steels due to differences in alloy content. To investigate the impact of alloys on the carbon footprint of steels, databases and literature papers have been consulted to get some values for the production of hardening alloying elements as listed in Table 3-11.

Alloying elements	GWP [kg CO ₂ eq/kg]	Source
Iron (Fe)	1.50	EcoInvent 2.2
Carbon (C)	3.66	CO ₂ =3.66*C
Ferrosilicon (FeSi)	11.34	Gabi 2021.1
Ferromanganese (FeMn)	1.50	IPCC 2006
Niobium (Nb)	12.5	EcoInvent 2.2
Aluminium (Al)	8.12	Gabi 2021.1
Ferrovandium (FeV)	33.1	EcoInvent 2.2
Titanium (Ti)	15.29	Gabi 2021.1
Ferronickel (FeNi)	6.5	EcoInvent 2.2
Ferromolybdenum (FeMo)	11.7	EcoInvent 2.2
Boron (B)	1.50	EcoInvent 2.2
Ferrochrome (FeCr)	2.4	EcoInvent 2.2
Copper (Cu)	3.99	Gabi 2021.1

Table 3-11. Greenhouse gas emissions of alloying elements [kg CO₂ eq/kg] according to [212], [213], [214].

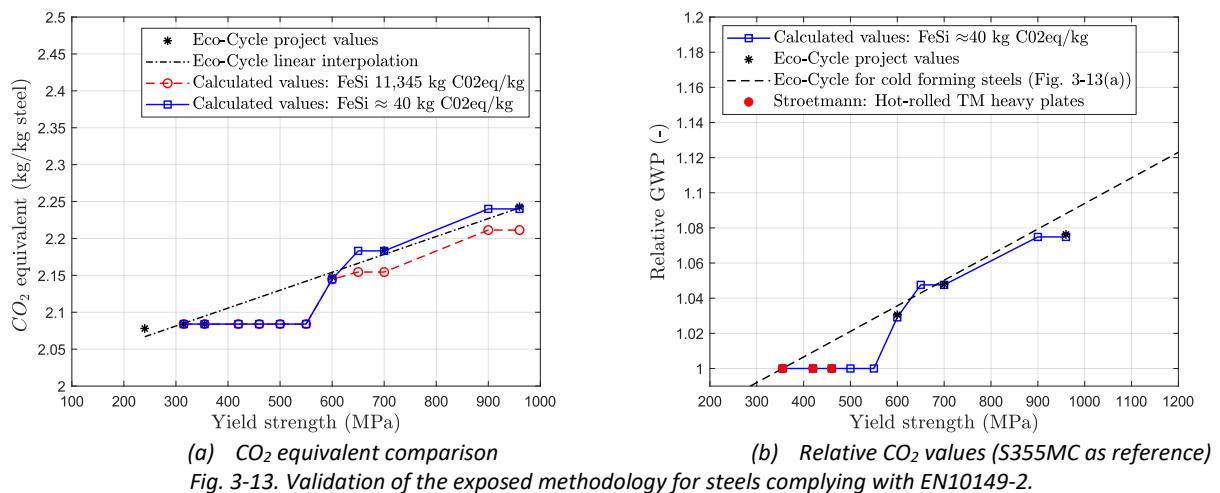
The pursued methodology consists of evaluating, for a given steel category, the relative GWP of high-strength steels based on their chemical compositions as it appears that differences in emissions between steel grades result from the production emissions of additional alloying elements. The upper threshold of the alloy percentages will be considered given that these maximum values are provided in the corresponding product standard. This approach is conservative as it may slightly overestimate the relative GWP of high-strength steels. The GWP of a given steel grade can therefore be conservatively derived through Eq. (3-11).

$$GWP_{grade} = GWP_{reference} + \sum_{i=1}^m \Delta_{alloy_i} \cdot GWP_{alloy_i} \quad (3-11)$$

where, $GWP_{reference}$ is the reference global warming potential for a given steel grade of a product category, m is the number of alloying elements present in the steel chemical compositions of this steel category, Δ_{alloy_i} is the difference between the percentage of the steel alloy “ i ” for the studied grade and the reference steel and GWP_{alloy_i} is the unitary GWP for the production of alloy i according to Table 3-11. The methodology has been validated using existing values from scientific literature for thermomechanically hot-rolled coils for cold-forming according to the chemical compositions of EN10149-2 [57], and for cold-formed hollow sections according to EN10219-3 [60].

3.4.3. Validation

The methodology developed reveals that the linear interpolation used in the scientific literature for high-strength low-alloy steels is unrealistic, as shown in Fig. 3-13. This is because the chemical composition remains unchanged up to S550MC, as only the Manganese (Mn) content changes to achieve higher yield strengths. Then, Titanium (Ti), Molybdenum (Mo) and Boron (B) must be added to the chemical compositions to reach higher yield strengths, as can be seen in Table 3-5. This explains the origin of the step in the evolution between S550MC and S600MC for steels belonging to EN10149-2 [57]. The first computation gave a good correspondence with literature emissions up to this step, but there is a small gap thereafter. As can be seen in Fig. 3-13a, this small gap may be explained by the emission factor of the Ferrosilicon (FeSi) production which may be underestimated in Table 3-11. Indeed, Ferrosilicons usually contain varying percentages of pure silicon (15%, 45%, 75% or 90%) and the production emissions differ accordingly. For instance, to obtain pure silicon, the environmental footprint is 85.6 kg CO₂ eq/t steel according to the EcoInvent 2.2 database which is almost eight times higher than the value in Table 3-11, the reality seems to be an intermediate value according to Fig. 3-13a.



It should be noted that the conclusion is comparable to the price investigations for steels from EN10149-2 [57] as when some hardening alloys must be added to reach higher yield strengths (i.e. from 600 MPa), the relative prices (respectively the carbon emissions) are affected by the unitary price (respectively the unitary GWP) of the corresponding alloying elements. A detail of the CO₂ equivalent computation for S600MC is provided in Example 3-5.

Example 3-5. CO₂ equivalent computation detail for S600MC

According to Table 3-5, the chemical compositions of S315 MC and S600MC including the iron content are:

Steel grade	Chemical composition in %. max											
	C	Mn	Si	P	S	Al (min)	Nb	V	Ti	Mo	B	Fe
S315MC	0.12	1.3	0.5	0.025	0.002	0.015	0.09	0.2	0.15	-	-	97.6
S600MC	0.12	1.9	0.5	0.025	0.015	0.015	0.09	0.2	0.22	0.5	0.005	96.4

Manganese, titanium, molybdenum and boron chemical elements must be added to reach a yield strength of 600 MPa. The methodology is illustrated for S600MC by using Eq. (3-11) and the unitary GWP listed in Table 3-11.

$$\begin{aligned}
 GWP_{grade} &= GWP_{reference} + \sum_{i=1}^n \Delta_{alloy_i} \cdot GWP_{alloy_i} \\
 &= 2.084 + (0.019 - 0.013) \cdot 1.5 + (0.0022 - 0.0015) \cdot 15.297 + 0.005 \cdot 11.7 + 0.00005 \cdot 1.5 \\
 &\quad + (0.964 - 0.976) \cdot 1.5 \\
 &= 2.144 \text{ kg CO}_2 \text{ eq / kg steel (Eco-Cycle project: 2.148 kg CO}_2 \text{ eq / kg steel)}.
 \end{aligned}$$

A second validation has been conducted for cold-formed hollow sections for which high-strength steels already exist. The same methodology has been applied considering the chemical compositions prescribed in EN10219-3 [60] and the carbon footprint of S355MH given in Fig. 2-7. The results are presented in Fig. 3-14.

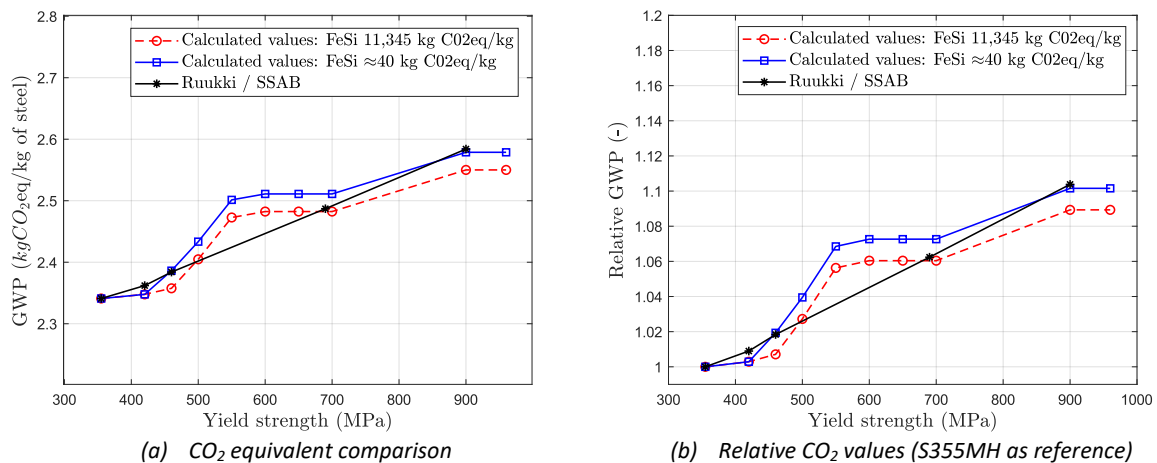


Fig. 3-14. Validation of the exposed methodology for cold-formed hollow sections (acc. to EN10219-3 [60]).

Fig. 3-14 demonstrates that the methodology can capture the evolution trend. The slight differences can be attributed to the fact that the literature data represent mean values for tubes, sections and tube lattices. Furthermore, depending on the database, there are some variations of the carbon factor for the hardening elements, as already expressed for the Ferrosilicon element. Therefore, the obtained results are considered acceptable for estimating carbon emissions. Example 3-6 provides a calculation of the CO₂ equivalent for S550MH based on the developed methodology.

Example 3-6. CO₂ equivalent computation detail for S460MH

According to EN10219-1, the chemical compositions of S355MH and S460MH focusing on strengthening alloys including the iron content are:

Steel grade	Chemical composition in %. max											
	C	Mn	Si	Cr	Ni	Al (min)	Nb	V	Ti	Mo	Cu	Fe
S355MH	0.14	1.5	0.5	-	0.3	0.02	0.05	0.10	0.05	0.2	-	97.1
S460MH	0.16	1.7	0.6	-	0.3	0.02	0.05	0.12	0.05	0.2	-	96.8

A series of hardening micro-alloys must be added to reach such a yield strength. Knowing that the carbon footprint (cradle-to-gate) of S355MH is 2.341 kg CO₂/kg. The computation of the GWP of S460MH is derived as follows:

$$GWP_{grade} = GWP_{reference} + \sum_{i=1}^n \Delta_{alloy_i} \cdot GWP_{alloy_i}$$

$$= 2.341 + (0.0016 - 0.0014) \cdot 3.66 + (0.017 - 0.015) \cdot 1.5 + (0.006 - 0.005) \cdot 11.34$$

$$+ (0.0012 - 0.001) \cdot 33.1 + (0.971 - 0.968) \cdot 1.5$$

$$= 2.358 \text{ kg CO}_2 \text{ eq / kg steel or } 2.387 \text{ kg CO}_2 \text{ eq / kg steel if } GWP_{Si} = 40 \text{ kg CO}_2/\text{kg}$$

The value from Ruukki is 2.384 kg CO₂ eq / kg steel.

This validation demonstrates that changes in alloying elements to achieve higher strengths inevitably lead to an increase in steel production emissions. Therefore, a simplified approach consisting of evaluating the GWP of a given grade with the maximum percentage differences of chemical elements prescribed in corresponding product standards can be used to align with values resulting from cradle-to-gate analyses in the literature. The significance of upstream emissions in determining the global environmental footprint of a product has been demonstrated. Therefore, in future decarbonisation roadmaps, it is essential to consider Scope 3 emissions as well.

3.4.4. Results

Based on Stroetmann's values (Fig. 3-12b), the relative GWP remains constant for yield strengths up to 460-500 MPa, regardless of the steel quality, even for heavy plates. Therefore, the developed methodology has also been applied to as-rolled steels (EN10025-2), thermomechanically hot-rolled steels (EN10025-4) and steel produced by quenching and self-tempering process (QST) to determine if similar conclusions can be drawn for other steel qualities. The reference emission for S355 is taken as 1.13 t CO₂ eq/t, according to a Bauforumstahl EPD for sections and heavy plates [94]. This EPD is considered as a reference in Europe for structural steel-products. The production shares in this EPD are 26% for the Basic Oxygen Furnace route (primary steel production) and 74% for the Electric Arc Furnace route (secondary steel production), which are realistic current market shares for steel sections, according to the World Steel Association [14]. All results are shown in Fig. 3-15 for each relevant steel quality.

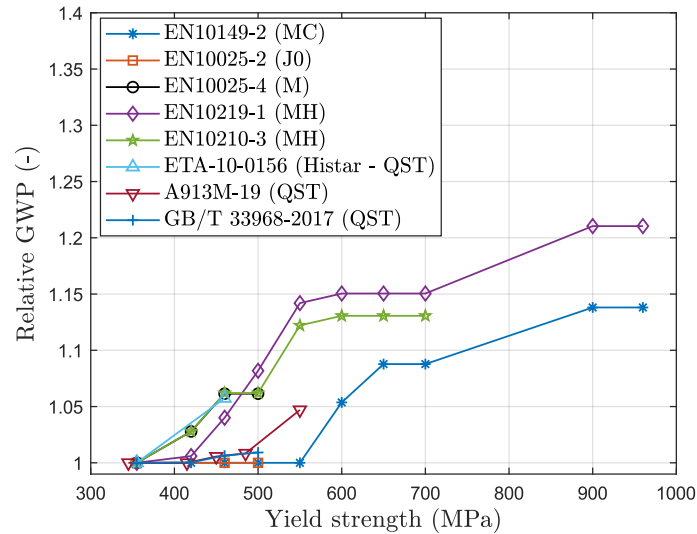


Fig. 3-15. Evolution of GWP as a function of yield strength and steel quality [53], [54], [57], [59], [60], [66], [67], [68].

In conclusion, the relative GWP remains constant at 1.0 until S500M-S550M for products covered in EN10149-2 [57], EN10025-2 [53] and for steels produced by the QST process [66], [67] because their chemical compositions do not change significantly until S500. Although the manganese content changes, the increase is offset by the reduction in iron content, resulting in identical unitary emissions (Table 3-11). Nonetheless, for EN10025-4 [54], EN10210-3 [59] and EN10219-3 [60], the alloy content increases with yield strength, which has an impact on the relative emissions as shown in Fig. 3-15. This is explained by the fact that thermomechanical high-strength steels use microalloying elements such as niobium (Nb) to develop fine grains to enhance low-temperature toughness performance and Vanadium (V) is also added to straighten those steels [76]. It is important to keep in mind that the methodology used is a rough estimation with upper percentages as given in the corresponding product standards, so the relative emissions are likely to be lower. Furthermore, thermomechanical steels present some other advantages such as the fine grain structure leading to a reduction of the crack risk after welding (good cold formability and toughness). Additionally, it has low carbon equivalent values, which usually eliminates the need for preheating before welding, resulting in significant time, cost and environmental savings.

With regards to the corresponding QST grades for the American steel market as prescribed in A913M-19 [66] and the Chinese equivalent grades from GB/T 33968-2017 [67], the maximum chemical percentages remain relatively unchanged up to Grade 70 (485 MPa), Q500 QST (500 MPa). Only a slight change in the Vanadium (V) content is contemplated, therefore no significant changes in terms of carbon emissions are observed in Fig. 3-15. This confirms that for steels produced by the quenching and self-tempering process (QST), the increase in carbon emissions is likely to be negligible up to 500 MPa, similarly to steels complying with EN10149-2 [57] and EN10025-2 [53].

Furthermore, the amplitude of Scope 1 and Scope 2 emissions influences such conclusions. In the upcoming years, producers will continue to grow the proportion of steel produced through the EAF route to achieve their carbon footprint reduction targets and to reach carbon neutrality by 2050; Scope 1 emissions will thus decrease. Moreover, the steel provenance can also impact steel carbon emissions. According to an AISC document about global warming and hot-rolled structural sections [215], hot-rolled sections produced in China emit 2.94 tonnes of CO₂ eq/t while the same sections in the US emit 0.98 tonnes CO₂ eq/t (cradle-to-gate scope). This difference can be attributed to the different production routes but also to the electricity production, as China still relies heavily on coal-fired

generation (Scope 2 emissions). Nevertheless, the same reference emission coming from the Bauforumstahl EPD has been considered regardless of the steel provenance. The impact of the production route on relative carbon emissions is the same as the impact of the base price on the relative prices, i.e. when the CO₂ intensity of steel production becomes lower by using low-carbon electricity in the EAF route for instance, the impact of micro-alloying production emission become larger on the relative emissions of high-strength steel grades. This feature has a negative impact on the environmental benefit of using high-strength steels. Therefore, the investigations demonstrate the necessity of targeting Scope 3 emissions related to the carbon footprint of alloy production to keep a benefit in increasing the yield strength, even though these emissions are not under the direct ownership of producers.

3.5. Discussions and conclusions

Steel producers can increase the yield strength of steel grades through adjustments of steel chemistry and process conditions. High-strength steels allow for the use of fewer resources than conventional steel grades while maintaining load-bearing capacity. However, the use of high-strength steel results in increased material costs and carbon emissions when considering the production stage of the life cycle.

On the one hand, as explained based on cost breakdowns, material costs typically represent only 33% of the total cost. Manufacturing costs should only be slightly affected by the yield strength increase given other costs (such as shot blasting, painting, transport, etc.) are generally positively affected by this increase in yield strength. This is due to the material savings resulting from the use of these steels, which leads to a reduction in surface area and weight. Furthermore, this weight gain compensates for the increased material costs, resulting in economic benefits when using these steels. Finally, as demonstrated, for certain types of sections, these steels are not yet commercially available or are only used when normal steel grades are no longer sufficient in terms of resistance. Demand for these steels will likely increase once their economic benefits are proven. As steel is a primary material, its prices are governed by the law of supply and demand. Therefore, base prices will continue to fluctuate over time, and it has been shown that, when the base prices of steel are high, the economic benefit of using these high-strength steels is higher because the impact of grade extras on the relative prices becomes negligible. To account for the variability linked to base price fluctuations, a proposal for relative price ranges was made at the end of the relative price investigations. These established ranges have been validated as all collected values fall within them.

On the other hand, this chapter demonstrates that the reduction in carbon emissions can be estimated as equal to the percentage of weight savings. This is because the increase in the relative carbon emissions resulting from using a higher yield strength is not significant up to S500 for several low-alloy steel qualities. This conclusion has been achieved through a developed methodology that evaluates the steel carbon footprint of a grade based on the maximum alloying contents prescribed in product standards. This methodology has been applied to all steel specifications for which grades higher than 460 MPa exist. Fig. 3-16 displays the obtained relative carbon emissions with the relative price ranges (Fig. 3-16) considering S235 or S355 as a reference and other values from the literature [96], [116] for the sake of comparison.

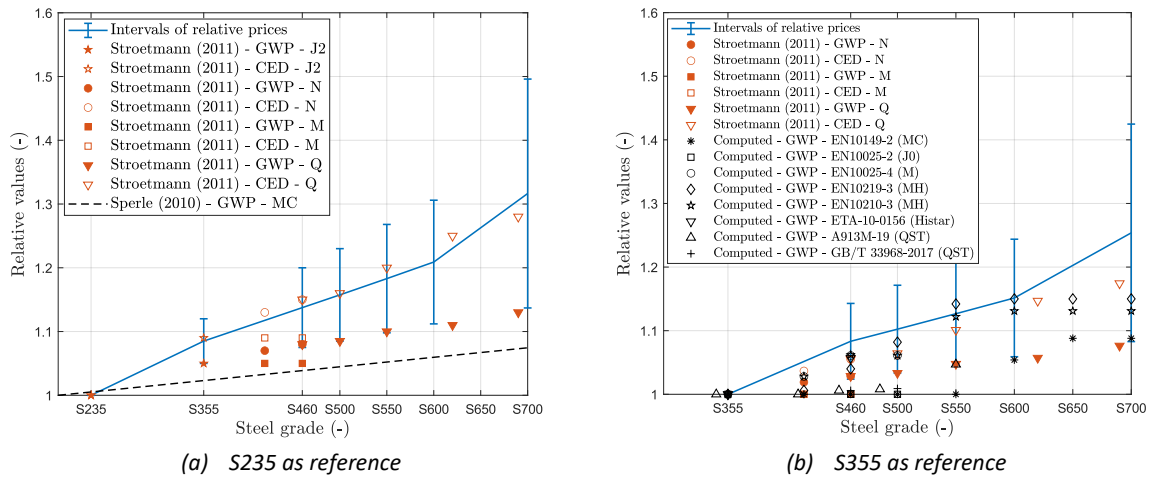


Fig. 3-16. Comparison between established relative prices (blue ranges) and relative carbon emissions.

Fig. 3-16 shows that the relevant environmental parameters (GWP and CED) of different steel productions are generally below the medium level of established relative prices. Except for quenched and tempered steels (category “Q”), these parameters are even below or equal to the low level of relative prices. Therefore, it is appropriate to consider the ranges of relative prices to justify the economic and environmental benefits of using an increased yield strength. Indeed, according to Fig. 3-16, if the selection of the steel grade is justified from an economical point of view, the so-obtained solution will also be performant from an environmental point of view as the increase of the relative carbon emissions is lower than the one of the relative prices. To conclude Chapter 3, the relative reference values to evaluate the economic and environmental benefits of using an increased yield strength are listed in Table 3-12 (considering S235 or S355 as reference).

Steel grade	Ref. S235			Ref. S355		
	LOW	MEDIUM	HIGH	LOW	MEDIUM	HIGH
S235	1.00	1.00	1.00	-	-	-
S275	1.00	1.00	1.00	-	-	-
S355	1.05	1.08	1.12	1.00	1.00	1.00
S420	1.06	1.11	1.17	1.01	1.06	1.11
S460	1.07	1.13	1.20	1.02	1.08	1.14
S500	1.08	1.15	1.23	1.03	1.10	1.17
S550	1.10	1.18	1.27	1.05	1.13	1.21
S600	1.11	1.21	1.31	1.06	1.15	1.24
S700	1.14	1.32	1.50	1.08	1.25	1.42

Table 3-12. Relative reference values (-) for comparison studies considering S235 or S355 as the reference grade.

Using the established relative reference values, it is possible to derive recommendations for developing and selecting appropriate steel grades, resulting in sustainable designs. Indeed, from the design stage, designers should achieve their design by positioning the right material in the right place enabling efficient exploitation of the material’s mechanical properties. This approach can significantly reduce the carbon footprint and total cost of building construction. However, the development and availability of the appropriate steel grade is a prerequisite, so manufacturers should adapt their product range to offer the possibility of structural optimisation. The following Chapter 4, entitled “The Right Steel at the Right Place”, addresses the crucial discussions for the selection of the appropriate steel grade for key structural members from an economic point of view while complying with the world’s climate and resource challenges.

Chapter 4

The Right Steel at The Right Place

4.1. Introduction

High-strength steels offer several advantages, including a reduction of the amount of material required, particularly for strength-governed members, thereby contributing to the “build less” approach of the hierarchy to net zero presented in Fig. 1-3. Indeed, when the resistance of the material is the design criterion, increasing the yield strength can lead to a significant gain in material usage by drastically reducing the section dimensions. Less material may lead to less environmental impact but also indirect benefits, such as cost and CO₂ emission savings on building foundations, reduced transport and a greater speed of construction. However, the execution of more slender structures is often associated with instability problems or excessive deflections and vibrations. These aspects, which are essential in civil engineering, depend on the modulus of elasticity which is the same regardless of the steel grade and can therefore sometimes limit the potential advantage of using these grades.

Within this context, the following question can be raised: what are the economic and environmental benefits of using high-strength steels in civil engineering?

Based on the research presented in Chapter 3, the aim of this chapter is, therefore, to identify the area of benefit from an economic point of view for existing grades (lower than S500) as well as for grades above the practical range (up to S690) for hot-rolled and hollow sections in steel structures as a prospective study. Additionally, recommendations will be provided regarding the slenderness limits below which using higher grades than the current practical range (above S500) would be advantageous.

The methodology and its validation are first described, and then different structural elements subjected to various loading conditions which are regularly encountered in steel structures are studied in order to compare the different steel grades on isolated members and to derive useful information to guide decision makers on grade selection and development. Finally, based on the knowledge gained with isolated members, the methodology is applied to case studies coming from the literature. The objective of these applications is to demonstrate the savings that could have been made by using high-strength steels on already-built structures.

4.2. Methodology

4.2.1. General structure

The work methodology adopted to achieve the research objectives consists of studying separately the impact of each design criterion on the benefit of using high-strength steels, i.e. to determine what is the appropriate steel grade in each design configuration for a given structural element as depicted in Fig. 4-1.

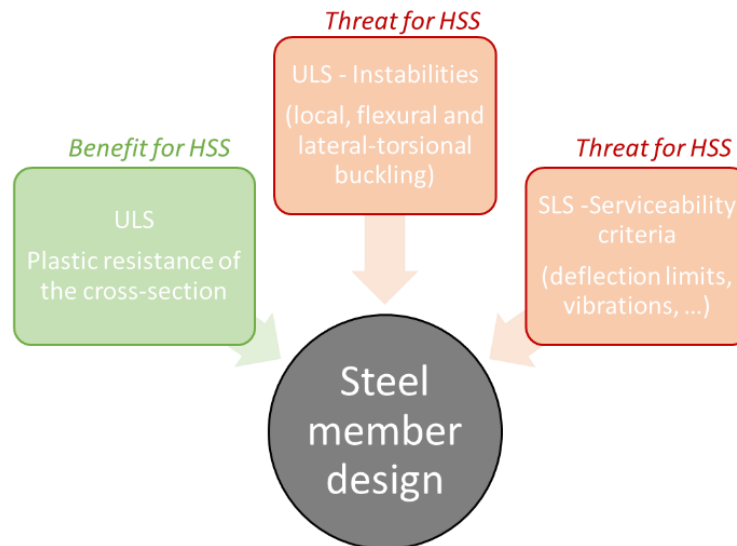


Fig. 4-1. Identification of aspects that govern the design of a steel structural member.

As long as a structural element is subjected to tensile forces, no instability phenomena can appear and affect its structural behaviour. The increase in yield strength thus results in a proportional reduction in the amount of steel used. The increase in material cost resulting from the use of a high-strength steel grade should be less significant than the increase in yield strength to present an economic benefit. This reasoning also applies to stocky elements for which the geometrical dimensions are such that no instabilities can occur. On the contrary, as soon as instability phenomena are likely to dominate the ULS design, the benefit of developing high-strength steels is likely to be reduced. Indeed, instability phenomena induce out-of-plane deformations that are more governed by the Young's modulus than by the yield strength. For very slender elements, the advantage of using high-strength steels may almost disappear as the buckling resistance becomes independent of the yield strength. Finally, to meet SLS criteria, deflections must be strictly controlled, which is also governed by Young's modulus rather than yield strength, so taking SLS conditions into account may penalise the benefit of using high-strength steels. These opportunities and threats for the benefit of using high-strength steels are summarised in Fig. 4-1. The aim of this research is therefore to identify whether there are situations in which the weight saving resulting from the use of high-strength steels will not be fully compensated by the instability phenomena (ULS) or the deflection requirements (SLS). Based on the conclusions obtained regarding the advantages of high-strength steels in terms of resistance to instabilities, the results of an optimisation routine will be presented for the analysis of real isolated members where all these opportunities and threats are simultaneously taken into account.

In the framework of Chapter 4, steel structures composed of beams and columns are analysed. For such applications, the floor is generally composed of a concrete slab and supporting beams. The size of the floor is directly proportional to the building size. According to the document "Steel building in

Europe – Multi-storey Steel Buildings – Part 2: Concept design” (in the framework of the SECHALO project) [216], the width of an office building is about 12m to 15m, which results in two spans of 6m to 7.5m. An example of a classical floor for an office building is illustrated in Fig. 4-2. Spans of 6m for flooring beams constitute a standard for residential buildings.

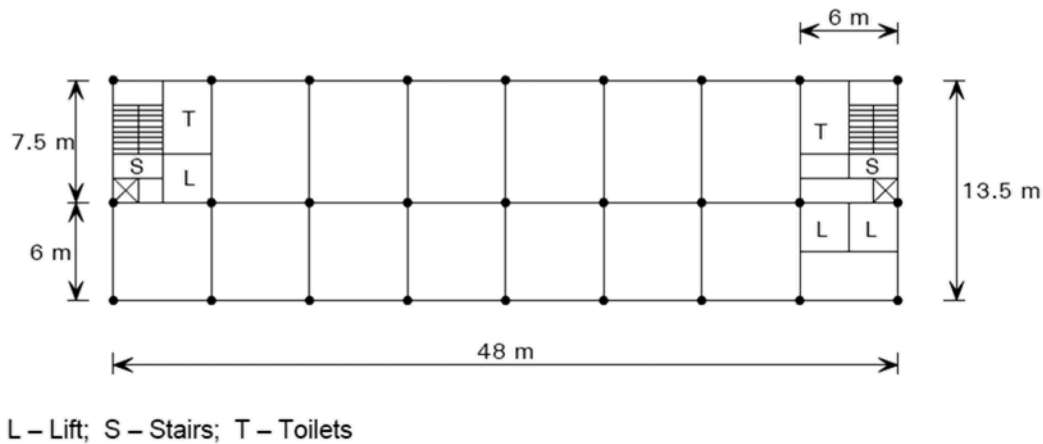


Fig. 4-2. Classical flooring system for an office building [216].

For this order of magnitude, the standard dimensions of steel sections as proposed in product catalogues for hot-rolled sections using mild steel grades (S235, S275, S355 or even S460) are relevant. Consequently, for such applications, the benefit of considering higher yield strength is likely to be limited; this is addressed in this Chapter 4. On the contrary, for exceptional steel structures associated with larger spans (over 20m), hot-rolled sections are no longer suitable and welded I-beams are therefore preferred. However, current investigations about high-strength steels often target welded I-beams, i.e. built-up members with flanges made of high-strength steels, particularly when bending resistance governs the design. Besides there exists research [45], [62], [76], [79], [86], [217], [218] that demonstrated the benefit of high-strength steels in hybrid girders. The scope of this study is therefore limited to the length range for which conventional hot-rolled sections are appropriate.

On the other hand, concerning the steel columns, the standard height of a building floor is generally between 3m and 5m [73], [116], the height being a function of the ceiling height as well as the chosen flooring system. These columns are subject to significant compressive forces in non-sway structures. Indeed, in this type of structure, the horizontal loads are carried by the bracing system and the columns only support the gravitational loads. On the contrary, for columns in sway structures, bending forces are added to the normal forces due to the horizontal forces that must be carried by the columns. Columns subjected to pure compression as well as those subjected to combined compression and bending are covered in this Chapter 4.

For classical buildings, the use of standard hot-rolled profiles in regular steel grades is a current practice. But, for architectural reasons, hollow sections can also be considered for columns. Chapter 4 therefore covers hot-rolled sections and hollow sections, intending to demonstrate the advantages of using high-strength steels for both section typologies.

4.2.2. Assumptions and case studies

High-strength steels (HSS) refer to steel grades between S500 and S690. These grades are today available for plates while, for hot-rolled sections, only steel grades up to S500 can be found on the European steel market. The investigations presented herein can thus be seen as a prospective study to determine whether there is a benefit in developing hot-rolled sections in steel grades above S500. To achieve this objective, comparisons will be performed using the current EN1993-1-1:2005 [70] and

the new version FprEN1993-1-1:2022 [52] of Eurocode 3 part 1-1 by adopting the methodology presented herein. The various individual elements included in the comparisons are reported in Fig. 4-3.

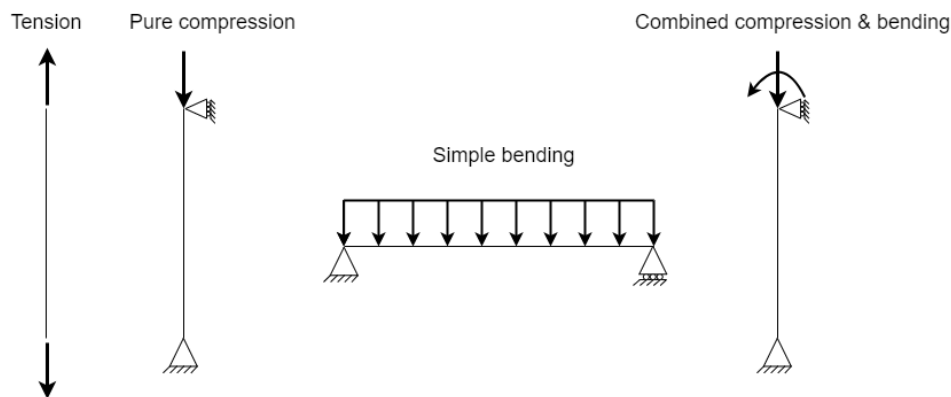


Fig. 4-3. Case studies covered in this research.

For each structural element, the effect of yield strength on each design criterion is first analysed. For instance, the effects of yield strength on the resistance to local buckling as well as to flexural buckling are first addressed before analysing the benefit of using a high-strength steel grade for members prone to both instability phenomena. The definition of load and length ranges to be considered for the different case studies must be established before starting the numerical investigations on the potential benefits of high-strength steels. The buckling lengths for columns are included in $L_{cr} \in [1; 12]$ m to cover non-sway and sway structural systems. For the span of steel beams, the same range of lengths is adopted as it is the range of lengths in which hot-rolled sections are suitable. Regarding the internal forces, an axial force of $N_{Ed} \in [500; 10000]$ kN is considered for columns in compression (up to 30000 kN for HD profile series) and $q_{Ed} \in [1; 120]$ kN/m for beams in bending. These loads are factored and can be directly used for the verification of the ultimate limit states (ULS). Besides that, unfactored characteristic loads must be defined for the serviceability limit states (SLS). In this study, the characteristic loads are assumed to be equal to the factored loads divided by an average safety factor assumed to be 1.4.

Only European hot-rolled steel sections are considered in the scope of this study including H-sections (comprising HEA, HEB, HEM and HD), I-sections (IPE) and hollow sections (CHS, SHS and RHS). These sections are available in a wide variety of sizes through European suppliers.

Some studies have shown that the lighter the structural elements, the more vulnerable they are to fire. The reduction factors associated with fire are also different for these steel grades [81], [82], [83]. The effect of the steel reduction factors is not reflected in the current specifications of Eurocode 3 [52], [70], [71] as the rules provided for steel grades above S460 do not differ from those for mild steels as expressed in Section 2.2.3. It is worth mentioning that investigations are carried out in a cold design situation, i.e. the above-mentioned aspects related to fire are not considered in this thesis. Furthermore, according to the basic dissipative concept called “the strong columns and weak beams” of seismic designs, where plastic hinges take place in the beams, the use of high-strength steels for the columns in combination with lower grades for the beams is suitable to favour the occurrence of the dissipative mechanism [79]. This feature is also beyond the scope of this study, but highly loaded columns are however covered.

Finally, the yield strength is assumed to be equal to the reference nominal values prescribed in Table 2-2 according to the forthcoming standard version FprEN1993-1-1:2022 [52]. Consequently, a yield strength reduction is applied for flange thicknesses greater than 40 mm.

4.2.3. Optimisation procedure and benefit criterion

To compare different steel grades, analytical comparative studies are carried out using the MATLAB software [193]; the objective is to define the cheapest structural element, i.e. the optimum design, respecting the current Eurocode 3 part 1-1 [70] and the new version of part 1-1 [52]. The flowchart of the developed optimisation routine is reported in Fig. 4-4.

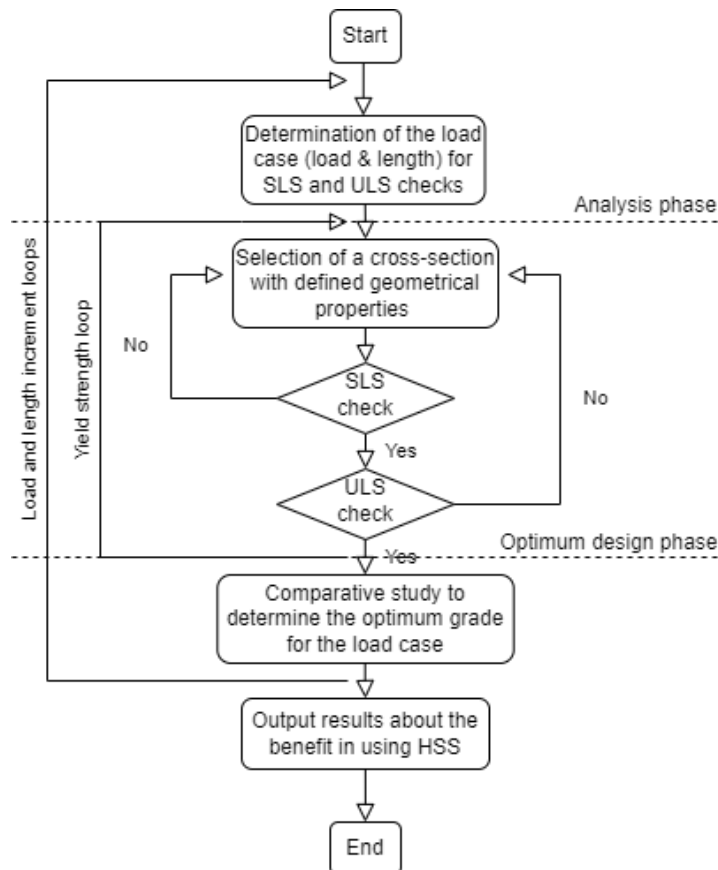


Fig. 4-4. Flowchart of the developed optimisation routines.

For each case study, the HSS benefit assessment is based on the comparison of the optimum designs of different grades: the regular steel (RS) grades and the high-strength steel (HSS) grades. An optimum design is defined as a design that returns the lightest profile, in a specific series of profiles (HEA, HEB, ...), thereby achieving the best material use. Then, a cost comparison between the optimum profiles is performed to determine whether there is an economic benefit in using a high-strength steel grade or not. When the applied load is such that the optimised profiles are the same for the compared steel grades, there is no economic benefit in using the high-strength steel grade instead of the RS grade because the latter is cheaper. Consequently, to present a benefit, the material savings resulting from the use of high-strength steels should compensate for the increase in material cost. In other words, the weight ratio between two optimum profiles must be greater than the relative cost $\left(\frac{C_{HSS}}{C_{RS}}\right)$ of the HSS grade (see Eq. (4-1)).

$$C_{rel} = \frac{A_{HSS} \cdot C_{HSS}}{A_{RS} \cdot C_{RS}} < 1 \rightarrow \frac{A_{RS}}{A_{HSS}} > \frac{C_{HSS}}{C_{RS}} \quad (4-1)$$

where A is the optimum cross-sectional area (mm^2) and $\frac{C_{HSS}}{C_{RS}}$ is the HSS relative cost (-).

The relative price ranges established in Chapter 3 are taken as a reference for assessing the benefits of using high-strength steels. Although grades above S500 do not yet exist for hot-rolled sections, the benefits of developing such grades are assessed for the sake of a prospective study. As a reminder, these reference values are listed in Table 4-1 depending on the steel grade and the intended relative cost level.

Steel grade	LOW	MEDIUM	HIGH
S235	1.00	1.00	1.00
S275	1.00	1.00	1.00
S355	1.05	1.08	1.12
S420	1.06	1.11	1.17
S460	1.07	1.13	1.20
S500	1.08	1.15	1.23
S550	1.10	1.18	1.27
S600	1.11	1.21	1.31
S700	1.14	1.32	1.50

Table 4-1. Reference relative prices of Chapter 3 for comparative studies.

The medium level is considered for the comparative studies presented in this chapter but, a parametric analysis has been carried out and conclusions are drawn based on the three cost levels defined in Table 4-1. As explained in Chapter 3, this thesis focuses on the sustainability assessment of high-strength steels. Consequently, as the relative carbon emissions have been evaluated below the relative prices, an economic assessment is pursued given it has been ensured that the economical solutions are also environmentally viable.

4.2.4. Establishment of continuous quantities

The geometrical properties of existing market catalogues have been interpolated to create fictitious continuous catalogues and to draw general conclusions on the domains for which there is a potential to consider high-strength steels. For hot-rolled sections, each geometrical property has been interpolated using a spline interpolation between the first and the last profile of each series. The spline interpolation is a piecewise continuous function composed of many polynomials to model the data set. The interpolation results for the HE and HD profile series are respectively shown in Fig. 4-5a and Fig. 4-5b. Concerning the hollow cross-sections, two variables were examined: the diameter and the wall thickness for CHS sections or the side dimension and the wall thickness for SHS elements. A paper written by Hoang in 2011 [219], expresses the constitutive condition $t \leq D/2$ for the optimum research problem but it means that being at the upper threshold of this condition implies that it is no longer a hollow section but a filled steel tube. According to manufacturers' catalogues available on the steel market, the diameter-to-thickness ratio varies between 7 and 127 for CHS while the width-to-thickness ratio varies between 8 and 50 for SHS. Therefore, on this basis, continuous quantities have been defined in order to respect the common geometrical properties commonly used in the current steel market. The continuous quantities and the discrete catalogues for cold-formed and hot-finished hollow sections are presented on the same graphs for CHS and SHS (see Fig. 4-5c and Fig. 4-5d).

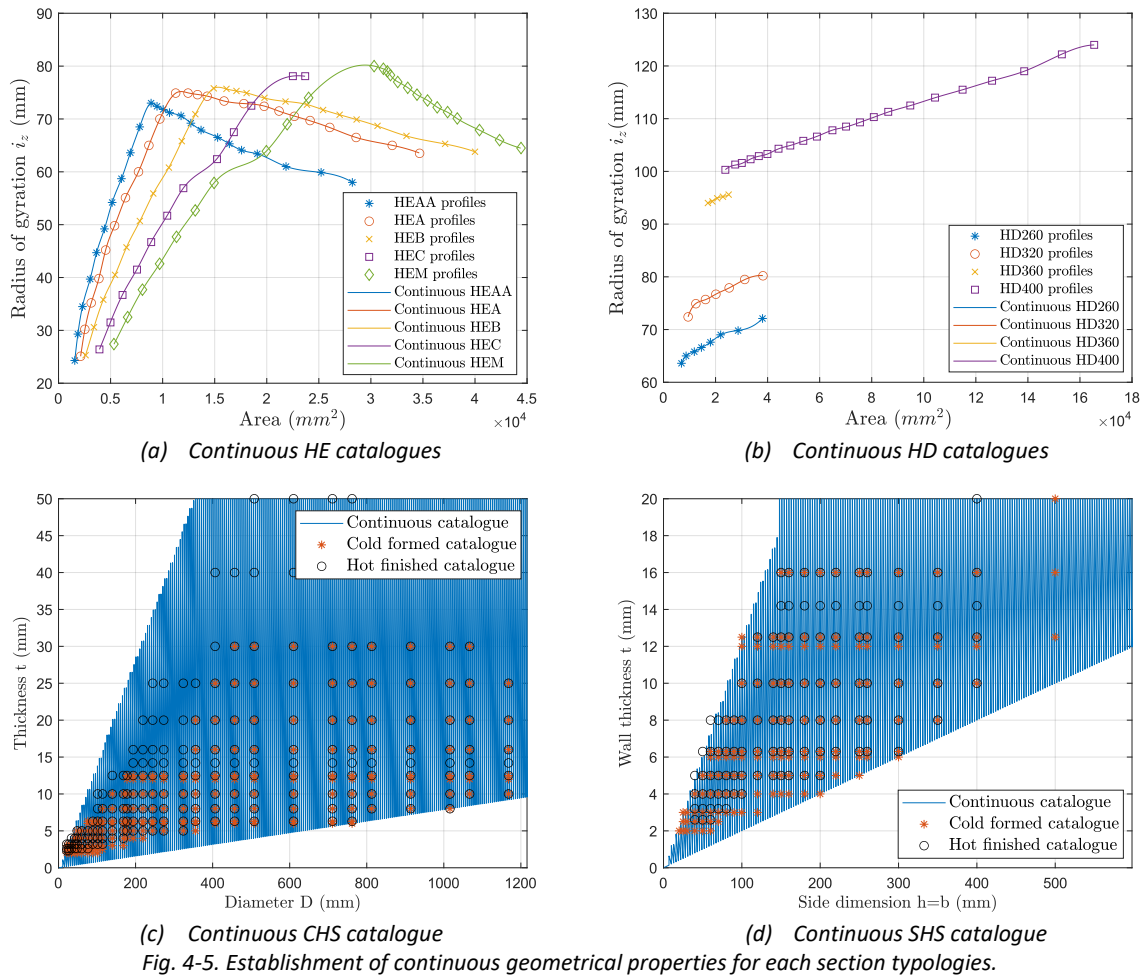
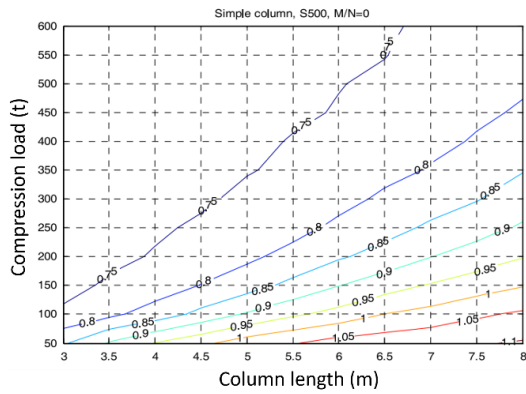


Fig. 4-5a and Fig. 4-5b show that, regardless the consideration of increased yield strengths, the different ranges are designed to target different load levels and need to be properly considered. For example, HD or HEM columns are designed to carry higher buckling loads than HEA or HEB columns (greater weak-axis inertia for the same cross-sectional area) and therefore do not offer any advantages in the load ranges of standard buildings but are more suitable for highly loaded columns in high-rise buildings. Finally, although these developed continuous quantities are used to draw conclusions, the effect of profile discretisation, that can be defined as the number of discrete profiles within a given catalogue, on the benefit of using high-strength steels is also addressed in the interpretation of the results.

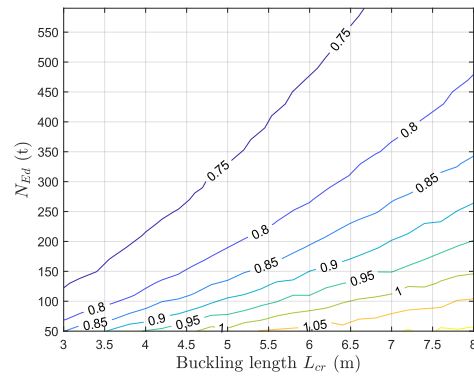
4.3. Validation

The MATLAB routine developed in this chapter to compare the various steel grades has been validated on circular hollow steel sections. Indeed, a research work on the economic benefit of high-strength steels for tubes was carried out earlier within the ATTEL project: “Performance-Based Approaches for High Strength Steel Tubular Columns and Connections under Earthquake and Fire Loading” leading to a publication on the economic benefit of using high-strength steels for tubular sections [219]. The MATLAB routine developed in the framework of the present thesis was validated through comparisons with the existing ATTEL algorithm and it perfectly reproduced the results. A constitutive condition ($t \leq D/2$) was fixed in the algorithm, so a continuous catalogue respecting this condition was established for the sake of comparison. In addition, this ATTEL algorithm assumed that all sections belong at least

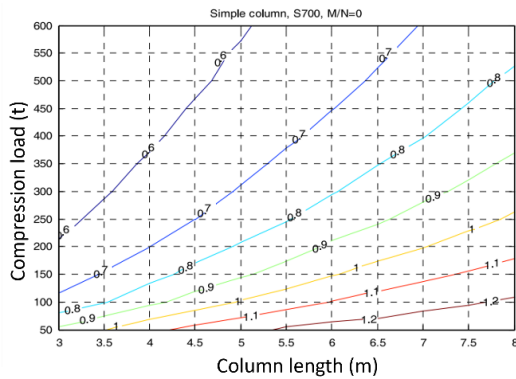
to class 3, to avoid any local buckling; so, the routine developed here was adapted accordingly by removing, again only for sake of comparisons with ATTEL, Class 4 sections from the considered continuous quantities. The validation of the results is shown in Fig. 4-6 by representing the area ratios between S500 / S355 and S700 / S355 optimum designs in the case of a simple column (subjected to pure compression, $e = M/N = 0 \text{ mm}$) and for a column subjected to combined compression and bending ($e = M/N = 100 \text{ mm}$).



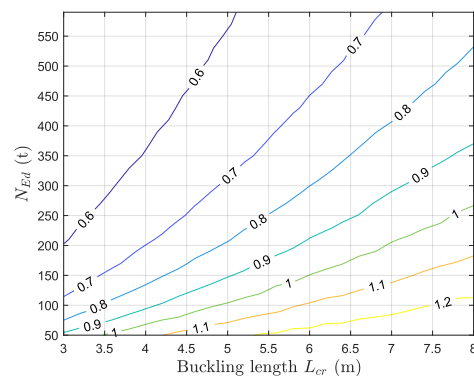
(a) S500/S355 – $e = 0 \text{ mm}$ – Hoang, 2011



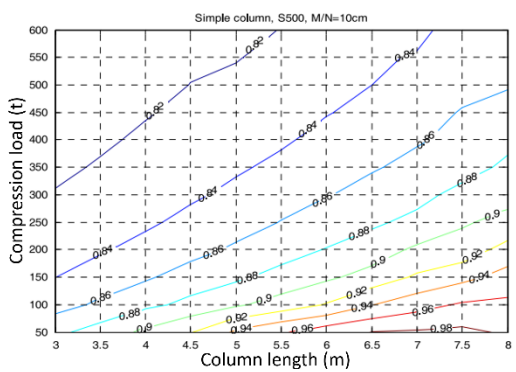
(b) S500/S355 – $e = 0 \text{ mm}$ – Dev. routine



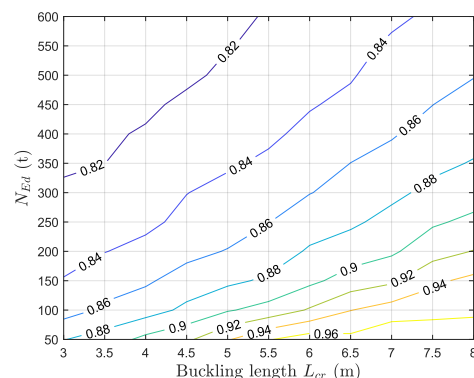
(c) S700/S355 – $e = 0 \text{ mm}$ – Hoang, 2011



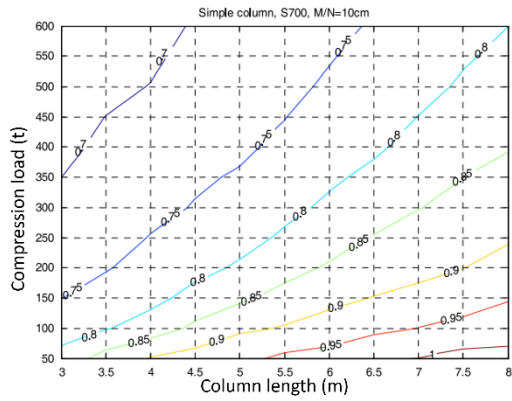
(d) S700/S355 – $e = 0 \text{ mm}$ – Dev. routine



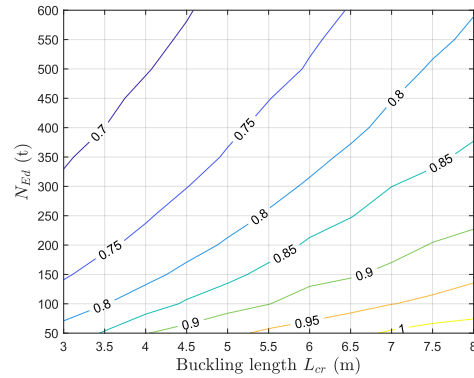
(e) S500/S355 – $e = 100 \text{ mm}$ – Hoang, 2011



(f) S500/S355 – $e = 100 \text{ mm}$ – Dev. routine



(g) S700/S355 – $e = 100 \text{ mm}$ – Hoang, 2011

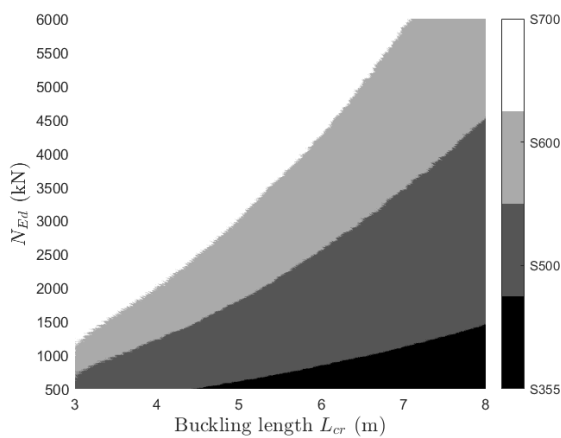


(h) S700/S355 – $e = 100 \text{ mm}$ – Dev. routine

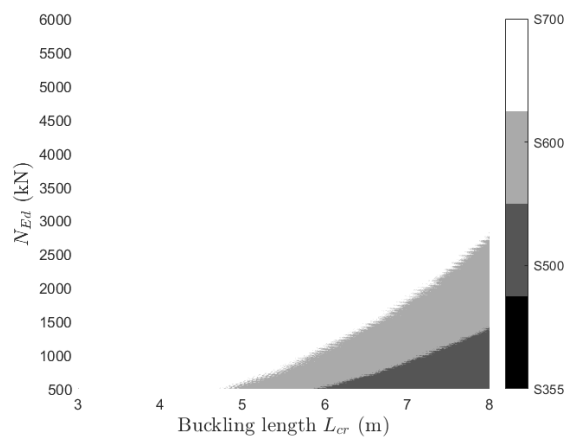
Fig. 4-6. Area ratios obtained through the developed methodology compared to an existing algorithm developed within the ATTEL project.

Fig. 4-6 testifies of the validity of the developed routine as the latter reproduces the results for two different grades and two different loading conditions.

This being, for the present study, some assumptions fixed in the ATTEL project have been removed. First, it has been decided to set the limit of the continuous quantities based on minimum and maximum diameter-to-thickness ratios from practical catalogues (as described in Section 4.2.4) instead of including filled columns ($t = D/2$). In addition, Class 4 sections have been included as many sections produced in the steel market have a wall slenderness above the Class 3 limit, especially when considering high-strength steel grades. Finally, the algorithm developed within the ATTEL project [219] gives the reduction in area between two selected grades and therefore does not give any indication about what is the most economical grade among the considered ones (S355, S500, S600 and S700) for each loading situation. So, the here developed routine has been designed to cover any type of catalogue as input (HE, HD, CHS, SHS, ...) and to return the optimum grade for any loading configuration depending on the type of optimisation targeted (cost or weight minimisation). For example, considering the validation example, Fig. 4-7 gives the optimum between the four grades considered in the ATTEL project [219] for continuous quantities, for both loading situations and for weight and cost optimisations. The range of buckling lengths corresponding to storey buildings (non-sway structures), buckling lengths between 3 and 5m as defined in Chapter 2, is also shown in Fig. 4-7d to indicate the advantage in considering grades above the practical range for this specific application [73], [116].



(a) Weight optimisation – $e = 0 \text{ mm}$



(b) Weight optimisation – $e = 100 \text{ mm}$

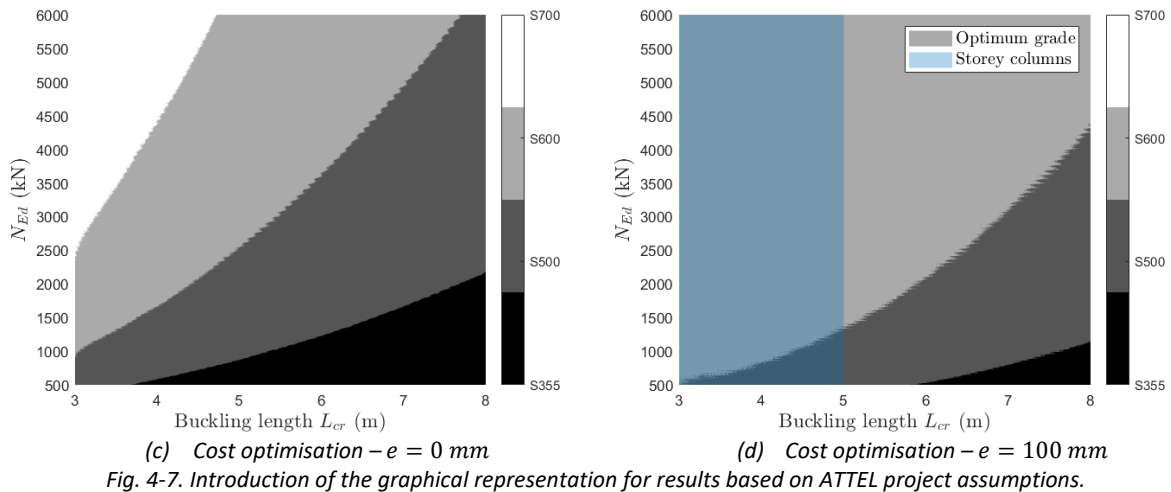


Fig. 4-7 shows an increase in the benefit for high-strength steels when the member is also subjected to a bending moment but, in this case, the results are highly dependent on the type of optimisation. Indeed, Fig. 4-7b shows no more advantage for the S355 grade while Fig. 4-7d shows a reduction of benefit for the S700 grade due to the relative cost increase. As the initial aim of the research is to derive a field of application for the use of high-strength steels in structural applications, the representation of Fig. 4-7 has been adopted throughout this Chapter 4, accounting for the selected grades and the medium relative price level (see Table 4-1) established in Chapter 3.

4.4. Results for hot-rolled sections

The hot-rolled sections are available in different shapes: I-shaped, U-shaped, or H-shaped. They are suitable for both columns and beams and are manufactured in various steel grades (up to 460-500 MPa in Europe and up to 80 ksi – 550 MPa in the USA). H-sections are the most used elements for columns but also for floor beams, trusses and engineering structural applications. They offer good resistance to instability phenomena and make it possible to overcome a current level/span height without maintaining them. The range of profiles available on the market is quite extensive, ranging from the simple HEA to the very massive HEM. Wide flange profiles, HD, are also produced to increase the resistance of columns subjected to significant normal stresses. For elements subjected to simple bending, IPE beams are considered due to their significant bending inertia along the main bending axis. The consideration of hot-rolled sections is therefore relevant to conclude on the areas of benefit for high-strength steels.

4.4.1. Members in tension

The first structural element studied is the tensile member. It is the simplest and the most efficient structural member. Its response is not at all guided by instabilities or SLS (serviceability limit states) conditions that are susceptible to reduce the economic benefit of using high-strength steels. The resistance of a tensile element only depends on its cross-sectional resistance, which is proportional to the yield strength of the steel, so large areas of economic benefit for high-strength steels are expected (as shown in Fig. 4-1). The relative material cost, considering that the strength can be fully utilised ($A = N_{Ed}/f_y$), can be derived as expressed in Eq. (4-2).

$$C_{rel} = \frac{A_{opt,grade\ 2}}{A_{opt,grade\ 1}} \cdot \frac{c_{grade\ 2}}{c_{grade\ 1}} = \frac{\left(\frac{N_{Ed}}{f_{y,grade\ 2}}\right)}{\left(\frac{N_{Ed}}{f_{y,grade\ 1}}\right)} \cdot \frac{c_{grade\ 2}}{c_{grade\ 1}} = \frac{f_{y,grade\ 1}}{f_{y,grade\ 2}} \cdot \frac{c_{grade\ 2}}{c_{grade\ 1}} \quad (4-2)$$

where; $A_{opt,grade\ i}$ is the cross-sectional area of the optimum profile considering grade “i”; $\frac{c_{grade\ 2}}{c_{grade\ 1}}$ is the relative cost of grade 2 as defined in Table 4-1; $f_{y,grade\ i}$ is the yield strength of grade “i” and N_{Ed} is the design axial load. In accordance to Eq. (4-2), the results for all steel grades are shown in Fig. 4-8 normalised to grade S235.

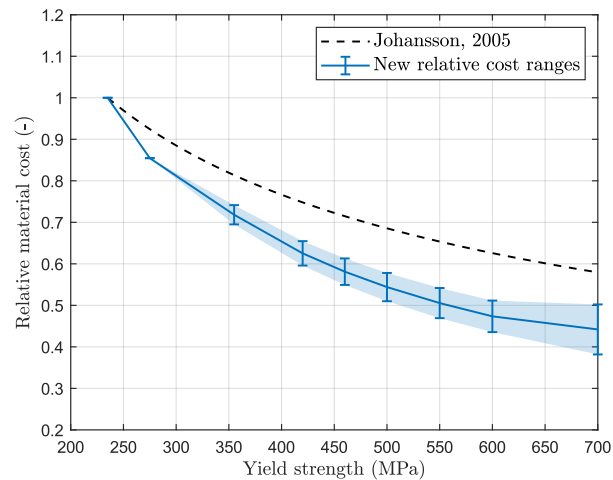
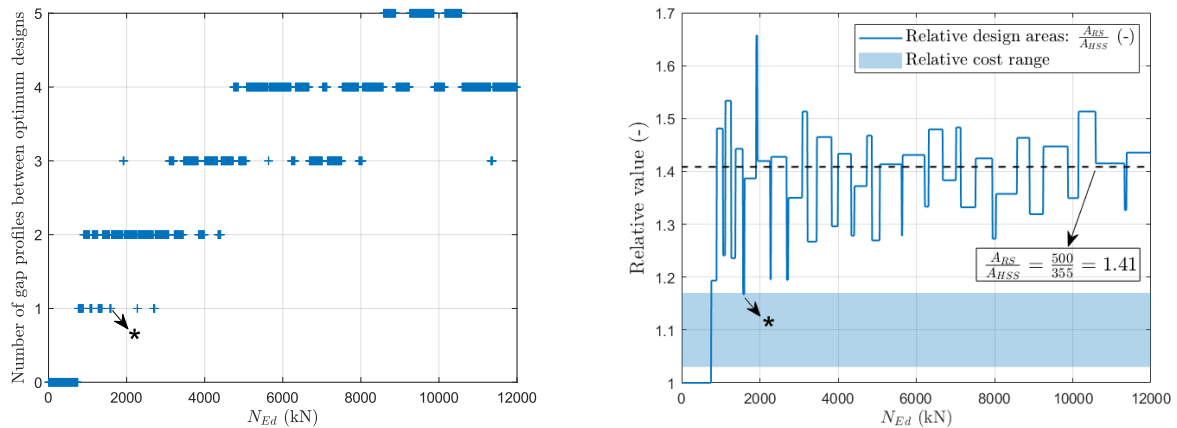


Fig. 4-8. Relative material cost for tension members normalised with S235 and by assuming that the strength can be fully mobilised.

Fig. 4-8 demonstrates that there is always a benefit in considering the highest grade, i.e. S700, when the optimum profile can mobilise the full strength of the material, However, the higher the relative price level, the lower the benefit for S700. Indeed, at the high relative price level defined in Table 4-1, the slope of the curve between S600 and S700 is close to zero, meaning that the relative material cost curve is closed to a horizontal asymptote for such yield strengths. The computed relative material costs are nonetheless well below the predictions made by Johansson in 2005 [86].

In addition, the market catalogues are always discrete, and the discretisation can affect the benefit of considering a higher yield strength. Consider a case in which only the HEA profile series is available in S500, the optimum designs provide the lightest HEA profiles required for S500 and S355 steel grades respectively. The number of “gap profiles” between the two optimum designs is represented in Fig. 4-9a. These ones correspond to the number of sections separating the two optimum sections. For example, if the optimum section in S355 steel grade is HEA140 and the optimum section in S500 steel grade is HEA120, it is considered that there is one gap profile given there is no existing section with an intermediate weight between these two ones. Fig. 4-9b shows the area ratios between the optimum designs for tension members in S355 and S500, considering only the HEA series of profiles.



(a) Number of gap profiles
 (b) Area ratios between optimum profiles
 Fig. 4-9. Comparative study between S500 and S355 for tension members and the HEA profile series.

Fig. 4-9 shows that there is no economic advantage in using the HSS steel grade when the HEA100 (the smaller cross-section in the HEA series) is sufficient for both steel grades (in this case, there are no gap profiles, see Fig. 4-9a). It means that the optimum profile is the HEA100 for both grades, so as long as the optimum design in S355 steel provides the first profile in the range, there is no benefit in using high-strength steels. For the rest of the field, there is an economic benefit if, for some gap profiles, the weight ratio between the two optimum profiles is greater than the cost ratio according to Eq. (4-1).

However, the area ratios fluctuate due to the catalogue discretisation and in some cases, the area ratio may fall below the relative cost. Example 4-1 details the design optimisations for a particular zone, marked with a (*) in Fig. 4-9, where the area ratio is equal to the upper bound of the relative cost range. This zone has only one gap profile between the two optimum designs as shown in Fig. 4-9a.

Example 4-1. Detail of optimisation for zone marked by "*" ($N_{Ed} = 1600$ kN, S355, S500)

The optimum profiles in S355 and S500 are:

$$A_{RS} \geq \frac{N_{Ed}}{f_{y,RS}} = \frac{1600 \cdot 10^3}{355} = 4507 \text{ mm}^2 \rightarrow \text{HEA180} (A = 4530 \text{ mm}^2) \rightarrow \text{Unity check} = 0.99$$

$$A_{HSS} \geq \frac{N_{Ed}}{f_{y,HSS}} = \frac{1600 \cdot 10^3}{500} = 3200 \text{ mm}^2 \rightarrow \text{HEA160} (A = 3880 \text{ mm}^2) \rightarrow \text{Unity check} = 0.82$$

The corresponding ratios are: $\frac{A_{RS}}{A_{HSS}} = 1.17$ which is close to the upper limit of the relative costs (as can be seen in Fig. 4-9b). In the case where the HEB series may also be ordered in S500, the optimum profile is: HEB120 ($A = 3400 \text{ mm}^2$) \rightarrow **Unity check = 0.94** (better optimised).

Considering the relative cost range of S500 and the corresponding area ratio ($\frac{A_{RS}}{A_{HSS}} = 1.33$), there is clear economic advantage in using the S500 grade.

Example 4-1 illustrates the negative impact of the non-availability of sections. The unity check also called the utilisation ratio, i.e. the ratio between actual stress and allowable stress ($N_{Ed}/N_{pl,Rd}$), testifies that the material use is not efficient for the high-strength steel grade and thus demonstrates the need to market as many profiles as possible in high-strength steel grades in order to optimise and achieve weight savings. Therefore, in order to ensure that high-strength steels lead to significant weight savings that compensate for the relative material cost and carbon footprint increases, the steel producers should adapt their production by either increasing the number of

profiles within a profile series that can be produced in high-strength steels, or at least by producing their entire existing catalogue in high-strength grades.

Another aspect to consider for tension members is the stiffness requirements. Tension members can be subject to bending induced by their self-weight, by certain eccentricities of the load or by dynamic effects. Therefore, the ESDEP (European Steel Design Educational Programme) [220] provides some recommendations for practitioners to avoid such problems that may negatively affect the benefits of using high-strength steels. Generally, the slenderness limits of 300 for main members and 400 for secondary members are given as good practice. Nonetheless, even with more restrictive values, these good practice recommendations are not significant for heavy hot-rolled sections as they are designed to target larger loads, and the radius of gyration is thus sufficient to meet such slenderness requirements.

Eventually, up to now, only the strength of the gross cross-section has been considered but the joints at the ends of the element require the drilling of holes. In accordance with Eurocode 3, the resistance considering the net area of the section is calculated by Eq. (4-3).

$$N_{u,Rd} = \frac{0.9 \cdot A_{net} \cdot f_u}{\gamma_{M2}} \quad (4-3)$$

Where, A_{net} is the net area of the section, f_u the ultimate strength of the steel and γ_{M2} the partial safety coefficient for connections. It can be seen from Eq. (4-3) that the resistance depends on the ultimate strength rather than the yield strength. As the ratio of ultimate strength to yield strength decreases with yield strength, the savings from using a high-strength steel grade is less than for the gross section. Langenberg et al. [73], [221] expressed a relationship between the ultimate and the yield strengths, i.e. $\frac{f_u}{f_y} = 1 - 0.72 \cdot e^{-0.0027f_y}$, based on coupon tests performed on various yield strengths, as expressed in Chapter 2. As an example, consider the weight saving resulting from the use of S690 grade instead of S355, the weight saving is equal to 49% (1-355/690) for the resistance considering the gross cross-section while it is 34% (1-510/770) by considering the net cross-section (assuming that the same holes are made for both grades).

Although joints at member ends, profile discretisation or slenderness limits may negatively affect the gain induced using a high-strength steel grade, there is almost always an economic benefit in developing high-strength steel grades for tension members as they are mainly strength-governed elements.

4.4.2. Members in pure compression

According to the design recommendations described in Chapter 2, the resistance of an element subjected to compression is checked using Eq. (2-7). Since members subjected to pure compression are susceptible to two main instability phenomena, i.e. local buckling and flexural buckling, the effect of the yield strength on the resistance associated with these two instability phenomena is first addressed to understand the key features that influence the benefit of using high-strength steels. Finally, comparative studies based on the developed optimisation routine are presented to define in which cases it is advantageous to consider high-strength steels for members under pure compression.

4.4.2.1. Resistance to local buckling

The presence of local buckling resulting from the use of a higher yield strength reduces the material efficiency. Besides, to account for local buckling, design standards recommend either evaluating an

effective width or evaluating an effective stress. The method prescribed in EN1993-1-5 [222] consists of determining an effective area obtained by virtually removing the part of the plate which is prone to local buckling ($A_{c,eff} = \rho \cdot A$ where ρ is the reduction coefficient to account for the risk of local buckling). The increase in terms of axial resistance as a function of the yield strength and accounting for the presence of local buckling is derived for a plate under pure compression, which is the worst scenario, as computed in Eq. (4-4) with S235 as reference.

$$\frac{N_{Rd,HSS}}{N_{Rd,S235}} = \frac{\rho_{HSS} \cdot A \cdot f_y}{\rho_{RS} \cdot A \cdot 235} = \left(\frac{\rho_{HSS}}{\rho_{RS}}\right) \cdot \left(\frac{f_y}{235}\right) \quad (4-4)$$

The results in terms of resistance ratios for outstand and internal elements to cover the various constitutive parts of hot-rolled H-shaped profiles are reported in Fig. 4-10.

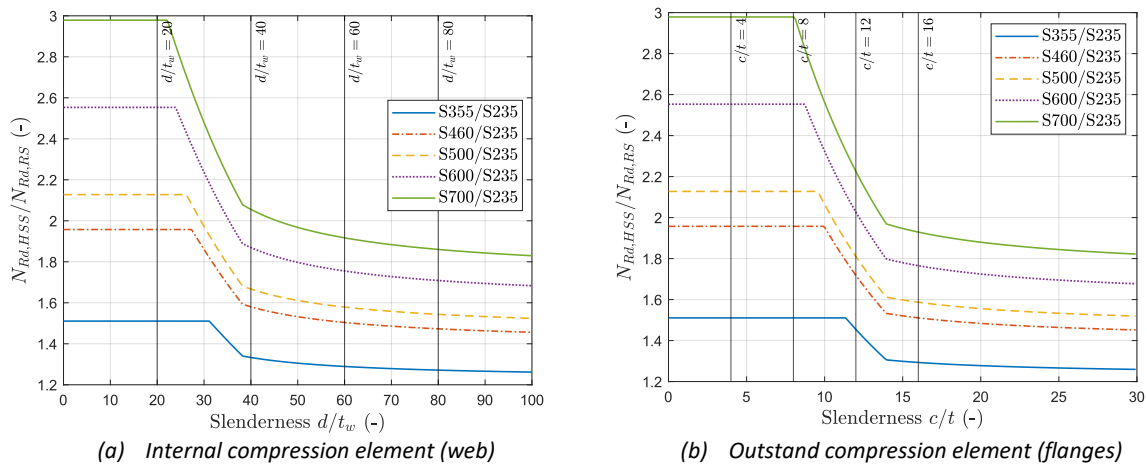


Fig. 4-10. Relative resistance to local buckling for hot-rolled sections under pure compression (S235 as reference).

Fig. 4-10 represents that, even for slender plates, there is still a gain in resistance resulting from the use of a higher yield strength but in a lower proportion than for stocky plates. Apart from the profiles of the HEAA series which have relatively slender flanges, there are only 3 profiles in the HEA series and only 5 profiles in the HD series for which the flange slenderness exceeds $c/t = 8$, the slenderness limit of the plastic plateau for S700 in Fig. 4-10b. Therefore, most of the profiles respect the slenderness limit of outstand elements as stocky plate. Otherwise, the slenderness of the internal compression elements, i.e. the web for H-shaped hot-rolled sections, increases with the weight for the HE profiles series. Generally, for the first sections of each series, the height-to-width ratio is less than 1.2 and the sections are more compact than the last ones which have a slenderer web.

Stroetmann presents some thoughts about material efficiency in the Practical Guide for Sustainable Steel Buildings [51]. For instance, he reported that there is still an advantage in considering high-strength steels even if a member is prone to local buckling. Nevertheless, this reduction should be reasonable compared to the relative cost increase, and this discussion has been covered by plotting the relative cost calculated through Eq. (4-5) considering only the internal plates (i.e. the web for H-sections).

$$\begin{aligned} C_{rel} &= \frac{A_{opt,grade 2}}{A_{opt,grade 1}} \cdot \frac{c_{grade 2}}{c_{grade 1}} = \frac{\left(\frac{N_{Ed}}{\rho_{grade 2} \cdot f_{y,grade 2}}\right)}{\left(\frac{N_{Ed}}{\rho_{grade 1} \cdot f_{y,grade 1}}\right)} \cdot \frac{c_{grade 2}}{c_{grade 1}} \\ &= \frac{\rho_{grade 1} \cdot f_{y,grade 1}}{\rho_{grade 2} \cdot f_{y,grade 2}} \cdot \frac{c_{grade 2}}{c_{grade 1}} \end{aligned} \quad (4-5)$$

The relative material costs in Fig. 4-11 are reported by assuming that the flanges are fully effective ($\frac{c}{t} \leq 8$) and thus, the local buckling may only occur in the web.

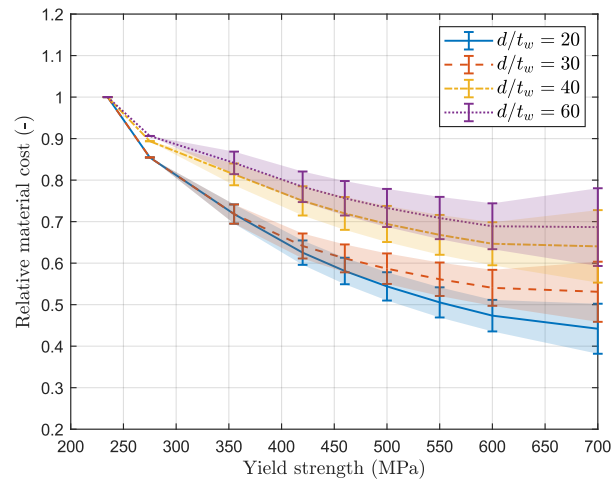


Fig. 4-11. Relative material cost for a hot-rolled member prone to local buckling (S235 as reference).

As can be seen in Fig. 4-11, the presence of local buckling has a slight effect on the material gain induced by the use of high-strength steels. In particular, for a high relative material cost, there is no more benefit in upgrading higher than S600. This example demonstrates that, although there is an overall benefit in increasing the yield strength, it should be relevant to limit the slenderness of the constitutive plates to improve the economic gain in considering high-strength steel grades. Otherwise, the material cost would be higher and the benefit of developing grades above S600 would even be null. In other words, steelmakers should develop new cross-sections or adapt existing ones with appropriate slenderness to optimise the material efficiency.

4.4.2.2. Resistance to flexural buckling

As expressed in Chapter 2, geometrical and material imperfections are accounted for through an imperfection parameter α , which defines the well-known European buckling curves. The relative importance of residual stresses decreases as the yield strength increases, which can have a positive effect on flexural buckling resistance. Regarding the current design recommendations reported in Table 2-11, the same buckling curve is assigned to grades included between S235 and S420 and an increase of one buckling curve is allowed for grades equal to or higher than S460. The relevance of this stepwise evolution will be discussed in Chapter 5. The gain of buckling resistance resulting from the use of a higher yield strength can be computed by evaluating the ratio of buckling resistances for a given column (same cross-sectional area for both compared grades) as given in Eq. (4-6), considering a Class 1, 2 or 3 column, one buckling axis and S235 as the reference grade.

$$\frac{N_{b,HSS}}{N_{b,S235}} = \frac{\chi_{HSS} \cdot A \cdot f_y}{\chi_{RS} \cdot A \cdot 235} = \left(\frac{\chi_{HSS}}{\chi_{RS}} \right) \cdot \left(\frac{f_y}{235} \right) \quad (4-6)$$

For example, in the case of members with height-to-width ratios above 1.2, flange thickness below 40 mm and flexural buckling about the major axis (curve “a” for mild steels and “a₀” for grades above S420 in design recommendations from FprEN1993-1-1:2022 [52]), the results in terms of buckling resistance ratios are given in Fig. 4-12a. As defined in Chapter 2, the critical buckling load depends on the slenderness λ and the shape of the section. The slenderness, denoted λ_{FB} in this study, is given by the ratio between the buckling length L_{cr} and the radius of gyration i_y for strong axis buckling (respectively i_z in case of weak axis buckling). The importance of the flexural buckling slenderness ($\lambda_{FB} = L_{cr}/i$)

on the benefit of using high-strength steels is demonstrated by plotting the relative resistances for 4 relevant slendernesses (40, 60, 80 and 100) as a function of the yield strength in Fig. 4-12b (for major-axis buckling in this represented case).

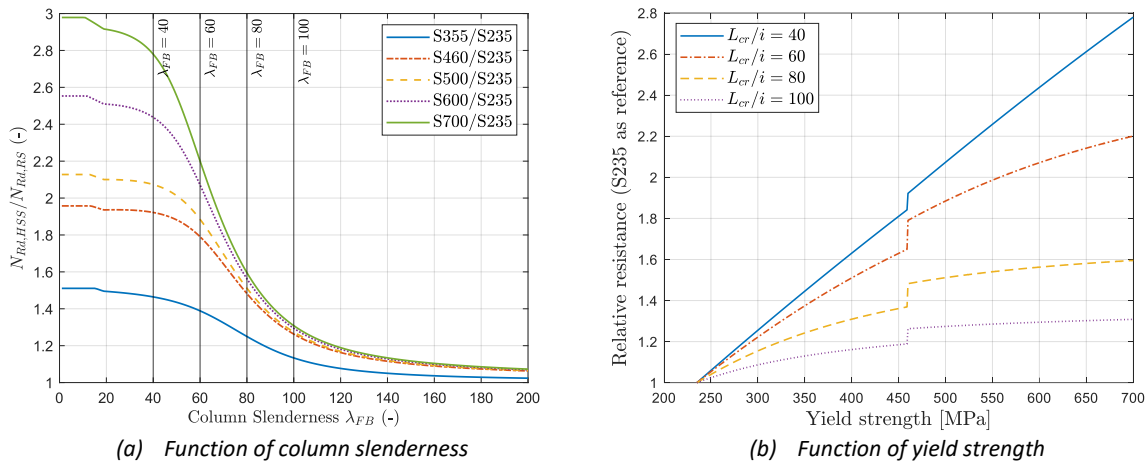


Fig. 4-12. Relative resistance to flexural buckling for hot-rolled sections (curve “a” up to S420 and curve “a₀” for S460 and above) considering grade S235 as reference.

The discontinuity in Fig. 4-12b is explained by the stepwise evolution of the imperfection factor α . Indeed, grade S460 benefits from a higher buckling curve according to the recommendations of FprEN1993-1-1:2022 [52]. In addition, it can be clearly seen in Fig. 4-12 that, for column slendernesses $\lambda_{FB} < 40$, the resistance ratio is closed to the yield strength ratio, i.e. the resistance is almost proportional to the yield strength. This slenderness limit was already cited by Johansson in 2005 [93] as it corresponds to the slenderness of stocky columns that are typical in multi-storey buildings where high-strength steels can lead to significant savings. On the contrary, for slender columns $\lambda_{FB} > 100$ (regardless of the buckling axis), the increase of resistance for grades higher than S460 becomes insignificant, and the flexural buckling phenomenon drastically reduces the benefit of considering higher yield strengths for such applications. This is the typical column slenderness met in sway structures as identified by Johansson [93]. This conclusion applies to any pair of buckling curves, i.e. any geometrical limit and buckling axis, and an illustration for a particular case study is given in Example 4-2.

Example 4-2. Relative resistance increases for HEA120 prone to minor-axis flexural buckling.

Considering a buckling length of $L_{Cr} = 3m$, which is relevant for non-sway structures and knowing that the radius of gyration of HEA120 is: $i_z = 30.2 mm$, the column slenderness ($\lambda_{FB,z} = L_{Cr}/i_z$) is thus equal to 100. The buckling resistance evolution is given below:

- S235: $\chi_z = 0.62 \rightarrow N_{b,Rd,S235} = 369 kN$
- S355: $\chi_z = 0.46 \rightarrow N_{b,Rd,S355} = 418 kN \rightarrow +13\%$
- S460: $\chi_z = 0.40 \rightarrow N_{b,Rd,S460} = 466 kN \rightarrow +26\%$
- S500: $\chi_z = 0.37 \rightarrow N_{b,Rd,S500} = 469 kN \rightarrow +27\%$
- S700: $\chi_z = 0.27 \rightarrow N_{b,Rd,S700} = 482 kN \rightarrow +31\%$

The increase, in terms of flexural buckling resistances, starts to be insignificant from S460. In fact, an increase in yield strength of about 10% (in case of using S500), represents only an increase in resistance of 1%. Therefore, the increase in resistance is unlikely to compensate for the increase in material cost for high-strength steel grades. For such slenderness, there is no benefit in going beyond S460.

Nevertheless, even a small increase in resistance may be sufficient, depending on the amplitude of the associated relative material cost. Consequently, to conclude on the benefit of higher grades, relative material costs have been derived based on the relative unitary costs reported in Table 4-1 and taking S235 as the reference - see Eq. (4-7) and Fig. 4-13. The same assumptions as for Fig. 4-12 still apply here.

$$C_{rel} = \frac{A_{opt,grade 2}}{A_{opt,grade 1}} \cdot \frac{c_{grade 2}}{c_{grade 1}} = \frac{\left(\frac{N_{Ed}}{\chi_{grade 2} \cdot f_{y,grade 2}}\right)}{\left(\frac{N_{Ed}}{\chi_{grade 1} \cdot f_{y,grade 1}}\right)} \cdot \frac{c_{grade 2}}{c_{grade 1}} = \frac{\chi_{grade 1} \cdot f_{y,grade 1}}{\chi_{grade 2} \cdot f_{y,grade 2}} \cdot \frac{c_{grade 2}}{c_{grade 1}} \quad (4-7)$$

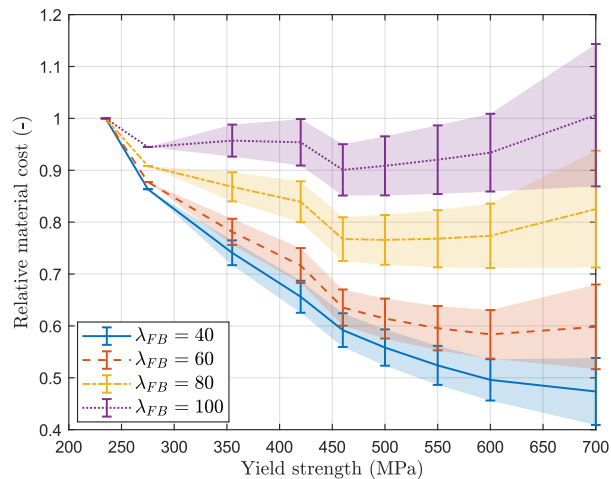


Fig. 4-13. Relative material cost for hot-rolled columns under pure compression and taking S235 as reference (curve “a” up to S420 and curve “a₀” for S460 and above).

As can be seen in Fig. 4-13, the benefit of using a higher grade is highly dependent on two parameters, i.e. the column slenderness and the relative cost level. In addition, Fig. 4-13 illustrates that there is a significant material reduction step between S420 and S460. This feature is attributed to the current design recommendations of Eurocode 3 which preconises to use one higher buckling curve for S460 while the grades below are grouped within the same buckling curve. Based on the current specifications of the forthcoming version FprEN1993-1-1:2022 [52], the optimum yield strength as a function of preconised buckling curves, column slenderness as well as the reference relative cost level is given in Table 4-2.

Reference cost level	$\lambda_{FB} = L_{cr}/i$	Buckling curve for S235				Lower strength
		a	b	c	d	
Low	40	700	700	700	700	700
	60	700	700	700	700	700
	80	600	700	700	700	600
	100	460	550	600	700	460
Medium	40	700	700	700	700	700
	60	600	600	600	600	600
	80	500	550	600	600	500
	100	460	460	460	500	460
High	40	600	600	600	600	600
	60	600	600	600	600	600
	80	460	460	500	500	460
	100	275	460	460	460	275

Table 4-2. Optimum yield strength (MPa) depending on the prescribed buckling curve for S235, the column slenderness, and the reference relative cost level.

Table 4-2 confirms that, for slender columns ($\lambda_{FB} > 100$), there is no benefit in using a yield strength above the practical range (presently limited to 460-500 MPa) while for $\lambda_{FB} < 40$, there is an advantage in developing the highest considered grade regardless of the buckling axis. For intermediate slendernesses, the optimum yield strengths are included between 500 MPa and 700 MPa and the benefit for high-strength steels should be assessed depending on the application.

The aforementioned conclusions are illustrated by plotting the slenderness limits of each steel grade, which define the field of application for a steel grade. For example, the ratio between the flexural buckling resistance of a given column made from steel grade S355 and the one from S235 is shown in Fig. 4-14a. Based on the relative prices defined in Table 4-1, it is feasible to derive the slenderness limit below which there is an economic advantage in using the S355 grade instead of S235, and this for the three material cost levels ($\lambda_{lim,H}$ the slenderness limit for the high level, $\lambda_{lim,M}$ for the medium level and $\lambda_{lim,L}$ for the low level) as depicted in Fig. 4-14a. The three limits for all steel grades are gathered in a single graph in Fig. 4-14b, facilitating the comparison of these relevant parameters for all steel grades. The figures have been plotted for the case of hot-rolled sections with height-to-width ratios above 1.2, flange thickness below 40 mm and flexural buckling about major axis (curve “a” for mild steels and “a₀” for grades above S420) selected as working example. This profile category is relatively common and represents the most unfavourable in Table 4-2. It should be noted, however, that the remaining charts for all the other cases are presented in Appendix A. These charts represent graphical tools to help designers determining the benefit for a higher grade as well as to steelmakers for developing new appropriate products.

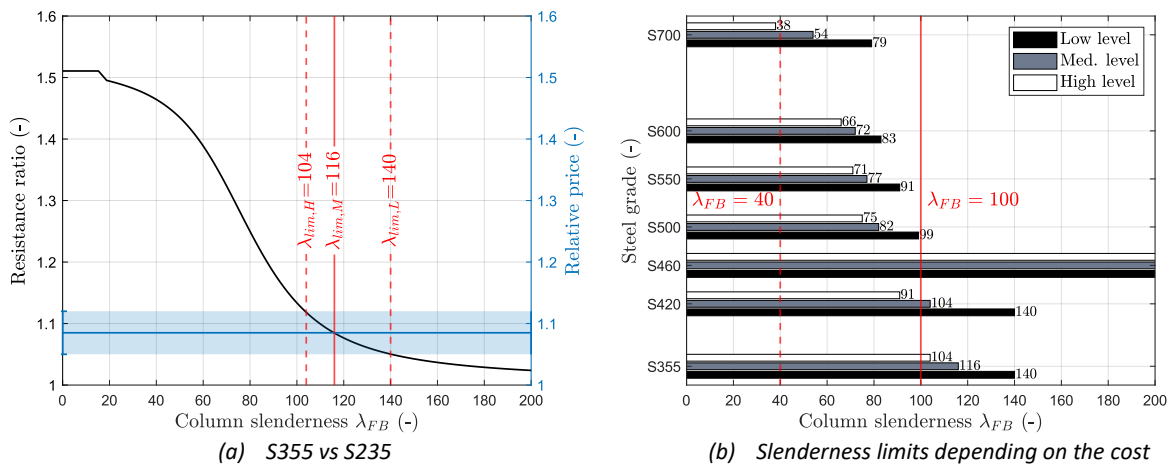


Fig. 4-14. Slenderness limits to justify the benefit of a higher grade for hot-rolled sections respecting $h/b > 1.2 / t_f \leq 40$ mm / major axis.

Fig. 4-14a confirms that, while the column slenderness remains below 100, there is always a benefit in substituting the S235 grade by the S355 grade, regardless of the relative cost level as the slenderness for the higher cost level (noted $\lambda_{lim,H}$) is 104. Based on the current unphysical stepwise evolution, there is always a benefit in considering the S460 grade instead of S420, as shown in Fig. 4-14b with slenderness limits exceeding the upper boundary of 200 in the chart. Furthermore, there is a benefit in considering the highest grade, i.e. S700, if the column slenderness does not exceed 40. For intermediate grades, the benefit should be evaluated in the slenderness range $\lambda_{FB} \in [40; 100]$ depending on the relative material cost, i.e. the following limits could be safely written $\lambda_{FB} \leq 75$ for S500, $\lambda_{FB} \leq 70$ for S550, $\lambda_{FB} \leq 65$ for S600. Nevertheless, based on Table 4-2 and Fig. 4-14, it should be conservatively concluded that it is relevant to investigate the possibility of using grades above the practical range for column slendernesses respecting $\lambda_{FB} < 80$.

4.4.2.3. Results of optimisation routine for hot-rolled sections

As a reminder, the conclusions expressed in Section 4.4.2.2 are for a Class 1, 2 or 3 column with a fixed slenderness for which the cross-section area decreases as the yield strength increases. But, in reality, the column slenderness increases with decreasing cross-sectional area, which is less favourable for high-strength steels. Furthermore, the consideration of a higher grade implies that some sections in the manufacturers' catalogues fall into the class 4 category, which means that they are susceptible to local buckling phenomena. It is therefore essential to consider both instability phenomena in order to draw conclusions. Furthermore, the profile range has an impact on the result as radius of gyration differs, as represented in Fig. 4-15.

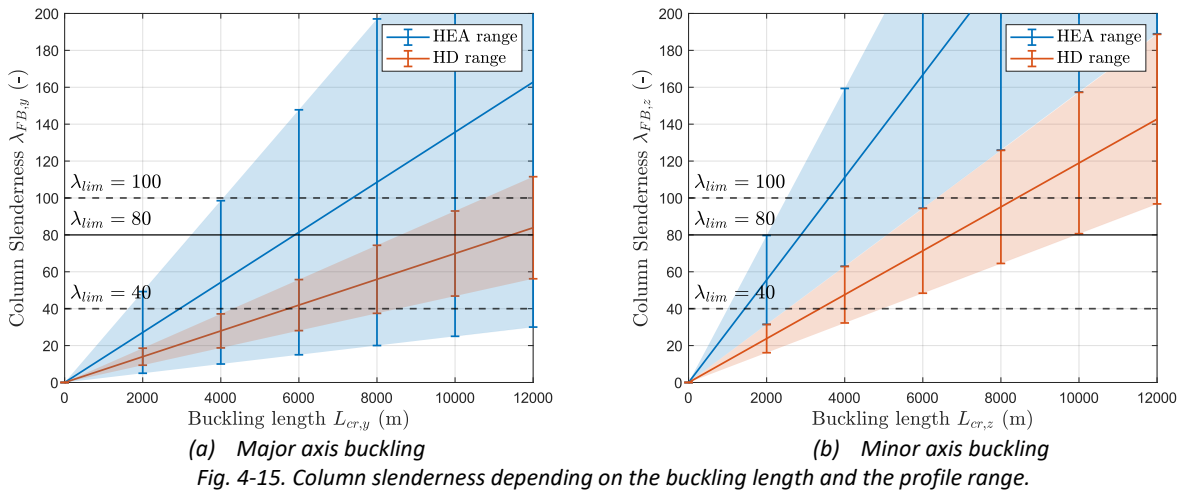
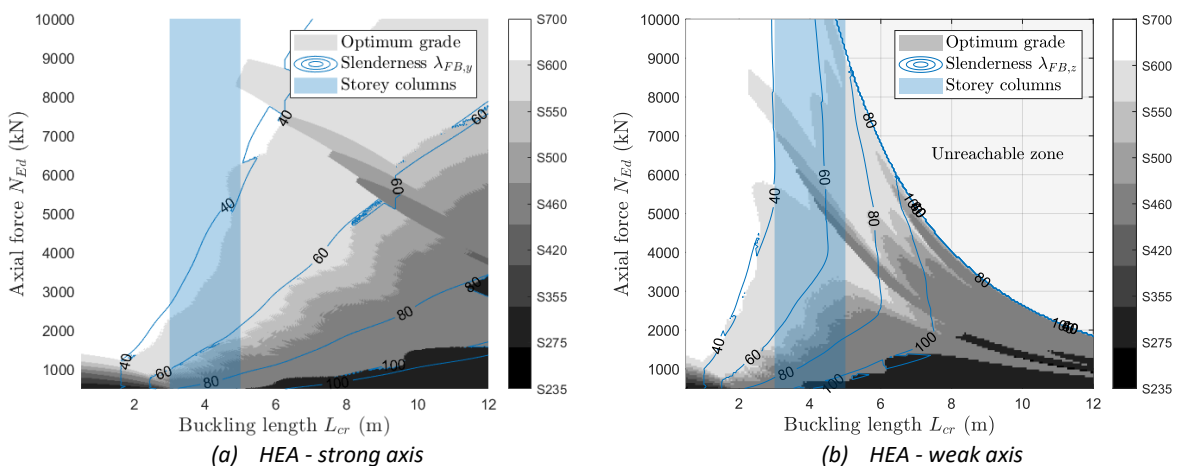


Fig. 4-15 illustrates that for massive cross-sections, like HD profiles, the column slenderness is below the slenderness limit $\lambda_{lim} = 80$ for typical multi-storey buckling lengths (between 3 and 5 m) and regardless of the buckling axis. On the contrary, lighter cross-sections like HEA profiles exhibit greater column slenderness for both buckling axes, meaning that the benefit of high-strength steel grades for such sections is likely to be limited. It has therefore been decided to consider these two ranges to draw conclusions. The results of optimisations carried out according to the procedure described in Section 4.2.3, considering the medium relative cost and the continuous quantities for HEA and HD catalogues (as established in Section 4.2.4) are shown in Fig. 4-16. The flexural buckling slendernesses $\lambda_{FB,y}$ (strong axis buckling) and $\lambda_{FB,z}$ (weak axis buckling) of the optimum profiles are also reported in order to identify the column slenderness ranges for which there is an advantage in developing new steel grades.



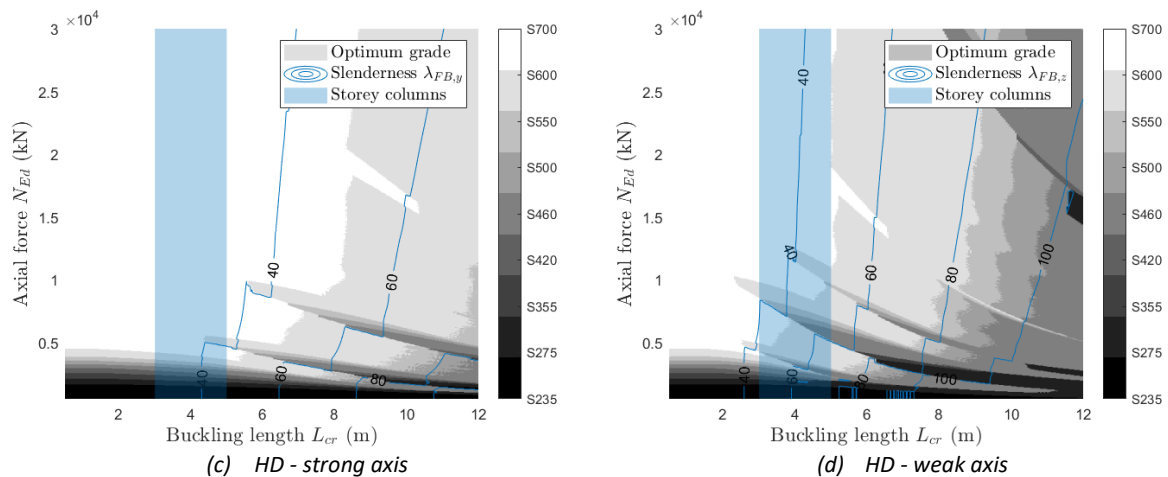


Fig. 4-16. Optimisation results for continuous hot-rolled sections (HEA and HD profile series) under pure compression and medium cost level.

As stated in reference [51], for profiles with a weight greater than 134 kg/m (HD360x134), the radius of gyration about the weak axis i_z becomes significantly higher than for HEA profiles. Indeed, as explained in Section 4.2.4, HD sections offer the best weak axis buckling resistance among the rolled sections available on the steel market. Given that the bigger the radius of gyration, the smaller the slenderness and the greater the benefit of increased yield strengths, this explains why the benefit for HD profiles is greater than for HEA profiles in Fig. 4-16. Fig. 4-16 also confirms the conclusions expressed in Section 4.4.2.2 regarding the slenderness limits, i.e. benefit of the maximum grade for $\lambda_{FB} < 40$ and no benefit for grades above the practical range when $\lambda_{FB} > 100$. The discontinuities observed in Fig. 4-16a and Fig. 4-16b, are caused by the sudden change of buckling curve prescribed in the Eurocode recommendations. Indeed, from a profile weight of 125 kg/m in the HEA profile series, the height-to-width ratio becomes greater than 1.2, leading to a change in the buckling curve. On the other hand, for the case of HD profiles, the two discontinuities are caused by the sudden increases in inertia between the HD320 and the HD400 profile series (see Fig. 4-5b), which explains why there are two specific transition zones in Fig. 4-16c and Fig. 4-16d. Indeed, in these zones, the lower grades change from one series to the other, resulting in a reduction of the cross-sectional area for the same radius of gyration which gives them an advantage in these specific areas. Finally, for the highly stressed columns in Fig. 4-16d, the flange thickness is greater than 40 mm and therefore the yield strength is reduced according to Table 2-2. Furthermore, as the optimum designs are performed for each steel grade and load case, such figures provide information on the domains (N_{Ed}, L_{cr}) for which there is a benefit in using higher yield strengths. For example, for storey columns characterised by buckling lengths between 3m and 5m (as shown in blue in Fig. 4-16), there is a benefit in considering higher yield strengths regardless the buckling axis. In contrast, for light profiles (HEA) and sway frames corresponding to higher buckling lengths, there is less benefit in considering new yield strengths for such applications.

Fig. 4-17 represents the same results as in Fig. 4-16 by considering the discrete HEA and HD profile series. As can be seen, the general trends based on the column slenderness are still valid for the discrete catalogue, but the profile availability affects the results. Example 4-3 reports the explanation of the area marked by an asterisk "*" in Fig. 4-17a.

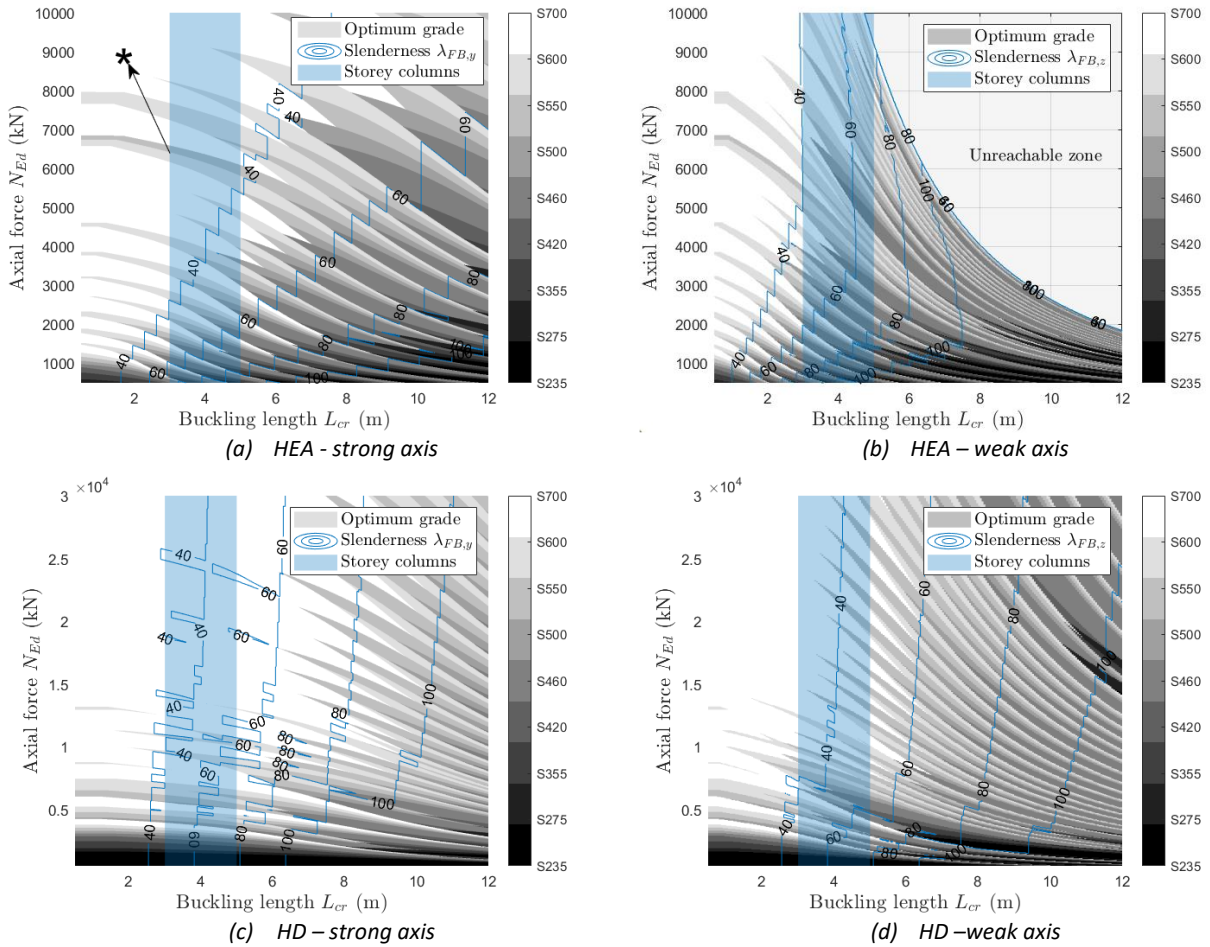


Fig. 4-17. Optimisation results for compression members considering the discrete HEA and HD profile series.

Example 4-3. Design details for zone marked by “*” ($N_{Ed} = 6500 \text{ kN}$, $L_{cr} = 3 \text{ m}$)

The optimum profiles for the various steel grades with their corresponding unity checks are reported below.

	S235	S275	S355	S420	S460	S500	S550	S600	S700
Opt. profile	HEA900	HEA650	HEA500	HEA400	HEA400	HEA360	HEA320	HEA320	HEA300
Area [mm ²]	32050	24160	19750	15900	15900	14280	12440	12440	11250
$\lambda_{FB,y}$ [-]	8.27	11.14	14.29	17.81	17.81	19.71	22.09	22.09	23.55
Unity Check [-]	0.91	0.99	0.93	0.98	0.90	0.93	0.99	0.91	0.90

This design example shows that, even if the slenderness ratio $\lambda_{FB,y}$ is less than 40, the highest grade is not always the optimum. It depends on the profile availability and thus on the material usage. Indeed, as shown in the table above, there is no profile in the HEA profile series that gives a unity check equal to 1.0 for S600 and S700, so S550 is the optimum grade.

The unity check, also called utilisation ratio, constitutes a good indicator to evaluate the material use efficiency (see Example 4-3). This study illustrates the column slenderness, the material cost but also the section typology dependency. Indeed, it has been shown that, above a certain load level, lighter

sections are no longer of interest. At a certain profile weight, the height-to-width ratio of HE sections becomes greater than 1.2 as the width no more increases with the weight, which means that the weak-axis inertia no longer increases with the cross-sectional area resulting in a smaller radius of gyration and therefore to a greater column slenderness. The choice of the appropriate range of profiles has been identified as important to realise larger weight savings. Finally, solutions may be found to reduce the column slenderness by reducing the buckling length, for example by using pre-stressed stayed columns [62], [76]. Nonetheless, the practical application of such a system is rare, and it is difficult to imagine such a concept in a building. On the contrary, an adequate consideration of the end fixity of the columns could reduce both the applied load and the buckling length. It should be remembered that these results have been plotted for the medium relative cost level and for two specific profile categories, but the above-mentioned discussions apply regardless of the profile category and the relative cost of the grades.

4.4.3. Members in simple bending

This third type of structural member refers to members subjected to simple bending, which is a loading situation generally met for beams. Two situations are considered for the ULS: (i) the beams are laterally restrained, so lateral torsional buckling cannot occur and (ii) the beams are unrestrained, so lateral torsional buckling can occur. In this study, the focus is made on simply supported beams (with fork supports at both ends) subjected to a uniformly distributed load along the beam.

4.4.3.1. Serviceability limit states

Beams are generally subjected to simple bending what requests to check SLS in addition to the ULS criteria. This means that the deformations must be limited to a certain threshold, regardless the yield strength. In fact, the deflection of a beam is a function of its flexural stiffness and not its yield strength. Consequently, as explained in Section 2.3.6, SLS conditions may significantly limit the economic benefit of using high-strength steels when determining the optimum design. Three different levels of deflection limits are considered as reported in Table 4-3.

Low	Intermediate	Restrictive
$L/100$	$L/300$	$L/500$

Table 4-3. Allowable deflection limits considered in the framework of this research.

The intermediate value of $L/300$ is adopted, except for the sensitivity study on the deflection threshold for which the three levels defined in Table 4-3 will be considered. To investigate the areas where SLS criteria govern the design, an analytical expression of a separation line has been derived. This line separates the area where SLS conditions govern from the area where ULS conditions govern.

For a beam subjected to a uniform load, the SLS check is determined by the following formula:

$$v = \frac{c_f \cdot q_{EK} \cdot L^4}{384 \cdot E \cdot I_y} \leq \frac{L}{300} \quad (4-8)$$

where $q_{EK} = q_{Ed}/1.4$, the characteristic load (unfactored) and c_f , the deflection coefficient ($c_f = 5.0$ for pinned end beams). Therefore, the maximum allowable design uniform load to respect the SLS requirements is:

$$q_{Ed,SLS} = \frac{1.4 \cdot 384 \cdot E \cdot I_y}{300 \cdot c_f \cdot L^3} \quad (4-9)$$

For ULS conditions, considering class 1 or 2 cross-sections and restrained beams (where lateral-torsional buckling is prevented), the check is:

$$M_{pl,Rd} = \frac{W_{pl,y} \cdot f_y}{\gamma_{M0}} \geq M_{Ed} = \frac{q_{Ed} \cdot L^2}{c_M} \quad (4-10)$$

with c_M the bending moment coefficient ($c_M = 8$ for pinned end beams). So, the maximum design uniform load to respect ULS conditions is:

$$q_{Ed,ULS} = \frac{c_M \cdot W_{pl,y} \cdot f_y}{\gamma_{M0} \cdot L^2} \quad (4-11)$$

To derive the separation line between the field governed by SLS conditions and the field governed by ULS conditions, both mathematical relations (4-9) and (4-11) must be equalised. The coordinates of the separation line in a (q_{Ed}, L) system can be computed using the expression Eq. (4-12).

$$(q_{Ed}, L) = \left(c_M^3 c_f^2 3.159 \cdot 10^{-4} \left(\frac{W_{pl,y}^3}{I_y^2} \right), \frac{1060.056}{c_M c_f} \left(\frac{I_y}{W_{pl,y}} \right) \right) \quad (4-12)$$

This line is intended to facilitate the interpretation of results in the next subsections.

4.4.3.2. Resistance to local buckling

For beams experiencing simple bending (about strong axis), the normal stress distribution is such that one flange is in pure compression while the web is in pure bending. The resistance gain for a given plate can be computed using the same method as for compression members – Eq. (4-13) and Fig. 4-18.

$$\frac{M_{Rd,HSS}}{M_{Rd,S235}} = \frac{\rho_{HSS} \cdot W_y \cdot f_y}{\rho_{RS} \cdot W_y \cdot 235} = \left(\frac{\rho_{w,HSS}}{\rho_{w,RS}} \right) \cdot \left(\frac{f_y}{235} \right) \quad (4-13)$$

Where; $W_y = W_{pl,y}$ for Class 1-2 cross-sections and $W_y = W_{el,y}$ for Class 3 cross-sections.

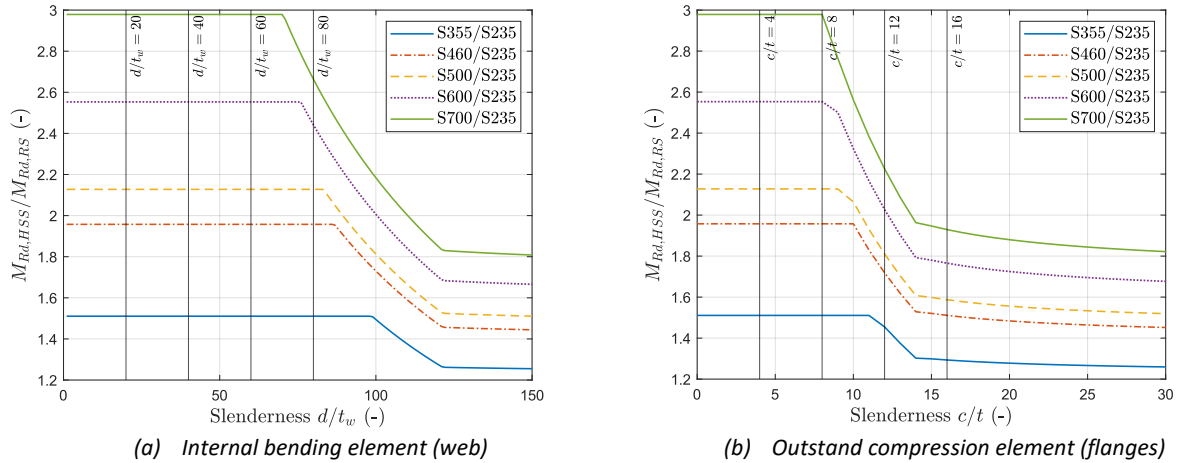


Fig. 4-18. Relative resistance to local buckling as a function of yield strength for hot-rolled sections under pure bending.

In the IPE profile series, the maximum web slenderness is 57, and the maximum flange slenderness is 7 for the slenderest profile IPE 750x134. Consequently, beams made from IPE profiles, are not affected by the local buckling up to 700 MPa. It is worth noting that the optimum plate in high-strength steels (HSS) may be of Class 3 and the optimum plate in regular steel (RS) of Class 1 or 2, which can lead to additional penalisation due to the type of verification allowed [76]. Indeed, for Class 3 cross-sections, only an elastic verification is allowed while for Class 1-2 cross-sections, a plastic verification is allowed. This feature will be accounted for in the optimisation results obtained using the developed routine (see Section 4.4.3.5).

4.4.3.3. Resistance to shear buckling

When a member is subjected to simple bending, it may carry a certain shear force that may cause a shear buckling of the web. This instability phenomenon reduces the shear resistance of the cross-section. The shear resistance ratio considering only the contribution from the web and a non-rigid end post, according to EN1993-1-5 [222] can be evaluated using Eq. (4-14) and the results are shown in Fig. 4-19 for various grades.

$$\frac{V_{b,HSS}}{V_{b,S235}} = \frac{\chi_{w,HSS} \cdot A_w \cdot f_y}{\chi_{w,RS} \cdot A_w \cdot 235} = \left(\frac{\chi_{w,HSS}}{\chi_{w,RS}} \right) \cdot \left(\frac{f_y}{235} \right) \quad (4-14)$$

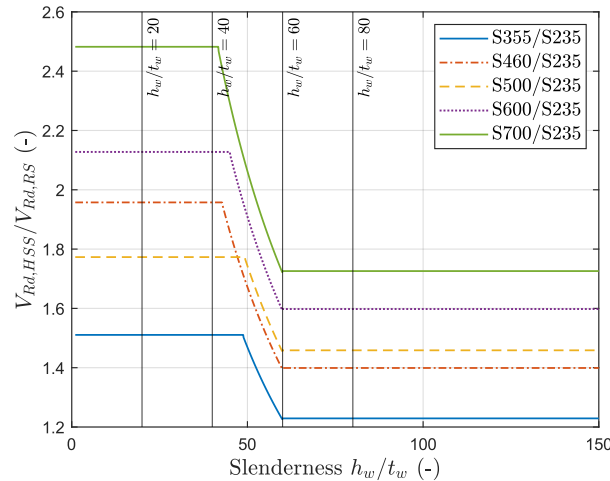


Fig. 4-19. Relative resistance to shear buckling as a function of yield strength and the web slenderness.

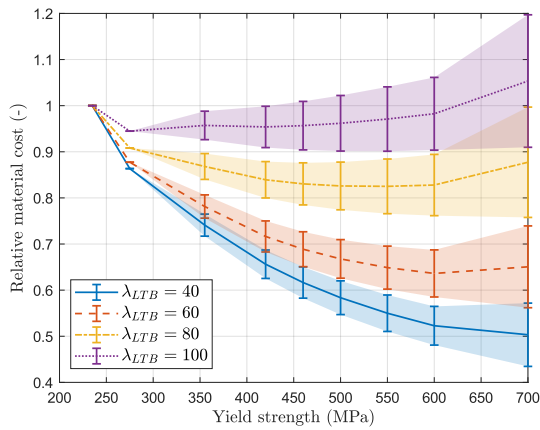
Fig. 4-19 illustrates that, in the shear resistance procedure, the reduction factor is equal to the coefficient η for non-slender webs. This coefficient is modified for grades higher than 460 MPa, i.e. $\eta = 1.2$ for grades up to S460 and $\eta = 1.0$ for grades above. This step in the design recommendations highly penalises the shear resistance of high-strength steel grades and explains why the relative resistance of S460 is higher than that of S500 in Fig. 4-19. The web slenderness limit of $h_w/t_w = 40$ is generally exceeded for built-up elements but the same is also observed for the last profiles of the IPE profile series; this is why this criterion is also addressed in this chapter.

4.4.3.4. Resistance to lateral torsional buckling

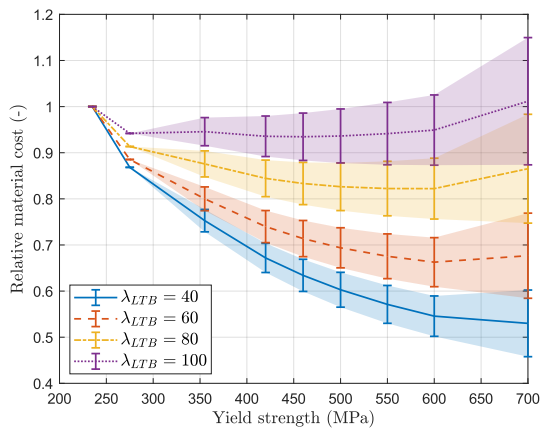
The resistance ratio to lateral-torsional buckling is calculated using Eq. (4-15) for a simple beam of either Class 1-2 or Class 3, for both compared grades.

$$\frac{M_{Rd,HSS}}{M_{Rd,S235}} = \frac{\chi_{HSS} \cdot W_y \cdot f_y}{\chi_{RS} \cdot W_y \cdot 235} = \left(\frac{\chi_{HSS}}{\chi_{RS}} \right) \cdot \left(\frac{f_y}{235} \right) \quad (4-15)$$

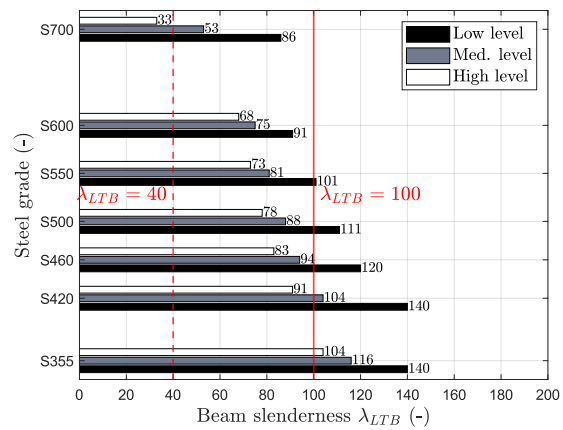
Where; $W_y = W_{pl,y}$ for Class 1-2 cross-sections and $W_y = W_{el,y}$ for Class 3 cross-sections. Fig. 4-20 reports the relative material costs and slenderness limits for both buckling limits, defined in Table 2-12, as a function of the beam slenderness. The critical moment resistance, as defined in Table 2-9, depends on the slenderness (λ) and the section's shape, through the coefficient ζ expressed in Eq. (2-6). The slenderness denoted λ_{LTB} for lateral-torsional buckling, accounts for the geometrical properties, the application point for the load, the support conditions, the moment distribution and the possible presence of a mid-span lateral restraint.



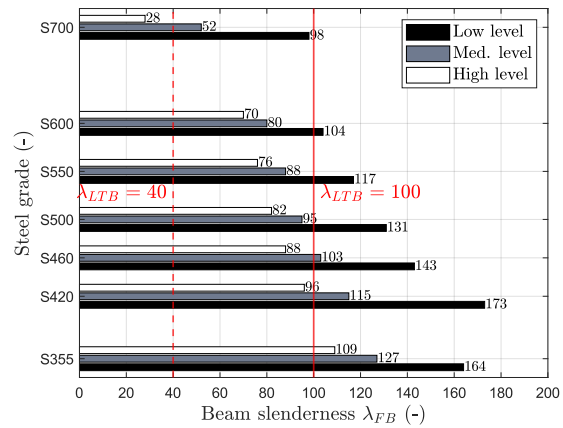
(a) $h/b \leq 2$ – relative costs



(c) $h/b > 2$ – relative costs



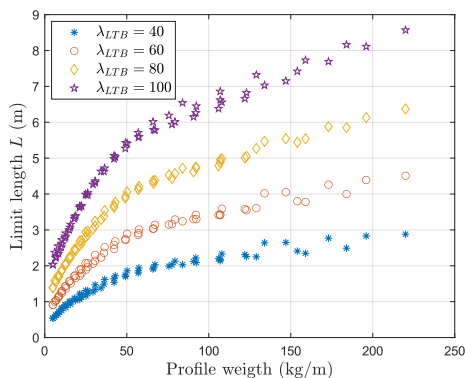
(b) $h/b \leq 2$ – slenderness limits



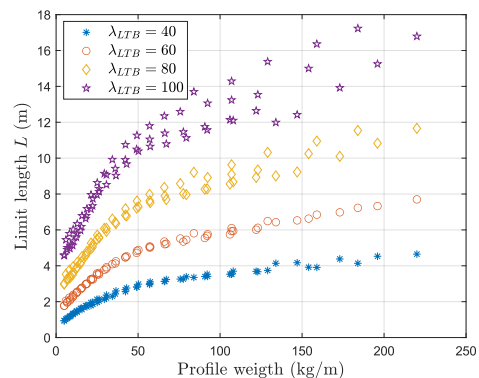
(d) $h/b > 2$ – slenderness limits

Fig. 4-20. Relative material cost and slenderness limits for members in simple bending.

Compared to the analysis of compression members, the analysis of beams shows a similar trend in terms of slenderness, i.e. λ_{LTB} should be below 40 to present a benefit in producing S700 grade while there is no more benefit in producing high-strength steels for beam slenderness λ_{LTB} above 100. Indeed, Fig. 4-20a illustrates that the relative material cost becomes higher than one above 460 MPa. This means that using a higher yield strength results in an economic loss compared to the use of mild steels (e.g. S235 or S355). As for compression members, a limit of $\lambda_{LTB} = 80$ could be adopted to justify the benefit of developing and considering grades above the practical range. The figures with the slenderness limits for each couple of steel grades are reported in Appendix B. Fig. 4-21 shows the evolution of the span length limit for each profile of the IPE profile series as a function of the beam slenderness (λ_{LTB}) and the profile weight. It includes (a) unrestrained simply supported beams and (b) simply supported beams with one lateral restraint at midspan.



(a) $C1=1.12$ and $k_2=1.0$



(b) $C1=1.33$ and $k_2=0.5$

Fig. 4-21. Limitations in terms of beam lengths for simply supported beams.

Fig. 4-21 indicates that, for a classical beam length of 6m, the beam slenderness for most profiles is above 80, limiting the benefit for high-strength steels. However, when a lateral restraint is positioned at mid-span (Fig. 4-21b), the last profiles of the range reach a slenderness of 60 resulting in a greater benefit for high-strength steels, particularly for heavy-loaded beams. However, this grade comparison is made without considering the eventual penalisation due to local buckling or shear buckling. The optimum design is also assumed to be governed by ULS criteria. Eventually, the conclusions presented are for beams belonging to the same section class, with a fixed slenderness λ_{LTB} for which the area decreases with an increased yield strength. As for columns, beam slenderness normally increases with a decrease in the cross-sectional area; the reality is therefore even less favourable for high-strength steels.

4.4.3.5. Results of optimisation routine for hot-rolled simply supported beams

The results, which account for all the design criteria and both discrete and continuous IPE catalogues, established on the same basis as expressed in Section 4.2.4, are represented in Fig. 4-22 for simply supported beams subjected to a uniform loading.

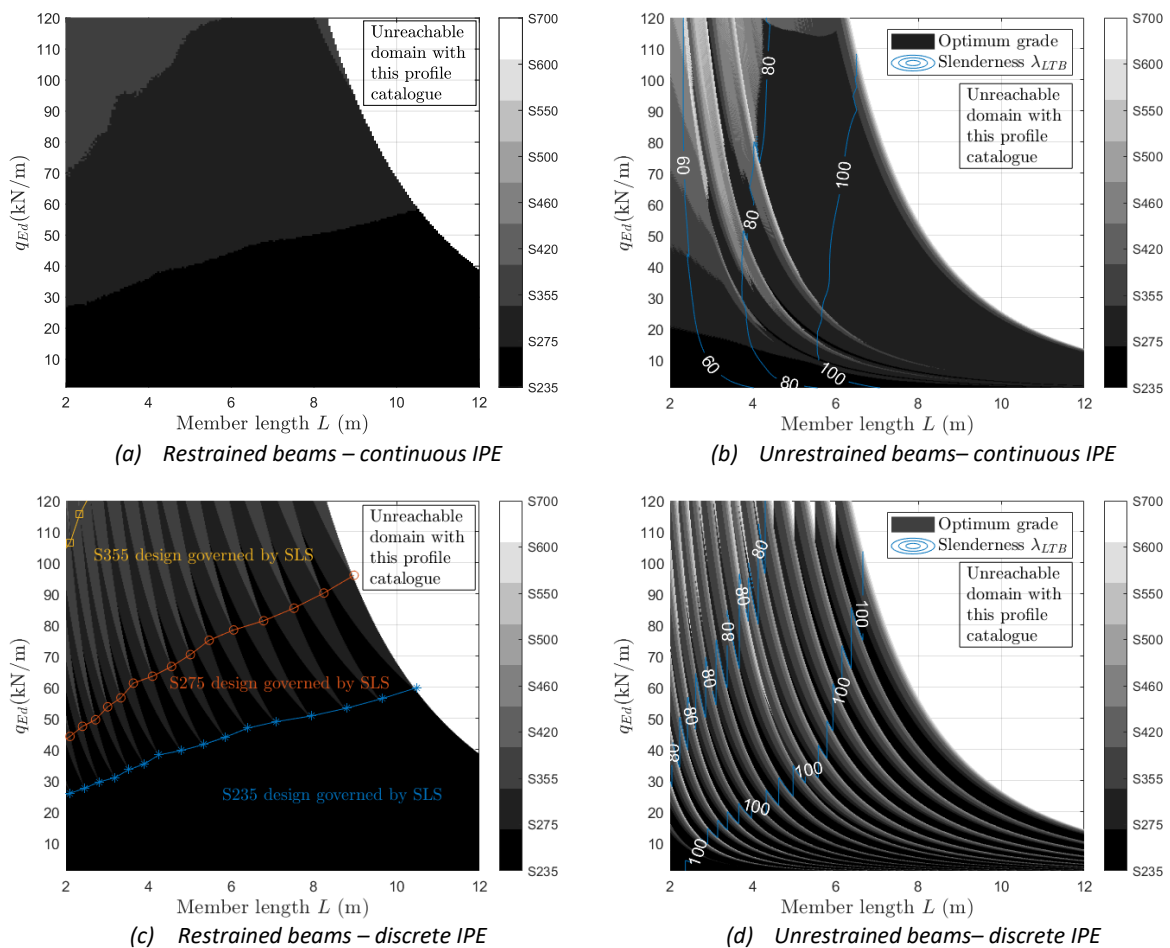


Fig. 4-22. Results of optimisation for simply supported beams and IPE profile series.

Fig. 4-22a and Fig. 4-22c demonstrate that SLS requirements govern the design for restrained simply supported beams in most cases. The separation line derived in Eq. (4-12) is reported in Fig. 4-22c to illustrate the dominance of SLS checks. Beyond a certain steel grade, size reduction is no longer possible due to the SLS checks that determine the optimum profile size. Example 4-4 provides a design example for which SLS conditions control the design. On the contrary, for unrestrained beams that are prone to lateral torsional buckling, the presence of this instability has the effect of strengthening the

ULS conditions (Fig. 4-22b and Fig. 4-22d). Indeed, for unrestrained beams, the ULS conditions are straighten due to the stability requirements, which leads to an increase in the potential areas of benefit for high-strength steels as the dominance of SLS checks is reduced. However, this beneficial effect can only be observed for reasonable beam slendernesses. Similarly to compression members, the beam's slenderness λ_{LTB} is reported in Fig. 4-22b and Fig. 4-22d to illustrate that the beam slenderness should be less than 80, to have a benefit in considering S460-S500 grades. This applies to very stocky and highly loaded beams. Based on these results, it seems that there is no advantage in developing grades beyond the practical range. Nevertheless, these conclusions are specific to a simply supported beam subjected to a uniform loading. A parametric study has thus been conducted to assess potential solutions for improving the advantage of high-strength steels.

Example 4-4. Optimum steel grade for a 6m simply supported beam subjected to $q_{Ed} = 100 \text{ kN/m}$

The maximum bending moment at midspan is equal to: $M_{Ed} = \frac{q_{Ed} \cdot L^2}{8} = 450 \text{ kNm}$ and $V_{Ed} = \frac{q_{Ed} \cdot L}{2} = 300 \text{ kN}$. The optimum profiles to respect SLS and ULS criteria are:

Steel grade	ULS	SLS	Optimum
S235	IPE500	IPE450	IPE500
S275	IPE450		IPE450
S355	IPE400		IPE450
S420	IPE400		IPE450
S460	IPE360		IPE450

The optimisation results demonstrate that, from grade S275, the optimum design is controlled by SLS criteria. Consequently, there is no more benefit in increasing the yield strength further.

4.4.3.6. Solutions to improve the benefit of high-strength steels

Section 4.4.3.5 brings the conclusion that the benefit of developing high-strength steel beams is relatively limited for stocky and highly loaded beams due to the combination of SLS requirements and the resistance penalisation to account for lateral torsional buckling. Solutions may be proposed to enhance the benefit of high-strength steels; these are reported below. The results are plotted for a continuous IPE catalogue to avoid any discretisation effect.

- **Solution 1 – To reduce the buckling length by accounting for rotational stiffness at supports or by positioning intermediate lateral supports**

The beam slenderness depends on various parameters including the buckling length, the geometrical properties, the application location of the transverse loads, the moment distribution, ... To decrease the beam slenderness and benefit from increased yield strengths, fixed purlins or bracings can be added to reduce the buckling length. The results for simply supported beams with reduced weak-axis buckling lengths are reported in Fig. 4-23.

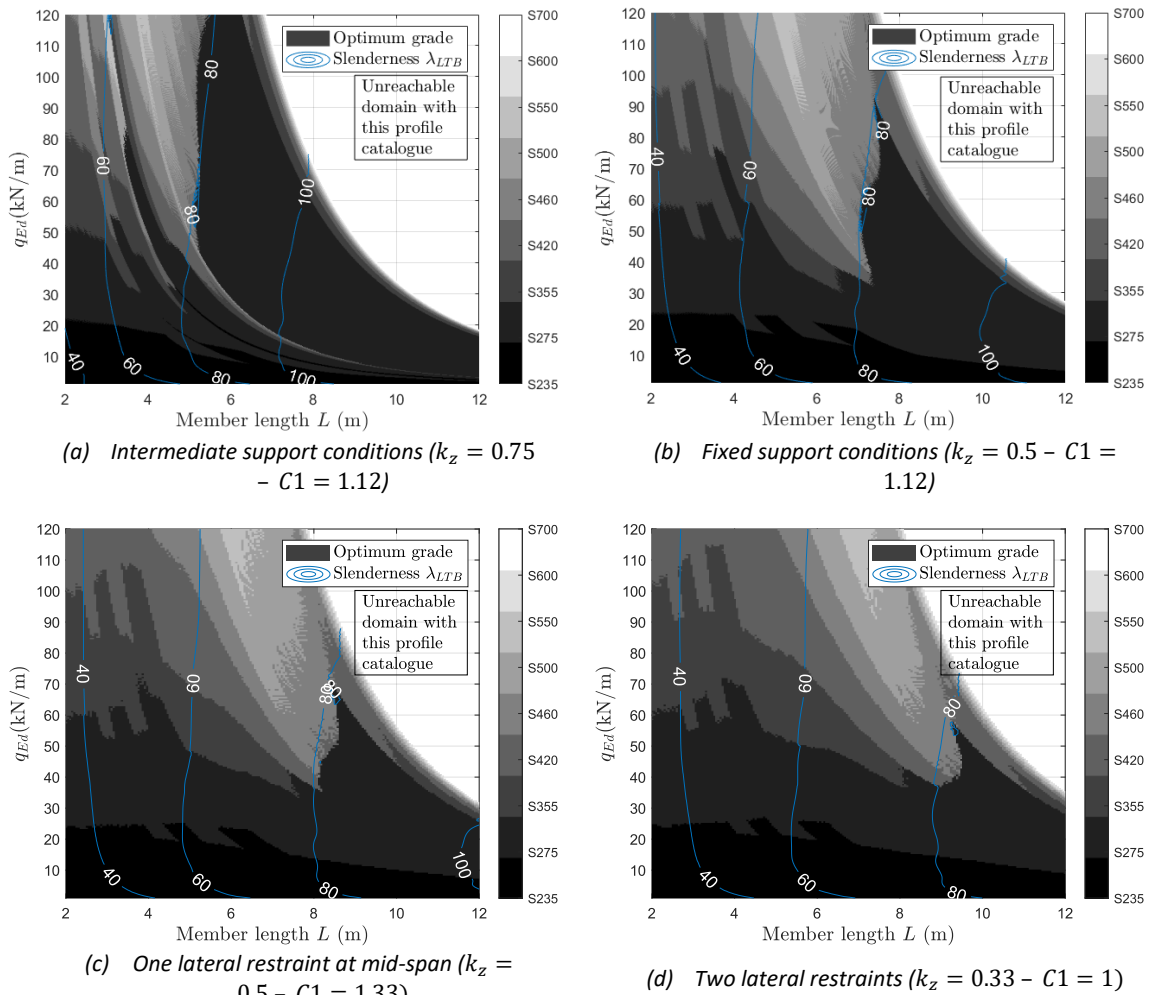


Fig. 4-23. Impact of intermediate lateral supports on the benefit of using high-strength steels for beams.

As can be seen in Fig. 4-23, reducing the buckling length of the beam element by adding lateral restraints decreases the risk of lateral torsional buckling. However, this weakens the ULS conditions, thus increasing the dominance of SLS. The more restrained the beams are, the closer the results from the unfavourable results obtained for fully restrained beams (Fig. 4-22a). The benefits of high-strength steels are limited to the already produced grades, namely S460 and S500. The benefit for these grades reduces as the number of lateral supports increases. Consequently, it appears that adding one support is the optimum configuration to maximise the advantage for S460-S500 grades but there is still no benefit to go beyond.

➤ **Solution 2 – To reduce the deflection limit**

Previous optimisation results have shown that the optimum designs should not be controlled by the serviceability criteria in order to have potential benefits of considering high-strength steels. Therefore, the impact of the deflection limit is analysed in Fig. 4-24 for the two extreme levels defined in Table 4-3. It is worth mentioning that the solution of pre-cambering the beam can be seen as a reduction of the deflection limit.

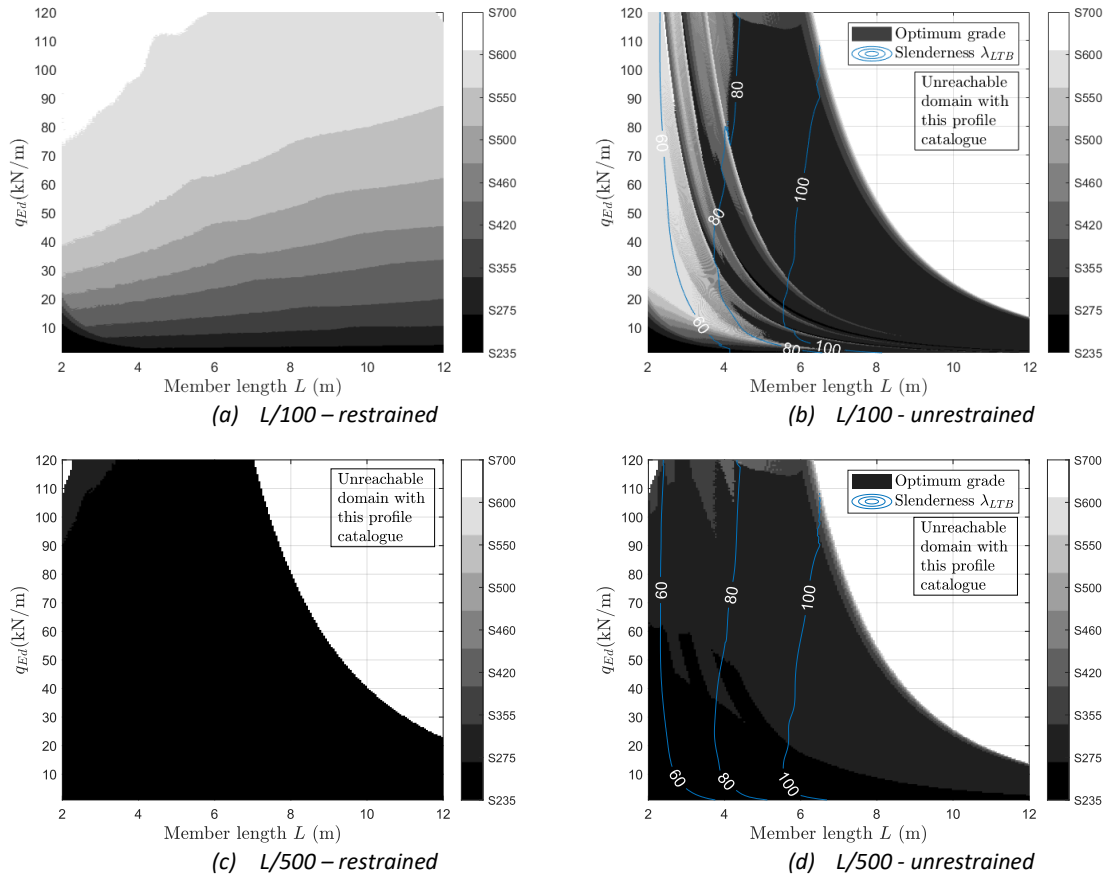


Fig. 4-24. Impact of the allowable deflection limit on the benefit of using high-strength steels for beams.

Fig. 4-24 demonstrates the significance of deflection limitations on the benefit of using high-strength steels. The benefits for grades above the practical range are significantly improved when deflections are reduced, or the deflection limit is relaxed to $L/100$ as shown in Fig. 4-24a and Fig. 4-24b. However, for beams prone to lateral-torsional buckling, the benefit is also limited by the beam slenderness, it appears that the benefit is concentrated for beam slendernesses below $\lambda_{LTB} = 80$. By contrast, if the deflection limit becomes stricter (e.g. $L/500$), there is no more benefit in considering other grades than mild steels, such as S235 or S275, regardless of the beam slenderness.

➤ **Solution 3 – To reduce deflections by considering a rotational stiffness at supports.**

Simple end support conditions are detrimental in terms of deflections. Therefore, considering a rotational restraint at beam supports could enhance the advantage of using high-strength steels as already suggested in previous studies [76], [223]. The studied cases considered are reported in Table 4-4.

Case studies	M_{max}^+	M_{max}^-	M_{max}	v_{max}	k_z	C1
1	$\frac{q_{Ed} \cdot L^2}{8}$	0	$\frac{q_{Ed} \cdot L^2}{8}$	$\frac{5 \cdot q_{Ek} \cdot L^4}{384 \cdot E \cdot I_y}$	1.0	1.12
2	$\frac{5 \cdot q_{Ed} \cdot L^2}{48}$	$\frac{q_{Ed} \cdot L^2}{48}$	$\frac{5 \cdot q_{Ed} \cdot L^2}{48}$	$\frac{4 \cdot q_{Ek} \cdot L^4}{384 \cdot E \cdot I_y}$		1.20
3	$\frac{q_{Ed} \cdot L^2}{12}$	$\frac{q_{Ed} \cdot L^2}{24}$	$\frac{q_{Ed} \cdot L^2}{12}$	$\frac{3 \cdot q_{Ek} \cdot L^4}{384 \cdot E \cdot I_y}$		1.20
4	$\frac{q_{Ed} \cdot L^2}{16}$	$\frac{q_{Ed} \cdot L^2}{16}$	$\frac{q_{Ed} \cdot L^2}{16}$	$\frac{2 \cdot q_{Ek} \cdot L^4}{384 \cdot E \cdot I_y}$		1.22
5	$\frac{q_{Ed} \cdot L^2}{24}$	$\frac{q_{Ed} \cdot L^2}{12}$	$\frac{q_{Ed} \cdot L^2}{12}$	$\frac{q_{Ek} \cdot L^4}{384 \cdot E \cdot I_y}$		2.60

Table 4-4. Case studies for the impact evaluation of the joint stiffness.

The best-case scenario is the beam fixed at both ends, the results for the last two cases listed in Table 4-4 are represented in Fig. 4-25.

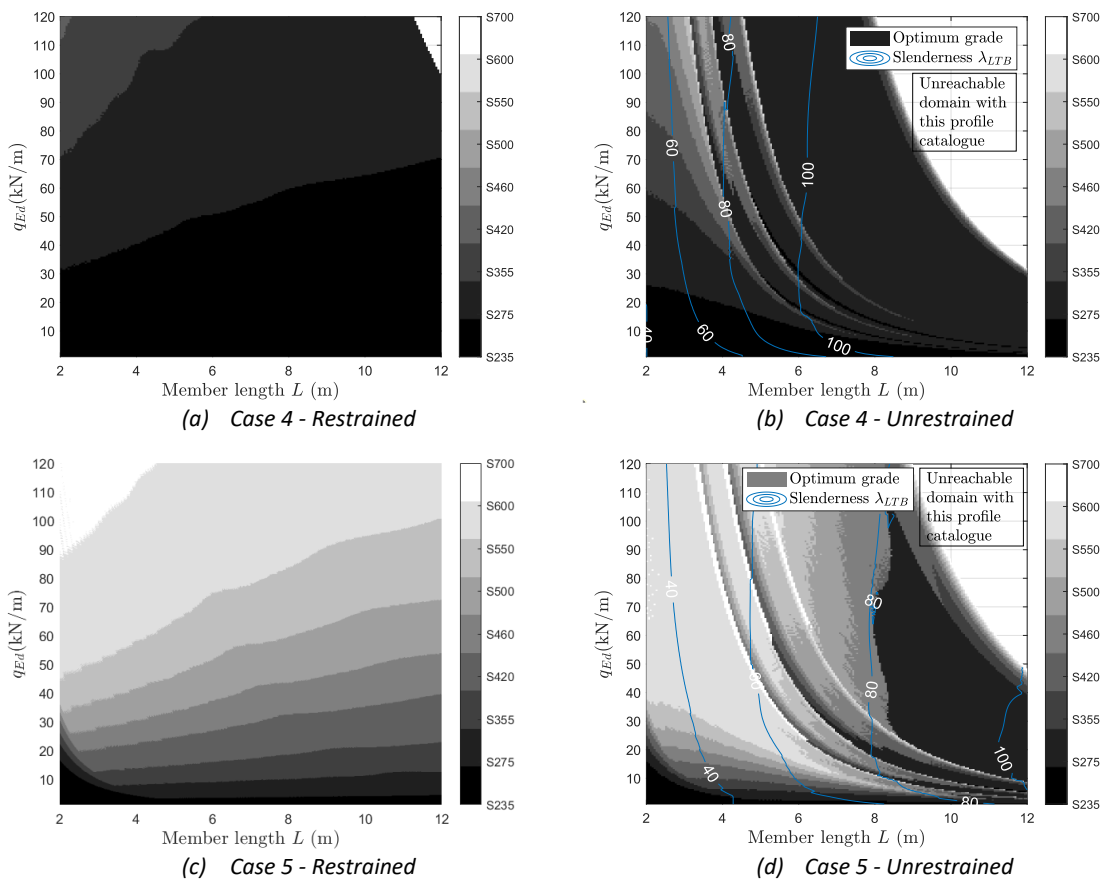


Fig. 4-25. Optimisation results for Cases 4 and 5 defined in Table 4-4.

As shown in Fig. 4-25, the fixed rotations at the extremities significantly reduce the vertical deflections at midspan (divided by 5) as well as the internal bending moments. However, a small loss of rotational rigidity directly induces a limitation of the benefit due to lateral torsional buckling.

Parametric studies have revealed that the benefit for grades above the practical ranges is limited to very specific case studies. Consequently, to enhance the benefit, it is important to address the various threats to high-strength steels simultaneously, as it appears that no single solution can solve the issue

alone. For instance, considering an intermediate lateral support and pre-cambering the beam may result in a benefit for high-strength steels. Furthermore, bending stiffness, EI , controls all instabilities and deflection requirements of the beam, but the Young's modulus remains the same for all steel grades. In the past, Bjorhovde [45] even suggested that metallurgists and engineers should focus on the development of new high-strength materials with a higher elastic modulus. Indeed, he stated that even a 10% increase could be highly beneficial as it plays simultaneously on all threats for high-strength steels.

4.4.4. Members subjected to combined compression and bending

The last section of the member study pertains to members that are subjected to combined compression and bending. Specifically, the studied members are columns that are axially loaded with a uniaxial bending in the strong axis plane, as illustrated in Fig. 4-26.

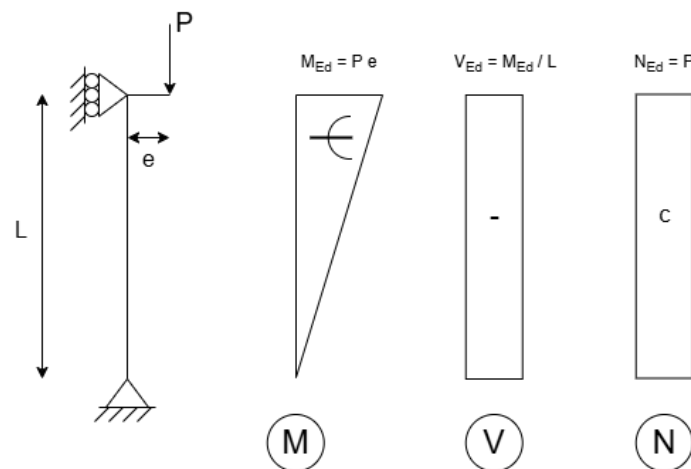


Fig. 4-26. Case study for hot-rolled members subjected to combined compression and bending.

This type of member is common because the compression load often has an offset with the centreline of the column. This means that there is often an eccentricity of the axial load, which produces an internal bending moment in the column. The purpose of this section is to evaluate the effect of this load eccentricity on the pure compression results shown in Section 4.4.2. It is important to mention that the boundary conditions (eccentricity $e = 0$ representing pure compression or $e = \infty$ corresponding to pure bending) were checked before interpreting the results to ensure consistency with the results presented in the previous sections. The scope of this study is limited to HD profiles as these profiles, due to their wide thickness, present a greater potential for high-strength steels (see Fig. 4-15). For HD profiles, none is subjected to shear buckling (the maximum h_w/t_w is 34.87 which is below the limit even for S700 grade – see Fig. 4-19). Two different cases are analysed:

- Case 1 – Out-of-plane instabilities are prevented;
- Case 2 – All instabilities may occur whatever the buckling axis.

The results are presented in Fig. 4-27 for both cases and a continuous HD catalogue.

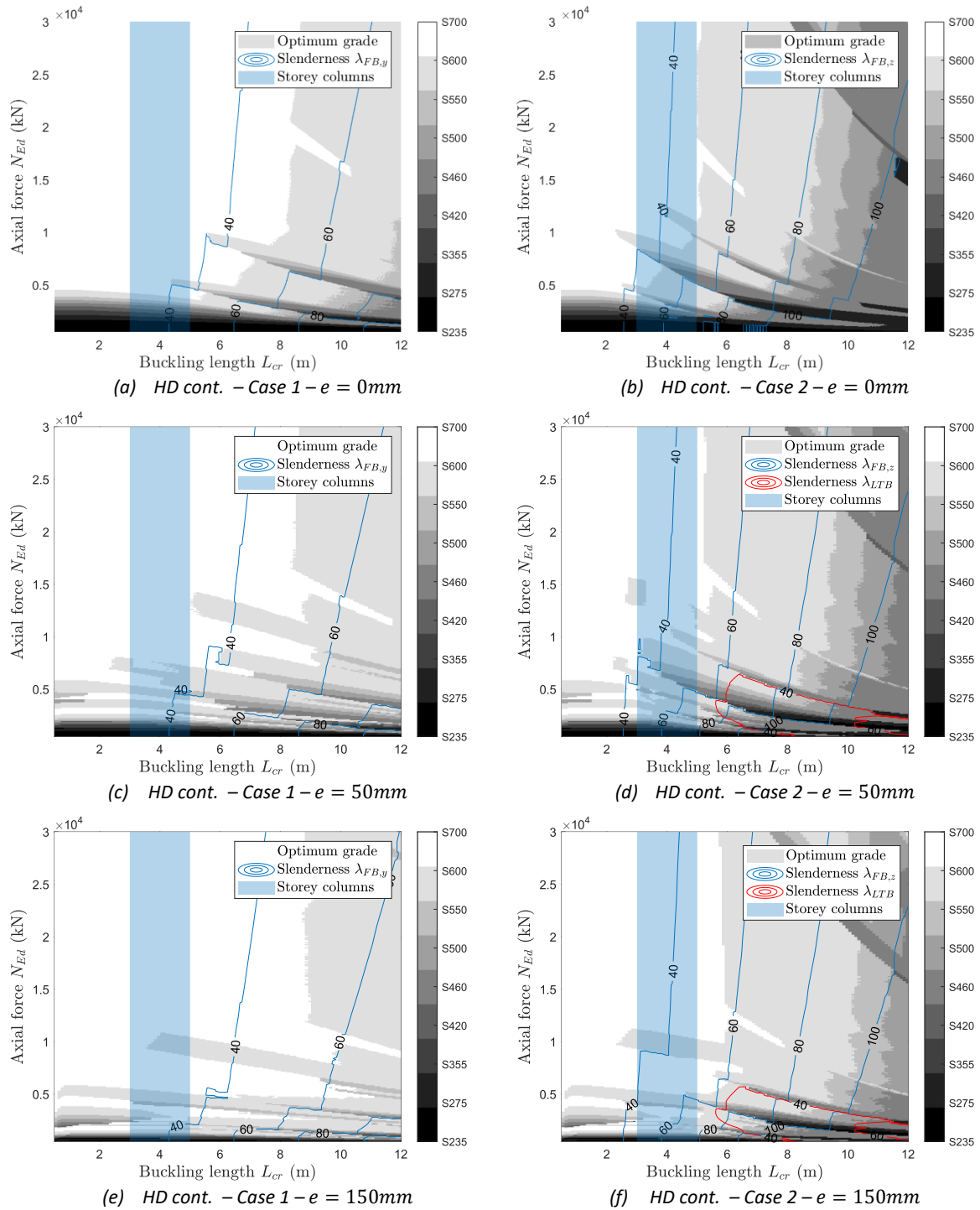


Fig. 4-27. Optimisation results for HD members subjected to combined compression and bending.

Regardless of the yield strength, an internal moment induced by the load eccentricity results in an increase in the size of the optimum profile. Consequently, for the same couple (L, N_{Ed}) , the slenderness of the optimum profile is reduced, making it less susceptible to instabilities. This feature explains why the benefit of high-strength steels globally increases with the load eccentricity. However, the second effect of considering an internal bending moment is to have shorter weight savings when using high-strength steels. Therefore, although the potential benefit for high-strength steels increases as instabilities are delayed, the actual benefit depends more on the relative prices. This feature was already observed in the validation (Fig. 4-6), the zones for which high-strength steels present an advantage increase but, the associated weight savings reduce when adding a bending moment to the

column. Therefore, although there is still a benefit in terms of weight optimisation, this reduction may influence the conclusion in terms of cost optimisation (see Fig. 4-7).

4.5. Results for hollow sections

Structural hollow sections have superior mechanical properties compared to opened sections, especially in torsion, compression and bending in all directions with a large variety of available sections and dimensions. Different typologies exist: circular (CHS), square (SHS) and rectangular (RHS) which can be either cold-formed or hot-finished. The compressive strength of a circular or square hollow section is very high, particularly in terms of flexural buckling, given that its inertia is maximum in all directions. The weight savings induced by the use of S500, S600 or S700 instead of S355 grade were already investigated in [219]. However, as explained in Section 4.3, fields of application for the various grades were not identified; thus, hollow sections have also been analysed in the framework of this research. This chapter does not cover the use of hollow sections under simple bending as they are generally less economical for bending members than classical I-shaped hot-rolled sections.

4.5.1. Members in tension

The geometrical properties of the optimum profiles are reduced in proportion to the increase in yield strength as the resistance to tensile forces is directly proportional to the yield stress. The same relation expressed in Eq. (4-2) applies, thus there is an economic benefit in using the highest considered grades for tension members as concluded for hot-rolled sections.

4.5.2. Members in pure compression

4.5.2.1. Resistance to local buckling

The impact of the yield strength on the resistance to local buckling for hollow sections is evaluated by Eq. (4-4) and the results are plotted for CHS (Fig. 4-28a) and SHS/RHS (Fig. 4-28b) as these are doubly symmetric cross-sections.

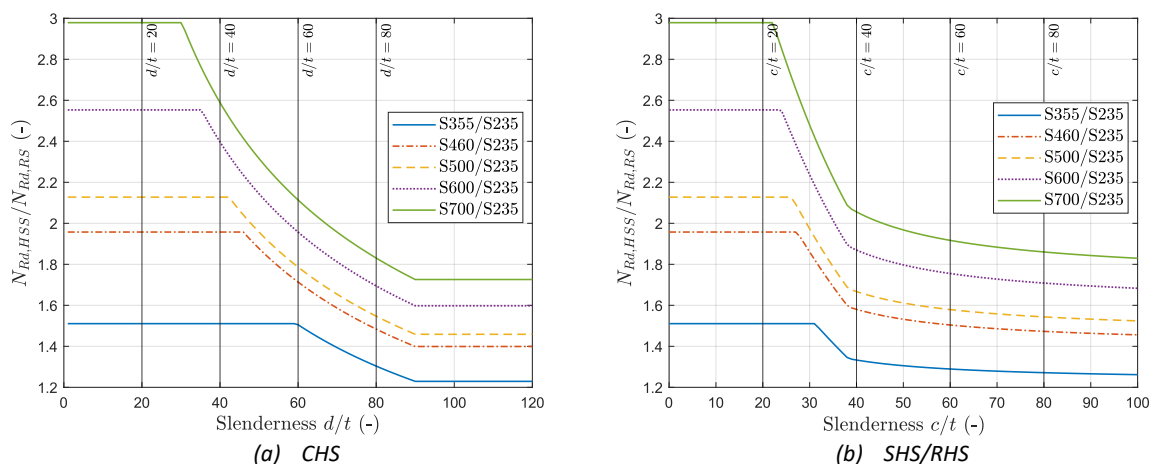


Fig. 4-28. Relative resistance to local buckling as a function of yield strength for hollow sections.

The practical guide for sustainable steel buildings [51] states that for SHS 260x8, increasing the width of this section without adapting the wall thickness (e.g. increasing to SHS 300x8) results in a negligible increase in terms of axial resistance for high-strength steel grades due to the presence of local buckling. Indeed, the slenderness of SHS 260x8 is equal to 32.5 which is on the decreasing slope for high-strength steels (see Fig. 4-28b). Therefore, increasing the wall thickness leads to an increase in column

slenderness associated with a higher reduction factor, which may counterbalance the increase in terms of cross-sectional area. In contrast to hot-rolled H-shaped and I-shaped sections, which typically have reasonable thicknesses, the walls in compression of hollow sections are generally slender. The diameter-to-thickness ratio for CHS varies between 7 and 127, while the width-to-thickness ratio for SHS varies between 8 and 50 (as stated in Section 4.2.4). This feature may particularly affect the benefit of using high-strength steels.

4.5.2.2. Resistance to flexural buckling

The relative resistance and material costs depending on the hollow section typology (hot-finished or cold-formed) for a given simple column with a fixed slenderness are described in Fig. 4-29 while the slenderness limits for each steel grade are represented in Fig. 4-30 and further details can be found in Appendix A.

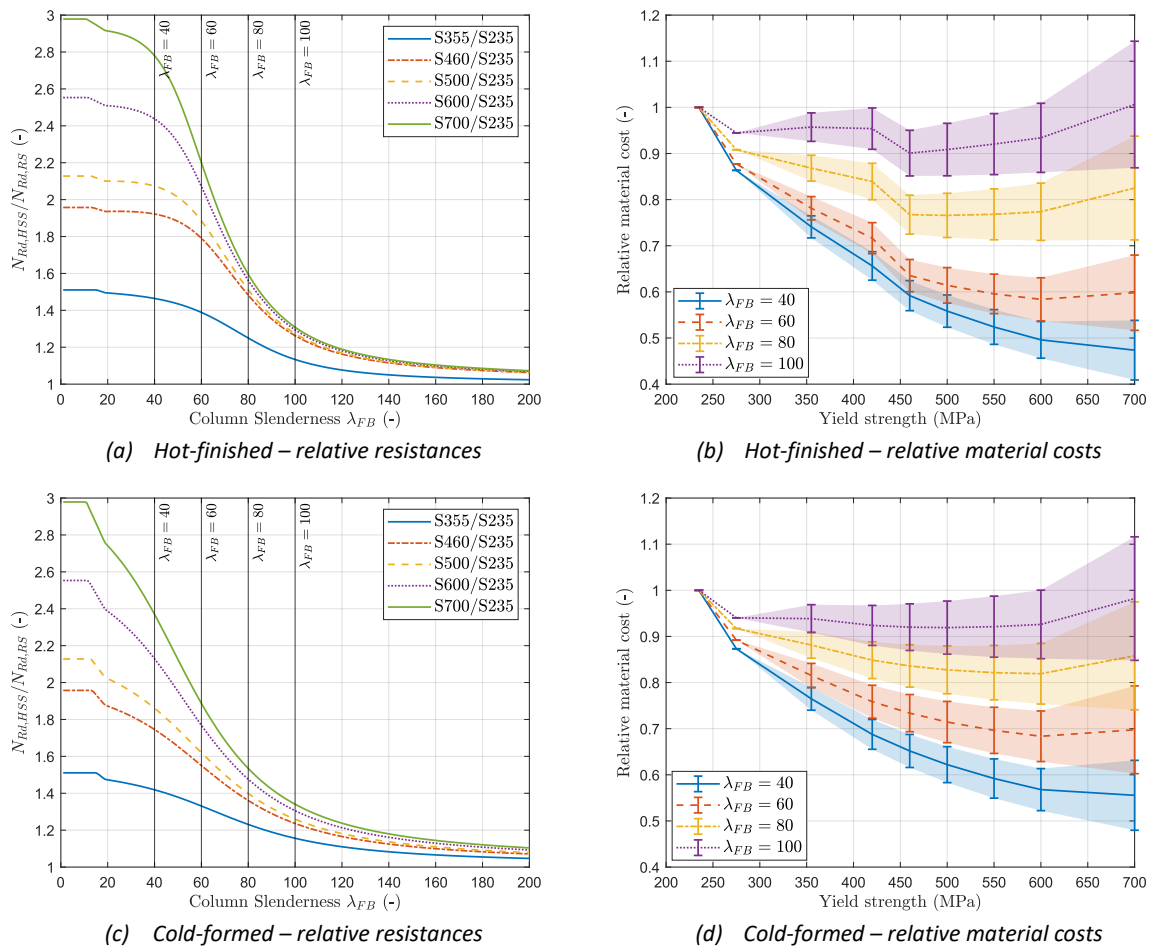


Fig. 4-29. Relative resistance and material cost for hollow sections under pure compression and considering S235 as reference.

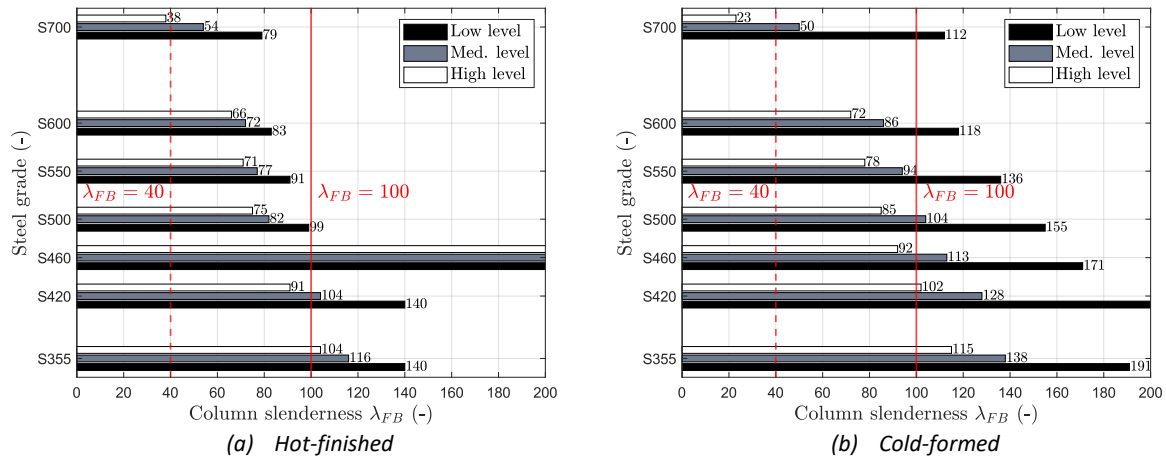
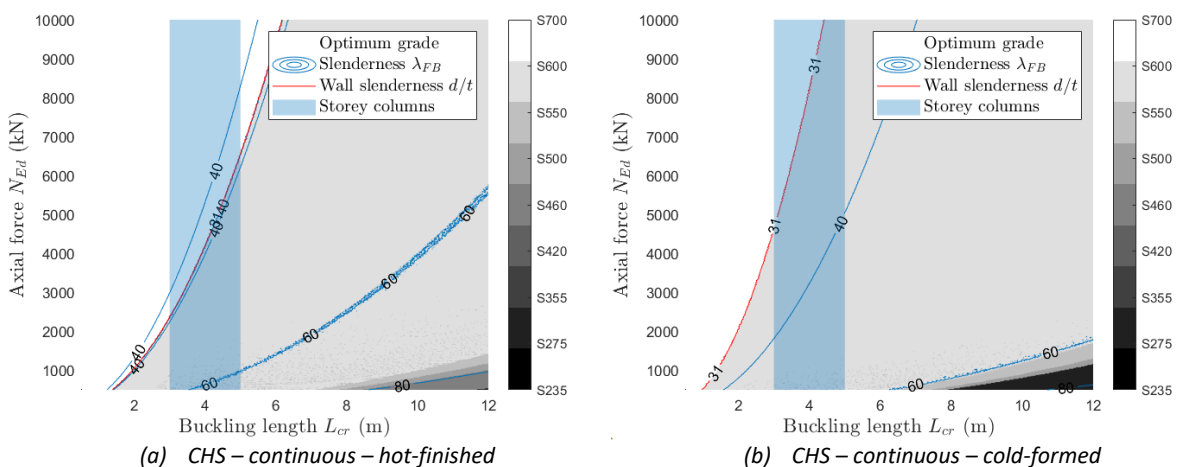


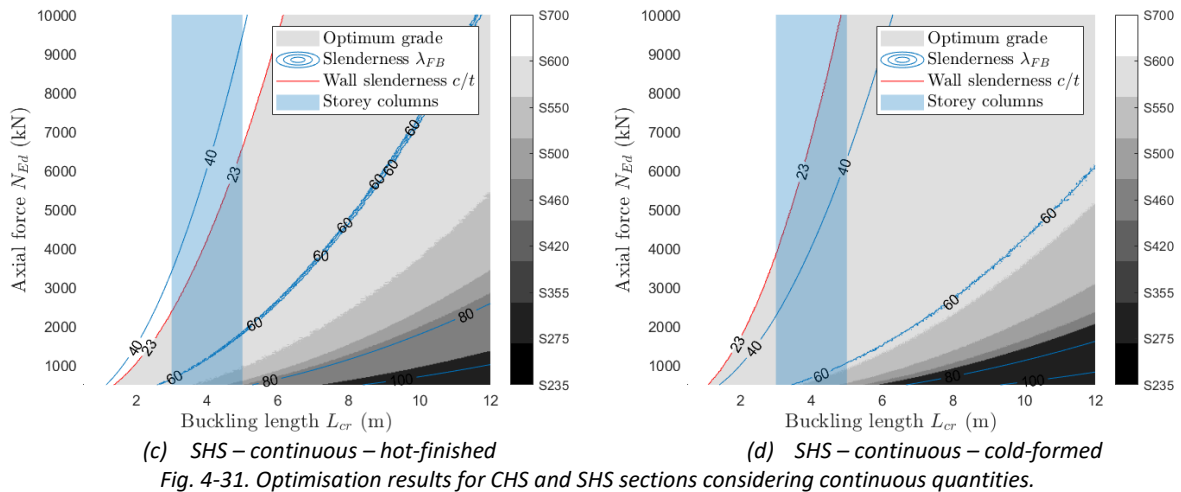
Fig. 4-30. Slenderness limits for each steel grade and for hollow profiles.

The conclusions expressed for hot-rolled sections still apply for hollow sections, i.e. for hot-finished hollow sections, the gap between the lines in Fig. 4-29a becomes smaller with the increased yield strength. It means that an increased yield strength results in a less favourable reduction factor for flexural buckling which offsets the increased cross-sectional resistance. According to Fig. 4-29 and Fig. 4-30, there is a benefit in considering grades above the practical range (i.e. at least S500) for column slendernesses respecting $\lambda_{FB} \leq 80$. The boundary limits are: $\lambda_{FB} < 40$, always a benefit in considering the highest steel grade, i.e. S700 and $\lambda_{FB} > 100$, no benefit in considering high-strength steel grades. It is worth pointing out that the same buckling curve is prescribed for cold-formed hollow sections, regardless of the steel grade, meaning that the S460 grade does not receive any preferential treatment for cold-formed hollow sections, this explains why the slenderness limit does not exceed 200 in Fig. 4-30b.

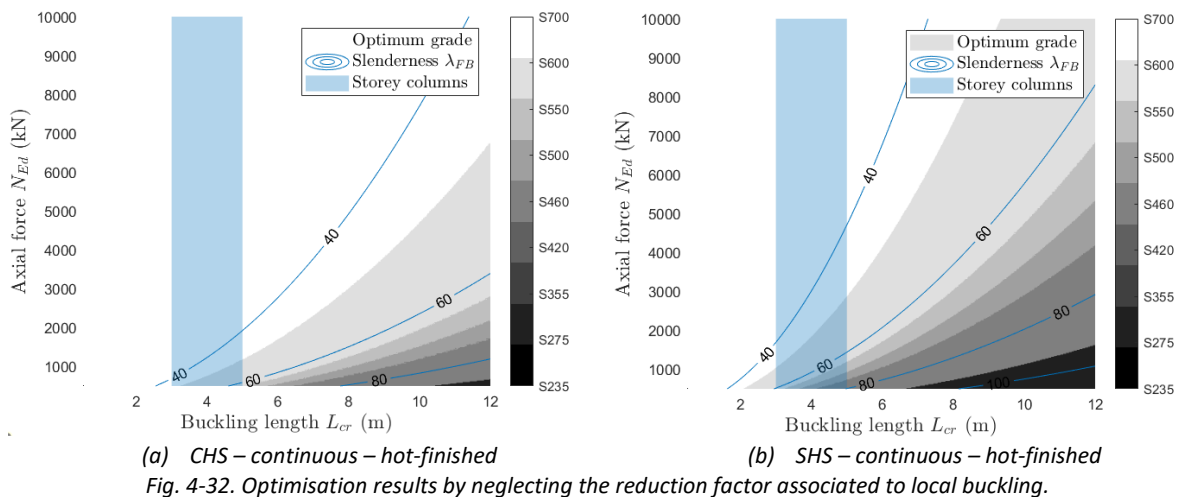
4.5.2.3. Results of the optimisation routine

The results of the optimisation routine for continuous CHS and SHS catalogues are gathered in Fig. 4-31. The wall slenderness limit for CHS in S700 is $90 \cdot \frac{235}{700} = 30.2$ and $38 \cdot \sqrt{\left(\frac{235}{700}\right)} = 22.0$ for SHS, these limits are included in the charts of Fig. 4-31 to demonstrate the impact of local buckling on the benefit of considering high-strength steels.





As shown in Fig. 4-31, there is a significant benefit for high-strength steels in steel tubes under pure compression. To benefit from grades above S460, the column slenderness should be below $\lambda_{FB} < 95$ for hot-finished and $\lambda_{FB} < 70$ for cold-formed sections. This applies to most of the domain under consideration for hollow sections. The cross-section classification, which refers to the resistance to local buckling, also affects the results as clearly demonstrated in Fig. 4-31 where the benefit for S700 is reduced due to local buckling. When comparing Fig. 4-29b and Fig. 4-29d, the relative material cost becomes close to a constant from S600, especially for cold-formed sections. This feature explains why a small loss of resistance due to the presence of local buckling may lead to a reduction of the benefit area for the S700 grade. Fig. 4-32 displays the same charts as Fig. 4-31a and Fig. 4-31c but without considering the reduction of resistance due to local buckling and, Example 4-5 illustrates the impact of local buckling on the optimum design. The conclusions drawn from this example apply to both CHS and SHS, and a significant benefit is expected for characteristic buckling lengths of storey columns as depicted in Fig. 4-31.



Example 4-5. Design details for a cold-formed column with: $N_{Ed} = 5000 \text{ kN}$, $L_{cr} = 4\text{m}$

The optimum profiles for S600 and S700 grades are reported here below.

Instabilities covered	Parameter	S600	S700	Weight saving (%)	Opt. grade
Flexural Buckling (FB) + Local Buckling (LB)	Opt. Profile	CHS 346.4x9.8	CHS 312.1x10.3	5.9	S600
	Area (mm ²)	10391	9773		
	λ_{FB} (-)	33.6	37.5		
	d/t (-)	35.2 (class 3)	30.3 (class 4)		
	Unity check (-)	0.99	0.99		
Flexural Buckling (FB)	Opt. Profile	CHS 601.8x4.7	CHS 564.8x4.4	11.9	S700
	Area (mm ²)	8888	7829		
	λ_{FB} (-)	18.95	20.19		
	d/t (-)	127	127		
	Unity check (-)	0.99	0.99		

This table shows that local buckling controls the design for the S700 grade. The maximum weight saving achievable is: $\left(\frac{700}{600} - 1\right) \cdot 100 = 16.7\%$. Therefore, for such slenderness, the local buckling highly affect the benefit of increased yield strengths.

Fig. 4-32 and Example 4-5 demonstrate the importance of local buckling on the advantage of using high-strength steels, and the necessity in reducing the importance of this buckling phenomenon. Besides, some authors already proposed in the past to develop innovative cross-sections to take better advantage of the increased yield strength [62], rather than simply using classical cross-sections. Various methods can be used to limit the width-to-thickness ratio of compression elements including the use of polygonal cross-sections, stiffeners (e.g. cold-formed folds) or corrugated webs [76], [90]. Nevertheless, such solutions can be costly and may offset the economic benefit of using high-strength steels. Despite the detrimental impact of local buckling, the overall benefit for high-strength steels remains significant within the defined domain, especially for buckling lengths corresponding to non-sway structures (as can be seen with the blue ranges in Fig. 4-31).

4.5.3. Members subjected to combined compression and bending

As for hot-rolled sections, the results for columns subjected to combined compression and bending are presented for specific loading situations, i.e. in the cases where the load eccentricity is equal to 0 mm, 50 mm or 100 mm. Hollow sections, which are “closed” sections by nature, exhibit bigger torsion performance compared to “opened” sections like H-shaped sections. Therefore, lateral-torsional buckling is not a concern for hollow sections in almost all practical applications. This comparison focuses on CHS due to the similarities between the results for CHS and SHS, as shown in Fig. 4-33.

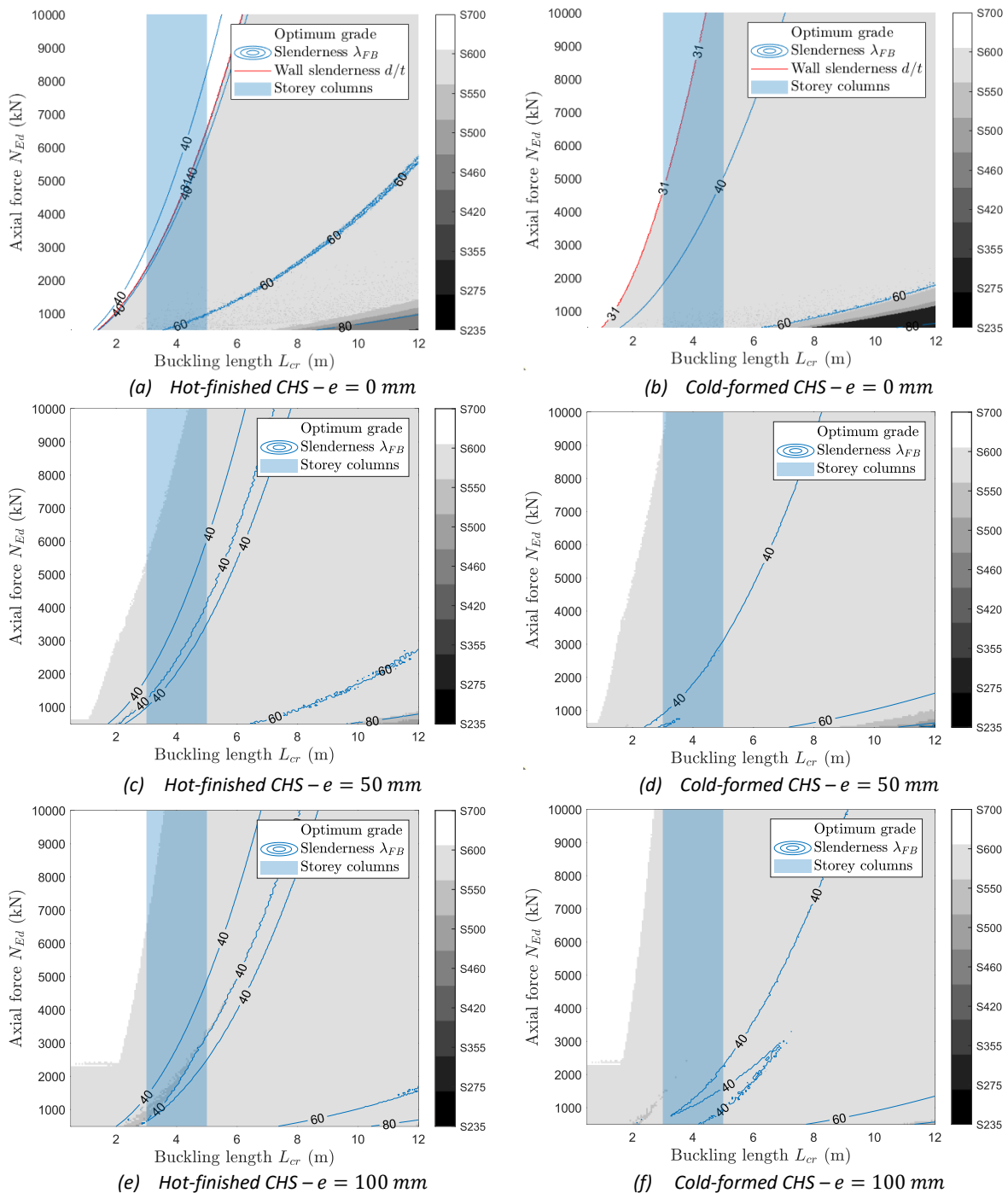
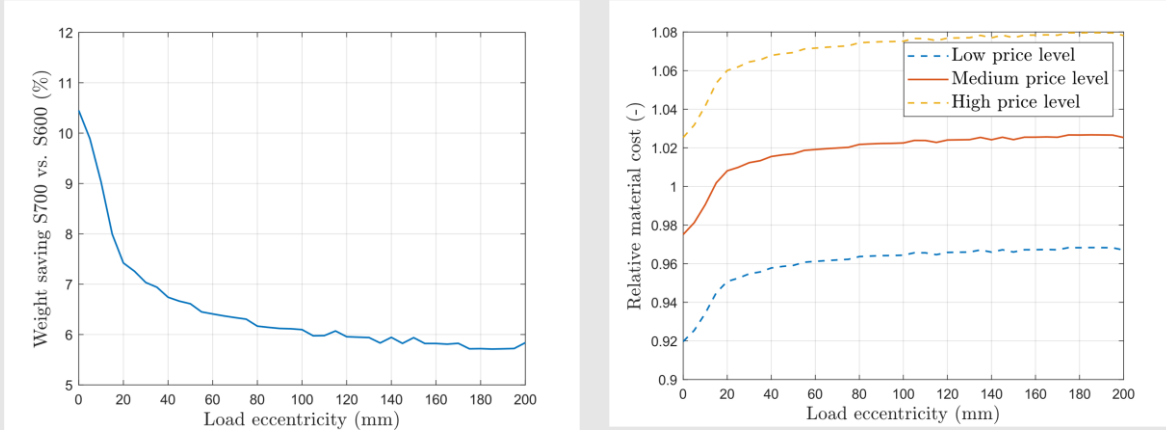


Fig. 4-33. Optimisation results for hollow sections subjected to combined compression and bending.

As shown in Fig. 4-33, the same observations as for HD sections are observed, i.e. the higher the load eccentricity, the higher the internal bending moment and thus, the higher the bending stiffness required to carry the load. As a result, for the same loading configuration, the column slenderness decreases with the load eccentricity, leading to an increased advantage for high-strength steels throughout the entire domain. When the load eccentricity is 100 mm, using at least S600 in the whole domain is beneficial. However, in the range of buckling lengths related to storey columns, the benefit of using S700 decreases with the increasing load eccentricity. This is because the reduction of cross-sectional area is limited by the bending stiffness required to carry the additional bending moment. Example 4-6 explains the reduction of benefit for S700 grade in a specific loading situation.

Example 4-6. Impact of load eccentricity on a specific case: $N_{Ed} = 6000 \text{ kN}$, $L_{cr} = 4\text{m}$

The charts below report the weight savings and the relative material costs of optimum designs in S600 and S700 as a function of load eccentricity for the three relative cost levels defined in Table 4-1.



These charts illustrate the reduction of economic benefit when using an increased strength due to an increase in load eccentricity. The reduction of area ratio induces that the benefit for S700 grade depends highly on its relative cost.

As illustrated in Example 4-6, although considering a bending moment reduces the weight saving and thus the economic advantage of high-strength steels, the benefits for high-strength steels beyond the practical range remain significant for hollow members subjected to combined compression and bending.

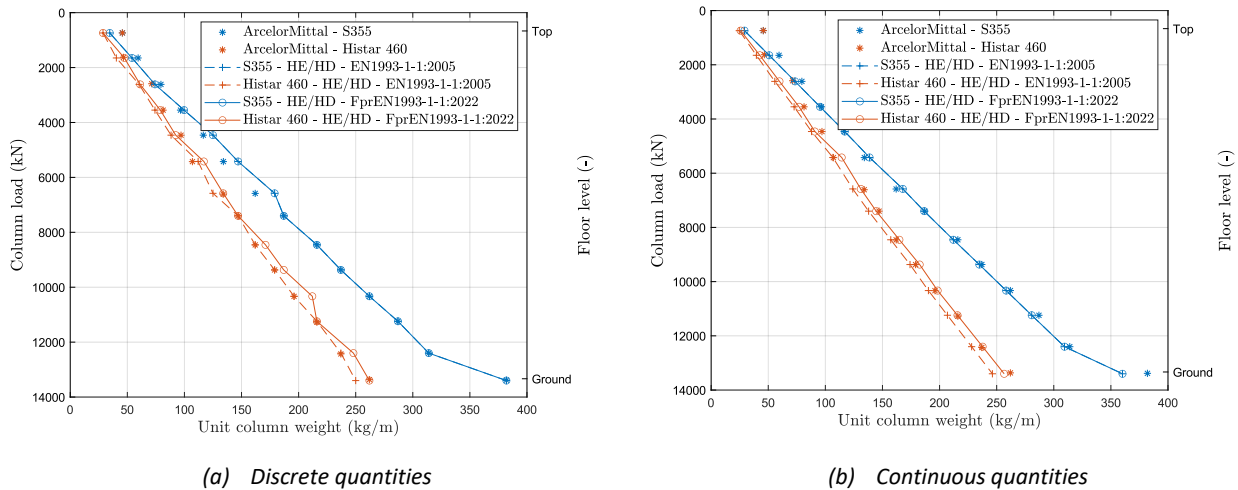
4.6. Case studies for compression members

This concluding section of Chapter 4 aims to quantify the advantages of using high-strength steels in practical applications, employing the methodologies developed in this thesis. As observed with the reference existing structures in Chapter 2, high-strength steels are particularly advantageous for compression members in high-rise buildings and in long-span structures. Consequently, two case studies have been selected to illustrate this, namely the Mapfre Tower in Barcelona for high-rise buildings and the NRG stadium in Houston for long-span structures. The first application is very detailed as this case study is well-documented while the second is intentionally concise.

4.6.1. Mapfre Tower in Barcelona

The highest grades produced today (e.g. S460-S500 for hot-rolled sections) are often used for high-rise buildings as these structures have highly stressed columns on the lower floors as expressed in Section 2.5. For these highly loaded columns, the optimisation potential by using S460 instead of S355 is between 20% and 40% according to the literature [51], [76], [115], [224]. In a promotional paper [28], ArcelorMittal promoted its HISTAR® 460 trademark steel by giving an example of its use in the Mapfre Tower in Barcelona. This 40-storey skyscraper with a total height of 154m was built in 1991 in HISTAR® 460 next to a similar building, the Hotel Olympia, with the same structural concept, similar dimensions and acting loads, but built in S355. The buckling length of the constitutive columns is 3.3m which is close to the lower bound of the buckling length range introduced in Section 4.3. ArcelorMittal compared the design of the Hotel Olympia in S355 with the design of the Mapfre Tower in HISTAR®

460 to derive the weight saving induced by the use of their innovative grade. The weight-saving amplitude for the ground-floor columns is 28% while, for the total column weight, an overall reduction of 24% is contemplated. Fig. 4-34 represents the unit column weights of each column for each floor in grades S355 and HISTAR® 460. As expected, it can be observed that the column weight decreases with the building height. This figure compares the column weights obtained by the column designs performed by ArcelorMittal with those returned by the optimisation routine developed in this thesis for the sake of validation. The designs in both selected grades were reproduced considering the European HE and HD profile series, with discrete quantities (Fig. 4-34a) or continuous quantities (Fig. 4-34b).



(a) Discrete quantities (b) Continuous quantities
 Fig. 4-34. Validation of ArcelorMittal's designs based on the optimisation routine.

As can be seen in Fig. 4-34, the optimal designs exhibit some discrepancies, particularly for the floors located near the top of the tower (less heavily loaded), which can be attributed to the availability of profiles. Indeed, for less loaded columns, there is a wider spectrum of available profiles compared to heavily loaded columns. Nevertheless, the calculated weight saving is 26% with the present optimisation routine, which is in close alignment with the results expressed in the reference [28]. It should be noted that the column's slenderness $\lambda_{FB,Z}$ significantly varies between floors, ranging from 30 at the ground floor to 70 at the top floor, so the benefit for high-strength steels may decrease with height. An optimisation routine has been developed to evaluate the potential benefit of developing high-strength steels, i.e. grades above S460, within the context of the present practical case study. The weight savings and relative costs as a function of yield strength are shown in Fig. 4-35, with S235 as a reference for the sake of continuity with the preceding investigations of this chapter. Continuous quantities have been used to establish the results.

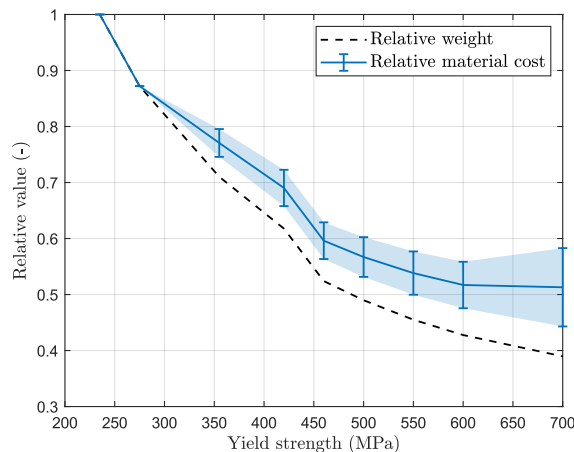


Fig. 4-35. Benefit in increasing the material yield strength for columns in the Mapfre Tower.

As can be seen in Fig. 4-35, there is an overall economic and environmental benefit to consider the highest considered grade, i.e. S700. Nonetheless, the aforementioned results assume that the same grade is used for all columns in the building, which is unlikely to be the optimum design. Fig. 4-36a represents the optimum grade returned by the optimisation routine as a function of the type of optimisation criterion and the column load, while Fig. 4-36b compares the slenderness range to the slenderness limits established in Section 4.4.2.2, in the worst-case scenario defined in Table 4-2 for sake of conservatism.

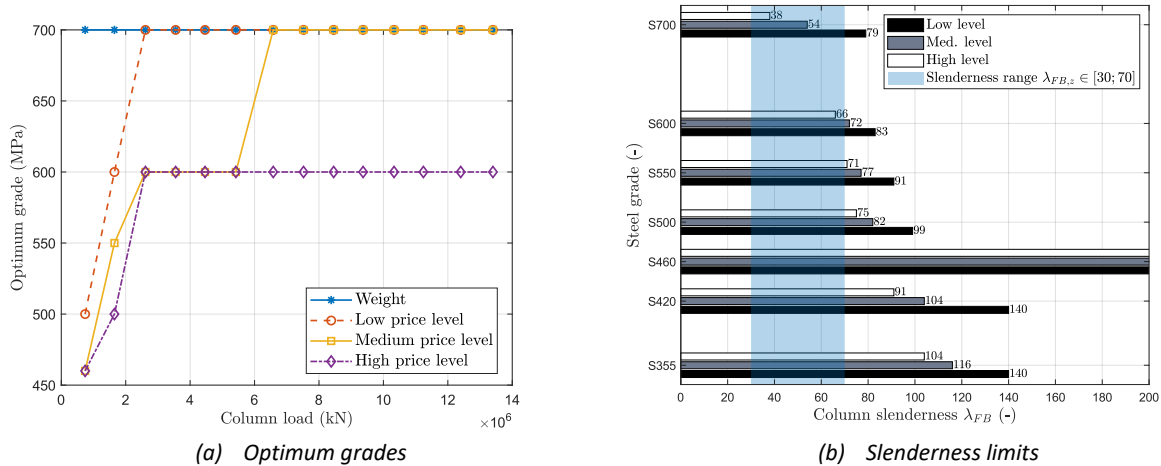


Fig. 4-36. Optimum grades and slenderness limits depending on the optimisation criterion.

Fig. 4-36a shows that, with regard to weight optimisation, it is beneficial to consider the highest considered grade for each floor of the tower. On the contrary, with regards to cost optimisation, the minimum is identified at a yield strength close to the maximum existing one for the two upper floors (optimum between S460 and S600 depending on the cost level), while it is advantageous to consider at least the S600 grade (in case of a high-cost level) for all the remaining floors. Fig. 4-36b presents the slenderness limits derived under the assumption that the same column is made of different steel grades, i.e. the column slenderness is not affected by the yield strength. Despite this assumption, Fig. 4-36b illustrates the same conclusion trends as the preceding ones, namely that there is a benefit in considering at least the maximum grades available in the European steel market (S460 and S500) irrespective of the material cost level and the floor level. On the contrary, the benefit for future emerging steel grades is highly sensitive to both the material cost level and the column slenderness. Indeed, there is a benefit to considering the S600 grade for column slendernesses below 60. This corresponds to the majority of floor levels, except for the two top floors. The advantage of utilising the maximum grade, specifically S700, is restricted to the bottom half of the structure and material costs that do not exceed the medium range. Therefore, this case study corroborates the suitability of the slenderness limits in providing an initial indication of the potential benefits of considering higher steel grades.

4.6.2. NRG Stadium in Houston

The Reliant Stadium was constructed in 2002 for multi-purpose activities such as concerts and professional or amateur sporting events. This stadium is scheduled to host multiple football matches in the 2026 FIFA World Cup. This was the first National Football League (NFL) stadium to be equipped with a retractable roof. In 2014, the stadium was renamed NRG Stadium. The specific design of the retractable roof was constructed using high-strength steels to achieve optimal efficiency. The advantage of opting for a Grade 65 (450 MPa) instead of a Grade 50 (345 MPa) was analysed and discussed in a paper [114]. For the highly loaded super trusses used for the retractable roof,

compression members were made from double W14-sections laced together with single angles. This approach was pursued to maintain the length of compression members at a minimum and maximise the benefit of using a higher grade. In the case of trusses with lower loads, single W14 chord members were employed, and the efficient bracing configuration ensures that the buckling lengths remain low. The authors presented a histogram of the member slenderness for the compression members employed in the stadium.

For the sake of conservatism, the worst-case scenario identified in Table 4-2 (see Section 4.4.2.2) has been considered to evaluate whether the maximum practical grade, i.e. S500, as well as future emerging grades (up to S690), would be of interest for this particular application. The results are reported in Fig. 4-37 on which the histogram of compression members used in the retractable roof is superposed.

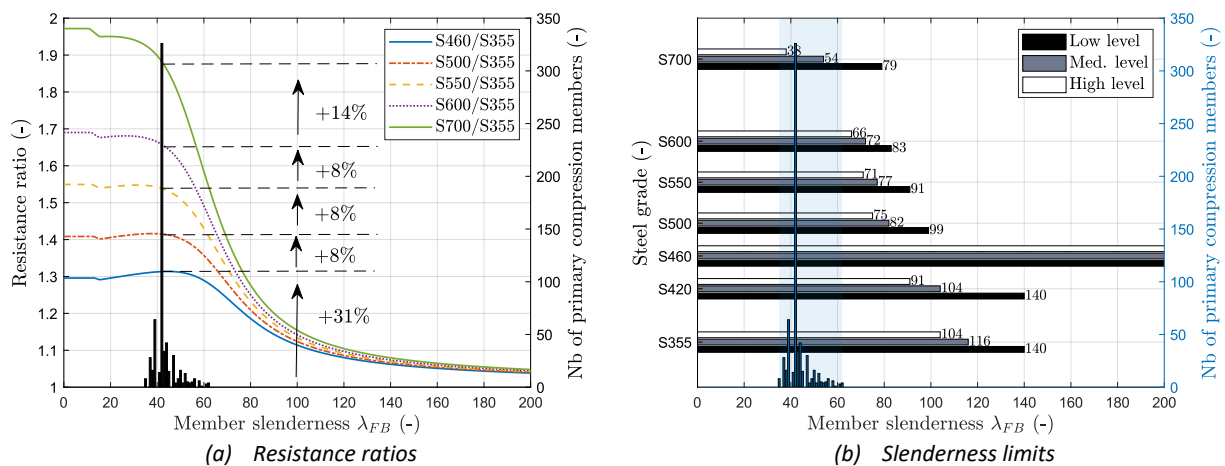


Fig. 4-37. Benefit of high-strength steels for the retractable roof of the NRG stadium at Houston.

This second case study demonstrates that, for the predominantly represented slenderness ratio ($\lambda_{FB} = 42$), there is a significant advantage in considering the maximum grade under concern. Indeed, Fig. 4-37a demonstrates that the relative resistance is frequently close to, or even occasionally higher than, the yield strength ratio. This phenomenon can be attributed to the gain of one buckling curve between grades S355 and S460, as recommended by current design guidelines [52]. Furthermore, as illustrated in Fig. 4-37b, most of the column slenderness values are close to the lower boundary of $\lambda_{FB} = 40$, meaning that there is an economic and environmental advantage in considering yield strength above the practical range in this specific application. It is nevertheless noteworthy that the designer employed a range of strategies with the objective of minimising the risk of structural instability by implementing an adequate structural system (with bracings to reduce the buckling lengths), thereby optimising the benefits of using high-strength steels. This highlights the importance of adequate designs for an optimum valorisation of the material performance.

In conclusion, these comparative investigations on case studies provide valuable insights into the advantages of high-strength steels in multi-storey buildings and long-span structures. The results of this study demonstrate that for a non-sway building or a well-designed super truss, the typical buckling length is such that the column slenderness remains within a range where there is a clear advantage in considering the highest available steel grade. In such applications, the development of higher grades beyond the practical range could therefore result in significant weight, cost and carbon savings.

4.7. Discussions and conclusions

This Chapter 4 presents a methodology for identifying the potential domains of benefit for high-strength steels. The methodology has been validated using a previously published comparative study. Several conditions have been identified which can assist manufacturers in updating their product catalogues to optimise the benefits of increased strength and allow designers to optimise their designs.

As commonly known, the benefits for high-strength steels are significant and undeniable as long as the steel elements are strength-controlled, which is the case for members subjected to tensile forces or stocky columns subjected to pure axial compression.

On the contrary, for stability-sensitive members, i.e. flexural buckling or lateral-torsional buckling, reference slendernesses (λ_{FB} for flexural buckling and λ_{LTB} for lateral-torsional buckling) have been identified as relevant to assess the suitability of a steel grade. In general terms, the slenderness λ should be less than 100 to have a benefit in using the maximum grades that are produced today (S460-S500 in the European steel market), less than 80 to have a benefit in developing grades above the practical range and less than 40 to have a full benefit in considering the highest considered grade (S700). Further details regarding the aforementioned slenderness limits can be found in Appendix A. However, these limits are influenced by material efficiency. Some parameters such as the decreasing yield strength with the thickness, the load eccentricity, the slenderness of the constitutive plates (presence of local buckling) and the serviceability requirements are independent of the steel strength, thereby reducing the benefit in considering higher grades when they are the governing design criterion. Indeed, serviceability requirements are controlled by the bending stiffness, EI , so the development of steel grades with a higher elastic modulus as well as a higher yield strength would thus be of great interest, as already suggested to steelworkers and research engineers in [45]. Alternative strategies, such as pre-cambering or the addition of lateral support at mid-span, can be employed to enhance the advantages of high-strength steels, particularly in the context of beams where the benefits are clearly limited. Nevertheless, the use of weak beams and strong columns may be of interest in case of seismic designs as explained in Section 4.2.2.

The availability of steel sections is another factor that can influence the benefit of using high-strength steels. In fact, the discrete nature of current product catalogues has been seen as detrimental to the advantage of using high-strength steels, as sometimes the profile that allows the material to be optimised is simply not available. Nevertheless, the increased use of such materials is likely to influence their availability. Current catalogues were developed for S235 and S355 in the past and adjustments should be made to optimise the benefits of new and emerging grades. For instance, massive profiles such as HD sections may be manufactured exclusively in high-strength steels, given their frequent deployment in heavily loaded structures and the geometrical characteristics that reduce the risk to any form of buckling. Conversely, the lighter sections could be only produced in mild steels. The benefit of considering a high-strength steel is also a function of the cost-effectiveness of the steel which is determined by base price fluctuations, demand and the availability of the steel grade. As previously stated in Chapter 3, the primary focus has been on the costs associated with the production stage. However, it is possible to achieve additional savings by reducing the section size such as: a reduction in primer coating costs, a reduction in size extras, a reduction in transport costs ...

This chapter illustrates that, in some cases, the conclusions regarding the benefits of high-strength steels can be diametrically opposite depending on the relative cost levels. However, while the cost of steel has been chosen as the driving factor for the sustainability assessment, the weight reduction may also be an objective, this is why some results have been expressed in terms of weight saving.

Furthermore, in the context of structural design, where weight is a primary consideration, the utilisation of high-strength steels presents a dual benefit. The reduction in the weight of the structural members consequently results in a reduction in the mass of the supporting elements, including columns and foundations. The selection of an appropriate steel grade thus necessitates a careful analysis and consideration of all the relevant factors identified in this chapter. From an early stage in the design process, designers should consider solutions to reduce the slenderness of structural elements to achieve an optimised and more sustainable design, as seen in the second benchmark example (Reliant Stadium). Finally, this research indicates that some design rules were established for mild steels (S235 to S355) and some were just adapted for S460; the design rules should be fully adapted to take full advantage of the yield strength. The following Chapter 5 presents contributions to the development of more appropriate design rules.

Chapter 5

Improvement of the Existing Design Rules for Flexural Buckling

5.1. Introduction

In the context of the “build clever” approach of the hierarchy to net-zero presented in Fig. 1-3 of Chapter 1, the adoption of appropriate design rules is important to enable designers in exploiting the material performance as efficiently as possible and thus lead to weight savings. The investigations in this thesis have been focused on members under pure compression.

The determination of the load-bearing capacity of a member under compression, presenting an initial out-of-straightness and residual stresses resulting from the manufacturing process, is a stability problem that is governed by the geometry of the member and the mechanical properties of its constitutive material.

On the one hand, the yield strength plays a key role as the influence of geometrical and material imperfections is reduced as the yield strength increases. As expressed in Chapter 2, high-strength steels represent the highest strength-to-weight ratio among the existing steels, thus providing the same strength with less material weight. However, Chapter 4 illustrates that the S460 grade is the sole one that benefits from the reduced influence of initial imperfections, resulting in a non-physical stepwise evolution in the current design recommendations for flexural buckling set forth in EN1993-1-1 [52], [70].

On the other hand, there are also straightening techniques that permit to respect tolerances in terms of bow imperfections. This chapter is devoted to a comprehensive analysis of the beneficial advantage of the roller-straightening process. The roller-straightening process is a steel cold production technique which consists of passing a steel element through a series of rolls that bend the member, thereby leading to a progressive reduction of the initial geometrical imperfections along its weak axis. As expressed in Chapter 2, this post-treatment process induces a continuous yielding of the steel member, which may present a second interest as it reduces the compressive residual stresses at flange tips. This modification of the residual stress pattern may result in an increase in the carrying capacity of steel columns. Nevertheless, despite the fact that all long products are now systematically straightened, the two versions of EN1993-1-1 standard [52], [70] do not take into account the potential beneficial effect of the roller-straightening process on the buckling capacity.

In view of the aforementioned shortcomings inherent to the existing design recommendations, an exhaustive numerical investigation has been conducted at the University of Liège. The objective was to derive a modified imperfection factor that accounts for the yield strength in the buckling resistance design procedure and to evaluate the potential benefit of the roller-straightening process on the carrying capacity of steel columns. The overarching objective was to enhance design recommendations in order to reduce the use of natural resources in future steel structures.

5.2. Establishment of a modified imperfection factor

As stated in Chapter 2, the residual stress-to-yield strength ratio decreases as the yield strength increases. However, this advantageous effect is only incorporated into the existing design recommendations for grade S460. As summarised in Table 2-14, some authors have already proposed some modified imperfection factors to adequately account for the yield stress [145], [148], [155], [156], [157]. The first part of Chapter 5 assesses the influence of the yield strength on the buckling resistance of hot-rolled columns subjected to pure compression, and to put forth a novel imperfection factor expression with the objective of restoring coherence in the design rules.

5.2.1. Methodology

The pursued methodology consists of calculating buckling resistances based on geometrically and materially non-linear analyses with imperfections (GMNIA). These analyses are conducted by using the FineLg finite element software, which was developed by the Greisch office and the University of Liège [225]. This software has been employed and validated in numerous studies conducted previously to model instability phenomena [226], [227], [228], [229], [230]. The numerical investigations focus on hot-rolled H-shaped and hot-finished hollow sections in existing grades ranging between S235 and S500, as well as in future emerging higher grades (up to S690), therefore in the framework of a prospective study.

In addition, for H-shaped cross-sections, the scope of this study is limited to low-thickness flanges as these profiles are the most prevalent and commonly represented in product catalogues ($t_f \leq 40$ mm and $t_f \leq 100$ mm for height-to-width ratios above and below 1.2 respectively). The yield strength f_y of steel grades is considered equal to the recommended values in FprEN1993-1-1:2022 [52] for grades up to S700 depending on the thickness domain, i.e. $t_f \leq 40$ mm or 40 mm $<$ $t_f \leq 80$ mm (see Table 2-2). The HISTAR® trademark steels of ArcelorMittal offer enhanced yield strengths up to higher flange thickness. For instance, the nominal yield strength is maintained up to 100 mm for HISTAR® 460 hot-rolled sections [69]. However, according to product standards EN10025-2 [53], EN10025-4 [54], EN10210-1 [59] and EN10210-3 [58] even for flange thicknesses below 40 mm, a small decrease in the yield strength is contemplated (see Fig. 2-1 in Chapter 2). The impact of this potential decrease is also addressed in this research by considering the reduced yield strength associated with the flange/wall thickness as prescribed in the above-mentioned product standards.

A previous study has already investigated higher thicknesses, observing a negative effect associated with a reduction in yield strength [231]. However, only a limited number of sections with thicknesses exceeding 100 mm for $h/b > 1.2$ (already investigated in [231]) are available while such sections are not present for $h/b \leq 1.2$ in product catalogues [231], [232]. In accordance with the geometrical properties defined in EN10210-2 [233] for hot-finished structural hollow sections, only five CHS profiles exceed a wall thickness of 40 mm. With regard to SHS and RHS, it can be observed that none of the standard profiles in either category exceed a thickness of 40 mm. Consequently, the yield stress reduction is limited to a small number of hollow profiles.

The present study examines flexural buckling about both buckling axes. In order to simulate a buckling curve, 13 simply supported columns have been modelled corresponding to 13 distinct relative slendernesses along the buckling curve (varying from 0.2 to 2.6). The specimen length for each numerical simulation is defined using the Eurocode relative slenderness, which is dependent on the classification – see Eq. (5-1):

$$\bar{\lambda} = \sqrt{\frac{\beta \cdot A_{FEM} \cdot f_y}{N_{cr}}} \rightarrow L = L_{cr} = \frac{i \cdot \pi \cdot \bar{\lambda}}{\sqrt{\frac{\beta \cdot f_y}{E}}} \quad (5-1)$$

Based on failure loads obtained by numerical simulations, the corresponding reduction factors can be derived as follows:

$$\chi = \frac{N_{u,FEM}}{\beta \cdot A_{FEM} \cdot f_y} \quad (5-2)$$

Where $N_{u,FEM}$ is the ultimate load obtained by numerical simulations and A_{FEM} is the area of the cross-section used in finite element simulations. The correspondence between Eurocode and numerical buckling curves is evaluated by calculating the mean value ($\bar{\chi}$), the standard deviation (COV) and the minimum and maximum values of the ratios between numerical and analytical reduction factors ($\frac{\chi_{FEM}}{\chi_{EC3}}$). A buckling curve is deemed suitable when the mean value exceeds 1.0, which aligns with the partial safety coefficient for stability design calculations ($\gamma_{M1} = 1.0$). The statistical evaluation and the figures presenting the results of the study were produced by means of the MATLAB software [193]. While the majority of the numerical simulations have been performed by using beam finite elements, when no local instabilities are expected, some shell finite element simulations have also been conducted to generalise the conclusions to Class 4 cross-sections. A summary of the extensive numerical campaign, comprising over 2000 columns, is presented in Table 5-1 for hot-rolled sections and Table 5-2 for hot-finished hollow sections. The tables include the geometrical properties of the selected cross-sections, and the type of finite elements employed, which varies according to the cross-section classification. It is noteworthy that a greater number of profiles have been considered for height-to-width ratios below 1.2, to cover a broader range of thicknesses (up to 100 mm). Moreover, supplementary numerical simulations were conducted for HEM500, HD400x818 and CHS 406.4x25 profiles, taking into account the reduction in yield stress in accordance with the specifications of product standards EN10025-2 [53], EN10025-4 [54] and EN10210-3 [59].

Limits	Designation	h (mm)	b (mm)	t _w (mm)	t _f (mm)	r (mm)	Class in S460	Class in S690	Type of FE
h/b > 1.2 / t _f ≤ 40 mm	HEB400	400	300	13.5	24	27	2	3	Beam
	HEM500	524	306	21	40	27	1	2	Beam
	HEB600	600	300	15.5	30	27	4	4	Shell
h/b ≤ 1.2 / t _f ≤ 100 mm	HEA240	230	240	7.5	12	21	3	3	Beam
	HD400x262	387	398	21.1	33.3	15	1	1	Beam
	HD400x634	474	424	47.6	77.1	15	1	1	Beam
	HD400x818	514	437	60.5	97.0	15	1	1	Beam
	HEA300	290	300	8.5	14	27	3	4	Shell

Table 5-1. Geometrical properties and type of finite elements for each selected hot-rolled cross-section.

Designation	d / b (mm)	t (mm)	Class in S460	Class in S690	Type of FE
CHS 406.4x25	406.4	25.0	1	1	Beam
CHS 508x50	508.0	50.0	1	1	Beam
SHS 150x6.3	150.0	6.3	2	3	Beam
SHS 350x16	350.0	16.0	1	2	Beam
SHS 200x5	200.0	5.0	4	4	Shell

Table 5-2. Geometrical properties and type of finite elements for each selected hot-finished hollow section.

5.2.2. Description of the numerical model

Buckling curves are simulated using geometrically and materially non-linear analyses with imperfections (GMNIA). The numerical simulations are realised by imposed load at the top of the modelled column. The non-linear analysis is solved by the arc-length method in order to capture the decreasing load trend after reaching the peak load. The $N_{u,FEM}$ is considered equal to the peak load, which corresponds to the maximum load on the load-displacement curve. A mesh sensitivity study was conducted to determine the optimum number of beam elements for modelling a column. The results indicated that ten beam elements were identified as sufficient. Before conducting the non-linear analysis, a linear bifurcation analysis (LBA) is undertaken to ascertain the first instability mode shape. This mode shape is introduced as a geometrical imperfection and amplified by $L/1000$ as buckling curves were derived based on this value and as it is commonly recommended in many studies [107], [231], [232], [234], [235]. Regarding the residual stress patterns, as presented in Section 2.4.2, the preconised distributions for hot-rolled sections from ECCS [231], [232], [234] are implemented in the model, with peak stresses of $0.3 \cdot 235 = 70.5$ MPa for sections with $h/b > 1.2$, $0.5 \cdot 235 = 117.5$ MPa for sections with $h/b \leq 1.2$ as well as for SHS sections and $0.15 \cdot 235 = 35.25$ MPa for CHS sections. These residual stress distributions are supposed to be constant over the thickness, and the f_y^* indicated in Fig. 5-1 is 235 MPa. This ECCS residual stress model is commonly used for wide flange hot-rolled sections regardless the yield strength as it has been confirmed that the yield strength is not influencing the residual stress distribution within a hot-rolled cross-section [110], [134], [155], [236], [237]. Thus, this model has been considered for each numerical model as recommended in new standard FprEN1993-1-14:2024 [135] and expressed in Chapter 2. The recommended residual stress model for hollow sections is also conservatively considered for such simulations as it has been demonstrated that they have a negligible impact on the results for high-strength steels [140], [141], [148], [238], [239]. It is noteworthy that RHS/SHS sections exhibit longitudinal residual stress distributions, whereas CHS sections exhibit flexural residual stresses. This difference of residual stress nature may affect the flexural buckling behaviour. However, the results for all hot-finished hollow sections are gathered irrespective of the cross-section shape to conserve the same distinction as it is in current Eurocode recommendations. The assumed material model is linear elastic – perfectly plastic material model without strain hardening. A nominal plateau slope of $E/10000$ has been applied for numerical stability reasons. The impact of strain hardening is deemed negligible for relative slenderness higher than 0.2 as failure mode is a flexural buckling instability mode; this was already assumed in another research [231], [235]. The underlying assumptions of the numerical models are graphically summarised in Fig. 5-1.

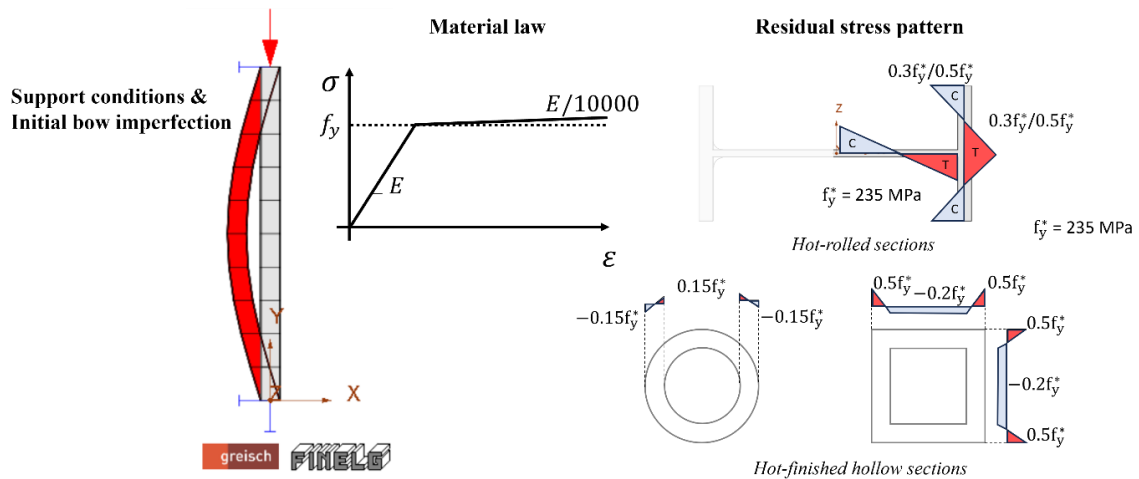


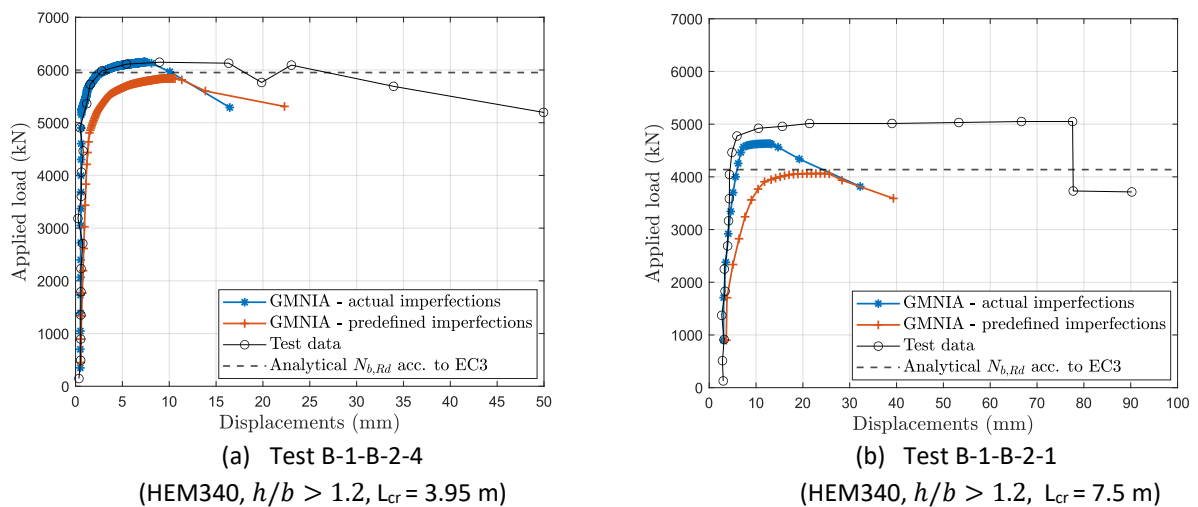
Fig. 5-1. Description of model assumptions for beam finite element modelling.

5.2.3. Validation of the numerical model

To validate the accuracy of the developed numerical model, a comparison has been carried out between the numerical data and the experimental data for both hot-rolled double-T cross-sections and hot-finished hollow sections.

5.2.3.1. Hot-rolled sections

The validation was conducted on the experimental tests carried out at the Fritz Engineering Laboratory in 1972 [240]. This campaign constituted an extension of the ECCS programme [105], targeting heavy shape cross-sections (thickness greater than 30 mm), which are covered in this study. The test programme consists of buckling tests of pinned end HEM340 ($h/b > 1.2$) and W12x161 ($h/b \leq 1.2$) columns for two distinct slenderness ratios ($L/i_z = 50$ and $L/i_z = 95$), and provides supplementary measurements (coupon tests, residual stress distribution, out-of-straightness). It has been determined that the numerical simulation of one test for each slenderness ratio is necessary to guarantee the accuracy of the numerical model in simulating the buckling curves. The linear elastic material law has been employed to reproduce these experimental tests with the objective of demonstrating the relevance of this law for such simulations. The results of these simulations are represented in Fig. 5-2.



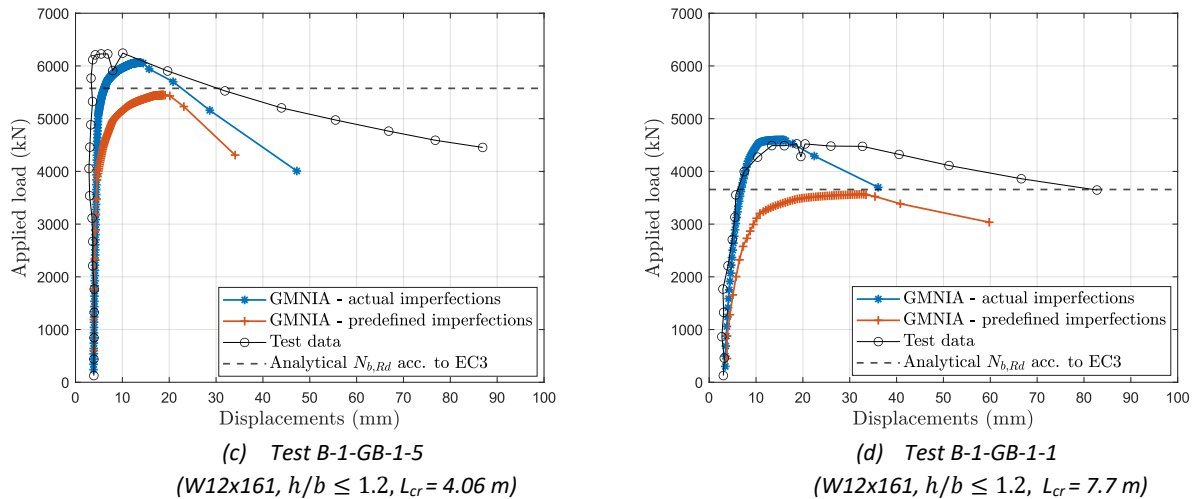


Fig. 5-2. Validation of the numerical model based on experimental results carried out in the Fritz Laboratory in 1972.

As shown in Fig. 5-2, the numerical model provides satisfactory predictions. It should be noticed that, for tests B-1-B-2-1 and B-1-GB-1-1, the numerical response is significantly influenced by the residual stress pattern as the relative slenderness for these columns is approximately 1.0. It should be noted that residual stress measurements are not provided for tests B-1-B-2-1 and B-1-GB-1-1. Consequently, the same residual stress patterns as those provided for tests B-1-B-2-4 and B-1-GB-1-5 have been applied, resulting in the observed discrepancy in terms of peak loads. Furthermore, as reported in Fig. 5-2, additional numerical simulations have been conducted by considering predefined imperfections, i.e. the ECCS residual stress model and a geometrical imperfection of $L/1000$, to demonstrate the correspondence between the numerical simulations and the Eurocode predictions based on these assumptions.

The present validation was conducted on the extant buckling tests for mild steels, as no buckling test results on hot-rolled double-T members in high-strength steels are currently available in the literature for compact sections (Class 1 to Class 3). Nevertheless, another study has already demonstrated the reliability of this finite element software to simulate the flexural buckling of hot-rolled high-strength angle members [229]. As the aforementioned research concerns a different cross-sectional shape of hot-rolled sections, an investigation was conducted on the residual stress pattern of similar shapes in increased yield strengths, as this has been identified as a key parameter affecting the resistance to flexural buckling. Although the forthcoming FprEN1993-1-14:2024 [135] recommends the use of the ECCS residual stress model scaled by 235 MPa regardless of the yield strength, a validation was carried out based on recent residual stress measurements performed on similar hot-rolled wide flange shapes of different grades [111], [124], [134], [241], [242], as shown in Fig. 5-3.

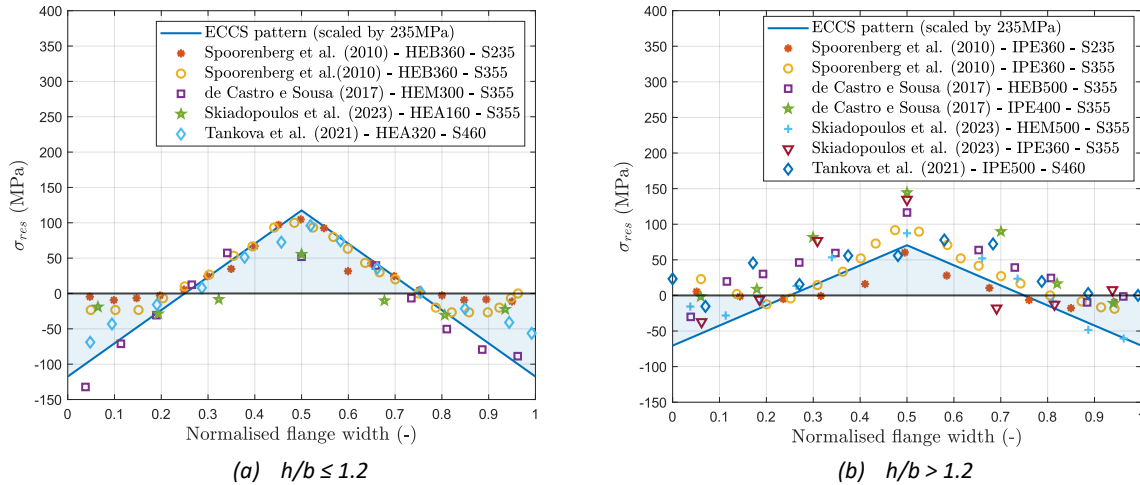


Fig. 5-3. Validation of the residual stress model used in the numerical simulations for high-strength steels.

Fig. 5-3 corroborated the assumption that residual stress levels remain unchanged in correlation with the yield stress. The residual stress measurements indicate that the compressive residual stress levels at the flange tips are lower than those predicted by the residual stress model. For a prospective study, it is assumed that this is also the case for grades above the practical range, i.e. grades above S460. It can therefore be concluded that the residual stress model is conservative, and that the finite element model is deemed appropriate for the numerical simulation of hot-rolled sections in mild and high-strength steel grades.

5.2.3.2. Hot-finished hollow sections

The validation of the numerical model for hot-finished hollow sections was conducted on experimental tests carried out by Wang & Gardner [140]. Several specimens were modelled in order to encompass a variety of structural shapes, different high-strength steel grades (S460 and S690) and slendernesses. The results of this validation are presented in Fig. 5-4. It is worth mentioning that these tests have been validated without consideration of residual stress distributions as it was admitted that residual stresses were deemed negligible based on residual stress measurements [140].

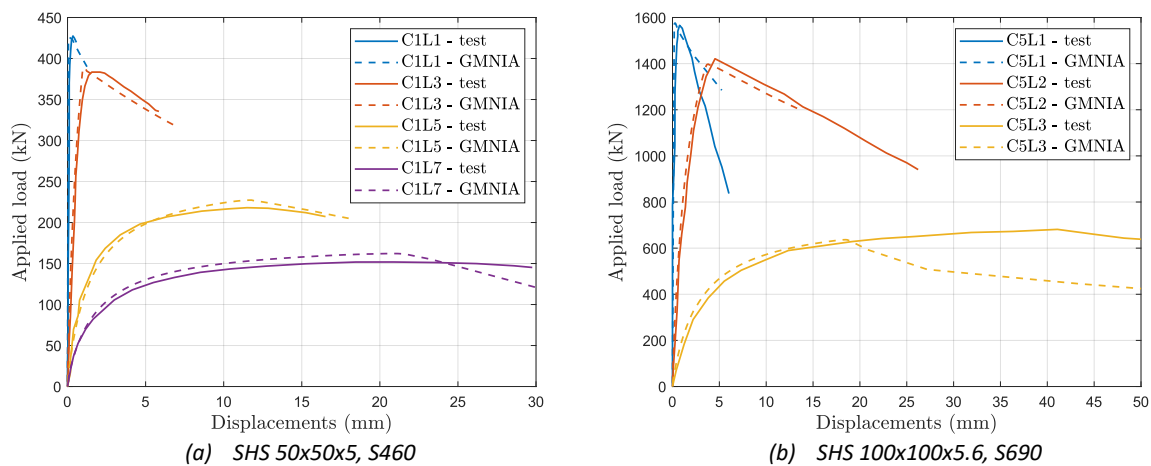


Fig. 5-4. Validation of the numerical model for hot-finished hollow sections.

The 14 simulation results, conducted for the purpose of validation, are presented for comparison with the findings of Wang & Gardner [140] in Table 5-3 with w_i the measured member out-of-straightness.

Specimen	L_{cr} (mm)	w_i (mm)	$\bar{\lambda}(-)$	$\frac{N_{u,FEM}}{N_{u,exp}} (-)$ (Wang, 2017)	$\frac{N_{u,FEM}}{N_{u,exp}} (-)$ (this study)
C1L1	427	0.42	0.36	1.00	1.00
C1L3	907	0.93	0.77	1.01	1.01
C1L5	1529	1.45	1.30	1.04	1.05
C1L7	1859	1.86	1.58	1.06	1.07
C3L1	858	0.91	0.35	1.07	1.07
C3L2	1759	1.73	0.72	1.12	1.12
C3L3	2949	2.24	1.22	1.05	1.06
C4L1	426	0.48	0.44	0.93	0.93
C4L3	905	0.93	0.94	0.93	0.92
C4L5	1529	1.60	1.59	0.95	0.93
C4L7	1860	1.77	1.93	1.00	0.99
C5L1	858	1.03	0.44	1.00	1.00
C5L2	1760	1.66	0.89	0.99	0.99
C5L3	2950	3.00	1.50	0.99	0.93

Table 5-3. Comparison between experimental and numerical results for hot-finished hollow sections.

Table 5-3 demonstrates the accuracy of the developed numerical model. A comparison of the shell model with the real stress-strain relationship and the developed beam model with an elastic-perfectly plastic material law reveals results which are very similar. This lends further support to the suitability of this simplified material law for the simulation of columns subject to flexural buckling. Eventually, although residual stress measurements in this testing programme exhibit negligible residual stresses for high-strength steel grades, it has been decided to adopt a conservative approach and consider the residual stress pattern prescribed in FprEN1993-1-14:2024 [135], which is scaled by 235 MPa.

5.2.4. Assessment of current recommendations for S235 and S460 grades

The buckling curve recommendations from the current and forthcoming versions of EN1993-1-1 [52], [70] are reported in Table 2-11. However, a summary of the rows under concern is made in Table 5-4.

Cross-section / Limits	Buckling about axis	EN1993-1-1:2005		FprEN1993-1-1:2022	
		S235-S275-S355- S420	S460	S235-S275-S355- S420	S460 up to S700
Rolled $h/b > 1.2$ / $t_f \leq 40$ mm	y-y	a	a ₀	a	a ₀
	z-z	b	a ₀	b	a
Rolled $h/b \leq 1.2$ / $t_f \leq 100$ mm	y-y	b	a	b	a
	z-z	c	a	c	b
Hollow Hot-finished	any	a	a ₀	a	a ₀

Table 5-4. Eurocode selection of buckling curves for flexural buckling and hot-rolled sections.

As can be seen in Table 5-4 for hot-rolled sections, the current buckling curves for the weak axis were found to be optimistic. Recent research has demonstrated that these curves were not appropriate [232], [243], [244] and that a lower buckling curve would be more appropriate. This modification has

been introduced in the upcoming version FprEN1993-1-1:2022 [52]. Therefore, as stated in Chapter 2, the ECCS situation of 1976 [110] in which one higher buckling curve was recommended for the high-strength steel grade once again applies for each hot-rolled section typology, geometrical limit and buckling axis. Prior to advancing further in the present study, numerical simulations of the two grades that are already covered in standards, namely S235 and S460, have been performed for the sake of confirming the aforementioned research. The results are presented in Fig. 5-5.

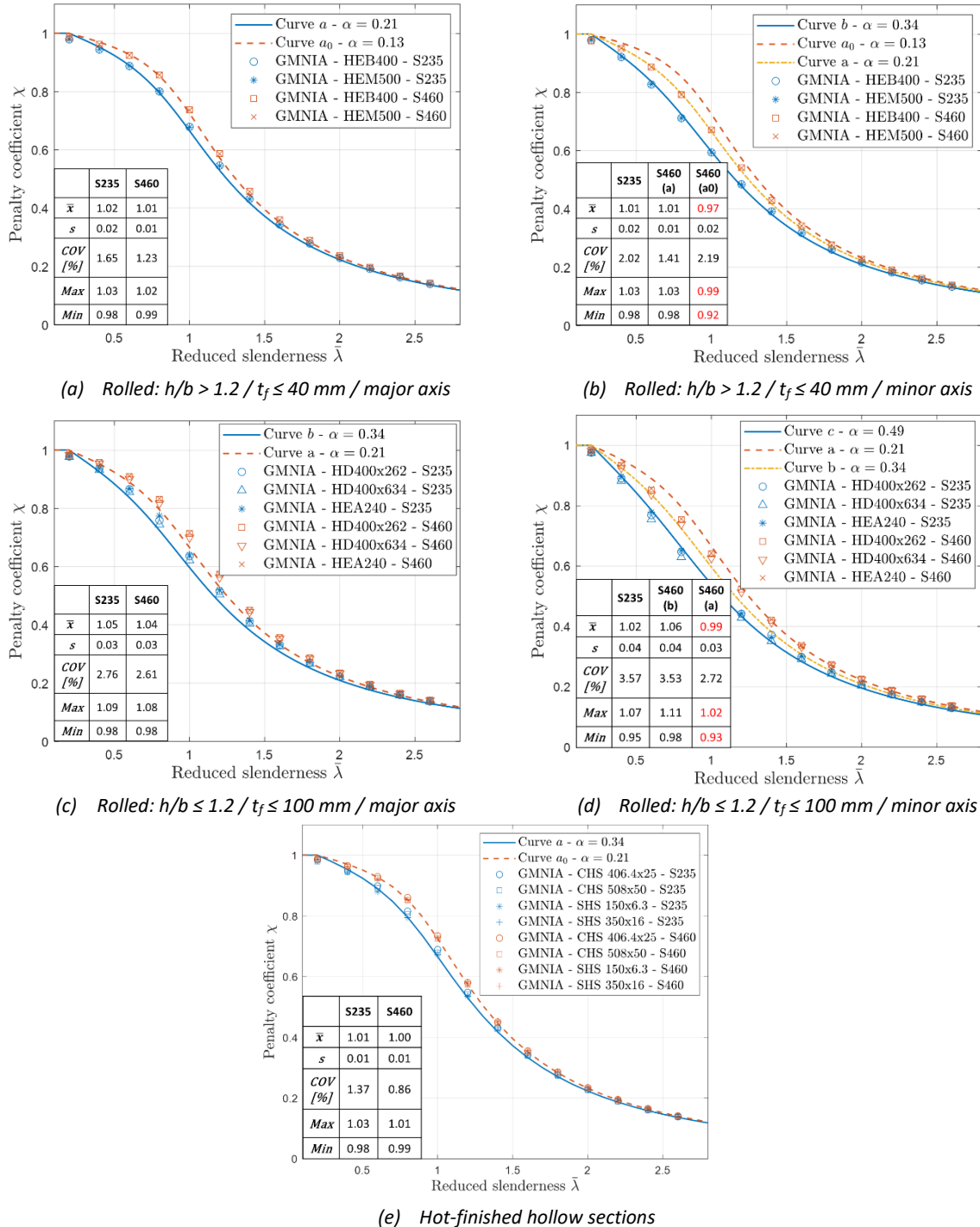


Fig. 5-5. Comparison between numerical simulations and Eurocode recommendations for grades S235 and S460.

According to Fig. 5-5, a reasonable fit is obtained by comparing results from the GMNIA FineLg analyses and the selected buckling curves from Eurocode, particularly for height-to-width ratios above 1.2 and hot-finished hollow sections as the mean values $\bar{\chi}$ are close to unity (as defined in the methodology).

In contrast, for height-to-width ratios below 1.2, the simulated buckling resistances are approximately 5% higher on average than the prescribed Eurocode curves. This indicates that there is a small margin of improvement, even for S235 and S460.

The reduction factor accounting for flexural buckling is highly dependent on the residual stress distributions, the geometrical imperfections, and the yield strength. Conversely, the cross-section geometries have a negligible impact for a same geometrical limit / table row defined in Table 8.3 of FprEN1993-1-1:2022 [52]. This observation justifies the methodology to consider only a limited number of profiles for the different geometrical limits / table rows studied. Eventually, the reduction factor is only slightly affected by geometrical tolerances, given the importance of the effect of initial imperfections, thus the inferences remain valid. Furthermore, as can be seen in Fig. 5-5e, despite the dissimilar residual stress nature of CHS (flexural) than SHS (longitudinal), the flexural buckling response is analogous. This substantiates the decision made in the current design rules to adopt a same buckling curve for all the cross-sectional shapes of hollow sections.

The numerical simulations for relative slenderness of 0.2 present a reduction factor $\chi < 1.0$, which suggests that, at this boundary limit between stocky and slender columns, flexural buckling occurs earlier than the yielding of the cross-section. This observation is consistent with the findings of other research studies that have identified a reduced reduction factor for this boundary slenderness [148], [155]. It can be seen that regardless of the constitutive law, the consideration of the strain hardening has no impact for $\bar{\lambda} \geq 0.2$ [155]. As can be seen in Table 2-14, some authors react to this phenomenon by proposing a continuous imperfection factor that shifts the yielding plateau: Meng & Gardner [148] propose a reduction of the yielding plateau from a relative slenderness of 0.2 to 0.1. Similarly, Jönsson & Stan [155] even suggest a yielding plateau length that is a function of the yield strength, applying the ε factor to the relative slenderness. In the framework of this research, following the mathematical model prescribed in FprEN1993-1-14:2024 [135], some simulations with a trilinear material law to account for strain hardening have been realised. The results demonstrate that the same peak loads were attained as illustrated in Fig. 5-6 for first slendernesses and selected profiles with height-to-width ratios above 1.2, thereby corroborating the observations previously expressed in the literature.

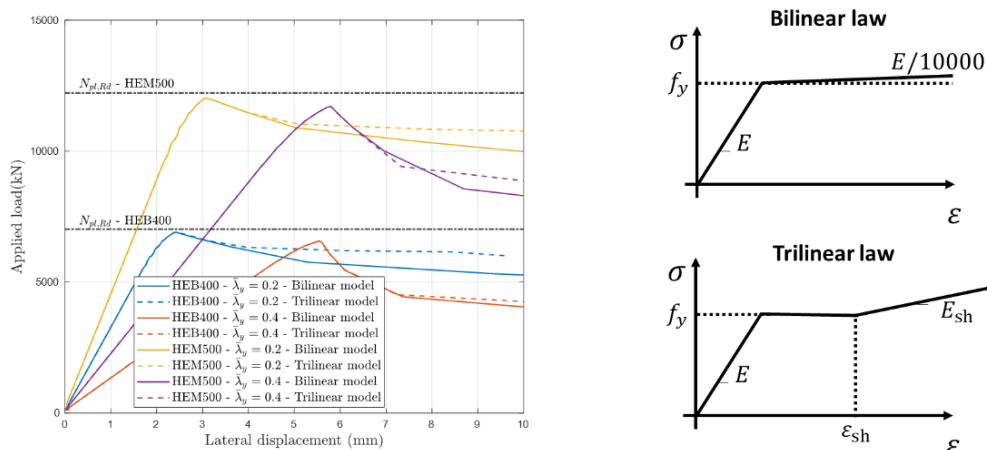


Fig. 5-6. Impact of strain-hardening on numerical simulations for low-slenderness columns.

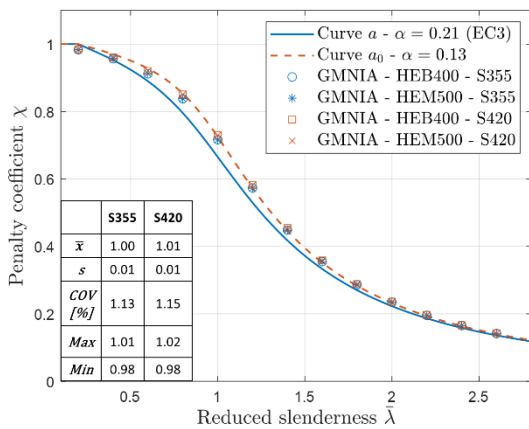
Fig. 5-6 testifies that the strain-hardening has no impact on the outcomes and the buckling load associated with a relative slenderness of 0.2 is slightly lower than the member's plastic resistance. It is nevertheless noteworthy that the value of 0.2 has been prescribed on the basis of experimental column tests, which are likely to exhibit fewer imperfections than those conservatively employed in numerical simulations. In addition, the yield strength is at least equal to the nominal value, thus it makes sense that this value was derived based on statistical analyses of experimental tests rather than

numerical simulations. In order to maintain consistency with existing recommendations, the length of the plateau has been retained in accordance with the specifications set forth in Eurocode 3.

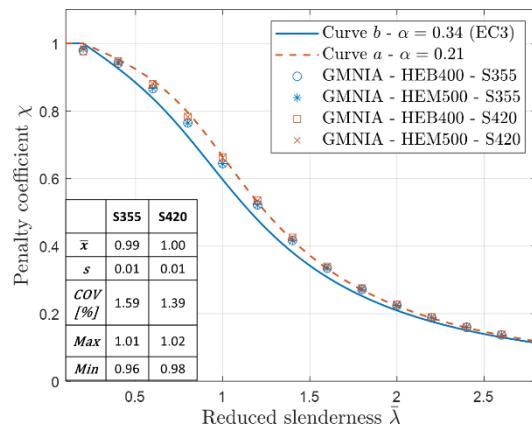
As previously outlined in Chapter 2, the modified Maquoi’s imperfection factor [145] aligns with the jump of one buckling curve that was recommended at the time for 430 MPa (in accordance with the earlier ECCS recommendations [110]). The current version of EN1993-1-1 [70] sometimes presents a two-curve jump for S460. However, it has been rectified in the last version of the standard FprEN1993-1-1:2022 [52]. Indeed, a difference of one buckling curve between S235 and S460 is once again prescribed in FprEN1993-1-1:2022 [52], irrespective of the h/b ratio and the buckling axis for the sections under consideration (Table 5-4). Consequently, given a jump of one buckling curve has been validated through numerical investigations and with the objective of maintaining the length of the yielding plateau, the approach proposed by Maquoi [145] presented in Section 2.4.3, is deemed the most appropriate for establishing a new, up-to-date imperfection factor.

5.2.5. Considerations for intermediary S355 and S420 grades

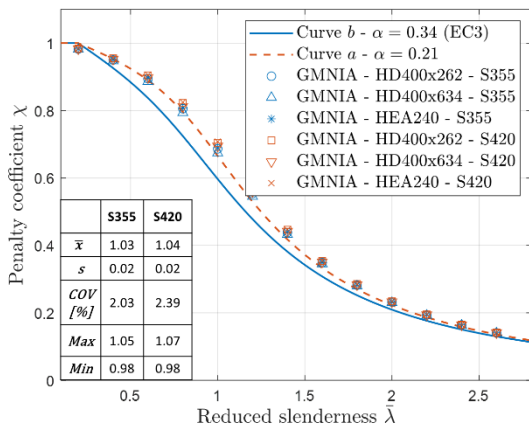
As discussed in Chapter 2 and in line with recent investigations [155], [232], grades between S235 and S460 are likely to be the most disadvantaged grades given the current Eurocode recommendations as the buckling curve calibrated for the S235 steel grade is imposed to these intermediate grades. These grades have been analysed by representing the preconised buckling curve (the blue lines) and the one just above (the red dashed lines), with the objective of determining whether a higher curve could be assigned to these grades (see Fig. 5-7). The statistical evaluation is conducted on the aforementioned higher buckling curve, i.e. curve a_0 in Fig. 5-7a and Fig. 5-7e, curve a in Fig. 5-7b and Fig. 5-7c and curve b in Fig. 5-7d.



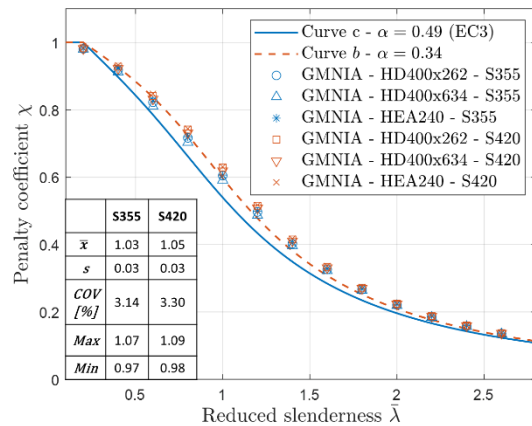
(a) Rolled: $h/b > 1.2 / t_f \leq 40$ mm / major axis



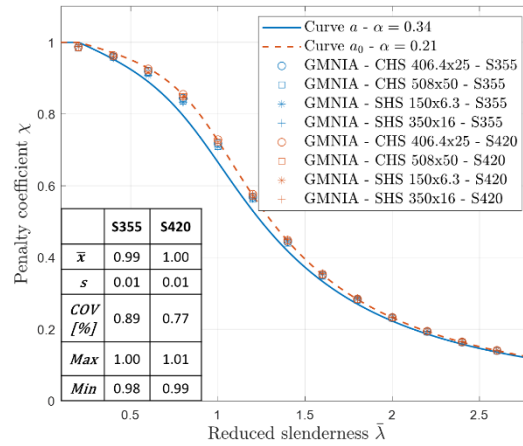
(b) Rolled: $h/b > 1.2 / t_f \leq 40$ mm / minor axis



(c) Rolled: $h/b \leq 1.2 / t_f \leq 100$ mm / major axis



(d) Rolled: $h/b \leq 1.2 / t_f \leq 100$ mm / minor axis



(e) Hot-finished hollow sections

Fig. 5-7. Evaluation of the possibility of selecting one higher buckling curve for S355 and S420.

As illustrated in Fig. 5-7, the results substantiate the expectations that the buckling resistances of S355 and S420 are underestimated, resulting in over-designs for those grades. This observation is particularly evident for sections with a height-to-width ratio below 1.2 as such sections encounter higher relative residual stress distributions. Regardless of the section typology and the height-to-width ratio, one higher buckling curve could have been prescribed for S355 and S420. However, the mean ratio $\bar{\chi}$ is equal to or just below 1.0 for S355 in the case of hot-rolled sections with a height-to-width ratio exceeding 1.2 or for hot-finished hollow sections. The safety aspects should therefore be discussed in the case of a higher curve selection. However, by defining a continuous imperfection factor, the increase could be less than one buckling curve, thus respecting the statistical evaluation in this case.

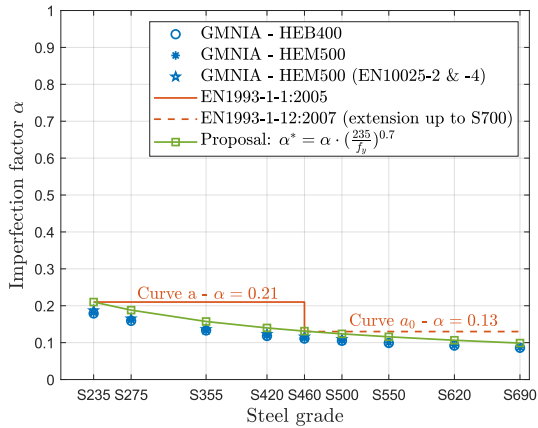
5.2.6. Modified imperfection factor for hot-rolled sections

In light of the outcomes of the preceding subsections, it may be concluded that grades S235 and S460 are correctly characterised in the forthcoming standard version FprEN1993-1-1:2022 [52]. The objective is therefore to propose a continuous imperfection factor α^* , while strictly adhering to the current recommendations for these two steel grades. It has been decided to consider the approach proposed by Maquoi [145], in which the exponent n is modified to 0.7 instead of 0.8, in order to respect the current imperfection factors for S235 and S460 – see Eq. (5-3). Indeed, by using this exponent, if $\alpha = 0.21$, $\alpha^* = 0.21$ for S235 and $\alpha^* = 0.13$ for S460. Similarly, if $\alpha = 0.34$, $\alpha^* = 0.34$ for S235 and $\alpha^* = 0.21$ for S460. These imperfection factors for S235 and S460 are in line with the current recommendations of Eurocode. However, if $\alpha = 0.49$, $\alpha^* = 0.49$ for S235 and $\alpha^* = 0.31$ for S460 which does not correspond to buckling curve “b” ($\alpha = 0.34$). This discrepancy was already stated with the Maquoi’s imperfection factor [145], and it has been considered acceptable given the potential margin of improvement observed in Fig. 5-5d. Based on the aforementioned considerations, the proposal is:

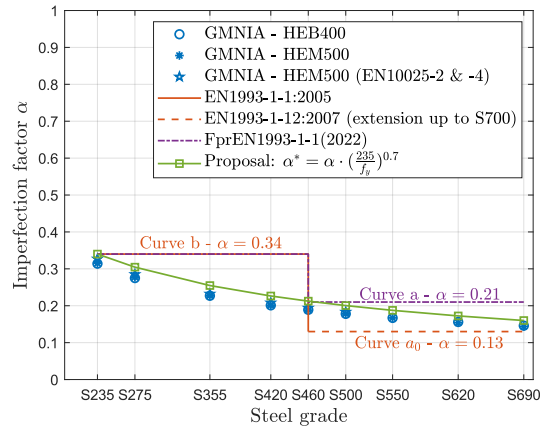
$$\alpha^* = \alpha \cdot \left(\frac{235}{f_y} \right)^{0.7} \quad (5-3)$$

The study consists of evaluating for which α the buckling curve fits with the GMNIA results (corresponding to a mean value $\bar{\chi}$ of 1.0 as defined in the methodology) considering a continuous vector of $\alpha \in [0.1: 0.001: 0.49]$. Fig. 5-8 illustrates the evolution of the calculated imperfection factor as a function of the yield strength and the proposed modified imperfection factor expressed in Eq.

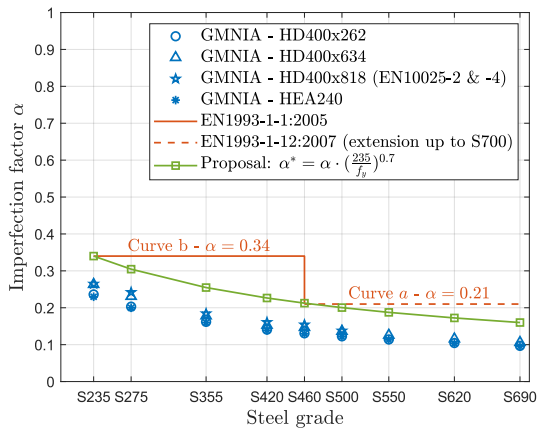
(5-3) for the sake of comparison. In addition, results considering the minimum yield strengths prescribed in EN10025-2 [53], EN10025-4 [54] and EN10210-3 [59] for profiles of Table 5-1 and Table 5-2, for which the thickness of the constitutive parts implies a yield stress reduction (see the strength reduction in Fig. 2-1 in Chapter 2), are also reported to evaluate the impact of this yield strength reduction on the results. For other cross-sections, the yield strength specified in Table 5.1 of FprEN1993-1-1:2022 [52] is considered.



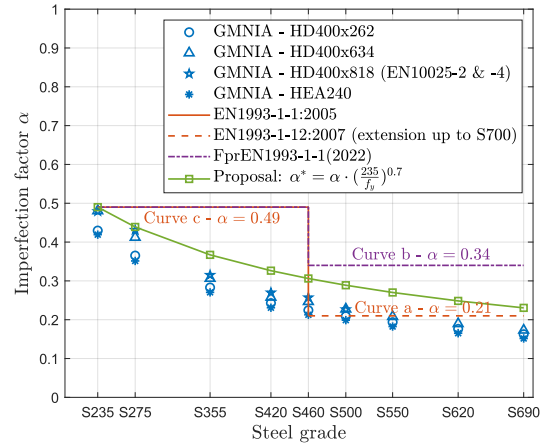
(a) Rolled: $h/b > 1.2 / t_f \leq 40$ mm / major axis



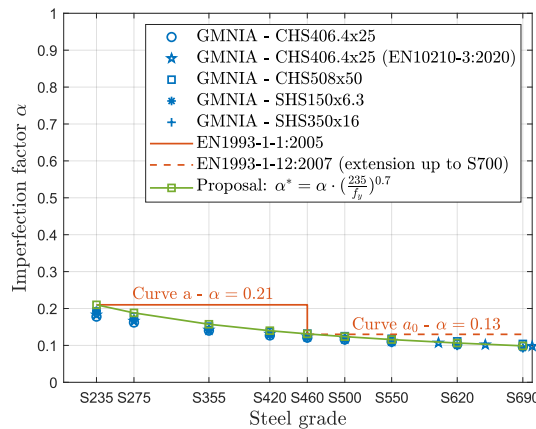
(b) Rolled: $h/b > 1.2 / t_f \leq 40$ mm / minor axis



(c) Rolled: $h/b \leq 1.2 / t_f \leq 100$ mm / major axis



(d) Rolled: $h/b \leq 1.2 / t_f \leq 100$ mm / minor axis



(e) Hot-finished hollow sections

Fig. 5-8. Evolution of the imperfection factor α as function of the yield strength.

The consideration of sections with higher thicknesses and thus reduced yield stresses in accordance with EN10025-2 [53] and EN10025-4 [54] results in higher imperfection coefficients which nevertheless remain below the corresponding modified imperfection factors of the proposal. Fig. 5-8 illustrates that the influence of the reduction in yield strength is negligible up to flange thicknesses of 40 mm. This finding aligns with the recommendations of FprEN1993-1-1:2022 [52], which recommend maintaining the nominal yield strengths up to 40 mm. For the limited number of hollow cross-sections with a wall thickness exceeding 40 mm, the proposal may be slightly unconservative for very high steel grades (above S460). This is illustrated by profile CHS 508x50 in Fig. 5-8e, which exhibits a maximum difference of 5% unconservative for grade S690. The relatively limited number of affected profiles (only five CHS profiles possess a wall thickness above 40 mm) and the fact that these numerical simulations consider residual stresses whereas recent research [140], [141], [148], [238] on hot-finished hollow sections has demonstrated that residual stress magnitudes obtained from measurements are very small and negligible compared to the yield strength, lead to the conclusion that the proposal with an exponent of 0.7 is deemed an acceptable compromise as it provides a satisfactory correlation with numerical simulations. This proposition offers a double advantage: (i) it provides a common buckling curve expression for all hot-rolled H-shaped and hollow sections regardless of the cross-section dimensions or the buckling axis, and (ii) it permits the conservation of the historical Eurocode curves (a₀, a, b, c, and d) for S235.

In the case of hot-finished hollow sections, there are some buckling test results available for the S460 and S690 grades. Consequently, the new formulation for flexural buckling prediction is evaluated based on the 83 test results identified in the literature [140], [147], [148]. The buckling reduction factors are calculated using the measured yield stress $f_{y,exp}$ and the measured cross-sectional area A_{exp} as expressed in Eq. (5-4).

$$\chi_{exp} = \frac{N_{u,exp}}{A_{exp} \cdot f_{y,exp}} \tag{5-4}$$

The comparison between the experimental reduction factors and the recommended buckling curves is presented in Fig. 5-9.

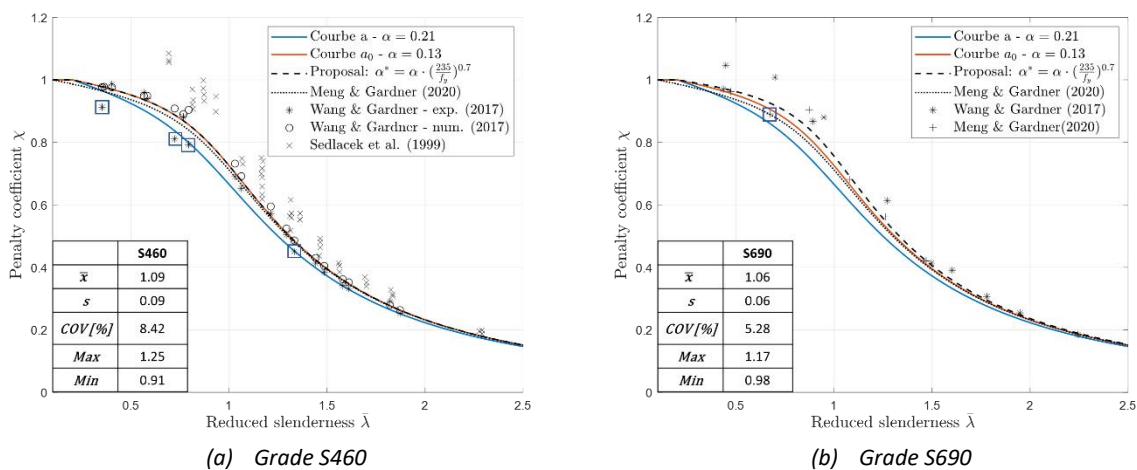


Fig. 5-9. Validation of the modified imperfection factor based on experimental tests for hot-finished hollow sections.

Fig. 5-9 demonstrates that, in general, the experimental test results are higher than the current Eurocode predictions and the predictions from the proposed model. It is noteworthy that five experimental reduction factors are, however, well below the proposed buckling curve and even below the currently recommended curve for the S460 grade, as boxed in blue in Fig. 5-9. For sake of

comparison, the results of numerical simulations carried out by Wang and Gardner [140] are also reported, to confirm the adequacy of the proposal with numerical simulations. The observed discrepancies in the results of some tests can be attributed to the fact that the measured yield stress represents a mean value derived from yield stress measurements obtained through coupon tests. Consequently, the actual yield strength of some tests may be lower, which could explain the observed reduced reduction factors. Furthermore, although the load eccentricity of all specimens was adjusted to achieve as close to a global imperfection of $L/1000$ as possible [140], some of the tests exhibited a bow imperfection larger than $L/1000$, while the buckling curves were established considering this level of initial bow imperfection.

Eventually, a recent study by Meng and Gardner [148] determined that the EC3 design approach is generally accurate in predicting column buckling resistances for grades above 460 MPa. However, the influence of yield stress on column buckling resistance is not fully captured in current Eurocode provisions resulting in a wide scatter band. Therefore, they also proposed a modified imperfection factor, and these special points are also below their proposal as represented in Fig. 5-9a. Based on a statistical evaluation conducted with a significant amount of numerical data, they concluded that their proposal with the currently recommended partial safety factor $\gamma_{M1} = 1.0$ was deemed as suitable. Consequently, given the limited number of unconservative experimental data points, it can be concluded through the presented comparisons that the proposal made in this chapter generally yields safe-sided buckling capacity predictions for hot-finished high-strength steel hollow sections. Nevertheless, further experimental investigations may validate the presented numerical conclusions, especially for high-strength hot-rolled sections.

5.2.7. Validity of the proposal for slender sections

The use of high-strength steels for sections implies that certain sections from producer catalogues fall within the Class 4 cross-section category, meaning that they are susceptible to an earlier failure due to local buckling. Consequently, supplementary numerical simulations using shell finite elements have been conducted to justify the validity of the modified imperfection factor for Class 4 cross-sections.

Geometrically and materially nonlinear analyses with imperfections (GMNIA) have been performed using the *Finelg* software [225]. The present study focuses on two profiles for hot-rolled H-shaped sections, i.e. HEB600 and HEA300 in S460 and S690, which are subjected to flexural buckling about their weak axis as well as the SHS200x5 profile for hot-finished hollow sections. These profiles are classified as Class 4 for yield strengths exceeding 460 MPa due to the web or wall slenderness. The shell modelling implies an overlapping of the web over the flanges to ensure continuity of the mesh and the fillets have been neglected (Fig. 5-10). A comparison of the geometrical properties between the actual cross-section and the modelled cross-section reveals a difference of less than 0.1% in terms of the weak-axis moment of inertia. This difference is, therefore, inconsequential concerning weak axis buckling. However, the exclusion of fillets results in a notable reduction in the cross-sectional area, particularly for the lighter sections (HEA300 and SHS200x5). Accordingly, the reduced area employed in the simulations noted A_{FEM} , has been used for determining the specimen lengths – see (5-1).

Eventually, support conditions were applied through the application of kinematic coupling constraints at column ends, represented by the dashed lines on the cross-sectional meshes in Fig. 5-10. A summary of the numerical modelling assumptions is provided in Fig. 5-10.

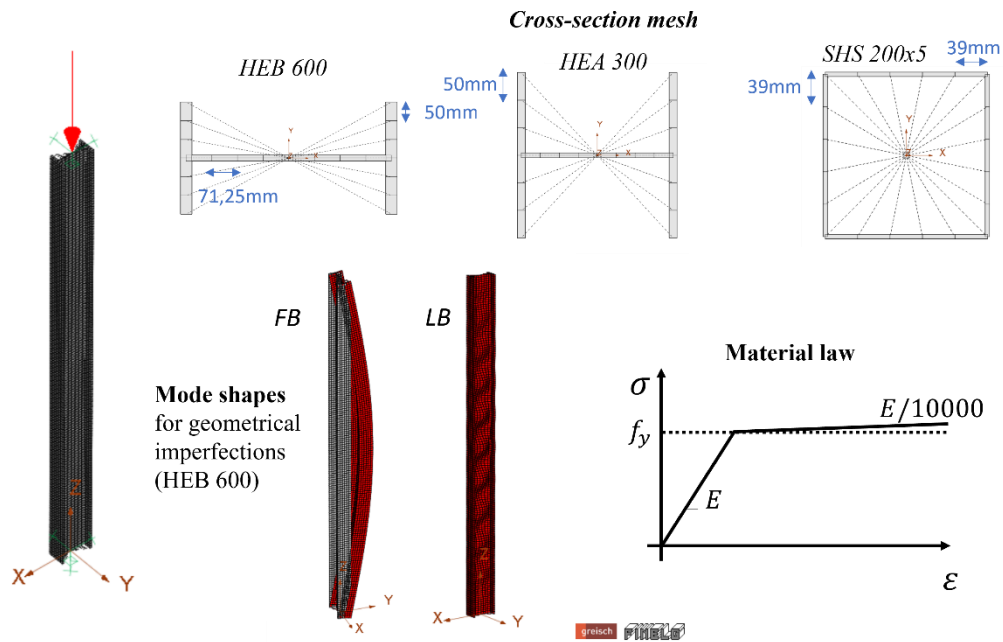


Fig. 5-10. Description of model assumptions for shell finite element modelling.

For hot-rolled sections, the classical ECCS residual stress model is implemented, while no residual stresses have been introduced for the SHS 200x5 profile. Indeed, as shown in Section 5.2.3.2, the residual stresses have a negligible impact on the behaviour of high-strength hot-finished hollow sections. Two geometrical imperfections are introduced based on a prior linear bifurcation analysis (LBA) performed on each member. The first geometrical imperfection is affine to the first flexural buckling mode shape, while the second geometrical imperfection is affine to the first local buckling mode shape (see Fig. 5-10). The flexural buckling mode shape is amplified by $L/1000$ while the local buckling mode shape is amplified by $c/200$, in accordance with the recommendations in EN1993-1-5 [222] and the forthcoming recommendations for numerical modelling FprEN1993-1-14:2024 [135]. In accordance with the latter standard, the defined value is adopted for the leading imperfection (mode appearing first in the linear buckling analysis) and the accompanying imperfection is reduced to 70% of the defined value.

A review of the literature about the combination of local and global imperfections in hollow sections reveals that a local imperfection magnitude of $c/400$ is more appropriate for representing the Winter curve (the design curve for local buckling) [245], [246], [247], [248], whereas a magnitude of $c/200$ remains the reference for I-shaped members. A mesh sensitivity study was conducted to ascertain the suitable longitudinal mesh and the appropriate local imperfection magnitude. This was conducted with stocky columns exhibiting a relative slenderness of 0.1, to focus on the local buckling behaviour and avoid any risk of flexural buckling. The reduction factors (β_{num}) for local buckling as well as those recommended in EC3 (β_{EC3}) are compared in Table 5-5 and the first local instability mode shapes for various longitudinal meshes are drawn in Fig. 5-11 for the HEB600 profile to evaluate whether the mode shape is well-modelled.

Cross-sections	Local imperfection magnitude	β_{EC3} (S460)	β_{num} (S460)					β_{EC3} (S690)	β_{num} (S690)				
			Longitudinal mesh (mm)						Longitudinal mesh (mm)				
			100	75	50	25	10		100	75	50	25	10
HEA 300	0	1.00	1.00	1.00	1.00	1.00	1.00	0.98	1.00	1.00	1.00	1.00	1.00
	c/400		0.98	0.99	0.99	0.99	0.99		0.97	0.98	0.98	0.98	0.98
	c/200		0.97	0.98	0.98	0.98	0.98		0.97	0.97	0.97	0.97	0.96
HEB 600	0	0.98	1.00	1.00	1.00	1.00	0.99	0.95	1.01	1.01	1.00	1.00	1.00
	c/400		0.99	0.99	0.99	0.99	0.98		0.99	0.98	0.98	0.98	0.98
	c/200		0.98	0.98	0.98	0.98	0.98		0.98	0.97	0.97	0.97	0.97
SHS 200x5	0	0.84	0.98	0.98	1.00	1.00	1.00	0.73	0.60	0.93	0.99	0.99	0.99
	c/400		0.78	0.82	0.84	0.85	0.85		0.62	0.67	0.69	0.70	0.71
	c/200		0.74	0.77	0.78	0.79	0.79		0.61	0.64	0.66	0.67	0.68

Table 5-5. Numerical sensitivity study of the longitudinal mesh and local imperfection magnitude influence.

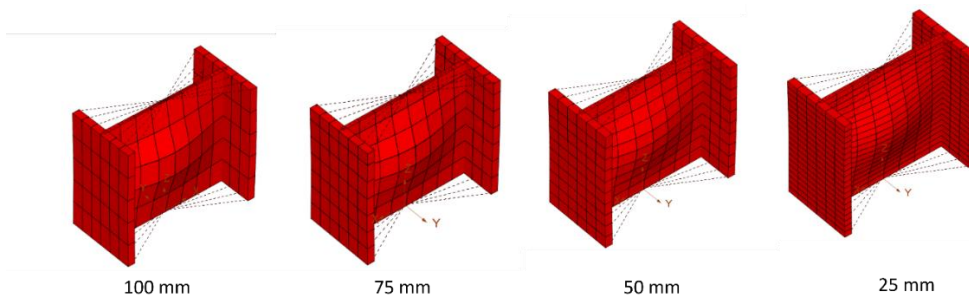
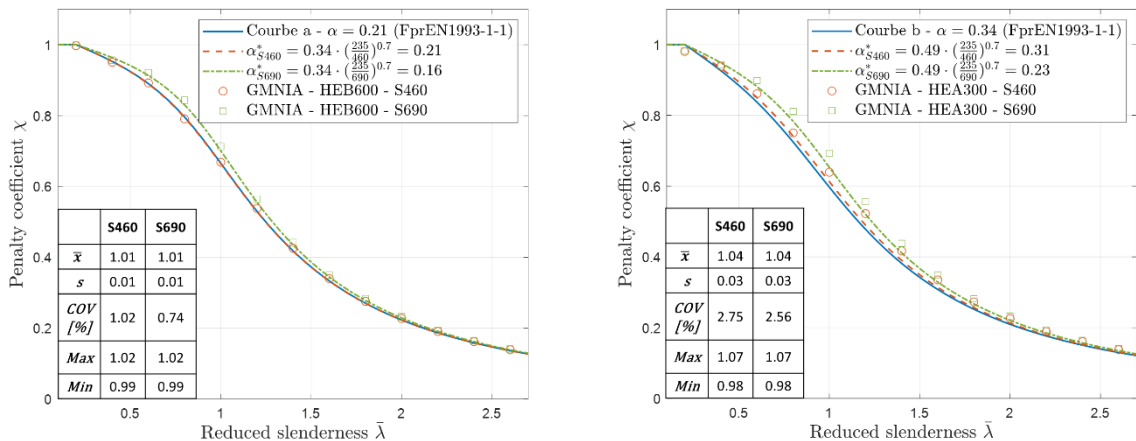


Fig. 5-11. Impact of the element size on the local instability mode shape (represented for the HEB600 profile).

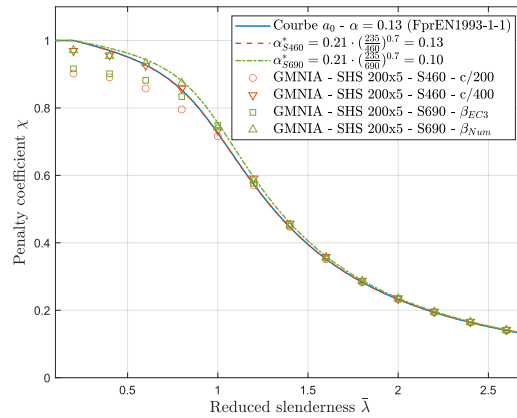
The sensitivity study confirms the numerical observations documented in the existing literature, indicating that a local imperfection magnitude of c/400 is more suitable for SHS members. However, for grade S690, the reduction factor obtained numerically is particularly sensitive to the local imperfection magnitude, which may have a notable impact on the instability response. Table 5-5 and Fig. 5-11 indicate that a longitudinal mesh of 50 mm is an appropriate choice for the three selected profiles.

The numerical campaign encompasses in total 78 columns, the three considered profiles being modelled for two grades (S460 and S690) and 13 slendernesses. A comparison with the modified imperfection factor curve is represented in Fig. 5-12.



(a) $h/b > 1.2 / t_f \leq 40 \text{ mm} / \text{minor axis (HEB600)}$

(b) $h/b \leq 1.2 / t_f \leq 100 \text{ mm} / \text{minor axis (HEA300)}$



(c) Hot-finished hollow sections (SHS 200x5)

Fig. 5-12. Comparison between shell numerical simulations and the modified imperfection factor for slender cross-sections.

The results shown in Fig. 5-12a and Fig. 5-12b as well as the corresponding statistical evaluations demonstrate a strong correlation between the shell model and the modified buckling curve proposal, indicating that this proposition is also valid for Class 4 hot-rolled cross-sections. In addition, Fig. 5-12b illustrates that, even though the proposal is not perfectly aligned with a “jump” of one buckling curve in the case where $\alpha = 0.49$ for S235, there is a good correlation between this imperfection factor proposal and the numerical results for S460, i.e. for $\alpha^* = 0.31$. Furthermore, an experimental campaign carried out at the University of Liège in 1993 [249] provided eight buckling tests on HEAA180 columns with the same buckling length ($L_{cr} = 3075 \text{ mm}$) with a yield strength of 550 MPa, for which the section is slender (Class 4). Based on the campaign findings, they concluded that a gain of 2 buckling curves compared to the one prescribed for mild steel, i.e. curve “a” for S550 and curve “c” for steels below S460, is justified. To validate the modified imperfection proposal, these experimental data have been reported on the buckling curve chart with a statistical evaluation, as can be seen in Fig. 5-13.

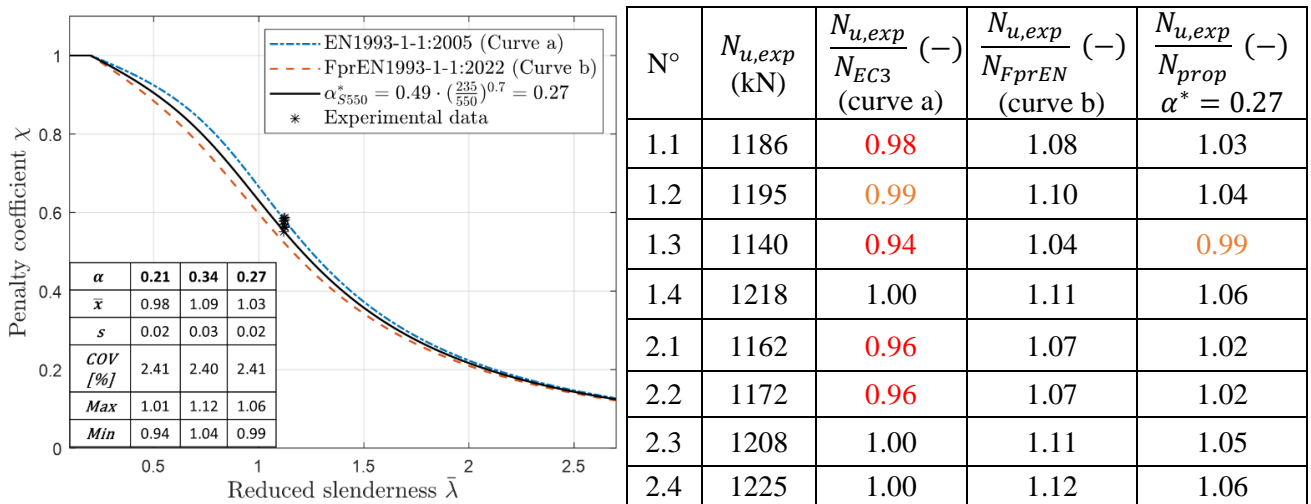


Fig. 5-13. Validity of the modified imperfection factor proposal for Class 4 cross-sections based on buckling tests.

N°	$N_{u,exp}$ (kN)	$\frac{N_{u,exp}}{N_{EC3}}$ (-) (curve a)	$\frac{N_{u,exp}}{N_{FprEN}}$ (-) (curve b)	$\frac{N_{u,exp}}{N_{prop}}$ (-) $\alpha^* = 0.27$
1.1	1186	0.98	1.08	1.03
1.2	1195	0.99	1.10	1.04
1.3	1140	0.94	1.04	0.99
1.4	1218	1.00	1.11	1.06
2.1	1162	0.96	1.07	1.02
2.2	1172	0.96	1.07	1.02
2.3	1208	1.00	1.11	1.05
2.4	1225	1.00	1.12	1.06

The results of this campaign, depicted in Fig. 5-13, demonstrate the relevance of the proposal but further buckling test results would be beneficial to confirm the suitability of the proposal for other slendernesses and grades. Furthermore, the numerical model could have been validated using these experimental results. However, the experimental report [249] lacks sufficient detail regarding the material law, the residual stresses and geometrical imperfections. Given the relative slenderness (close

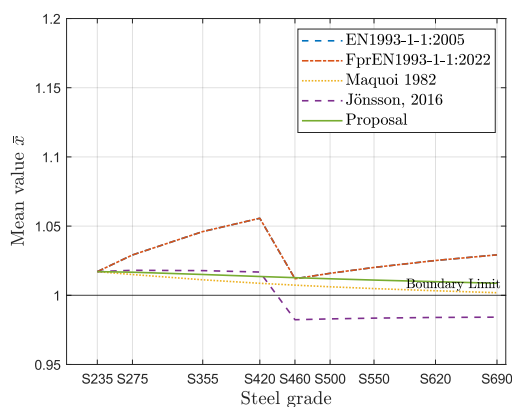
to 1.0), these imperfections play a key role in the instability response. Therefore, the tests were deemed insufficiently detailed to allow a model validation.

On the other hand, for hot-finished hollow sections, the results of the literature [245], [246], [247], [248] and those reported in Fig. 5-12c demonstrate that the results for the SHS 200x5 profile are highly sensitive to the local imperfection magnitude. For the S460 grade, the combination of imperfections consisting of considering 70% of the accompanying imperfection with a magnitude of $c/400$ shows a better agreement with the buckling curve proposal as shown in Fig. 5-12c. However, achieving a comparable correspondence for the S690 grade is difficult to reach. The discrepancy may be attributed to the difference between the reduction factor for local buckling obtained by the Winter curve and the factor numerically simulated, as shown in Table 5-5. Indeed, a better correspondence is observed in Fig. 5-12c when considering the numerical reduction factor, denoted β_{num} .

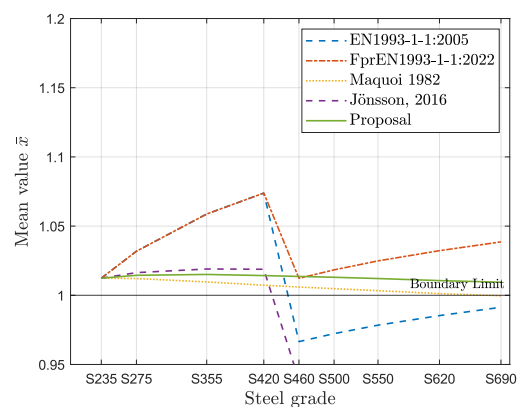
Finally, the out-of-straightness tolerance, as defined in the product standard EN10210-2 [233] about geometrical tolerances for hot-finished tubes, is $L/500$. This value is twice the imperfection tolerance adopted to establish the European buckling curves. In addition, this standard prescribes that the concavity/convexity of square hollow sections is accepted up to $c/100$, which is also twice the recommended local imperfection magnitude for numerical simulations, and even four times the required magnitude obtained by numerical simulations. The unsafe experimental result observed in Fig. 5-9b corresponds to one of the tests for which the failure was dominated by local buckling. This test (SC1-2 – $L = 1.35\text{m}$) exhibited a lower resistance ($N_u = 1054\text{ kN}$) than the longer one (SC1-3 – $L = 1.75\text{m}$) also dominated by local buckling and for the same global imperfection magnitude ($N_u = 1071\text{ kN}$). This unexpected result may be attributed to the amplitude of the local imperfection. It is mentioned in the paper that the measured local imperfections were, on average, slightly smaller than $c/200$ [148]. However, further details are provided in an accompanying publication [250], in which it can be clearly seen that some of them have a higher value (see Fig. 6 in [250]). It can be concluded from the aforementioned numerical investigations and the related papers dealing with local imperfections [245], [246], [247], [248], that further experimental and numerical investigations on the local buckling behaviour of hot-finished hollow sections in high-strength steel grades are necessary in order to ascertain the suitability of the modified imperfection factor in cases where the local buckling is the dominant failure mode.

5.2.8. Confrontation with other existing expressions from literature

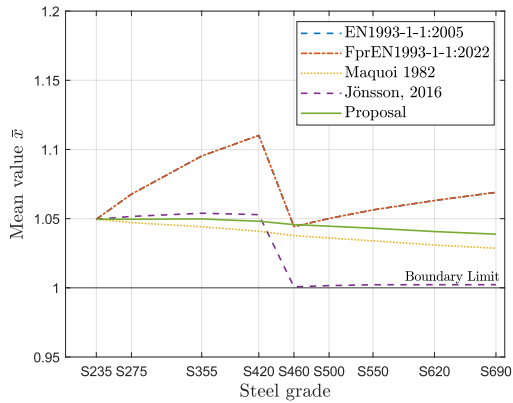
Comparisons are made based on the mean value of the ratios of the buckling reduction factors proposed in this study and other modified imperfection factors proposed in the literature. The mean values $\bar{\chi}$ of $\frac{\chi_{FEM}}{\chi_{EC3}}$, $\frac{\chi_{FEM}}{\chi_{prEN}}$, $\frac{\chi_{FEM}}{\chi_{Maquoi}}$, $\frac{\chi_{FEM}}{\chi_{Jönsson}}$ and $\frac{\chi_{FEM}}{\chi_{Meng}}$ are reported in Fig. 5-14.



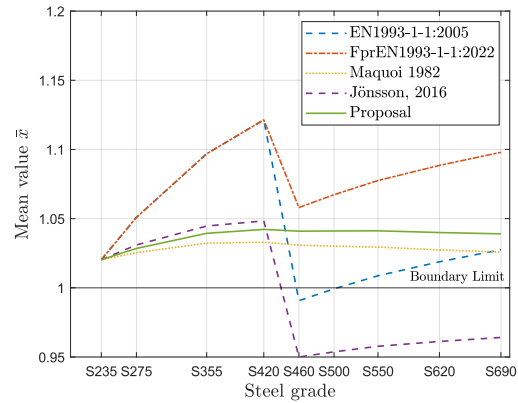
(a) Rolled: $h/b > 1.2 / t_f \leq 40\text{ mm} / \text{major axis}$



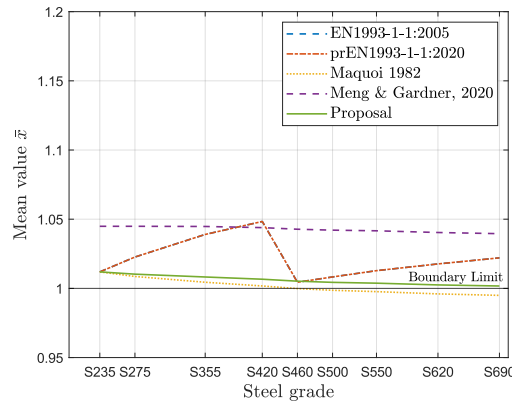
(b) Rolled: $h/b > 1.2 / t_f \leq 40\text{ mm} / \text{minor axis}$



(c) Rolled: $h/b \leq 1.2 / t_f \leq 100 \text{ mm} / \text{major axis}$



(d) Rolled: $h/b \leq 1.2 / t_f \leq 100 \text{ mm} / \text{minor axis}$



(e) Hot-finished hollow sections

Fig. 5-14. Evolution of the mean values depending on the imperfection factor reference.

The current and forthcoming versions of the Eurocode recommendations provide appropriate design recommendations for S235 and S460, but they do not consider the beneficial impact of yield strength for intermediate grades and future emerging grades (yield strengths higher than 460 MPa).

Whilst Jönsson & Stan [155] focused their research on hot-rolled sections subjected to strong axis buckling only, the applicability of this modified factor for weak axis has also been assessed. However, even in the case of strong axis buckling, the mean value \bar{x} is sometimes found to be below unity. The partial safety coefficient $\gamma_{M1} = 1.0$ should in this case be revised to be on the safe side. Furthermore, it can be observed that the mean value \bar{x} is always below unity for grades exceeding S460 for weak axis buckling. According to Fig. 5-14, this modified imperfection factor appears to be fully applicable up to 420 MPa but, beyond this grade, its applicability is more questionable, particularly for weak axis buckling.

In a recent contribution, Meng & Gardner (2020) [148] proposed a modified imperfection factor associated with a shifted yielding plateau (limited to $\bar{\lambda} = 0.1$ instead of $\bar{\lambda} = 0.2$). As can be seen in Fig. 5-14e, the mean values remain approximately constant about 4.5%. However, the new proposed imperfection factor gives a better resistance prediction. The difference between the two modified imperfection factors is illustrated in Fig. 5-15 for the S235 and S460 grades, for which the buckling resistances are already accurately predicted in Eurocode provisions.

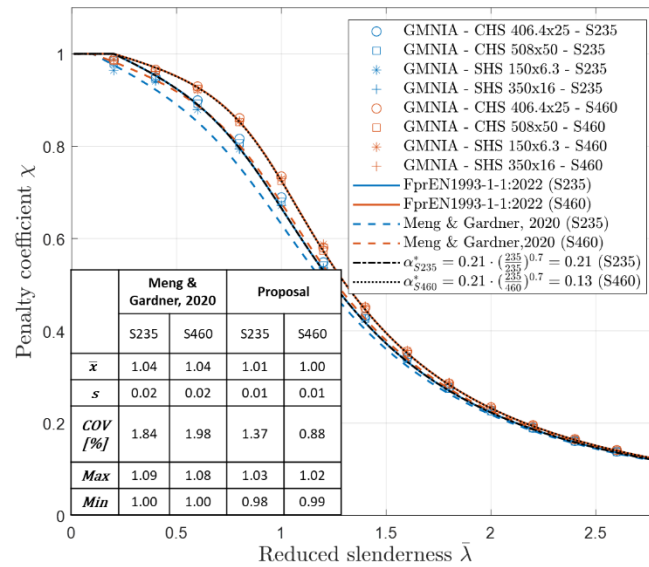


Fig. 5-15. Comparison between the modified imperfection factor of Meng & Gardner and the new proposal for already covered grades.

Fig. 5-15 illustrates that, there are no more numerical simulations below unity for the modified imperfection factor of Meng & Gardner [148], due to the shift in the yielding plateau. Aside the ongoing debate surrounding the length of the yielding plateau, the new proposal offers a better prediction for the reduction factors associated with relative slendernesses above 0.2, which is in line with the current recommendations for S235 and S460, as shown in Fig. 5-15.

Regarding the modified imperfection factor of Maquoi [145], the results in Fig. 5-14 are good, particularly for grades below S460. In addition, this factor was calibrated in such a manner that the curves adjust themselves on the classical imperfection factors for 235 MPa and 430 MPa. The objective of this work is to propose an adjustment of this factor so that it aligns with the current imperfection factors for 460 MPa instead of 430 MPa. Indeed, as can be seen in Fig. 5-14, the proposal of Maquoi [145] does not respect the current recommendations for S460, which have been deemed suitable by recent research and by this work (see Section 5.2.4).

The adaptation of this factor with an exponent of 0.7 yields interesting results, with mean values (\bar{x}) that do not exceed 5% for height-to-width ratios below or equal to 1.2 while the mean values \bar{x} are lower than 1.02 for height-to-width ratios beyond 1.2 and for hot-finished tubes. This proposal could therefore enable each grade of the range covered by new upcoming standards to benefit from the beneficial effect of yield strength linked to the decreasing relative importance of the residual stresses, assuming that the production process for these new steels will result in similar residual stress levels. Furthermore, this proposal is consistent with the observed transition in the buckling curve between S235 and S460, except in the case where $\alpha = 0.49$, $\alpha^* = 0.49$ for S235 but $\alpha^* = 0.31$ for S460. However, even with $\alpha^* = 0.31$ for S460, the mean value \bar{x} remains above 1.0, as can be seen in Fig. 5-14d. Finally, this proposal offers the advantage of being applicable to both section typologies covered in this research. This may result in the establishment of a common modified imperfection factor applicable to all hot-rolled sections.

5.2.9. Benefit in terms of buckling resistance

The advantages in terms of member buckling loads resulting from the utilisation of the proposed modified imperfection factor instead of upcoming Eurocode recommendations are represented in Fig. 5-16.

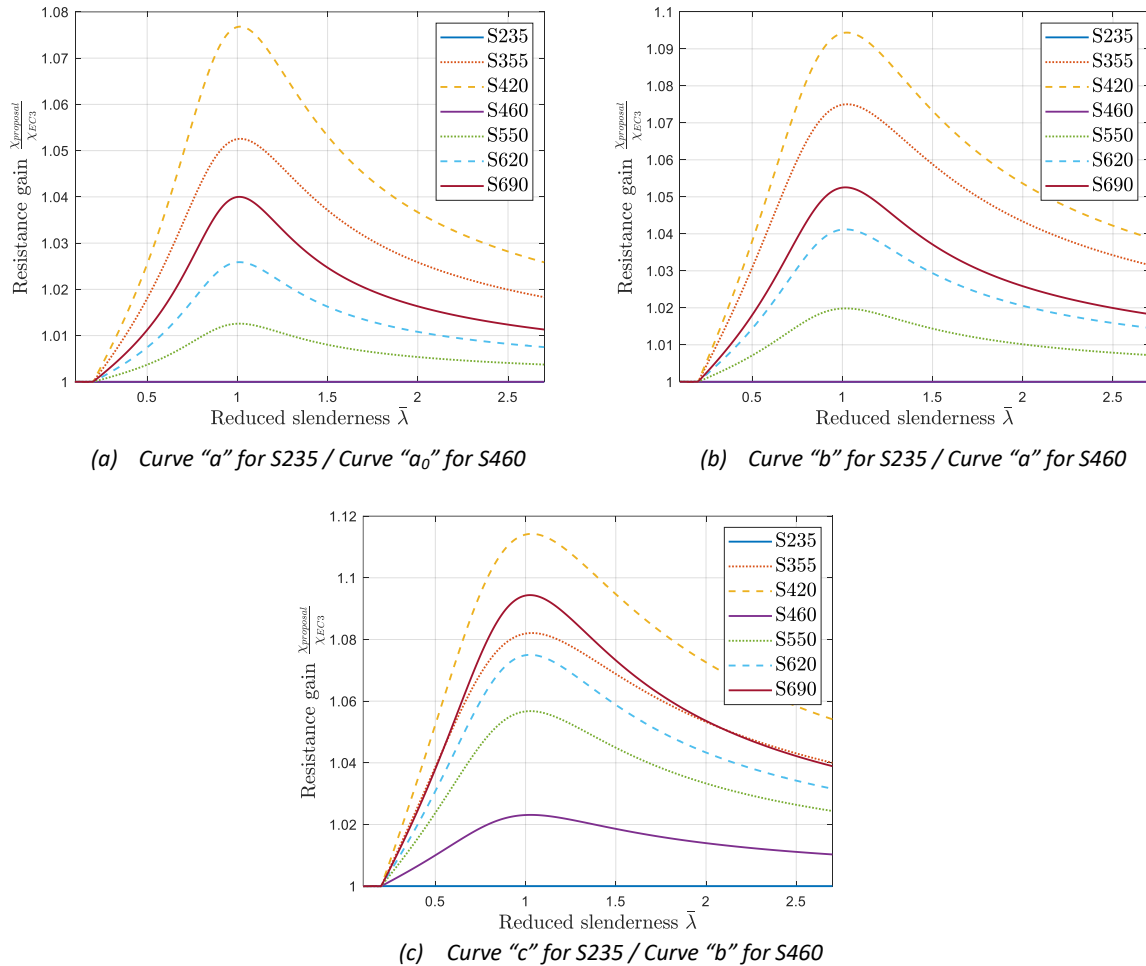


Fig. 5-16. Resulting gains from the use of the modified imperfection factor compared to forthcoming Eurocode recommendations [52].

Fig. 5-16 reports a significant rise in resistance, particularly for the intermediate grades S355 and S420 for which the flexural buckling resistances are currently underestimated in Eurocode. The peak increase corresponds to a non-dimensional slenderness of 1.0, for which the residual stress distribution has a significant impact on the results. The resistance gain is ranging from 1 to 12% but, even a small increase in the buckling resistance may result in a gain of one profile, thereby leading to a non-negligible reduction in the overall structure weight. Example 5-1 illustrates this affirmation by providing a practical design example.

Example 5-1. Detail example to illustrate the improvement benefit ($L_{cr} = 3.3m, N_{Ed} = 12400 kN, S460$)

Let us consider the second floor of the case study described in Section 4.6. The buckling length of the columns is 3.3m and the design axial load is $N_{Ed} = 12400 kN$, the optimum profile for the S460 grade is HEM340 considering the current design rules and HD400x237 with the modified imperfection factor (see table below).

Specimen	Area (mm ²)	Imperfection factor (-)	$N_{b,Rd}$ (kN)	Unity check (-)
HD400x237	30090	$\alpha = 0.34$	12335.7	1.01
HD400x237	30090	$\alpha^* = 0.31$	12467.0	0.99
HEM340	31580	$\alpha = 0.34$	12803.3	0.97

The table above shows that even though the modified imperfection proposal provides a negligible increase in resistance of about 1%, it leads to different optimum profiles corresponding to a weight saving of 5%.

Moreover, this modification contributes to the enhancement of existing design rules, avoiding a non-physically justified stepwise evaluation of the buckling resistance when yield stress increases, and thus, it contributes to the global objective of reducing the use of materials in future steel structures.

5.2.10. Summary and conclusions

The research proposes an adaptation of the design rules provided in Eurocode 3 for a member under pure compression prone to flexural buckling through the use of a modified and continuous expression of the so-called imperfection factor. This first part of Chapter 5 presents the results of numerous numerical simulations conducted to assess the buckling resistance of hot-rolled columns for a range of existing and forthcoming grades. These simulations enabled the derivation of a continuous expression of the imperfection factor, which accounts for the reduction in the impact of residual stresses on the flexural buckling resistance as the yield strength increases. A summary of the proposed modification is provided in Fig. 5-17.

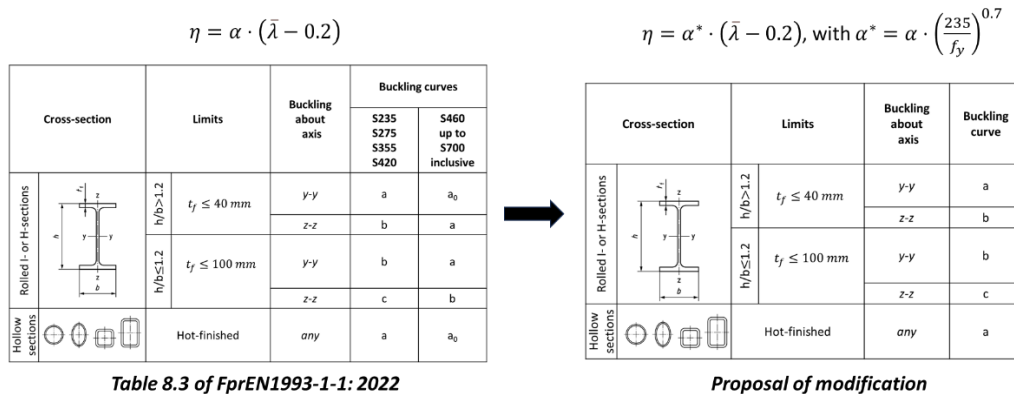


Fig. 5-17. Summary of the modification proposal.

This factor represents a slight modification of an existing modified imperfection factor proposed by Maquoi in 1982 [145], respecting the present normative recommendations made for S235 and S460 steel grades, which can be considered appropriate. This factor presents the second advantage of being applicable to all section typologies and dimensions covered in this research. The classical buckling curves recommended in Table 5-4 are conserved for grade S235, while the yield strength is accounted for by a modified imperfection factor. As a consequence, all grades beyond S235 would thus be freed from any undue penalisation caused by a non-continuity of design recommendations in terms of imperfection factors. Although this work initially focused on high-strength steels, it was demonstrated that several existing grades were also disadvantaged by current rules. It is particularly the case for the S355 steel grade, which is seen as the reference grade nowadays and for which the flexural buckling resistance is currently underestimated in Eurocode provisions.

5.3. Beneficial influence of the roller-straightening process

The Section 5.2 illustrates that, compressive residual stresses, which persist in a profile following the cooling phase of the rolling process, have a detrimental effect on column buckling resistances, as they lead to a premature yielding at the flange tips. However, most hot-rolled profiles must undergo a straightening process in order to comply with the specific tolerances set out in EN10034:1994 [251]. In current practice, the roller-straightening process is used to straighten the as-rolled profiles along their weak-axis. But this post-treatment presents a second advantage, namely the generation of a modified residual stress pattern in the profile which is less detrimental for the column buckling capacity. The literature review presented in Chapter 2 provides an overview of the existing experimental studies on the impact of the roller-straightening on residual stress distributions and the resulting beneficial impact on the column stability. Although most profiles are straightened, research on column stability did not consider this beneficial impact due to uncertainty about whether straightening had been done as already stated by Alpsten in 1975 [165], so this advantageous effect has never been incorporated in the design rules. In addition, the aforementioned experimental studies lack sufficient detail regarding the methodology employed to straighten the profiles, rendering the results unexploitable. Nevertheless, Alpsten [165] presented residual stress measurements, in addition to coupon tests and full buckling tests for different straightening situations. This study has been chosen as a reference to validate the developed numerical model. Consequently, this research focuses on the impact of the roller-straightening process on the residual stress pattern by, (i) modelling the post-treatment process to establish a straightened residual stress pattern, and (ii) evaluating the positive impact of this favourable residual stress pattern on the column bearing capacity.

In order to address this topic, a reference straightening process will be considered and modelled as described in the next section. Then, the model will be validated through comparisons to existing measurements of Alpsten [165]. With the so-validated model, parametrical studies will be conducted to investigate the influence of key parameters on selected case study profiles with the final aim to define a straightening process allowing the generation of an optimised residual stress pattern. Finally, the influence of the improved residual stress patterns on the bearing capacity of columns is investigated.

5.3.1. The reference machine setting and the model description

To conduct the investigations, a reference roller-straightening machine is defined as represented in Fig. 5-18 based on a confidential project with an industrial partner. This process can be modelled as a continuous beam on five pinned supports subjected to four imposed displacements at each mid-span. For the latter, the values 9 mm, 6 mm, 3 mm and 0.75 mm have been selected as a reference. The setting of the machine is determined by the worker's expertise, this appears to remain the case in current practice.

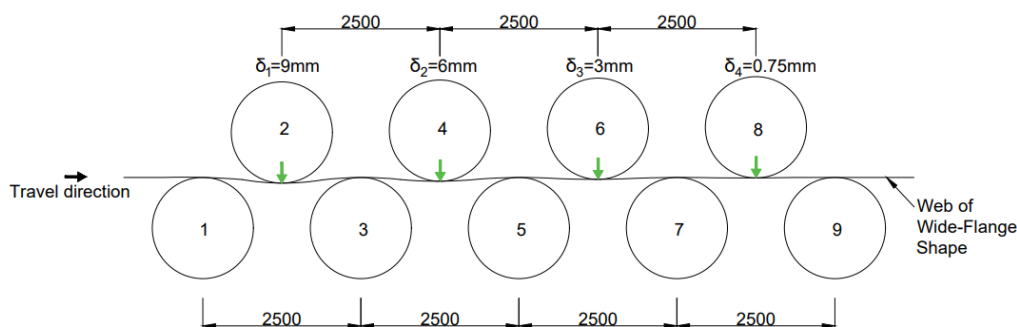


Fig. 5-18. The reference roller-straightening process.

The system represented in Fig. 5-18 is statically indeterminate and represents the stage in which the member is fully inside the machine. However, the support and loading conditions are subject to change throughout the straightening process, i.e. between the stages the profile is entering and leaving the straightening machine. Accordingly, an evolutive model has been selected to simulate this process, defined as a model allowing for modifications of the static scheme throughout the course of the calculation. This approach permits, through a single calculation, the incorporation of support condition changes observed during the straightening process. This modelling approach is particularly well-suited for studying particular construction techniques such as cantilevering, lifting and launching and this approach is fully integrated into the Finelg software [225] used for the present study. Furthermore, this single calculation also accounts for the history of yielding, which is of paramount importance for the prediction of residual stresses resulting from the straightening process.

The computation of straightened residual stress distributions is based on geometrically and materially non-linear analyses with imperfections (GMNIA). These non-linear numerical simulations are conducted by imposing displacements at each moving roller and are solved using the Newton-Raphson (constant load) method. In the FINELG software, these evolutive computations impose the use of beam finite elements. In accordance with the principles of the beam theory, it is noteworthy that plane sections are assumed to remain plane during deformation. Also, shear deformations are neglected; this latter assumption will be discussed subsequently.

The material law implemented in numerical model is a trilinear model with a yielding plateau and accounts for strain hardening according to the recommendations of FprEN1993-1-14:2024 [135]. Although there is a certain degree of variability in the material properties across the cross-section, it is assumed that the yield stress remains constant throughout the web and flanges. In addition, the residual stresses are assumed to be uniform across the flange thickness. Through a sensitivity study, it has been concluded that the self-weight of the beam can be neglected in the numerical modelling, what improves the numerical stability. The idealisation of the roller-straightening process is schematically reported in Fig. 5-19.

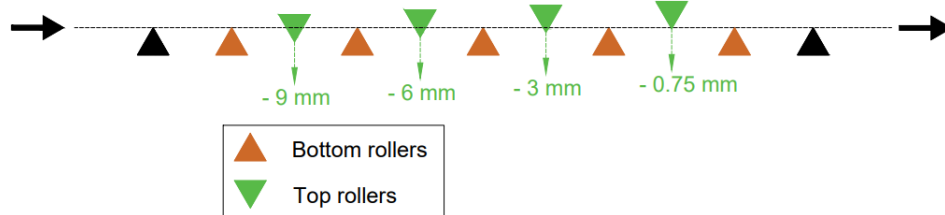


Fig. 5-19. Free body diagram of the reference roller-straightening process.

For sake of illustration of the computation process, the various main computation steps, the corresponding bending moment diagrams and the associated values for a specific cross-section (indicated by a black bullet) travelling within the straightening process are listed in Table 5-6 for the roller-straightening of a HEM500 profile.

Computation step	Bending moment diagram (kNm)	Applied moment (kNm)
1		+662
2		-750
3		+732
4		-654
5		+423

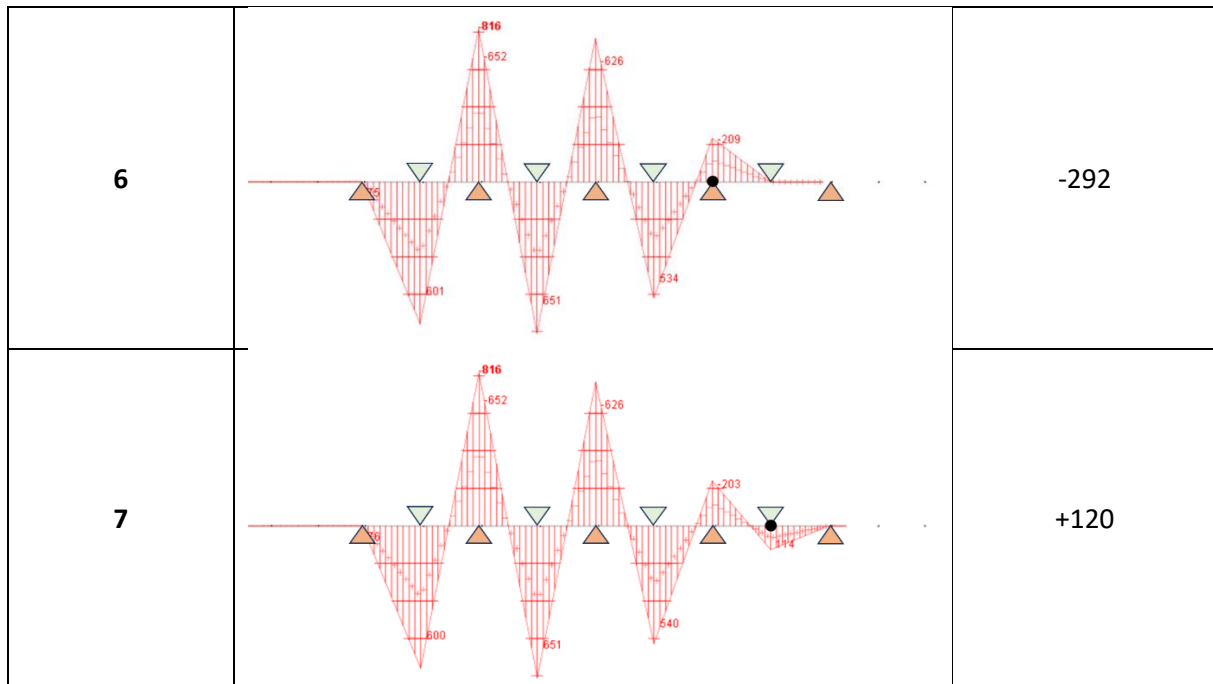


Table 5-6. Numerical steps to simulate the roller-straightening process of a HEM500 profile.

As represented in Table 5-6 and in the following Fig. 5-20, the section marked with a black bullet point is alternatively subjected to positive and negative bending moments, leading to several yielding within the cross-section. Indeed, in Fig. 5-20, it can be observed that the applied bending moments are in a range between the elastic and plastic bending resistances. These consecutive yielding events induce a redistribution of the residual stresses over the flanges.

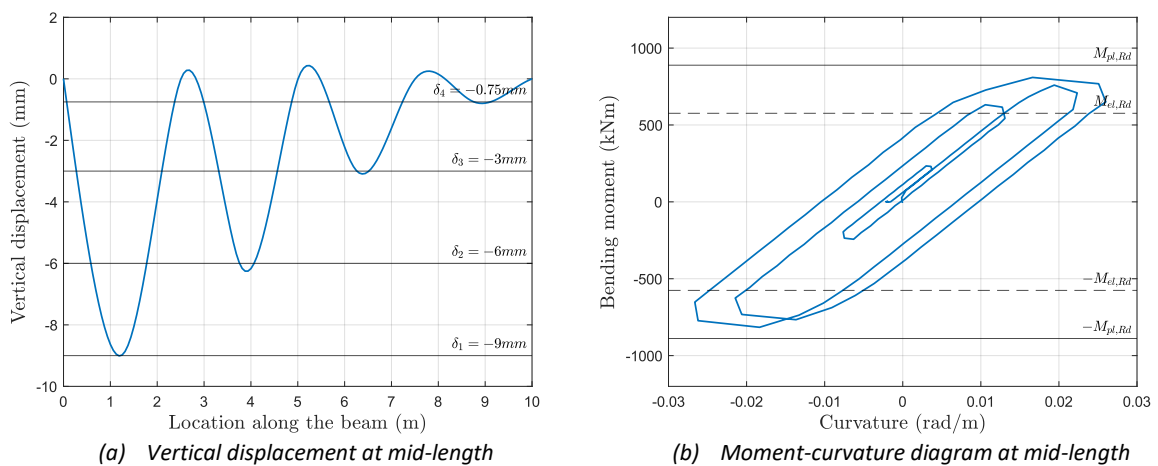


Fig. 5-20. Vertical displacement and moment - curvature diagram at mid-length of the HEM500 profile during the roller-straightening process.

Before analysing the results in terms of residual stresses, numerical simulations considering relevant imperfections as well as geometrical and material non-linearities were performed and validated based on the results of experimental data from a testing programme that was conducted in 1975. The results of this experimental campaign are presented in the following section.

5.3.2. Validation on experimental measurements

A testing campaign was realised by Alpsten et al. in 1975 [165] on a wide flange shape HEA200 profile, manufactured by the Norrbottens Järnverk steel mills at Luleå in Sweden. The steel grade was identified as SIS 1412, which is equivalent to S275JR. The various members were subjected to three distinct controlled roller-straightening procedures:

- Classical roller-straightening;
- Classical roller-straightening repeated twice;
- Modified roller-straightening with imposed displacements 2.5% larger than in the classical process.

The machine setting for the classical roller-straightening processes is reported in Fig. 5-21.

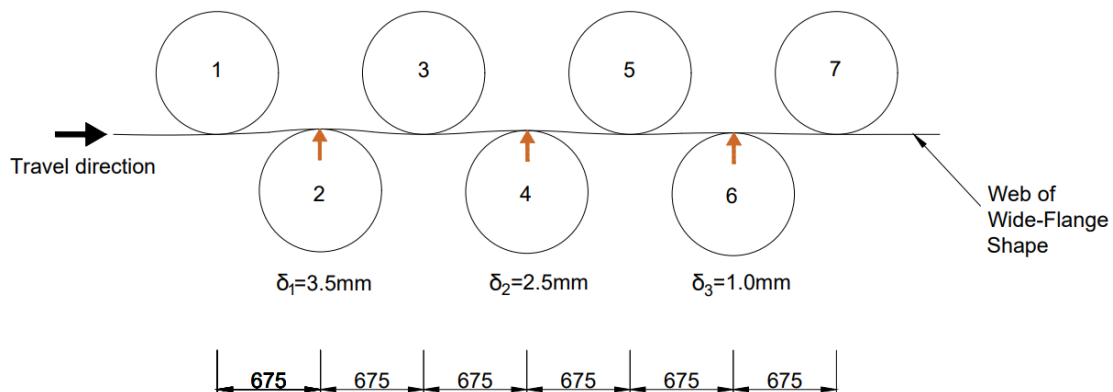


Fig. 5-21. Machine setting for the roller-straightening process in the Alpsten's experimental campaign.

As detailed in the scientific report of this experimental campaign [252], the four upper rollers are fixed in the vertical direction, while the lower rollers are adjustable. The post-treatment is uniform across the entire member length, except for edge sections that have exhibited side effects. The free-body diagram of the numerical model is shown in Fig. 5-22.

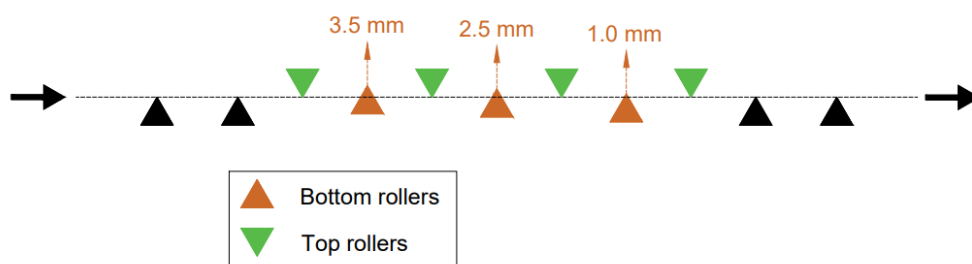


Fig. 5-22. Free body diagram of the roller-straightening process.

Coupon tests, residual stress measurements and column tests were realised. These measurements will allow the calibration and the validation of the developed numerical model of the straightening process. The measured yield stresses after rolling but before straightening are reported in Fig. 5-23 based on the measurements provided in [165].

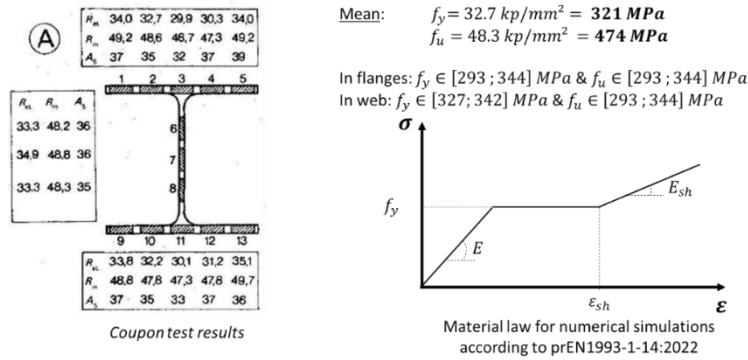


Fig. 5-23. Material law for numerical simulations based on coupon test results.

The residual stress distributions were measured prior to and following the roller-straightening process. The mean distributions in flanges with the ECCS pattern are drawn in Fig. 5-24.

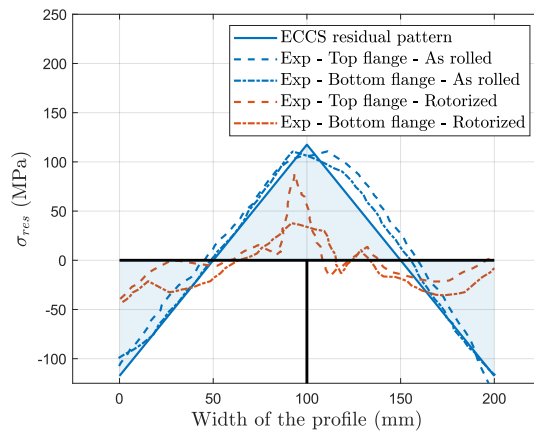


Fig. 5-24. Residual stress measurements during the test campaign.

Fig. 5-24 illustrates the accuracy of the ECCS model for residual stress distributions after the rolling process, this model has been used to introduce initial residual stresses into the numerical model. Moreover, the residual stress measurements performed after the straightening have revealed a significant reduction in compressive residual stresses at the flange tips. The residual stresses in question have been found to be almost negligible in comparison to those measured prior to the straightening process. It seems reasonable to expect that this reduction will have a beneficial effect on the bearing capacity of compressed columns. A comparison between experimental measurements and numerical simulations using the developed model is reported in Fig. 5-25. This comparison is made by applying either the average yield stress or the yield stress at flange tips to the entire cross-section.

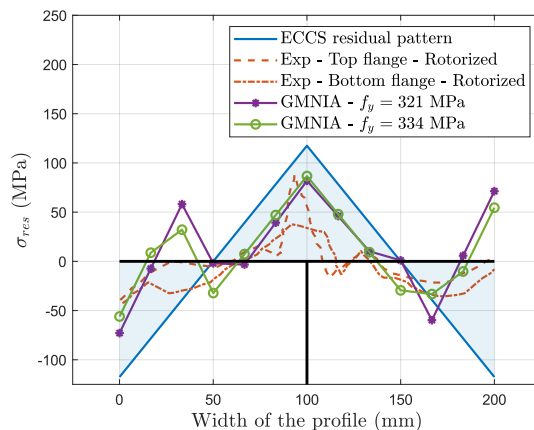


Fig. 5-25. Comparison between residual stress from experiments and from numerical simulations.

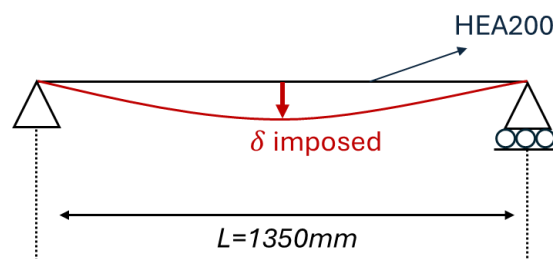
As shown in Fig. 5-25, the general trend of the residual stress distribution is well reproduced by the developed model. Nevertheless, discrepancies between the experimental and numerical simulations are observed, particularly with regard to the amplitude of the residual stress distribution. These differences may have various causes:

- The measured residual stresses exhibited considerable variability in their distribution throughout the thickness as shown in detail in [165]. The experimental data reported in Fig. 5-24 and Fig. 5-25 represent the average residual stresses on each flange;
- The effect of the variability of the yield strength is illustrated in Fig. 5-25, in which the results are plotted for two measured yield strengths. The measured yield strengths at the flange tips are typically higher than those observed near the web junction while the numerical model considers the same yield strength for the whole cross-section;
- The shear deformations are neglected in the numerical model. This implies that the numerical model exhibits a larger yielding of the cross-section to achieve the same imposed displacement;
- The sections remain plane based on the beam theory. The local effects, such as local plasticity resulting from the contact with rollers, are not considered.

The third proposed cause has been subjected to further analysis. It can be assessed that the shear contribution is not insignificant, given that the distance between two fixed rollers is relatively short in comparison to the profile height. This indicates that the assumption of the beam theory ($L/h \geq 10$) is unsatisfied. In the straightening process under concern, the profile is positioned along its weak axis, the beam height is thus $b = 200 \text{ mm}$, and so the length-to-height ratio is $L/b = 6.75$. This value is clearly below the limit prescribed by the beam theory. Regarding bending moment resistance, the shear area is the area of two flanges: $A_{vy} = 2 \cdot 200 \cdot 10 = 4000 \text{ mm}^2$, so, the shear resistance is:

$$V_{Rd} = V_{pl,Rd} = \frac{A_{vy} \cdot f_y}{\sqrt{3} \cdot \gamma_{M0}} = 741.32 \text{ kN} \quad (5-5)$$

A comparison of the shear force obtained in the evolutive numerical model with the shear resistance indicates that the shear force satisfies the following condition: $V_{Ed} \leq 0.5 \cdot V_{pl,Rd}$. This implies that the bending moment resistance is not affected by the presence of shear forces. However, the shear contribution in the total deformation is expected to affect the yielding as considering the shear contribution will inevitably result in reduced internal forces for a given imposed displacement. Numerical simulations with beam and shell finite elements have been compared to illustrate the impact of the shear contribution on the cross-sectional yielding and thus, on the residual stress distribution after straightening. The static scheme and the results for a one-span simply supported model, with a span length equal to the distance between two fixed rollers (1350 mm) and for the profile under consideration (HEA200), are presented in Fig. 5-26. Four levels of imposed displacements have been selected to encompass a bending moment range from M_{el} to M_{pl} (as depicted in Fig. 5-26b).



(a) Static scheme of the model.

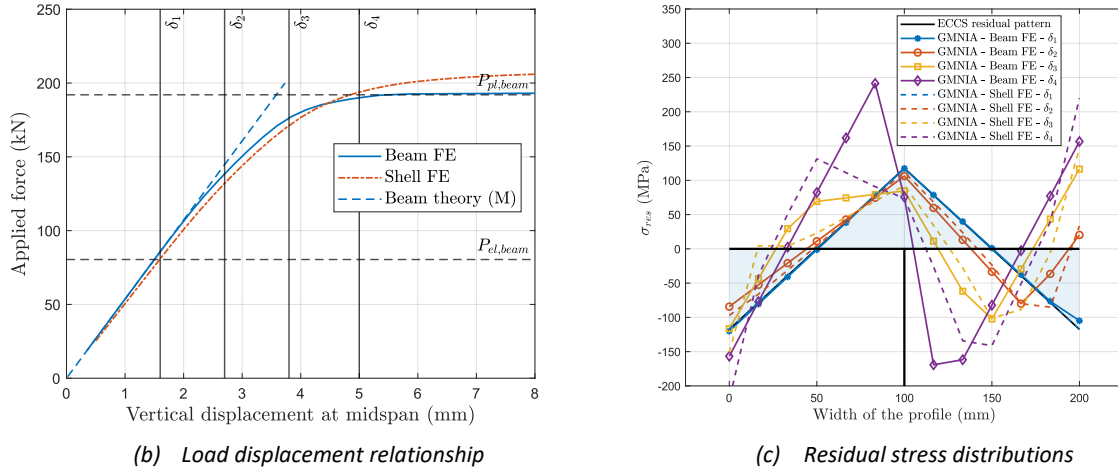


Fig. 5-26. Impact of the shear deformations on the residual stress distribution for the tested profile (HEA200).

The results represented in Fig. 5-26c demonstrate the fact that neglecting the shear deformations in the developed numerical model may explain the higher amplitude of residual stresses observed in Fig. 5-25. Neglecting the shear contribution will therefore lead in most cases to an over-estimation of the residual stresses. In other words, the residual stress distributions obtained by the developed numerical model could be actually obtained with slightly greater imposed displacements. As stated above, the employed modelling technique required the use of beam elements that does not allow to account for the shear deformation in this software. However, the numerical model was deemed appropriate for establishing realistic residual stress distributions. Indeed, the purpose of these distributions, as a reminder, is to determine whether the roller-straightening would improve the load-bearing capacity of steel columns. If this is indeed the case, then experimental residual stress measurements should be carried out before and after roller-straightening to allow for model validation on more recent and well-documented data. In addition, a more accurate model, that accounts for all the identified discrepancies, will be necessary to calibrate the machine settings and obtain the most favourable residual stress distribution. However, this will only be relevant if this study proves the beneficial advantage of roller straightening.

5.3.3. Straightened residual stress patterns for selected profiles

For the sake of continuity within Chapter 5, the same reference profiles that were employed in Section 5.2 have been selected for the purpose of investigating the advantageous impact of roller-straightening. The reference steel grade is S460, and the geometrical properties of the selected profiles are listed in Table 5-7.

Limits	Designation	h (mm)	b (mm)	t_w (mm)	t_f (mm)	r (mm)	Class in S460
$h/b > 1.2$ $/ t_f \leq 40$ mm	HEB400	400	300	13.5	24	27	2
	HEM500	524	306	21	40	27	1
$h/b \leq 1.2$ $/ t_f \leq 100$ mm	HEA240	230	240	7.5	12	21	3
	HD400x262	387	398	21.1	33.3	15	1

Table 5-7. Selected profiles to evaluate the potential benefit of the roller-straightening process.

All the profiles defined in Table 5-7 are at least class 3 in S460; thus, the use of beam elements is justified as no local buckling may occur. About the shear contribution, the length-to-height ratios (L/b) are 8.33, 8.17, 10.42 and 6.28, respectively, for HEB400, HEM500, HEA240 and HD400x262. Except for the latter, the effect of the shear contribution is expected to be less pronounced as the length-to-

height ratio is approaching the limit prescribed by the beam theory. The impact of the shear deformations on the residual stress distributions for the lightest profile (HEA240) is represented in Fig. 5-27 considering the same approach as at the end of the previous section for the HEA200 profile.

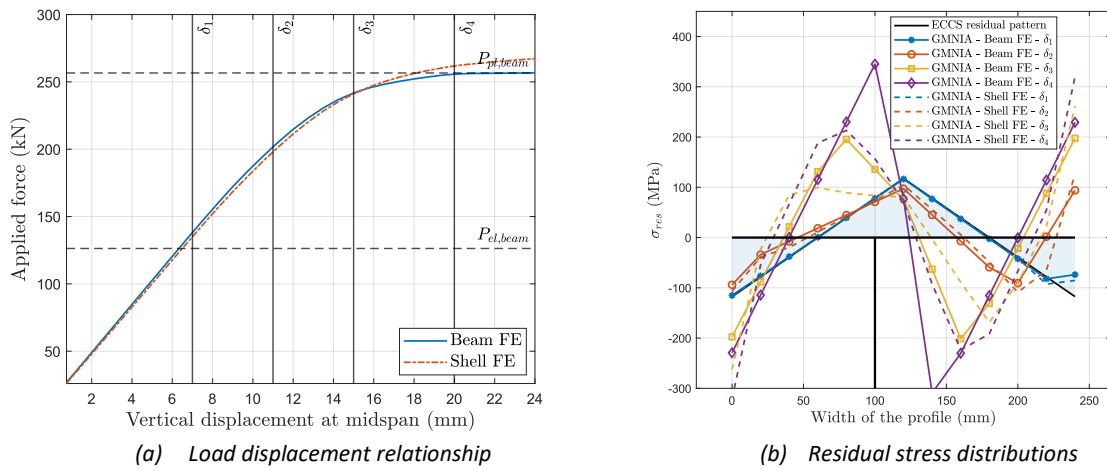


Fig. 5-27. Impact of the shear deformations on the residual stress distribution for HEA240.

Fig. 5-27 shows that the impact of the shear deformations is less for higher length-to-height ratios, however, this assumption may still slightly affect the residual stresses for large yielding. Considering the imposed displacements defined for the reference machine setting, the straightened residual stress distributions for each selected profile obtained numerically are shown in Fig. 5-28.

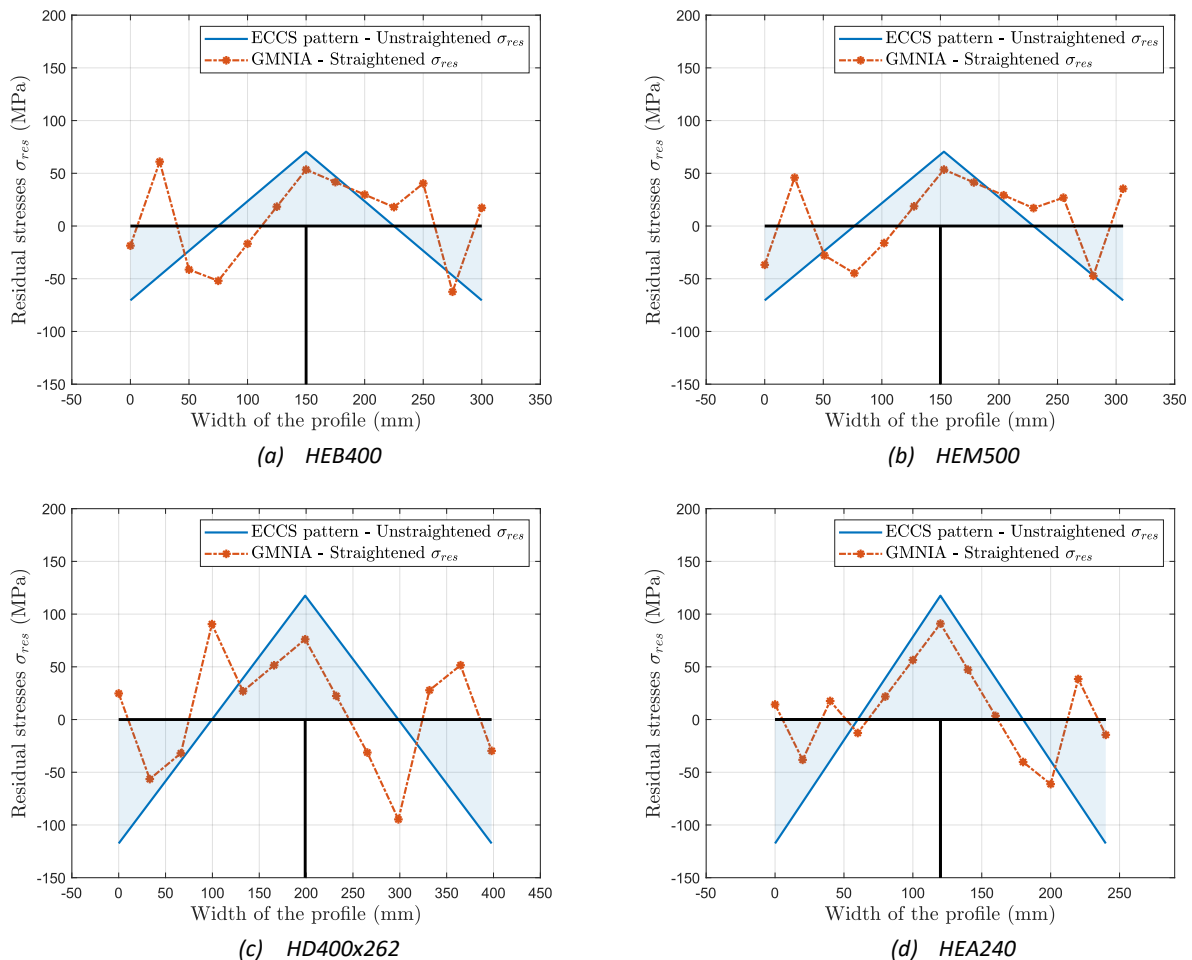


Fig. 5-28. Residual stress patterns for each selected profile and for the reference machine setting.

Fig. 5-28 illustrates the fact that the magnitude of the compressive residual stresses is greatly reduced at both flange tips. Indeed, the sign of the residual stress changes at the edges of each flange, which may lead to an increase in buckling resistance. The consideration of several sections, i.e. the consideration of different bending stiffnesses, while keeping the same imposed displacements for the straightening process implies that the number and amplitude of the yielding vary. Indeed, the lightest section (HEA240) exhibits less yielding than the others while the heaviest (HD 400x262) yields at each step defined in Table 5-6. The moment-curvature diagrams for these sections are shown in Fig. 5-29.

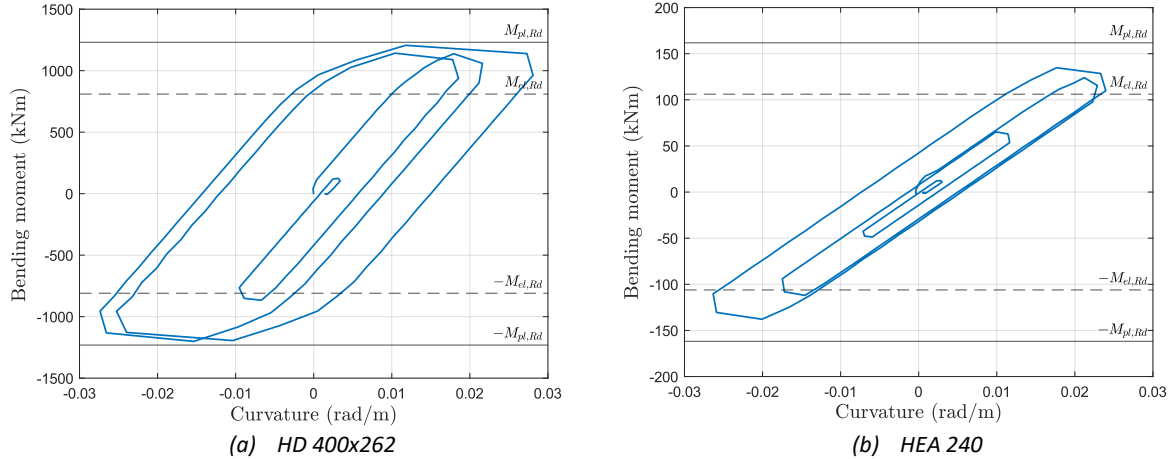


Fig. 5-29. Moment-curvature diagrams for HD400x262 (a) and HEA240 (b) considering the reference machine setting.

The moment-curvature comparison, shown in Fig. 5-29, and the residual stresses reported in Fig. 5-28, demonstrate that the yielding should be limited to have a reduced amplitude of compressive residual stresses across the flanges. This comparison illustrates the dependence between the machine setting, i.e. the imposed displacements, and the bending stiffness of the section to be straightened to target an optimised residual stress distribution. A sensitivity study was therefore carried out to identify the key parameters affecting the residual stress distributions.

5.3.4. Optimisation of machine setting

For the sake of conciseness, the sensitivity study has been conducted on the HEM500 profile only.

5.3.4.1. Effect of several successive yielding

Several numerical models have been realised to understand the effect of each numerical step (defined in Table 5-6). Hence, for instance, the modelling of the first computation step consists of applying only the first positive bending moment, the second step only considers the two first bending moments, ..., as shown in Fig. 5-30a. The residual stress patterns for each numerical step are reported in Fig. 5-30b.

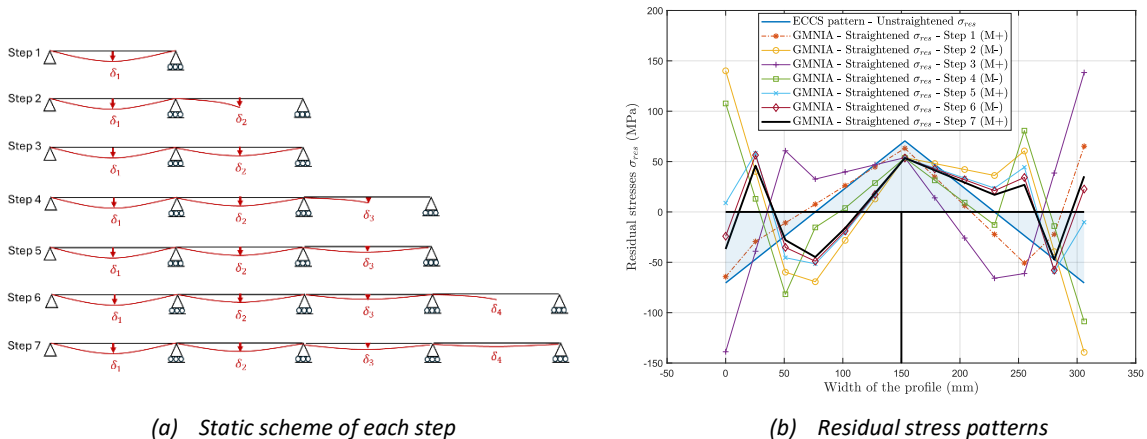


Fig. 5-30. Effect of each maximum bending moment on the residual stress distribution for the HEM500 profile.

Fig. 5-30b illustrates the fact that the magnitude of the compressive residual stresses at the right flange tip is greatly reduced, after the first numerical step, i.e. the first yielding of the cross-section. Indeed, at the right edge of the flanges, the sign of the residual stresses undergoes a change which should lead to an increase in the buckling resistance, even after only one cross-section yielding.

After the first yielding, the compressive residual stresses at the left flange tip are approximately the same as before the process. Consequently, in the case of a single yielding, the positive effect of the roller-straightening process on the buckling resistance depends on the direction in which the profile will buckle, thus on the out-of-straightness direction. However, the advantage of the roller-straightening process over the gag straightening process (both defined in Section 2.4.4) is that it reduces the amplitude of the residual stress on both sides of the flanges, since this process consists of a series of applied bending moments of opposite sign (see Table 5-6). In fact, as can be seen in Fig. 5-30b, the yielding induces different bends in the residual stress distributions at the flange tips, gradually reducing their amplitude. This could be beneficial in view of the expected increase in buckling resistance of the columns. Accordingly, it seems that an optimised selection of imposed displacements could be found in such a way as to reduce the amplitude of the residual stresses at both flange tips.

5.3.4.2. Modification of the first imposed displacement

This subsection consists of evaluating the influence of the first yielding amplitude on the resulting residual stress distributions, considering three values of the first imposed displacement δ_1 without modifying the other displacements. The residual stress patterns for three different settings are shown in Fig. 5-31.

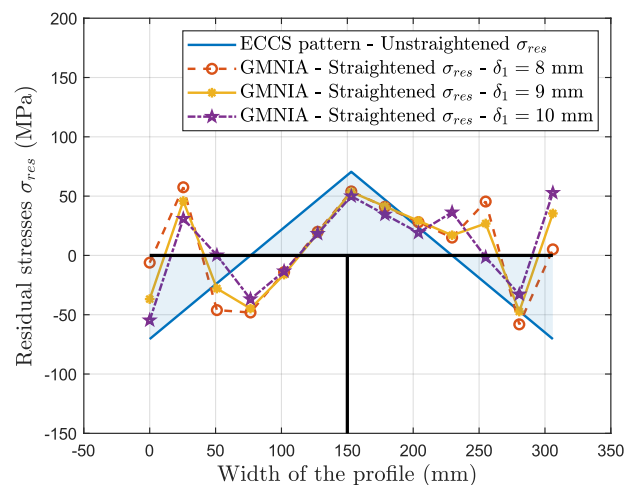


Fig. 5-31. Residual stress distributions for the HEM500 profile depending on the first imposed displacement.

Fig. 5-31 shows that the higher the first imposed displacement, the higher the residual stresses at flange tips. Accordingly, it increases tensile residual stresses on one side and compressive residual stresses on the other side, so the benefit of roller-straightening on the buckling resistance depends on the direction of the initial geometrical imperfection. In addition, the smaller the first imposed displacement, the smaller the amplitude of residual stresses at flange tips. Therefore, the first imposed displacement must be well targeted in such a way to maximise the benefit of the roller-straightening on the column buckling capacity.

5.3.4.3. Modification of the second imposed displacement

In the same manner as for the previous subsection, three different cases of second imposed displacement were selected to evaluate the effect of the amplitude of the first negative bending moment. The other imposed displacements remain the same. The different residual stress patterns

after the roller-straightening process in the different setting cases (here only the displacement δ_2 is affected) are given in Fig. 5-32.

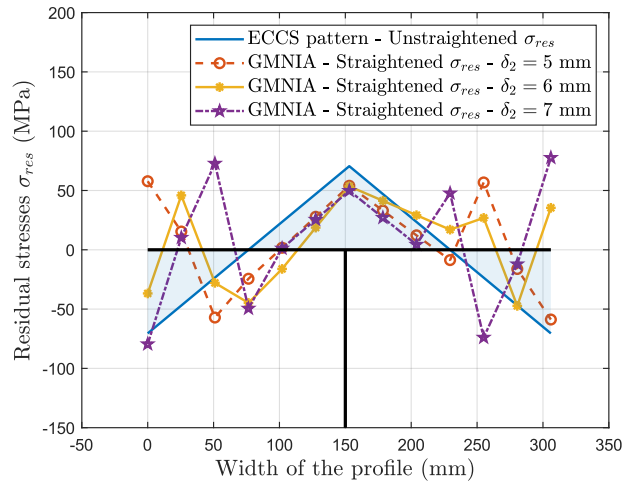


Fig. 5-32. Influence of the second imposed displacement on the residual stress distribution for the HEM500 profile.

As can be seen in Fig. 5-32, from a second imposed displacement of 6 mm, the second yielding of the section induces a bend in the residual stress distributions at the flange tips. This could be beneficial in view of the expected increase in buckling resistance of the columns. Accordingly, it appears that an optimised set of the first two imposed displacements could be found to further reduce the amplitude of the residual stresses at both flange tips.

5.3.4.4. Influence of yield strength

The reference setting was applied to three different grades, i.e. S355, S460 and S500. The comparison of the residual stress distributions obtained for the three steel grades is shown in Fig. 5-33.

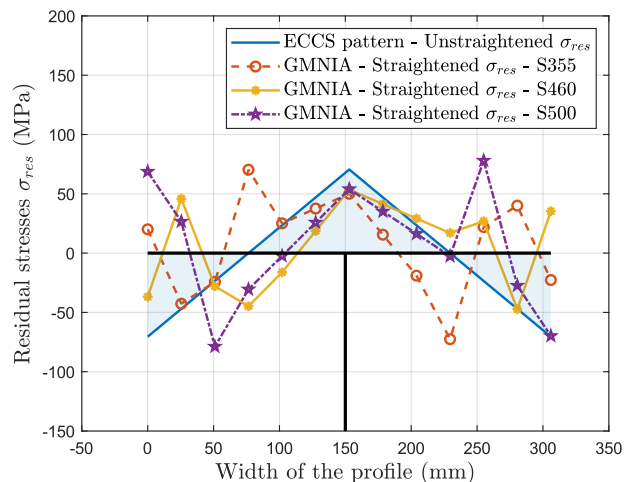


Fig. 5-33. Influence of the yield strength on the residual stress distribution for the HEM500 profile.

As expected, Fig. 5-33 illustrates a considerable variability of results depending on the yield strength. This was expected as the yield strength has a direct influence on the level of yielding in a cross-section and the related yielding history. Therefore, it can be concluded that the machine setting should be adjusted in accordance with the material yield strength.

5.3.4.5. Effect of a second straightening pass

A second pass through the machine imposes the same hysteresis on all sections, so a second pass does not induce further yielding. To ensure that the profile is straight after the process, two successive

passes through the machine in two directions (180° rotation along the axis) could be considered. Alpsten [165] reported some measurements carried out during the experimental campaign as shown in Fig. 5-34a. In addition, although it is not applied in current practice, it was decided here to numerically simulate this second pass for the reference straightening of the HEM500 profile, to see its effect on the residual stress distributions – see Fig. 5-34b.

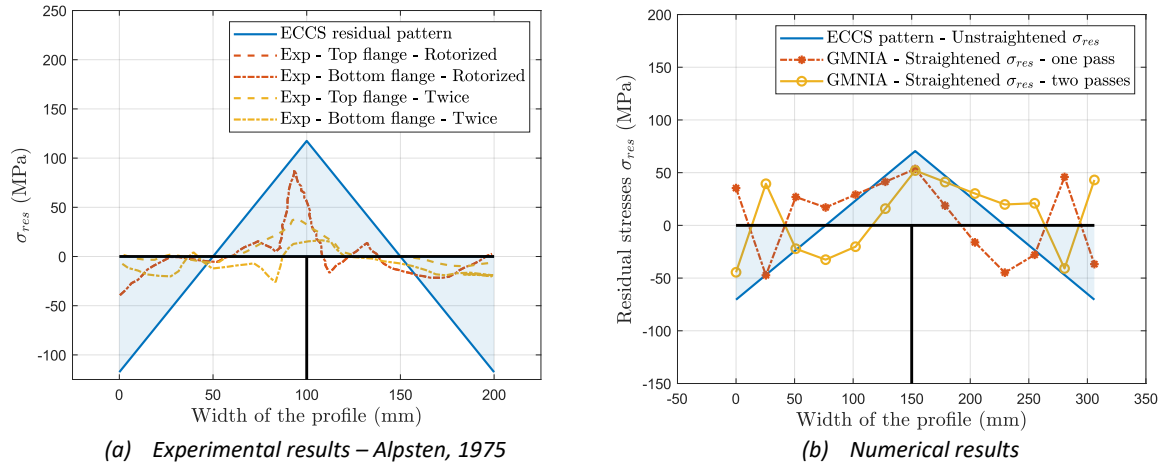


Fig. 5-34. Effect of a second pass in the straightening machine.

Fig. 5-34 illustrates that there is no advantage in terms of residual stresses to straighten a profile twice, as the residual stress pattern is simply the inverse. Indeed, the second one-way pass on the other side induces the same hysteresis with the opposite bending moments sign. Consequently, the residual stress values for two passes are the mirror values of those for the one-way pass. The effect of these patterns on the buckling capacity depends on the direction of the initial geometrical imperfection, as discussed in the following subsection. In fact, the tension residual stresses are located at different flange tips depending on the number of passes.

5.3.4.6. Proposal for an optimised straightened residual stress pattern

Several conclusions can be drawn from this sensitivity study to calibrate the process settings:

- The machine setting should be adjusted according to the profile size and yield strength to achieve a reduced residual stress distribution;
- Only a single yielding of the cross-section induces a bend in the residual stress distributions, but in this case, the benefit of the roller-straightening process will be highly dependent on the sign of the initial geometrical imperfection. Multiple yielding, i.e. the roller-straightening, should be preferred as it leads to a homogeneous reduction of residual stresses;
- A second straightening pass does not present any advantage, so there is no need to consider it further.

To study the influence of the roller straightening on the load-bearing capacity of columns in compression, relevant residual stress patterns must be selected for each of the four profiles. The first residual stress pattern considered is the one obtained by considering the reference-imposed displacements, i.e. 9/6/3/0.75 mm (as defined in Fig. 5-18). An "optimised" pattern is also considered in order to evaluate the benefit in terms of buckling resistance that could be obtained when calibrating the process settings. An optimised setting is defined as a setting that provides a lower residual stress amplitude than that obtained with the reference setting. This corresponds to a setting which has the potential to further increase the column bearing capacity. The optimised settings are reported in Table 5-8 while the optimised residual stress patterns for each selected profile are shown in Fig. 5-35.

Specimen	δ_1 (mm)	δ_2 (mm)	δ_3 (mm)	δ_4 (mm)
HEB400	8	5	4	0.75
HEM500	8	5	3.5	0.75
HD400x262	5	4	3	0.75
HEA240	10	5	4	0.75

Table 5-8. Optimised machine setting for each selected profile.

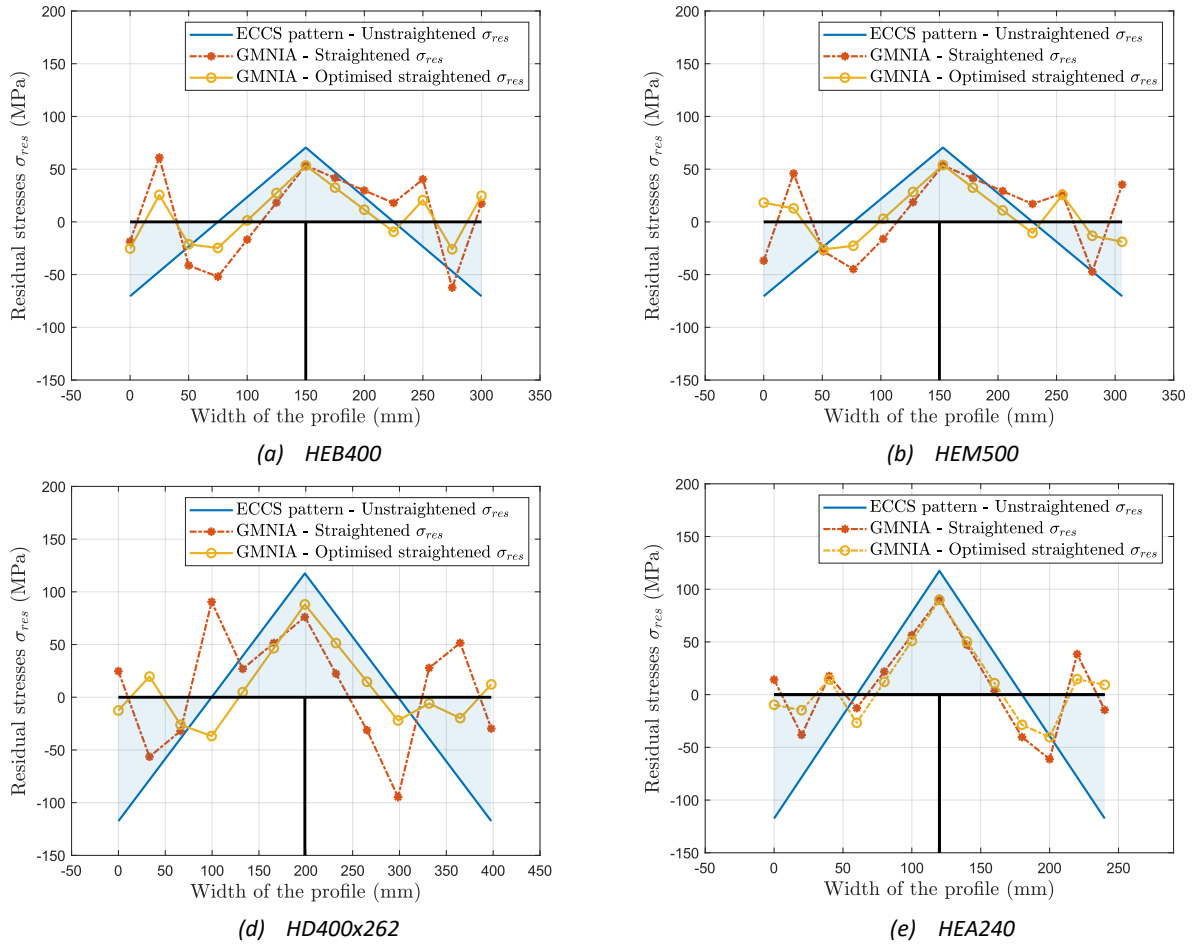


Fig. 5-35. Residual stress patterns for evaluating the benefit of the roller-straightening process on the column bearing capacity.

It is noteworthy that this optimisation is only based on the knowledge gained from the developed model, which does not perfectly represent the reality as already stated. In fact, the purpose of this numerical model is not to calibrate the straightening machine, but rather to establish straightened residual stress patterns that are physically realistic, to draw conclusions about the potential benefit of the straightening on the load bearing capacity of the columns. Based on the positive results of this research, considering the beneficial effect of the straightening should be considered in the future as a way to increase the competitiveness of steel sections, so further studies with experimental measurements should be carried out in order to model accurately and calibrate the machine. It is difficult to generalise the conclusions as the machine properties are likely to be different depending on the manufacturer. For instance, the reference straightening setting shown in Fig. 5-19 differs significantly from the machine setting of Alpsten shown in Fig. 5-22, so optimising the setting depends on the straightening machine. Nevertheless, the optimisation conducted in this research makes it possible to establish plausible residual stress distributions that can be used in column numerical models to assess the benefit of the straightening on the column bearing capacity as reflected in the next section.

Finally, it is also important to note that the flexural buckling about minor axis presents two opposite stress patterns depending on the sign of the initial deformed shape. The application of an axial force to a geometrically imperfect column generates bending moments to which corresponds a bi-triangular stress pattern. Compressive stresses develop at the intrados, left or right side of the column, depending on the sign of the initial imperfection. For a common residual stress pattern, such as the ECCS model, the orientation (sign) of the geometrical imperfection does not affect the buckling resistance because the residual stress pattern is symmetrical with respect to the column web. However, this is not the case for a "straightened" pattern as graphically shown in Fig. 5-36. In fact, Fig. 5-36b illustrates a case where the yielding is delayed for only one of the two orientations. If the signs of the residual stresses at the flange tips are opposite in the two patterns, thus the residual stresses resulting from the roller-straightening process offset the flexural stresses. Consequently, the orientation of the initial geometrical imperfection could potentially affect the carrying capacity of straightened columns in which non-symmetric residual stress patterns have been generated; this is safely addressed in the following section by considering the worst case for each buckling curve.

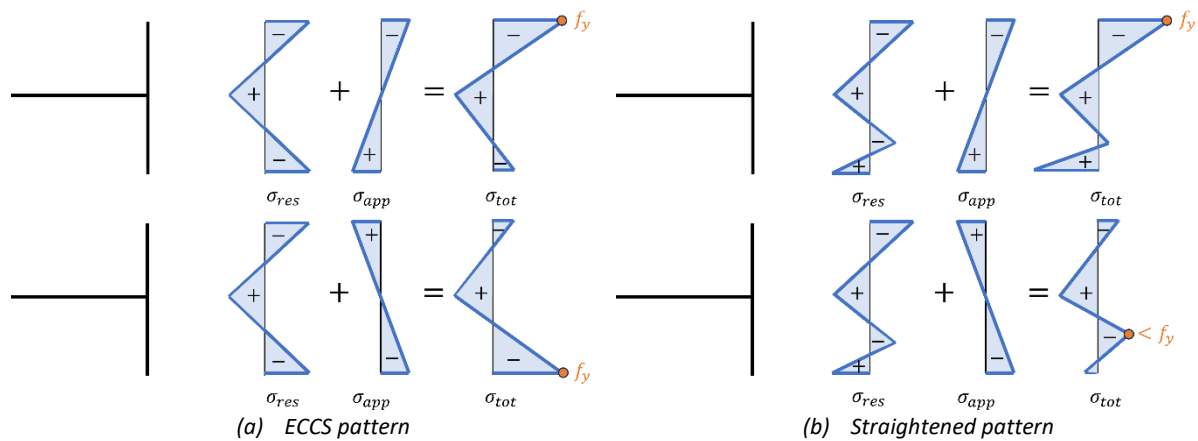


Fig. 5-36. Effect of the sign of the initial geometrical imperfection on the column bearing capacity.

5.3.5. Influence of roller-straightening on column buckling resistance

The final part of the adopted methodology consists of deriving buckling curves for straightened members, successively for the two straightening configurations defined in the previous section, i.e. reference and optimised straightening processes. In a second phase, the numerical curves are compared with those recommended by Eurocode 3 (see current recommendations in Table 2-11) to quantify the effect of the roller-straightening process on the load bearing capacity of columns. The buckling curves were obtained by evaluating the column instability loads for 13 different non-dimensional buckling slendernesses according to the methodology described in Section 5.2.2. The steel stress-strain relationship, shape and amplitude of the initial geometrical imperfection are the same as those considered in Section 5.2.2. The S460 grade is the target grade in the framework of the presented investigations, but the benefit is likely to be greater for lower grades due to the increased relative importance of residual stresses for lower yield stresses. It was therefore decided to also consider S355, which is now considered as the reference grade, with the same straightened residual stress distributions. It is worth noting that such residual stress distributions could not be achieved with the same machine settings for both grades (as explained in Section 5.3.4.4), but nevertheless, the aim here is to evaluate the effect of straightened residual stress patterns on buckling resistance. The implementation of initial stresses in FineLg is not automatic and therefore successive iterations may be required to reach the stress equilibrium in the section. For instance, Fig. 5-37 shows the residual stresses for the reference and optimised cases of the HEM500 section before and after adjustments in

the software. This adjustment check was carried out for each residual stress distribution introduced in the software.

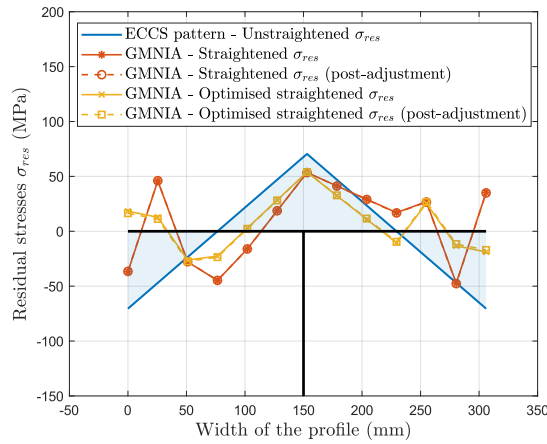
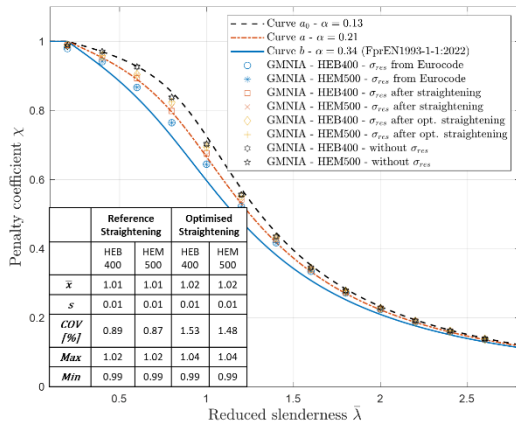
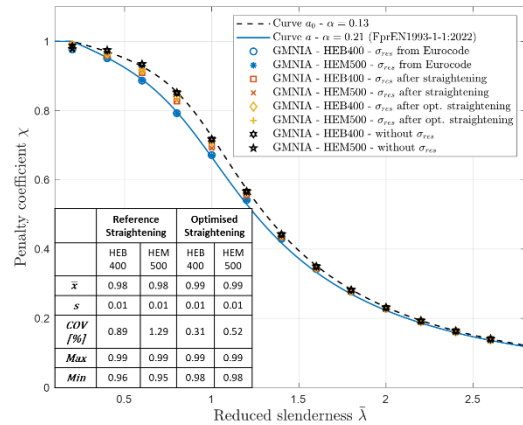


Fig. 5-37. Residual stress distributions for HEM500 before and after the stress adjustment into the software.

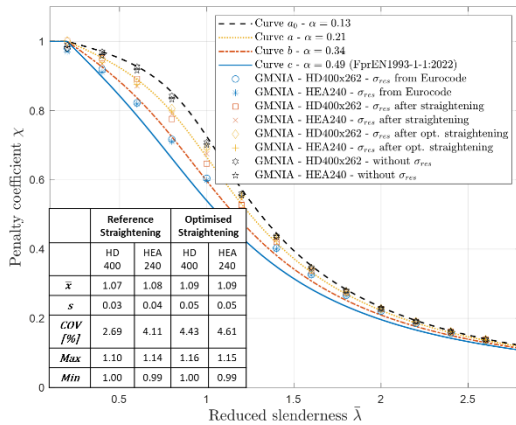
The numerical results are presented on the buckling curves in Fig. 5-38 with a statistical analysis to evaluate the possibility of considering a higher buckling curve for roller-straightened profiles. The blue curves represents the recommended curve in FprEN1993-1-1:2022 [52] for each case while the statistical evaluation is performed on the higher buckling curve, i.e. curve a_0 in Fig. 5-38b, curve a in Fig. 5-38a and Fig. 5-38d and curve b in Fig. 5-38c.



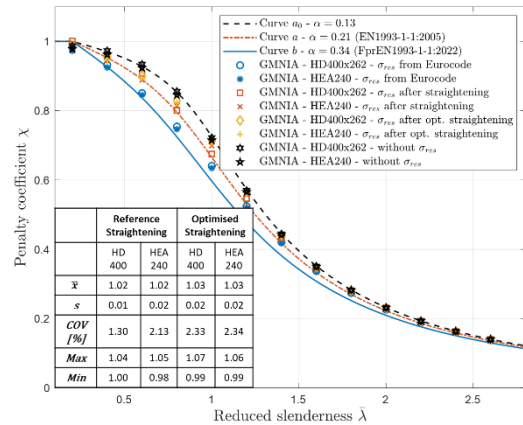
(a) Rolled: $h/b > 1.2 / t_f \leq 40 \text{ mm} / S355$



(b) Rolled: $h/b > 1.2 / t_f \leq 40 \text{ mm} / S460$



(c) Rolled: $h/b \leq 1.2 / t_f \leq 100 \text{ mm} / S355$



(d) Rolled: $h/b \leq 1.2 / t_f \leq 100 \text{ mm} / S460$

Fig. 5-38. Beneficial influence of the roller-straightening on the buckling resistances for grades S355 and S460.

Fig. 5-38 shows the significant effect of straightening on the load-bearing capacity of columns in compression. Indeed, in most cases, taking straightening into account results in an increase of one buckling curve for both S355 and S460 grades. Some simulations were carried out in the absence of residual stresses to show the optimum case that could be achieved with a machine setting that totally removes residual stresses. As expected, these numerical results were consistent with an a_0 curve that had originally been established for profiles without residual stresses. Fig. 5-38 shows that, the results tend to be closer to this idealised case when considering optimised process settings. For grade S355, it has already been shown that its buckling resistance is underestimated in the existing design rules (see Section 5.2.5). As can be seen in Fig. 5-38a and Fig. 5-38c, considering the beneficial effect of the straightened residual stress pattern in addition, systematically leads to a gain of at least one buckling curve for the S355 grade. However, for the S460 grade, curve “a” is already recommended for cross-sections with a height-to-width ratio above 1.2. Therefore, to gain one buckling curve, the effect of residual stresses would have to be completely eliminated (see Fig. 5-38b). In conclusion, the consideration of an optimised roller-straightening process could permit to consider a **buckling curve “a”** for flexural buckling about weak axis for both grades whatever the dimensions of the section. The increases in buckling resistance are thus equal to the ratios of the reduction factors between the buckling curve “a” (respectively “ a_0 ”) and the buckling curve currently prescribed in FprEN1993-1-1:2022 [52], as reported in Fig. 5-39.

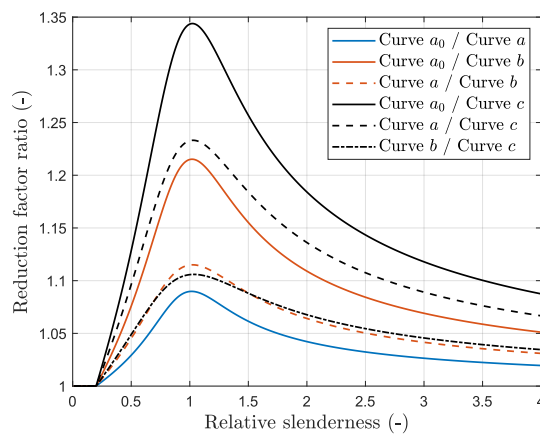


Fig. 5-39. Resulting gains from the consideration of a higher buckling curve.

Fig. 5-39 demonstrates the significant increase that could be achieved by reducing the deleterious impact of residual stresses through innovative production processes. This confirms the necessity in investing research to determine a way to account for the beneficial influence of the straightening in the current design recommendations.

5.3.6. Discussions and conclusions

A numerical model has been developed to simulate the roller-straightening process. This model has allowed to establish realistic residual stress patterns which enable to evaluate the positive impact of the roller-straightening process on column stability.

Throughout this study, two realistic residual stress distributions have been considered for four profiles selected as study cases. The first residual stress distribution is obtained by the imposed displacements taken as reference while the second is an “optimised” distribution based on the knowledge gained during the present research. The aim of the research was to determine whether a “jump” in the selection of relevant European buckling curves could be contemplated when considering straightened residual stress patterns. The present work presents some encouraging results regarding the potential benefit of the roller-straightening process on residual stress distributions. It has been shown that a

buckling curve “a” can be adopted in all minor axis buckling cases when the beneficial influence of the roller-straightening is considered regardless the curve recommended by Eurocode.

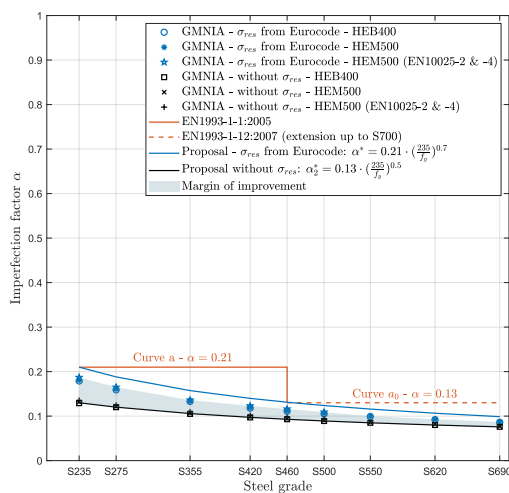
Nevertheless, this study was carried out for a specific machine configuration and settings. A different machine would have resulted in a different residual stress distribution. As a perspective, some residual stress measurements, before and after straightening, for different machine configurations and settings should be carried out to calibrate and validate a more accurate numerical model with the aim of proposing a standardised residual stress pattern function of the machine setting. In addition, some buckling tests should be carried out to validate the beneficial impact of the roller-straightening process on column carrying capacity, i.e. the prescription of the buckling curve “a” for straightened columns. The final aim is to identify optimised machine settings for a range of profiles typically used in columns. This will ensure that a more favourable buckling curve applies to a whole range of sections and not just a few specific ones.

5.4. Modified imperfection factor for columns without residual stresses

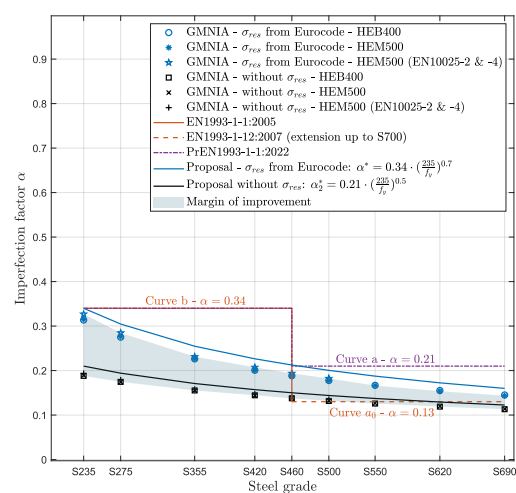
The investigations on the influence of the roller-straightening process on the stability of steel columns have highlighted a significant improvement in terms of buckling capacity but, it has also been shown that the benefit of this post-treatment process is highly dependent on the machine setting. The amplitude of the benefit will depend on the manufacturer and the level of optimisation of the machine settings. It was therefore decided to carry out several simulations in the idealised case where there are no residual stresses, to derive an idealised modified imperfection factor. On the basis of these numerical simulations, the following imperfection factor has been derived - see Eq. (5-6) with $\alpha_{ref} = 0.13$ for strong-axis and $\alpha_{ref} = 0.21$ for weak-axis buckling.

$$\alpha_2^* = \alpha_{ref} \cdot \left(\frac{235}{f_y} \right)^{0.5} = \alpha_{ref} \cdot \varepsilon \quad (5-6)$$

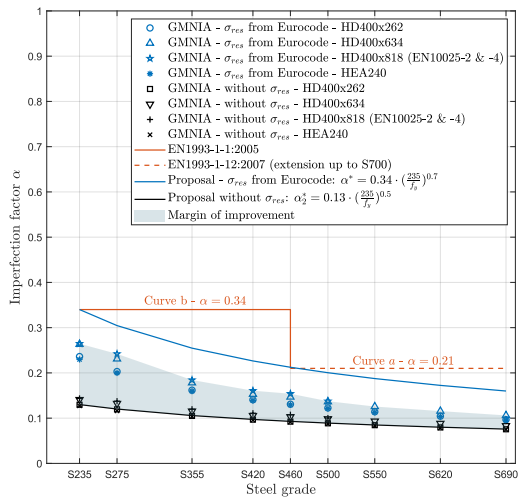
It should be recalled the value $\alpha_{ref} = 0.13$ refers to a buckling curve “a₀” developed in the past for sections without residual stresses. This modified imperfection factor has been reported with the corresponding numerical simulations in Fig. 5-40 to show its relevance for each section typology and buckling axis. Furthermore, the potential for improvement, in terms of residual stress reduction, is indicated by an area called “Margin of improvement” in Fig. 5-40.



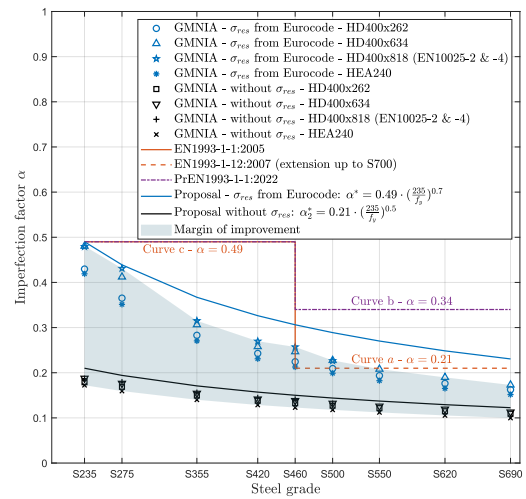
(a) Rolled: $h/b > 1.2 / t_f \leq 40$ mm / major axis



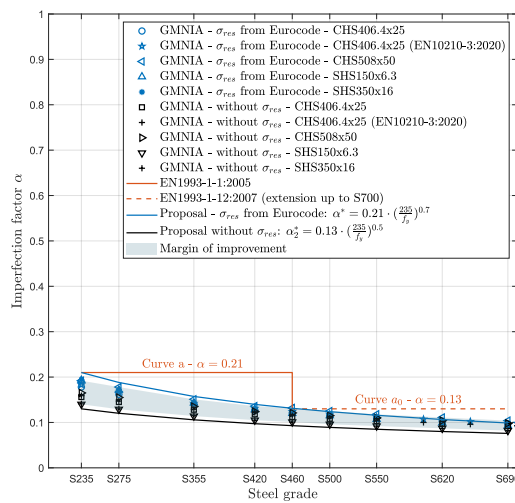
(b) Rolled: $h/b > 1.2 / t_f \leq 40$ mm / minor axis



(c) Rolled: $h/b \leq 1.2 / t_f \leq 100$ mm / major axis



(d) Rolled: $h/b \leq 1.2 / t_f \leq 100$ mm / minor axis



(e) Hot-finished hollow sections

Fig. 5-40. Evolution of the imperfection factor with or without the consideration of residual stresses.

Fig. 5-40 demonstrates that the idealised modified imperfection factor expressed in Eq. (5-6) shows a good agreement with the simulations neglecting the residual stresses. However, the reduction in residual stresses has a greater effect on columns prone to weak axis buckling, as the improvement margins are larger in Fig. 5-40b and Fig. 5-40d. In addition, the use of post-treatment techniques to reduce residual stresses, such as the roller-straightening process, has mainly an advantage on mild steels as the margin of improvement decreases with the yield strength (see Fig. 5-40). This explains why the beneficial impact of the roller-straightening reduces with the yield strength increase. Therefore, the resistance of sections made of intermediate mild steels (i.e. S355, S420) is particularly underestimated, as the beneficial effects of the yield strength and the systematic straightening are not adequately accounted for in current design recommendations. Finally, these numerical simulations show that the development of new techniques to reduce the amplitude of residual stresses for sections prone to strong-axis buckling or hot-finished hollow sections is unlikely to be significant regarding the related small margins of improvement. This feature is also illustrated by plotting the increase in buckling resistance as a function of a change in the imperfection factor – see Fig. 5-41. The imperfection factor denoted α_0 is the reference imperfection factor prescribed by the standard for a specific application.

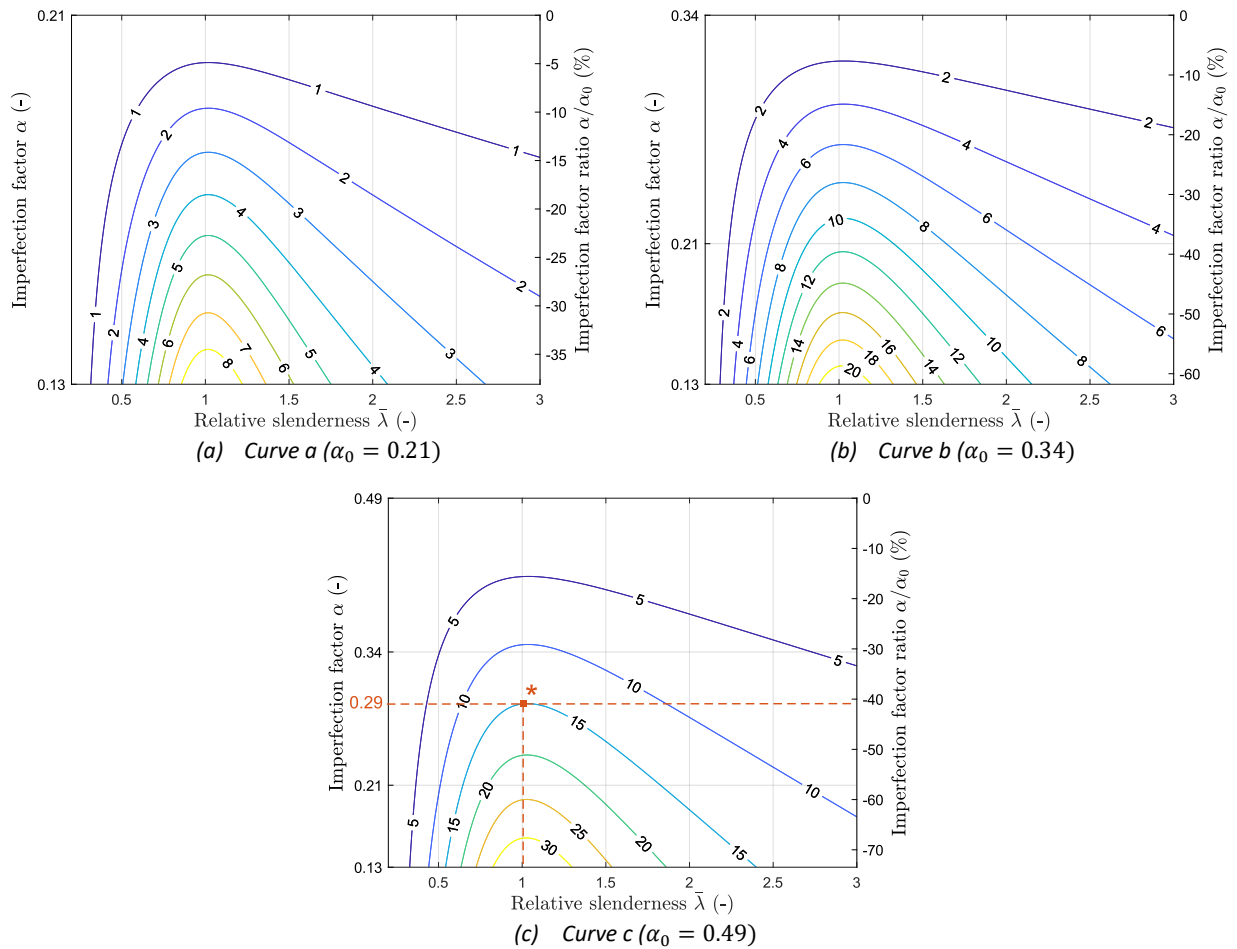


Fig. 5-41. Buckling resistance increase (%) as function of the imperfection factor reduction and the relative slenderness.

In order to facilitate the understanding of the curves plotted in Fig. 5-41, an illustrative example is provided in Fig. 5-41c. For a member with a relative slenderness of 1.0 and for which a curve “c” is prescribed (imperfection factor of 0.49), a gain of 15% in buckling resistance is observed when a reduction of 41% of the imperfection factor is achieved through a reduction of the residual stress amplitude (corresponding to an imperfection factor of 0.29). As can be seen in Fig. 5-41, if a curve “a” is already recommended for a given member, the increase in buckling resistance resulting from a reduction in residual stresses is very small, while higher percentages are contemplated for buckling curves “b” and “c” as the margin of improvement is larger in these cases. Nonetheless, it has already been shown that even though the increase in resistance is low, it may lead to a greater reduction in weight (see Example 5-1).

5.5. Discussions on the right choice of steel grade

5.5.1. Resistance to flexural buckling

The effect of the two modified imperfection factors, which have been proposed in this study, on the relative buckling resistances, is shown in Fig. 5-42 for the cases in which buckling curve “a” is recommended for steel grades up to S420 and curve “a₀” for grades above, which have been evaluated as the most detrimental in Chapter 4. Fig. 5-42a demonstrates the beneficial impact of the established modified imperfection factors on the relative buckling resistance of the S355 grade compared to S235. The slenderness limits for the medium relative price are provided, which illustrates the beneficial

impact of the established modified imperfection factors. Those reference slendernesses are provided for each steel grades in Fig. 5-42b, which demonstrates the beneficial advantage in considering a modified imperfection factor for the benefit of using higher steel grades. Furthermore, the results are depicted for the medium relative cost level and further results can be found in Appendix C and Appendix D.

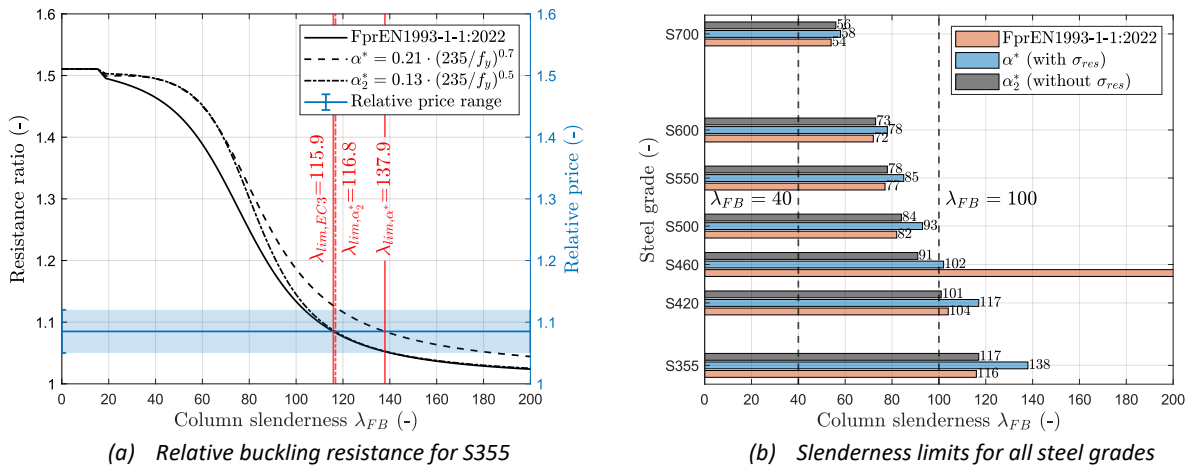
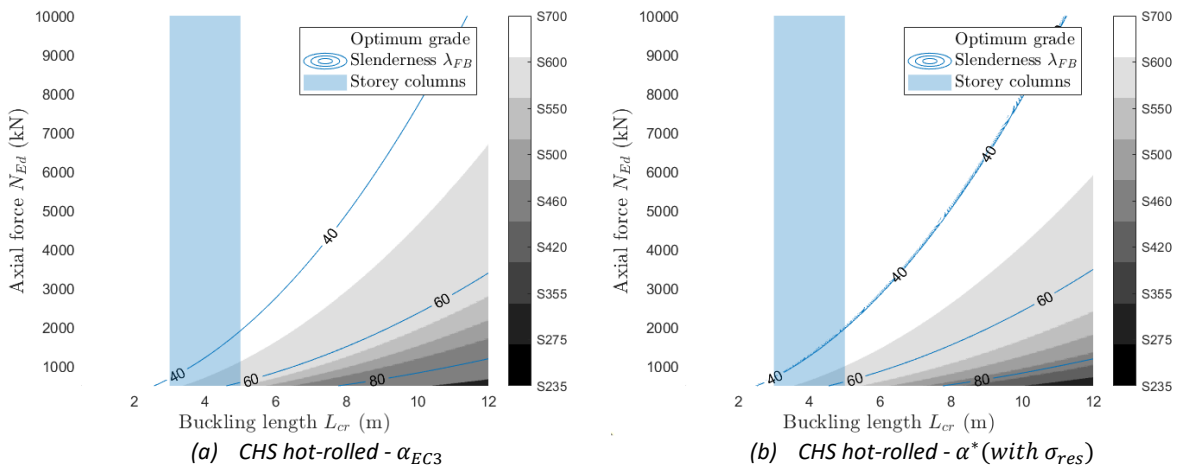


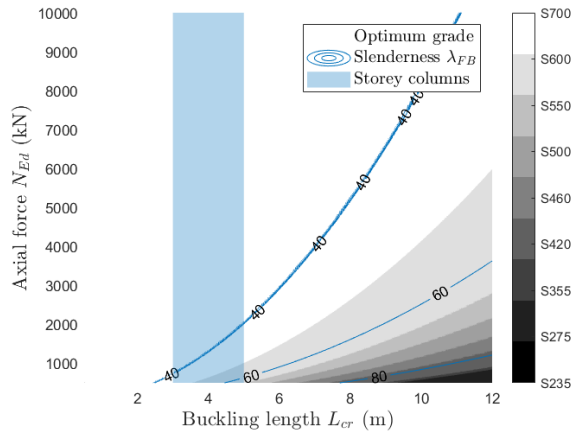
Fig. 5-42. Influence of a modified imperfection factor on relative buckling resistances and slenderness limits (Rolled: $h/b > 1.2$ / $t_f \leq 40$ mm / major axis or hot-rolled hollow sections considering a medium base cost).

As illustrated in Fig. 5-42, the modified imperfection factor α^* increases the benefit of using a higher steel grade to larger column slenderness as the curve representing the resistance ratio in Fig. 5-42a is shifted to the right. This is particularly the case for intermediate grades between S235 and S420. Conversely, reducing the amplitude of residual stresses by accounting for the straightening increases the benefit for the mild steel grades, but reduces the benefit of using high-strength steels.

5.5.2. Results of the optimisation routine

The optimum grade as a function of the buckling length and axial load is reported in Fig. 5-43. It has been chosen to focus on hot-finished hollow sections in the absence of local buckling (similarly as Fig. 4-32). This assumption is made as the observed conclusions are similar for each section typology, geometrical limit and buckling axis and because Chapter 4 concludes that it is the most detrimental case. The absence of local buckling assumption is made in order to concentrate on the effect on the resistance to flexural buckling.





(c) CHS hot-rolled - α_2^* (without σ_{res})

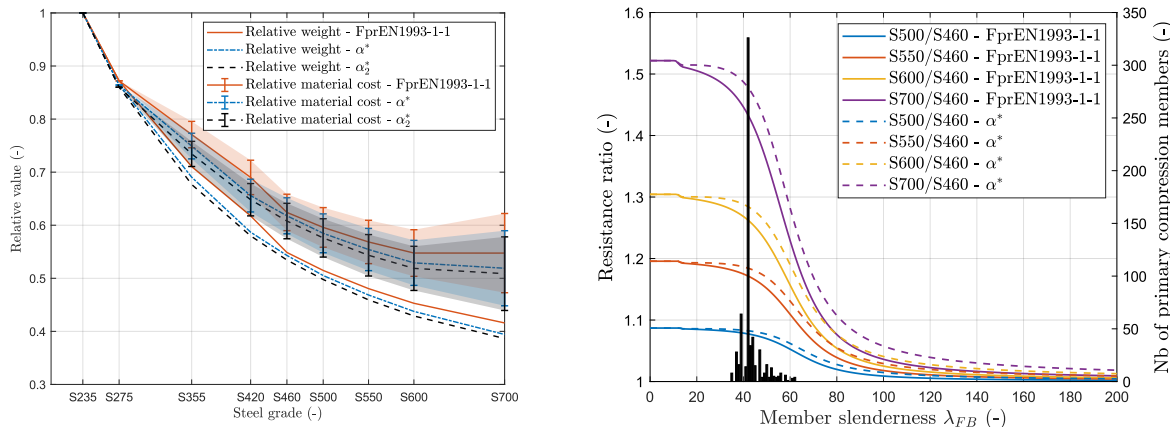
Fig. 5-43. The impact of the proposed imperfection factors on the right choice of steel grade.

The modified imperfection factors proposed in this chapter have a slight impact on the optimum steel grade selection, as illustrated in Fig. 5-43.

A comparison of Fig. 5-43a and Fig. 5-43b reveals that the zones of benefit for intermediate grades (i.e. grades between S235 and S460) and those above S460 increase as expected when the modified imperfection factor is taken into account. However, the benefit of selecting S460 is diminished as the resistance of S420 is increased. Indeed, with the modified imperfection factor, there is no more one buckling curve of gap between these two grades. This feature is also contemplated by the slenderness limits which no more exceed the upper bound of 200 for S460 in Fig. 5-42b. Fig. 5-43c shows the results for an imperfection factor that corresponds to the idealised scenario where there are no more residual stresses. The benefit of mild steels is even more pronounced as the detrimental effect of residual stresses is diminished. Nevertheless, the column slenderness limit of $\lambda_{FB} = 80$ remains relevant as there is still a benefit in developing grades above S460 for slenderness below this limit.

5.5.3. Case studies for compression members

The effect of the modified imperfection factors on the practical case studies presented in Chapter 4 is evaluated in Fig. 5-44.



(a) Mapfre tower, Barcelona

(b) NRG Stadium, Houston

Fig. 5-44. Influence of the modified imperfection factors on the case studies discussed in Chapter 4.

Fig. 5-44 illustrates the usefulness of the developments made in this chapter, with a clear benefit increase for intermediate grades between S235 and S460, as well as for grades above S460. Indeed,

regarding the Mapfre tower in Barcelona, the relative weight and material costs are shifted downwards in Fig. 5-44a, further increasing the benefit for grades higher than S460. The beneficial effect of the increased yield stress is, however, more pronounced for ground floor columns, which are the most loaded and therefore the least slender as expressed in Chapter 4. Similarly, for the NRG Stadium in Houston (Fig. 5-44b), the consideration of a modified imperfection factor, α^* , leads to an increase in relative resistances for grades above the practical range. The resistance increase is such that, for most members encountered in the structure, the gain for a higher grade is practically the full yield strength ratio. Finally, for both case studies, the conclusion remains that there is a benefit of increasing the yield strength up to S700 in terms of weight savings, but the economic advantage of considering the S700 grade becomes debatable when considering a high level of relative costs, as shown in Fig. 5-44a.

5.6. Conclusions

The numerical investigations in Chapter 5, consisting of about 4500 numerical models, have highlighted the importance of optimised design rules to take full advantage of the yield strength. In the context of growing resource scarcity issues, it becomes crucial to adapt the design rules to optimise the material usage in the building sector. This chapter is divided into two main parts, both aimed at increasing the load-bearing capacity of compressed columns. The first part consists in adapting the existing design rules to account for the reduced relative importance of residual stresses for an increased yield strength while the second part consists in considering the beneficial impact of the roller-straightening process on the residual stress distribution and thus on the load-bearing capacity of columns.

The first part showed that, in terms of the flexural buckling resistance, only the buckling resistance of S235 and S460 grades is correctly predicted in current design standards. Although the detrimental effect of residual stresses decreases with yield strength, intermediate grades between S235 and S460 are assigned to the same buckling curve as for S235. Similarly, grades above S460 are assigned to the same buckling curve as for grade S460. A numerical model of a steel column under pure compression has been validated and used in an extensive numerical study to check the validity of existing recommendations and to restore continuity by defining a new modified imperfection coefficient that takes full advantage of the yield strength for all different steel grades.

The second part investigates the beneficial effect of the roller-straightening process on the residual stress distributions and hence the load carrying capacity of columns under compression. A numerical model has been developed to model this cold-forming post-treatment process and has been used to establish straightened residual stress patterns for a reference and optimised machine settings. These residual stress patterns were then used to assess the beneficial influence of the roller-straightening process on the carrying capacity of columns. The study concluded that a minimum gain of one buckling curve may be achieved for S355 and S460 grades for cases when the profile is roller-straightened. Although accounting for the straightening of the profiles represents a significant challenge in the evaluation of the load-bearing capacity of a column, given the multitude of possible machine settings and the related residual stress distributions, the neglect of the beneficial influence of this systematic straightening is highly detrimental in the context of weight optimisation and should be the subject of future studies.

These numerical investigations have highlighted a series of possible improvements but also a few research perspectives to increase the load-bearing capacity of compressed columns. Such improvements contribute to the global goal of reducing the amount of material used in the construction leading to weight, cost and carbon savings.

Chapter 6

Consideration of Inherent Sources of Stabilisation in Storage Racks

Confidential

Confidential

Confidential

Confidential

Confidential

Confidential

Confidential

Confidential

Confidential

Confidential

Confidential

Confidential

Confidential

Confidential

Confidential

Confidential

Confidential

Confidential

Confidential

Confidential

Confidential

Confidential

Confidential

Confidential

Confidential

Confidential

Confidential

Confidential

Confidential

Confidential

Confidential

Confidential

Confidential

Confidential

Confidential

Confidential

Confidential

Confidential

Confidential

Confidential

Chapter 7

General Conclusions

7.1. The challenges of sustainable construction

This thesis addresses the complex issue of making tomorrow's construction more sustainable, both in economic and environmental terms. The concept of sustainable construction prioritises the use of eco-friendly materials and practices with the objective of reducing the carbon footprint of the construction sector and ensuring a healthier planet for future generations. In recent years, as the world has faced the growing effects of climate change, there has been a notable increase in environmental awareness, giving rise to the adoption of several environmentally conscious initiatives. The construction industry, which is one of the most polluting sectors, has a crucial role to play in this context.

One of the most significant challenges to the implementation of sustainable construction practices is the higher initial cost which may be associated with these practices, in comparison to more traditional approaches. For instance, a low-carbon material is frequently more expensive than a traditional material, and the incorporation of a stabilising element to reduce the weight of a structural element may result in more elevated global fabrication costs. Furthermore, sustainable construction requires the coordination of multiple stakeholders, including designers, architects, manufacturers and policymakers. The process of aligning the conflicting interests and managing the complex collaborations can be challenging and very time-consuming. The solution necessitates not only a change in mindset regarding environmental sustainability, which varies considerably between individuals, but also an in-depth comprehension of the necessity of investigating the potential consequences of resource scarcity and of developing a comprehensive understanding of the solutions that may lead to a more sustainable construction sector. It is imperative to promote innovative materials and solutions to emphasise the long-term advantages of decarbonising the construction sector and to increase demand, thereby enhancing the availability of sustainable materials and solutions.

The thesis represents a contribution towards the development of a sustainable future in construction through several scientific developments. The overarching objective is to demonstrate and promote the importance of selecting the right material at the right place, adopting suitable design rules, as well as of promoting innovative materials and design solutions with the aim of achieving reductions in weight, cost and carbon emissions.

Every action, regardless of whether it is undertaken individually or within a professional context, will contribute to the creation of a more sustainable future.

7.2. Summary of contributions

The current climate crisis has highlighted the need for a significant reduction in the carbon footprint of the construction industry. The introduction (**Chapter 1**) indicates that the reduction of the emissions associated with the steel production process is currently underway. Nevertheless, the complete decarbonisation of the steel industry will require a considerable investment in time. Concurrently, it is imperative to achieve efficient designs by combining smart specifications and smart designs to accelerate the reduction of embodied carbon before 2030. This will ensure the achievement of the Paris Agreement, which mandates the limitation of global warming to 1.5-2°C in 2050. In the context of the “build less” and “build efficiently” approaches, high-strength steels may have a significant role to play as an innovative material, reducing the weight of structures. In the context of the “build clever” approach, the use of appropriate structural configurations and appropriate design criteria is also imperative, as they facilitate the exploitation of material properties and realise weight savings. These approaches are included in the hierarchy to net zero, as presented in Chapter 1, and have been addressed by different scientific developments throughout this thesis.

Chapter 2 presents a review of the literature on the physical and material properties of high-strength steels, the existing provisions of product and design standards, and the reference papers and projects that highlight the benefits of such materials. Based on their increased strength, their use results in the consumption of less resources for the same load-bearing capacity. It is important to note that these savings are not always sufficient to offset the increased cost and carbon footprint associated with these steels. Consequently, designers who lack practical guidance on the applications for which these steels offer an advantage are sometimes reluctant to use them. This reluctance of designers has resulted in a relatively marginal demand for these steels, which has not provided sufficient encouraging reasons for producers to invest in more efficient production lines capable of producing even stronger hot-rolled steels. This creates a vicious circle, in which the research community has a role to play in attempting to resolve this situation, which is detrimental to the optimisation of structures.

To evaluate the economic and environmental benefits associated with the use of such steels, the initial objective was to establish a correlation between the material cost and the yield strength, as well as to identify a relationship between the carbon footprint and the yield strength. Based on price lists available online by the past and on the history of steel base prices, realistic relative price ranges have been established in **Chapter 3** and validated based on the existing values and models from the literature. This approach allows for the consideration of both the multiplicity of production techniques and the variability of the base price associated to the market demand, which has a significant impact on the economic advantage of using a higher specific grade. Indeed, during periods of base price peaks, such as those experienced during the pandemic crisis or the energy crisis, the extra costs associated with a particular grade, which are constant values, become relatively insignificant, thereby increasing the economic gains generated by using high-strength steels. Furthermore, **Chapter 3** has demonstrated that the increase in carbon emissions as a function of yield strength for low-alloy steels is insignificant, given that the alloy content is identified as the determining parameter. However, as for the effect of the base price on relative cost, the impact of Scope 3 emissions relating to the extraction of these alloying elements is more negligible when Scopes 1 and 2 emissions are at high levels (see definitions of each scope at Section 3.4.1). An analysis of the decarbonisation plans of producers reveals that most of the focus is placed on Scope 1 and 2 emissions, which are within their direct responsibility. It can be reasonably deduced that a reduction in Scope 1 and 2 emissions without concomitant attention to Scope 3 emissions may result in an increased relative carbon footprint for high-strength steels in the future. This Chapter 3 has demonstrated the considerable variability of

these relative parameters and the inherent difficulty in providing data that are reliable over time, given the variations in the base price and carbon emissions relative to steel production. Accordingly, reliable ranges of variation have been established for these parameters to encompass this unpredictability and to encompass both economic and environmental considerations. These ranges of variation have been used for the present thesis developments and can serve as reference for future studies examining the economic and environmental benefits associated with the covered steel grades ranging from S235 to S700.

Comparative studies have been carried out between the various existing and future possible emerging grades in **Chapter 4**, based on the realistic ranges of relative prices and carbon emissions. A methodology and optimisation routines were developed by means of the MATLAB software. The optimisation results were validated through comparisons to previous studies published in the literature, in which an alternative optimisation algorithm is used. These numerical comparisons were conducted on hot-rolled European sections, as well as on hot-finished and cold-formed tubes. The analysis revealed several factors that either limit or increase the advantages of the use of higher steel grades. In the case of members that are sensitive to stability, reference slenderness ratios, denoted λ_{FB} (for flexural buckling) and λ_{LTB} (for lateral-torsional buckling), were discussed. It appears that there is always a benefit to be gained from using the highest grade (under consideration within the present study) for slenderness ratios below 40. Conversely, for slenderness ratios exceeding 100, the advantage of developing grades above the practical range becomes very limited. To ascertain the advantage of producing a specific profile with higher yield strength, a series of reference figures were plotted, delineating the various dimension limits with the associated costs and establishing reference slenderness limits. The aforementioned information is collated in Appendix A. This result can assist producers in producing their profiles in appropriate steel grades and the promotion of the most suitable steel grade for a given application. In the case of more complex structural elements, such as members subjected to combined compression and bending, it may be beneficial to provide practitioners with numerical tools to assist them in the selection of the optimal structural option. Indeed, it has been demonstrated that the unavailability of specific grades for particular profiles results in utilisation ratios that are less than unity in the design process, demonstrating an irrational use of raw materials. In the context of the “build efficiency” of the hierarchy to net zero, it becomes crucial to adapt product catalogues to offer the widest range of available profiles in the relevant steel grade, to realise optimised designs (utilisation ratio close to 1) and of maintaining a benefit in considering hot-rolled sections. The selection of the right steel at the right place may result in significant weight, carbon and cost savings. However, this requires effective communication and collaboration between the designer and the supply chain to ensure the efficiency of the performed designs.

Chapter 5 addresses the necessity of implementing appropriate design rules, in particular to improve the prediction of the flexural buckling resistance, by appropriately accounting for the effect of an increased yield stress, and thus achieving substantial weight reduction. The initial objective was to assess the reliability of extending existing design rules for flexural buckling up to S700. However, through the performed developments, it has been demonstrated that even the resistance for conventional grades S355 and S420 is underestimated in current design recommendations. Based on these observations, a modified imperfection factor has been derived through a wide numerical campaign, offering the potential for significant weight savings for conventional grades as well as those yet to emerge as a prospective study.

In addition, the effect of cold-formed straightening after rolling (regularly used in modern production processes) on the distribution of residual stresses in the section has been investigated. This straightening process results in a decrease of the amplitude of these residual stresses and even a

change of sign of residual stress at flange tips. The beneficial impact of this process on the buckling capacity of steel columns has been demonstrated, and an idealised imperfection factor in the case of negligible residual stresses has been established. The advantage of adopting reliable design rules has been assessed by comparison with the conclusions presented in Chapter 4. In particular, slenderness limits similar to the ones derived in Chapter 4 were established by considering the modified imperfection factors. These are compared in Appendix C, and the details for the first imperfection factor are reported in Appendix D. A graphical summary outlining the specific developments and milestones of the above-described chapters is represented in Fig. 7-1 for members subjected to pure compression.

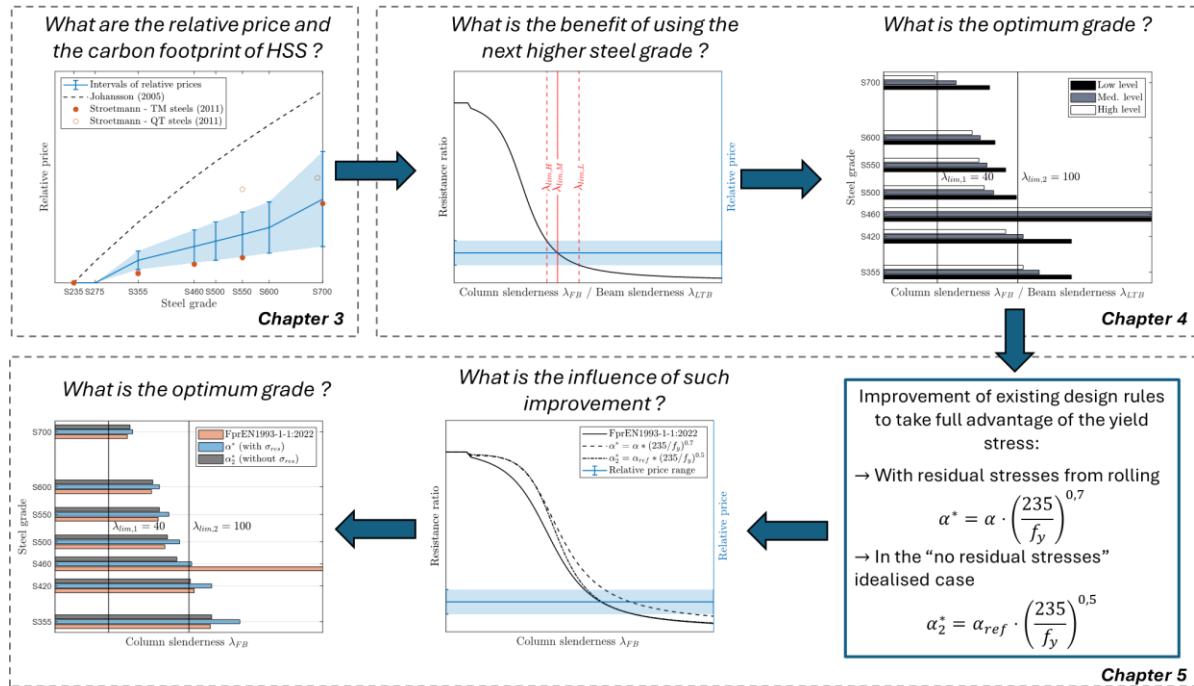


Fig. 7-1. Summary of the Chapter 3 to Chapter 5 contributions for members under pure compression.

Confidential

The objective of this thesis was to answer a series of research questions, expressed in Section 2.6. Here is a brief summary of the key conclusions:

- The increase in relative price, compared to S235, is between **5%** and **12%** for S355, **7%** and **20%** for S460, **10%** and **27%** for S550 and **14%** and **50%** for S700;
- The increase in carbon emission is almost **negligible** for all existing grades for hot-rolled sections;
- There is a full benefit in considering grades above the practical range (i.e., above S460) for low slenderness columns, i.e. for column slenderness ratios $\lambda_{FB} < 40$;
- There is no benefit in considering such grades for high slenderness columns, i.e. for column slenderness ratios $\lambda_{FB} > 100$;
- The economic and environmental benefit in developing grades higher than S460 for intermediary column slenderness ratios, i.e. for column slenderness ratios respecting $40 \leq \lambda_{FB} \leq 100$, is highly influenced by the level of relative price and carbon emission;
- A new modified imperfection factor as a function of f_y has been established for hot-rolled sections, allowing for a more accurate prediction of the buckling resistance of members through the use of the buckling curve concept. This factor has been validated for hot-rolled sections and hot-finished tubes;
- The roller-straightening process positively impacts the residual stress distributions, by significantly reducing their amplitude at flange tips. This beneficial impact increases the column bearing capacity;

Confidential

7.3. Limitations and perspectives

This doctoral thesis is composed of various works which are based on different assumptions and simplifications. As a result, further research that could be carried out on the various treated subjects has been identified as a potential perspective for future investigation. This section presents a summary of the limitations and perspectives of every chapter of this thesis.

In **Chapter 3**, the primary assumption is to only consider the production stage of the life cycle, i.e. modules A1 to A3 (see definitions in Table 3-1), when establishing relationships between price, carbon emissions and steel grade. Indeed, the increase in steel strength can be attributed to the addition of alloying elements or energy during the production process. The difference between two different grades is therefore mainly limited to the production phase, especially as the dissertation deals with passive structures rather than active structures such as cars. Indeed, the use of high-strength steels in automotive applications has the potential to significantly reduce fuel consumption during the operational phase, due to the weight reductions resulting from these materials, thereby resulting in further cost and carbon savings during the structure lifetime. For passive structures, there are no notable differences expected in other phases. However, the semi-finished steel produced by the steelmaker is provided to a hot-rolling mill to be shaped and finished before its delivery to the construction site for assembly. It can be reasonably assumed that the rolling and finishing process, as well as erection, will not be significantly affected by the yield strength, given that only the semi-finished product is actually affected by the material production. The cost of each step is equivalent to one-third of the final price. Indeed, the material cost is generally around 700€/t while the final

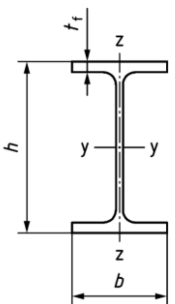
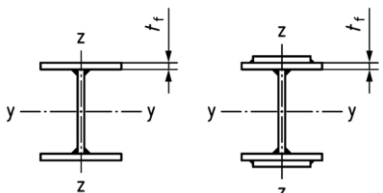
manufacturing price is generally around 2000€/t. Consequently, even if the increase in material cost is approximately 10% for a higher grade, the relative final manufacturing cost between both compared grades is negligible. In addition, for the sake of conservatism and with the aim of providing clear and readable results, the focus was realised on grade extras. The consideration of a lower profile by using a higher yield strength may result in a reduction in the size extras, which may offset the grade extra. Eventually, a size reduction may result in a reduction in costs for the supporting elements (columns, foundations, etc.), thereby offsetting the increase in material costs. In conclusion, high-strength steels are undoubtedly more expensive but, when the whole cost of the whole building is considered, the cost difference is found to be quite marginal, even negligible. This Chapter 3 demonstrates the relationship between the base price of steel and the relative prices of high-strength steels. The relative price ranges have been established by considering the lower and upper bounds of base prices over time. Similarly to the relative prices of Johansson which were identified as no more realistic due to the increase of base price and the change in production process, these bounds may evolve in the future, necessitating an adaptation of the relative prices. Throughout this PhD thesis, the price of steel has moreover exhibited significant volatility, reaching historic peaks in 2021 and subsequently declining. This year, the prices have significantly dropped since the beginning of the year. The observed decline in steel prices has brought them closer to the equilibrium state that was previously observed before the various crises. This demonstrates the time dependency of the expressed findings.

For relative carbon emissions, it is anticipated that the emissions of each scope will be significantly reduced in the forthcoming years because of the expansion of initiatives undertaken by steelmakers to reduce their emissions. This will undoubtedly impact the relative carbon emissions of high-strength steels, particularly given that Scope 3 emissions will gain greater significance in the coming years, given the significant energy consumption associated with the extraction of rare elements. However, the selection of a high-strength grade, with an inherently higher environmental load, is likely to result in a reduced environmental impact when considering the induced weight savings and the full life cycle, but it requires to have detailed data on the existing products and grades. Therefore, there is a need for carbon transparency for new materials or products, as opposed to the current practice which consists in grouping all the greenhouse gases of a whole production mill, as reflected in environmental product standards (EPD). It is important that designers can distinguish between products and grades in the EPD, otherwise accuracy in the estimation of the environmental impact is not possible. In parallel to the assistance to designers in evaluating the environmental benefit of increasing the yield strength, the carbon transparency will force to either reduce the quantity of alloying elements through innovative production process or cut off the Scope 3 emissions. In conclusion, while the weight savings achieved through the utilisation of high-strength steels typically counterbalance the marginal increase in carbon emissions with yield strength, there is a necessity for more comprehensive measurement data in the forthcoming iteration of EPD declarations to allow for life cycle assessment with well-documented data in order to facilitate the selection of the optimum product.

In the context of the comparative studies presented in **Chapter 4**, it has been determined that, in a society where cost remains a primary determinant of decision-making, the cost should be identified as the primary driver parameter. However, the benefits to the environment are significantly greater. Consequently, according to the ecological crisis, it may be argued that the environmental optimum should become the determinant parameter of decision-making in the near future, so the conclusions may be drawn in another way. The advantage of high-strength steels is illustrated on case studies, but analogous comparative studies may be conducted on a series of pertinent structures to generalise the positive conclusions and promote the use of high-strength steels to designers and producers. The routines developed in the MATLAB software may be adapted in another code format to be used in an application that could serve as a tool for structural engineers, particularly for members subjected to

combined compression and bending. In addition, steel simply cannot be used (with a few exceptions) without protective coatings; these coatings will have a defined life that will determine future maintenance costs. It would be prudent to incorporate fire design into the existing routines to address this aspect as well. It is believed that the methodology employed in this study can be applied to other problems, such as those involving partially or fully encased steel-concrete composite sections. It may be feasible to also undertake comparative studies with welded members, given the enhanced flexibility in terms of dimensions, which may lead to efficient designs.

In **Chapter 5**, on the one hand, the pursued approach for establishing the proposal of modified imperfection was based on the expression initially proposed by R. Maquoi in 1982. This approach was subsequently employed by Hungarian researchers as part of the European project RUOSTE [80]. This approach consists of conserving the classical buckling curves for grade S235, i.e. curves a_0 , a , b , c , d , while employing a multiplication factor function of the material yield strength to account for the smaller influence of the residual stresses on the member stability when the yield strength increases. In contrast, in the context of another RFCS project, STROBE [92], the research team led by L. Gardner from the Imperial College of London proposed a different approach. They suggested shifting the plateau length to a relative slenderness of $\bar{\lambda} = 0.1$ and to give up classical buckling curves, as shown for various rows in Table 7-1. As a perspective, it would be beneficial to conduct a statistical analysis of these two approaches to ascertain which is the most relevant for incorporation into design recommendations. Some buckling tests in various grades should be realised to confirm the numerical conclusions. Furthermore, the remaining lines in Table 7-1 that have not yet been studied should be addressed. A master's thesis is planned for completion next year at the University of Liège, the objective of which is to validate the existing approaches for cold-formed hollow sections. Based on the knowledge gained by the team about the stability of hot-rolled angles [229], [230], [272], some investigations are also planned to cover hot-rolled angles to generalise the proposed modified imperfection factor to all hot-rolled sections, frequently used in construction. Finally, the initial local imperfection has been demonstrated to exert a significant influence on the numerical results for hollow sections. Further investigations could therefore be conducted to assess the reliability of the modified imperfection factor for slender hollow sections.

Cross-section		Limits		Modified imperfection factor	Author, year
Rolled I- or H-sections		$h/b > 1.2$	$t_f \leq 40 \text{ mm}$	$\alpha^* \cdot (\bar{\lambda} - 0.2)$ $\alpha^* = \alpha \cdot \left(\frac{235}{f_y}\right)^{0.7}$	Saufnay, 2024
			$t_f > 40 \text{ mm}$	No existing works	
		$h/b \leq 1.2$	$t_f \leq 100 \text{ mm}$	$\alpha^* \cdot (\bar{\lambda} - 0.2)$ $\alpha^* = \alpha \cdot \left(\frac{235}{f_y}\right)^{0.7}$	Saufnay, 2024
			$t_f > 100 \text{ mm}$	No sections exist in current catalogues	
Welded I-sections				$\alpha^* \cdot (\bar{\lambda} - 0.2)$ $\alpha^* = \alpha \cdot \left(\frac{235}{f_y}\right)^{0.6}$	Somodi, 2017 (RUOSTE)
				$\alpha^* \cdot (\bar{\lambda} - 0.1)$ $\alpha^* = 0.45 \varepsilon_f$ for y-y $\alpha^* = 0.55 \varepsilon_f$ for z-z	Yun, 2023 (STROBE)

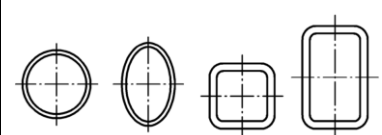


Hollow sections		Hot-finished	$\alpha^* \cdot (\bar{\lambda} - 0.1)$ $\alpha^* = 0.24\epsilon$	Meng, 2020
		Cold-formed	$\alpha^* \cdot (\bar{\lambda} - 0.2)$ $\alpha^* = \alpha \cdot \left(\frac{235}{f_y}\right)^{0.7}$	Saufnay, 2024
			$\alpha^* \cdot (\bar{\lambda} - 0.2)$ $\alpha^* = \alpha \cdot \left(\frac{235}{f_y}\right)^{0.5}$	Somodi, 2017 (RUOSTE)
		$\alpha^* \cdot (\bar{\lambda} - 0.1)$ $\alpha^* = 0.24\epsilon$	Meng, 2020	
L-sections		Rolled sections	No existing works	
		Welded sections ($t_f \leq 40 \text{ mm}$)	No existing works	

Table 7-1. Perspective works on the establishment of modified imperfection parameters for flexural buckling.

Eventually, the current recommendations for lateral torsional buckling prescribe the same buckling curve for all steel grades. Consequently, the effect of the yield strength on this instability mode should be investigated, with a view to potentially deriving a comparable modified imperfection factor for lateral-torsional buckling. The identical procedure as that reported in Fig. 7-1 could be pursued for members subjected to pure bending and prone to lateral-torsional buckling. Nevertheless, the results of Chapter 4 demonstrate that SLS requirements for beams are dominant. Therefore, it is of the utmost importance to identify solutions that will reduce deflections and the dominance of SLS requirements (e.g. the systematic beam cambering, the increase of the Young’s modulus for new material, ...).

On the other hand, the finite element model for roller straightening was found to require improvement for some assumptions. It would be beneficial to conduct residual stress measurements before and after the straightening process to validate or calibrate a more refined version of the FE model developed in this thesis. The residual stress measurements and potential buckling tests would be helpful to validate the conclusions obtained in this thesis and to calibrate the straightening machine settings. Moreover, the machine settings could be calibrated to target a lower out-of-straightness than $L/1000$. However, the setting that results in a lower global imperfection amplitude may also lead to a less beneficial residual stress distribution. Therefore, the calibration of this process is not straightforward and further extensive experimental and numerical campaigns are required to adequately account for its beneficial effect in future design rules. Discussions have been initiated with industrial partners, with the objective of conducting residual stress measurements on this topic at the University of Liège.

Confidential

7.4. Thoughts about tomorrow's practice

7.4.1. Closing the loop

As indicated by the market share estimation for hot-rolled sections conducted by ArcelorMittal in 2015 [48] and reported in Table 7-2, the market share of steel in building construction in the USA, Canada, the UK and Scandinavian countries was approximately 70% and the estimated market share for the S355 / Grade 50 grade was about 90% in these countries. In Western Europe, the market share for steel is approximately 20%, with the lower steel grades S235 and S275 remaining the preferred choice (at around 80-85%). It can thus be inferred that there is likely a correlation between the market share of steel and the utilisation of a higher steel grade [48]. As discussed in Chapter 3 about the British sections, the grades S235 and S275 are currently considered as special orders within the United Kingdom, for which extra costs are applied while S355 is considered as the basis grade. It is probable that, in response to an increasing demand from designers, the S460 grade will replace the S355 as the basis in the future [92]. The availability of steel sections in grades S235 and S275, particularly the larger sections, has become extremely limited in some countries as the market has shifted towards the higher standard grade S355. In the upcoming years, it seems possible that there will be cost, and programme penalties imposed for specifying grades S235 and S275 even for Western countries.

	S235, S275 / A36	S355 / Grade 50	S420, S460 / Grade 65	Market share of Steel in building construction
<i>USA, Canada</i>	<1%	>95%	>1%	70%
<i>UK</i>	10%	90%	<1%	70%
<i>Scandinavian</i>	10%	90%	<1%	40%
<i>Poland</i>	60%	40%	<1%	30%
<i>Italy</i>	50%	50%	<1%	20%
<i>Benelux</i>	85%	15%	<1%	20%
<i>France</i>	90%	10%	<1%	20%
<i>Germany</i>	80%	20%	<1%	10%

Table 7-2. Estimation of the market share of hot-rolled sections in building construction.

It is the responsibility of the scientific community to persuade designers of the necessity of optimising structural designs on benchmark examples and to provide them with guidance for such optimisation, e.g. providing useful graphs or optimisation routines to facilitate their optimisation. The price of steel is determined by the fundamental supply and demand law that governs the pricing of any other materials. It follows that an increase in market demand for these innovative materials will therefore result in an increase in supply, which will in turn lead to a reduction in prices. Furthermore, the market demand for materials that do not currently exist, will force steel manufacturers to modify their production processes. Consequently, steelmakers will be required to adapt their product range in accordance with the market demand in order to facilitate the optimisation process for designers. In light of the thesis outcomes, it seems reasonable to affirm that the use of HD sections in S235, inevitably leads to the creation of inefficient designs, which are disadvantageous for both designers and manufacturers. It thus falls upon the steelmakers to adapt their product range and set their margins in order to guarantee the competitiveness of steel in comparison to other materials from an economic and environmental point of view. This action may allow to close the loop of the storytelling of this thesis as depicted by the red arrow in Fig. 7-2.

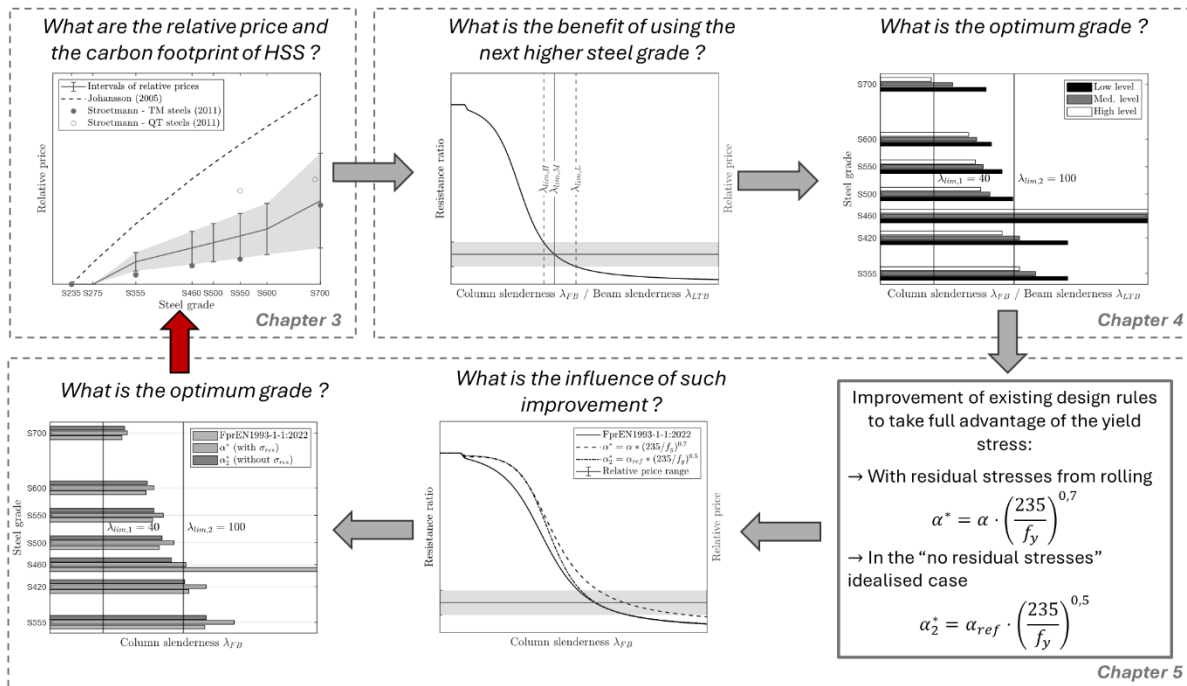


Fig. 7-2. Closing the loop of these thesis contributions.

As steel is 100% recyclable and reusable, there is a common interest in increasing the market share of this material for a sustainable future. Furthermore, to solve the upcoming issues of overpopulation and overcrowding due to population growth, it would be advantageous to limit horizontal growth by building more vertically to preserve green lands and the associated eco-systems. As illustrated in **Chapter 2** with the numerous examples in the United States, the construction of high-rise buildings leads to higher loading levels, for which the use of wide-flange profiles in high-strength steels presents a great advantage. The case studies analysed in **Chapter 4** demonstrate that the designers could have gone even further in resistance than the practical range. Consequently, policymakers and those responsible for the product standards should also accelerate the adaptation of product standards to allow designers to use higher grades that respect the requirements of the construction industry. S550 grade was added to the American product standard ASTM A913 in 2019 [66] and used for the first time in the BMO Tower in 2021. This grade could appear on the European market in the medium term, but it generally takes about 10 years for a material to appear and be used in construction. The buildings that are scheduled for completion in 2030, the first milestone in decarbonisation roadmaps, are currently being designed, so these deadlines should therefore be accelerated to allow efficient designs as soon as possible.

7.4.2. Collaboration for a sustainable future

The thesis demonstrates the necessity for stakeholders in the construction industry to collaborate in order to develop more efficient designs and thereby contribute to a more sustainable future. As illustrated in the preceding subsection, the responsibility to close the loop lies with steelmakers and policymakers in response to the increasing demand for eco-friendly material solutions. However, each stakeholder must contribute to this endeavour, as depicted in Fig. 7-3.

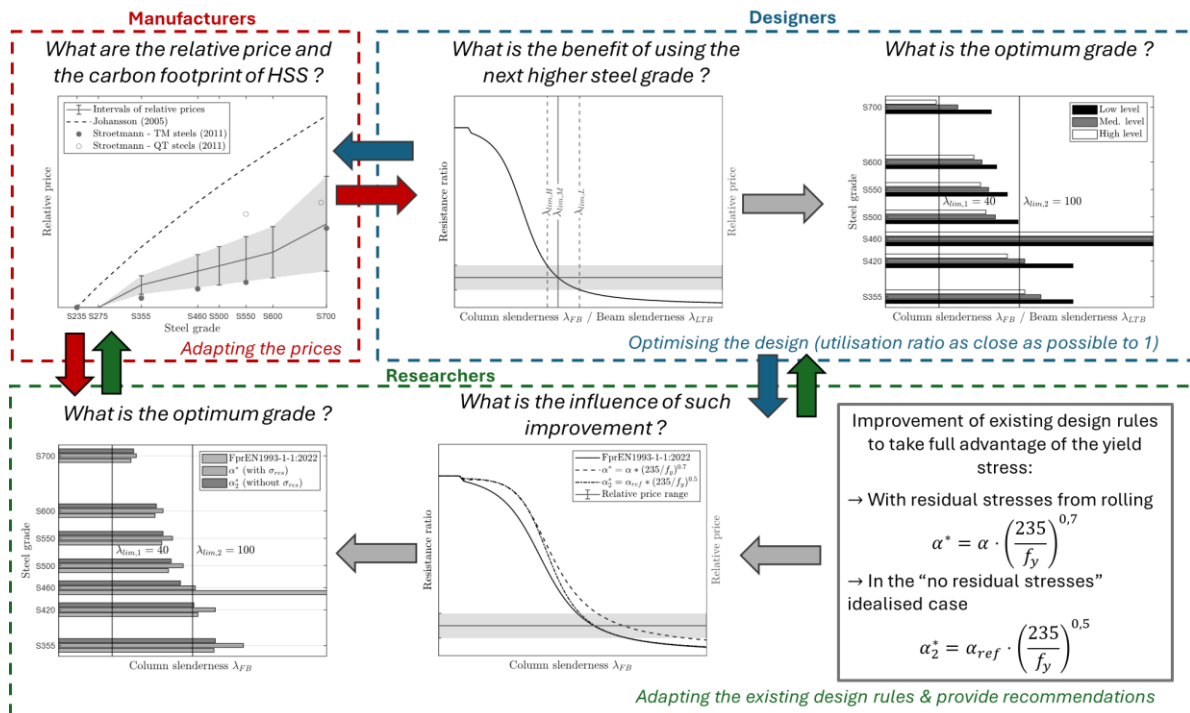


Fig. 7-3. Responsibility of each stakeholder for realising weight, cost and carbon savings.

On the one hand, designers could exert pressure on steelmakers to decarbonise their process, but the introduction (**Chapter 1**) illustrates that they should be realistic about timescales and understand that reducing material volume is also a priority, which is more under their responsibility. They should think about material efficiency and circularity from the early stages of the design process. There is a clear need to carry out systematic life cycle assessments of the different grades and products available to consider the best solution. Based on the recommendations or tools provided by researchers and on the statistical distribution of member slendernesses obtained from a pre-design, they can have some information about the optimum grade for their application and adapt the solution for the final design. Based on the pre-design, some exchanges between the steelmaker and the designer can facilitate the elaboration of the best available solution from production.

On the other hand, researchers and the scientific community have a responsibility to educate. Education is essential to teach to future structural engineers that, safety is obviously important, but material efficiency is also important. Research has a responsibility to develop appropriate design rules and to assist the industry to change and achieve efficient designs. **Chapter 4** illustrates the need to provide graphical or numerical tools to assist designers in adopting the right material at the right place. Furthermore, **Chapter 5** shows the importance of having appropriate design rules to fully exploit the material performance and **Chapter 6** the necessity of investing research time to help industrials in finding innovative design solutions for their structural optimisation.

At every stage of the design and construction process, all involved stakeholders (architects, engineers, construction professionals and others) have a responsibility to contribute to the creation of a more sustainable built environment. In this context, researchers, designers and manufacturers should work together to achieve significant weight, cost and carbon savings for a more sustainable building sector, as shown in Fig. 7-4.

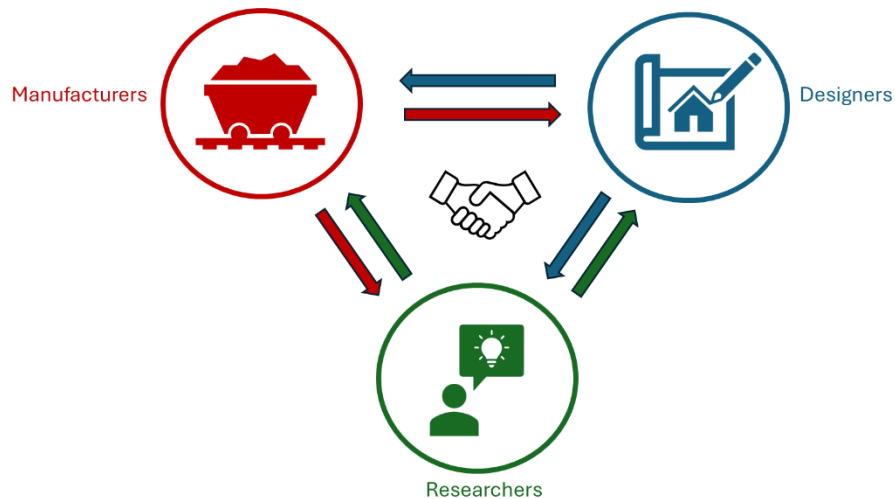


Fig. 7-4. Collaboration between stakeholders for reducing carbon emissions.

An increasing number of practitioners are recognising the necessity to reduce their emissions, and they will undoubtedly require assistance to contribute to a sustainable future. It is incumbent upon researchers to provide the industrial sector with education, guidance and support in the context of ongoing transformation and change. The more people are aware of what is happening, the more they will be equipped with the motivation they need to implement sustainable, cost-effective and eco-friendly, solutions based on their capabilities. The future is promising and there is reason for optimism as industry continues to innovate, education continues to improve, and policies are reformed to bring the necessary change.

“We cannot solve our problems with the same thinking we used when we created them”

Albert Einstein

List of Publications

The present PhD thesis has resulted in several scientific publications, including contributions to international journals (3) and conference proceedings (6). The conference proceedings were presented at several scientific events held during the thesis. Furthermore, the supervision of several Master's theses (8) has contributed to some additional developments of the present work. These references are accessible via the institutional repository (MATHEO). Finally, industrial projects related to the research topics have led to the preparation of scientific reports. Please refer to the PDF version for direct hyperlinks.

Publications in reviewed academic journals

- Saufnay, L., & Demonceau, J. F. (2025). *The beneficial effect of the roller-straightening process on the column stability – under preparation*
- Saufnay, L., & Demonceau, J. F. (2025). *The right selection of steel grade for hot-rolled columns in high-rise buildings. Journal of Constructional Steel Research – under preparation*
- Saufnay, L., Jaspard, J. P., & Demonceau, J. F. (2024). Improvement of the prediction of the flexural buckling resistance of hot-rolled mild and high-strength steel members. *Engineering Structures*, 315, 118460.
<https://doi.org/10.1016/j.engstruct.2024.118460>
- Saufnay, L., & Demonceau, J. F. (2023). Establishment of reliable relative price predictions for high-strength steel members. *Steel Construction*, 17: 136-145.
<https://doi.org/10.1002/stco.202300013>
- Saufnay, L., Beyer, A., Jaspard, J. P., & Demonceau, J. F. (2023). Experimental and Numerical Investigations on Closely Spaced Built-Up Angle Members. *Journal of Structural Engineering*, 149(4), 04023012.
<https://doi.org/10.1061/JSENDH.STENG-1164>

Publications in proceedings, presented at international conferences

- **SDSS 2025 – Barcelona (Spain) – abstract submitted**

Saufnay, L., & Demonceau, J.-F. (2025). High-strength steel columns in multi-stored buildings – Establishment of reference slendernesses to select the appropriate steel grade

- **Nordic Steel 2024 – Luleå (Sweden)**

Saufnay, L., & Demonceau, J.-F. (2024). Flexural buckling of mild and high-strength steel hot-rolled sections: Improvement proposal of the flexural buckling design rules. Nordic Steel Construction Conference 2024 (NSCC 2024), Luleå, Sweden.

<https://doi.org/10.5281/zenodo.12192458>

- **EUROSTEEL 2023 – Amsterdam (Netherlands)**

Saufnay, L., & Demonceau, J. F. (2023). Economic and environmental assessment of high-strength steel grades. *ce/papers*, 6(3-4), 527-532.

<https://doi.org/10.1002/cepa.2291>

Saufnay, L., Renotte, T., Mahieu, L., & Demonceau, J. F. (2023). Design optimisation of welded I-beams made of high strength steels. *ce/papers*, 6(3-4), 568-573.

<https://doi.org/10.1002/cepa.2471>

- **CTA 2022 – Pescara (Italy)**

Saufnay, L., Jaspert, J. P., & Demonceau, J. F. (2022, October). Sustainability Assessment of High Strength Steel Elements. In *Le Giornate Italiane Della Costruzione in Acciaio (The Italian Steel Days)*.

- **SDSS 2022 – Aveiro (Portugal)**

Saufnay, L., Tibolt, M., Jaspert, J. P., & Demonceau, J. F. (2022). The Beneficial Influence of the Roller-straightening Process on the Bearing Capacity of Steel Columns. *ce/papers*, 5(4), 889-897.

<https://doi.org/10.1002/cepa.1832>

- **EUROSTEEL 2021 – Sheffield (UK)**

Saufnay, L., Jaspert, J. P., & Demonceau, J. F. (2021). Economic benefit of high strength steel sections for steel structures. *ce/papers*, 4(2-4), 1543-1550.

<https://doi.org/10.1002/cepa.1454>

- **HPSSRC II 2020 – High Performance Steel Structures Research Council – Delft (Netherlands)**

“Economic benefit of using high strength steel sections in steel structures” [Oral presentation].

Master theses or internship supervision

- **2024-2025** (planned):
 - (1) L. Duchêne – Modified imperfection factor for cold-formed hollow sections
 - (2) N. De Bastiani – Optimisation of steel structures with high-strength steels
- **2022-2023**:
 - (1) H. Delsemme – Continuation of the D. Defoy’s master thesis
 - (2) L. Mahieu (internship) – Continuation of the T. Renotte’s master thesis
 - (3) F. Delsemme – Optimisation of welded I-beams with high-strength steels
- **2021-2022**:
 - (1) F. Dechamps – Impact of fire design on the benefit of high-strength steels
 - (2) D. Defoy – Optimisation of trusses by the use of high-strength steels
 - (3) T. Renotte – Optimisation of welded I-beams with transversal stiffeners: awarded as Best Master thesis by the AILG (Association des Ingénieurs de Liège)
- **2019-2020**:
 - (1) B. Franck – High-strength materials in composite structures

Side projects

- Saufnay, L., Jaspert, J. P., & Demonceau, J. F. (2023). Stability behaviour of cold-formed elements for self-supporting storage racks. Research project realised for Kocher in collaboration with the Greisch office.
- Saufnay, L., Jaspert, J. P., & Demonceau, J. F. (2020). Pre-study about the effect of the roller-straightening process on the buckling resistance capacity of rolled profiles. Research report for ArcelorMittal
- Saufnay, L., Bezas, M. Z., Jaspert, J. P., Demonceau, J. F., Verstraete, M., & Bustos Hermosilla, M. (2020). ANGELHY-D3.2: Report on experimental tests on closely spaced built-up members. *ANGELHY project*

References

- [1] S. L. der Linden, A. A. Leiserowitz, G. D. Feinberg, and E. W. Maibach, "The scientific consensus on climate change as a gateway belief: Experimental evidence," *PLoS One*, vol. 10, no. 2, p. e0118489, 2015, doi: <https://doi.org/10.1371/journal.pone.0118489>.
- [2] M. H. Goldberg, A. Gustafson, S. van der Linden, S. A. Rosenthal, and A. Leiserowitz, "Communicating the scientific consensus on climate change: diverse audiences and effects over time," *Environ Behav*, vol. 54, no. 7–8, pp. 1133–1165, 2022, doi: <https://doi.org/10.1177/00139165221129539>.
- [3] J. Cook, S. van der Linden, E. Maibach, and S. Lewandowsky, "The Consensus Handbook - Why the scientific consensus on climate change is important," Mar. 2018. doi: DOI:10.13021/G8MM6P.
- [4] International Energy Agency (IEA) and United Nations Environment Programme (UNEP), "Global Status Report: Towards a zero-emission, efficient and resilient buildings and construction sector," *International Energy Agency and the United Nations Environment Programme*, 2018.
- [5] H. Ritchie, P. Rosado, and M. Roser, "CO₂ and Greenhouse Gas Emissions," Met Office Hadley Centre (2024). Accessed: Aug. 22, 2024. [Online]. Available: [OurWorldInData.org/co2-and-greenhouse-gas-emissions](https://www.ourworldindata.org/co2-and-greenhouse-gas-emissions) | CC BY
- [6] 2030 Architecture, "Why the built environment?," 2022, Accessed: Aug. 22, 2024. [Online]. Available: <https://www.architecture2030.org/why-the-built-environment/>
- [7] P. Levi, W. Hall, and T. Vass, *Emissions Measurement and Data Collection for a Net Zero Steel Industry*. 2023.
- [8] A. Dyson, N. Keena, M.-L. Lokko, B. K. Reck, and C. Ciardullo, "Building materials and the climate: constructing a new future," Paris, 2023. Accessed: Aug. 21, 2024. [Online]. Available: <https://wedocs.unep.org/handle/20.500.11822/43293>
- [9] United Nations, "Adoption of the Paris Agreement," *Conference of the Parties on its twenty-first session*, vol. 21932, no. December, 2015.
- [10] H. Lee *et al.*, "Climate change 2023 - synthesis report summary for policymakers," *Intergovernmental Panel on Climate Change (IPCC)*, 2024.
- [11] UN Environment Program, "New research identifies remaining global carbon budget for twelve main industries," Nov. 2021. Accessed: Aug. 23, 2024. [Online]. Available: [https://www.unepfi.org/themes/climate-change/new-research-identifies-remaining-global-carbon-budget-for-twelve-main-industries/#:~:text=The%20global%20carbon%20budget%20to,Gt%20CO2%20\(1.6%25\)](https://www.unepfi.org/themes/climate-change/new-research-identifies-remaining-global-carbon-budget-for-twelve-main-industries/#:~:text=The%20global%20carbon%20budget%20to,Gt%20CO2%20(1.6%25)).
- [12] F. Delasalle *et al.*, "Mission Possible Partnership, Making Net-Zero Steel Possible - An industry-backed, 1.5°C-aligned Transition Strategy," 2022. Accessed: Aug. 23, 2024. [Online]. Available: <https://www.missionpossiblepartnership.org/action-sectors/steel>

- [13] Material Economics, “The Circular Economy a Powerful Force for Climate Mitigation: Transformative innovation for prosperous and low-carbon industry,” Stockholm, Sweden, Jun. 2018.
- [14] “World Steel Association.” Accessed: Aug. 19, 2022. [Online]. Available: <https://worldsteel.org/>
- [15] International Energy Agency (IEA), *Iron and steel technology roadmap: Towards more sustainable steelmaking*. OECD Publishing, 2020.
- [16] Climate Action Tracker (CAT), “Paris Agreement Compatible Sectoral Benchmarks: Elaborating the Decarbonisation Roadmap,” Berlin, Germany, 2020. Accessed: Aug. 23, 2024. [Online]. Available: https://climateactiontracker.org/documents/753/CAT_2020-07-10_ParisAgreementBenchmarks_FullReport.pdf
- [17] G. Di Foggia and M. Beccarello, “Decarbonization in the European steel industry: Strategies, risks, and commitments,” *Environmental Challenges*, vol. 16, p. 100988, 2024, doi: <https://doi.org/10.1016/j.envc.2024.100988>.
- [18] World Green Building Council (WGBC), “Bringing embodied carbon upfront: Coordinated action for the building and construction sector to tackle embodied carbon,” World Green Building Council (WGBC) London, Sep. 2019.
- [19] London Energy Transformation Initiative (LETI), “Climate Emergency Design Guide,” *How New Buildings can Meet UK Climate Change*, Jan. 2020.
- [20] N. Cabassud, “Guide RE2020: réglementation environnementale: Eco-construire pour le confort de tous,” Jan. 2024.
- [21] M. J. de Villafranca Casas, S. Smit, A. Nilsson, and T. Kuramochi, “Climate targets by major steel companies: an assessment of collective ambition and planned emission reduction measures,” *Energy and Climate Change*, vol. 5, p. 100120, 2024.
- [22] ArcelorMittal, “Climate Action Report 2,” Jul. 2021. Accessed: Aug. 23, 2024. [Online]. Available: https://corporate-media.arcelormittal.com/media/ob3lpdom/car_2.pdf
- [23] USS United States Steel, “Roadmap to 2050: Our vision to achieve our net-zero greenhouse gas emissions goal.” Accessed: Aug. 23, 2024. [Online]. Available: <https://www.ussteel.com/roadmap-to-2050>
- [24] The Institution of Structural Engineers (IStructE), “The hierarchy of net zero design.” Accessed: Aug. 23, 2024. [Online]. Available: <https://www.istructe.org/resources/blog/the-hierarchy-of-net-zero-design/>
- [25] N. Watson, “Material decarbonisation - where are we heading?,” Jul. 14, 2023. Accessed: Aug. 23, 2024. [Online]. Available: <https://www.istructe.org/resources/training/climate-emergency-e-conference-2023/>
- [26] M. White, “Engineering in the climate emergency: doing less, better,” *The Structural Engineer: journal of the Institution of Structural Engineer*, vol. 100, no. 10, pp. 10–12, 2022.
- [27] M. Jungclaus, R. Esau, V. Olgyay, and A. Rempher, “Reducing embodied carbon in buildings: low-cost, high-value opportunities,” 2021.

-
- [28] C. F. Dunant, M. P. Drewniok, J. J. Orr, and J. M. Allwood, "Good early stage design decisions can halve embodied CO2 and lower structural frames' cost," *Structures*, vol. 33, pp. 343–354, 2021, doi: <https://doi.org/10.1016/j.istruc.2021.04.033>.
- [29] A. Kanyilmaz, V. Hoi Dang, and A. Kondratenko, "How does conceptual design impact the cost and carbon footprint of structures?," *Structures*, vol. 58, p. 105102, 2023, doi: <https://doi.org/10.1016/j.istruc.2023.105102>.
- [30] Ove Arup and Partners Ltd, Working together for a world without waste (WRAP), and The Climate Centre (TCC), "Low Carbon Routemap for the UK Built Environment," Mar. 2013. [Online]. Available: <https://scbrims.wordpress.com/wp-content/uploads/2013/10/routemap-final-report-05032013.pdf>
- [31] H. Treasury, "Infrastructure carbon review," *London: HM Treasury*, Nov. 2013.
- [32] E. Halliwell, "Putting the net-zero hierarchy into practice: Build nothing," *The Structural Engineer: journal of the Institution of Structural Engineer*, vol. 102, no. 1, pp. 10–11, 2024.
- [33] W. Algaard, "Persuasion and influence in a climate emergency," *The Structural Engineer: journal of the Institution of Structural Engineer*, vol. 98, no. 9, pp. 10–12, 2020.
- [34] T. Ibell, J. Norman, and O. Broadbent, "Nothing is better than something," *The Structural Engineer*, vol. 98, no. 6, p. 12, 2020.
- [35] J. Norman, T. Ibell, and O. Broadbent, "How can we create an engineering industry while building nothing?," *The Structural Engineer: journal of the Institution of Structural Engineer*, vol. 98, no. 7, p. 31, 2020.
- [36] M. Sansom, A. Girao Coelho, R. M. Lawson, and others, "Reuse and demountability using steel structures and the circular economy (REDUCE)," *Final Report, Project*, no. 710040, 2020.
- [37] M. Charlier and O. Vassart, "A paradigm shift in designing circular steel buildings: Some key principles and pioneering projects," *Steel Construction*, vol. 16, no. 4, pp. 209–214, 2023.
- [38] M. C. Moynihan and J. M. Allwood, "Utilization of structural steel in buildings," *Proceedings of the Royal Society A: Mathematical, Physical and Engineering Sciences*, vol. 470, no. 2168, p. 20140170, 2014.
- [39] G. Sabau, "Flexural Buckling of High-Strength Steel Columns," *Luleå University of Technology*, 2020.
- [40] C. Hickman *et al.*, "Climate anxiety in children and young people and their beliefs about government responses to climate change: a global survey," *Lancet Planet Health*, vol. 5, no. 12, pp. e863–e873, 2021.
- [41] E. Barbiroglio, "Generation Z fears climate change more than anything else," *Forbes, December*, vol. 9, 2019.
- [42] R. B. Salguero, D. Bogueva, and D. Marinova, "Australia's university Generation Z and its concerns about climate change," *Sustainable Earth Reviews*, vol. 7, no. 1, p. 8, 2024.
- [43] J. Allwood *et al.*, "Absolute zero," 2019, doi: DOI: 10.17863 / CAM.46075.
- [44] J. Orr, O. Gibbons, and W. Arnold, "How to calculate embodied carbon," *The Institution of Structural Engineers*, 2020.
-

- [45] R. BJORHOVDE, "Performance and design issues for high strength steel in structures," *Advances in Structural Engineering*, vol. 13, no. 3, pp. 403–411, 2010.
- [46] R. WILLMS, "High strength steel for steel constructions," in *Proc. of the Nordic Steel Construction Conference*, Malmö, Sweden: NSCC, 2009, pp. 597–604.
- [47] SAMUELSSON ANDERS and SCHRÖTER FALKO, "High-Performance Steels in Europe," in *Use and Application of High-Performance Steels for Steel Structures*, 2005. doi: 10.2749/sed008.099.
- [48] M. MAY, "How we all can increase the competitiveness of steel ? [Presentation]," Nov. 2015.
- [49] M. MAY, "How the right choice of rolled sections, steel grades and subgrades can economically impact your project? [Webinar Steligence]," Jun. 16, 2021.
- [50] H. BAN and G. SHI, "A review of research on high-strength steel structures," *Proceedings of the Institution of Civil Engineers-Structures and Buildings*, vol. 171, no. 8, pp. 625–641, 2018.
- [51] M. VELJKOVIC, *Sustainable Steel Buildings: A Practical Guide for Structures and Envelopes*. John Wiley & Sons, 2016.
- [52] CEN, "FprEN1993-1-1:2022: Eurocode 3: Design of steel structures - Part 1-1: General rules and rules for buildings," Brussels, 2022.
- [53] CEN, "EN10025-2: Hot rolled products of structural steels - Part 2: Technical delivery conditions for non-alloy structural steels," Brussels, 2019.
- [54] CEN, "EN10025-4: Hot rolled products of structural steels - Part 4: Technical delivery conditions for thermomechanical rolled weldable fine grain structural steels," Brussels, 2019.
- [55] CEN, "EN10025-3: Hot rolled products of structural steels - Part 3: Technical delivery conditions for normalized/normalized rolled weldable fine grain structural steels," Brussels, 2019.
- [56] CEN, "EN10025-6: Hot rolled products of structural steels - Part 6: Technical delivery conditions for flat products of high yield strength structural steels in the quenched and tempered condition," Brussels, 2019.
- [57] CEN, "EN10149-2: Hot-rolled flat products made of high strength steels for cold forming - Part 2: Technical delivery conditions for thermomechanically rolled steels," Brussels, 2013.
- [58] CEN, "EN 10210-1:2006 - Hot finished structural hollow sections of non-alloy and fine grain steels - Part 1: Technical delivery conditions," Brussels, 2006.
- [59] CEN, "EN 10210-3:2020 - Hot finished steel structural hollow sections - Part 3: Technical delivery conditions for high strength and weather resistant steels," Brussels, 2020.
- [60] CEN, "EN 10219-3:2020: Cold formed welded steel structural hollow sections - Part 3: Technical delivery conditions for high strength and weather resistant steels," Brussels, 2020.
- [61] CEN, "EN10219-1:2006: Cold formed welded structural hollow sections of non-alloy and fine grain steels - Part 1: Technical delivery conditions," Brussels, 2006.
- [62] M. LUKIC, "Réflexions sur la mise en pratique des éléments en acier HLE," *Revue de construction métallique (CTICM)*, 2019.
- [63] S. FINNIGAN, B. CHARNISH, and R. CHMIELOWSKI, "Steel and the skyscraper city: A study on the influence of steel on the design of tall buildings," in *CTBUH Conference, New York*, 2015.

-
- [64] R. Zanon and D. Zaganelli, "Wide Flange Beams: Trends Towards Higher Steel Performance," *Current Trends in Civil & Structural Engineering*, 2019.
- [65] G. Axmann, "Steel going strong," *Modern Steel Construction*, vol. 43, no. 1, pp. 56–61, 2003.
- [66] ASTM, "A913/A913M – 19: Standard Specification for High-Strength Low-Alloy Steel Shapes of Structural Quality, Produced by Quenching and Self-Tempering Process (QST)," Pennsylvania United, United states.
- [67] National Standard of the People's Republic of China, "GB/T 33968-2017: Hot Rolled Steel Sections with improved weldability (translated)," Jul. 2017.
- [68] DIBt-Deutsches Institut für Bautechnik, "ETA-10/0156 Long products made of HISTAR 355/355L und HISTAR 460/460L," DIBt Berlin, Berlin, Germany, 2015.
- [69] ArcelorMittal, "HISTAR® : Innovative high strength steels for economical steel structures," 2020. Accessed: Oct. 17, 2023. [Online]. Available: https://sections.arcelormittal.com/repository2/Sections/5_3_1_HISTAR_web.pdf
- [70] CEN, "EN1993-1-1:2005: Eurocode 3: Design of steel structures - Part 1-1: General rules and rules for buildings," Brussels, 2005.
- [71] CEN, "EN1993-1-12:2007: Eurocode 3 - Design of steel structures - Part 1-12: Additional rules for the extension of EN 1993 up to steel grades S 700.," Brussels, 2007.
- [72] P. Langenberg, T. Nießen, and W. Dahl, "Bruch-und Verformungsverhalten von hochfesten Stählen mit Streckgrenzen von 690 bis 890 MPa," *Stahlbau*, vol. 69, no. 4, pp. 283–291, 2000.
- [73] R. Stroetmann, P. Deepe, U. Kuhlmann, and C. Rasche, "Bemessung von Tragwerken aus höherfesten Stählen bis S700 nach EN 1993-1-12," *Stahlbau*, vol. 81, no. 4, pp. 332–342, 2012, doi: <https://doi.org/10.1002/stab.201201545>.
- [74] Gardner Leroy, "Designing HSS structures: Eurocode rules and practical guidance.," Presentation for the HILONG workshop. Accessed: Jul. 13, 2021. [Online]. Available: <http://news-sci.com/wp-content/uploads/2015/07/6-hillong-leroy-gardner.pdf>
- [75] CEN, "EN1993-1-10:2005: Eurocode 3: Design of steel structures - Part 1-10: Material toughness and through-thickness properties," Brussels, 2005.
- [76] N. Baddoo and A. Chen, "High Strength Steel Design and Execution Guide," *SCI (the Steel Construction 397 Institute)*, vol. 398, 2020.
- [77] P. Langenberg, "Relation between design safety and Y/T ratio in application of welded high strength structural steels," in *Proceedings of International Symposium on Applications of High Strength Steels in Modern Constructions and Bridge-Relationship of Design specifications, Safety and Y/T ratio. Beijing*, 2008, pp. 28–46.
- [78] CEN, "EN1993-1-2:2005: Eurocode 3: Design of steel structures - Part 1-2: General rules - Structural fire design," Brussels, 2005.
- [79] Thierry Kretz (head of AFGC), "Les aciers à Haute Limite d'Elasticité," Oct. 2012.
- [80] M. Feldmann *et al.*, "Rules on high strength steels (RUOSTE): Final report," 2016. Accessed: Jul. 13, 2021. [Online]. Available: <https://op.europa.eu/en/publication-detail/-/publication/515285b0-c820-11e6-a6db-01aa75ed71a1>
-

- [81] X. Qiang, F. S. K. Bijlaard, and H. Kolstein, "Post-fire mechanical properties of high strength structural steels S460 and S690," *Eng Struct*, vol. 35, 2012, doi: 10.1016/j.engstruct.2011.11.005.
- [82] M. Neuenschwander, C. Scandella, M. Knobloch, and M. Fontana, "Modeling elevated-temperature mechanical behavior of high and ultra-high strength steels in structural fire design," *Mater Des*, vol. 136, 2017, doi: 10.1016/j.matdes.2017.09.041.
- [83] C. Maraveas, Z. C. Fasoulakis, and K. D. Tsavdaridis, "Mechanical properties of High and Very High Steel at elevated temperatures and after cooling down," *Fire Sci Rev*, vol. 6, no. 1, 2017, doi: 10.1186/s40038-017-0017-6.
- [84] F. Dechamps, "Quantification of the impact of fire design on the interest of using" high yield strength" steels [Master's thesis]," University of Liège, Liège, 2022.
- [85] CEN, "FprEN1993-1-9: 2023: Eurocode 3: Design of steel structures - Part 1-9: Fatigue," Brussels, Mar. 2023.
- [86] P. Collin and B. Johansson, "Eurocode for high strength steel and applications in construction," in *International Conference Super-High Strength Steels*, Associazione Italiana di Metallurgia, Ed., Nov. 2005.
- [87] Stroetmann Richard, "High strength steel for improvement of sustainability," in *EUROSTEEL 2011*, Budapest, Hungary, Sep. 2011.
- [88] T. Lehnert, "Special heavy plate solutions for bridges," *Steel construction: design and research.*, vol. 11, no. 3, pp. 192–195, 2018, doi: 10.1002/stco.201800011.
- [89] M. Gkantou, "Response and design of high strength steel structures employing square and rectangular hollow sections," University of Birmingham, 2017.
- [90] M. Veljkovic, "The most recent results on high strength steel for constructions [Course]," 2016, *Delft*.
- [91] G. Q. Li, Y. B. Wang, and S. W. Chen, "The art of application of high-strength steel structures for buildings in seismic zones," *Advanced Steel Construction*, vol. 11, no. 4, 2015.
- [92] N. Baddoo *et al.*, "Stronger steels in the built environment (STROBE): Final report," 2021.
- [93] B. Johansson, "Buckling Resistance of Structures of High Strength Steel," in *Use and application of high-performance steels for steel structures*, IABSE., International Association for Bridge and Structural Engineering (IABSE), 2005, ch. 5.3, pp. 120–128.
- [94] Bauforumstahl e.V., "Environmental Product Declaration: Structural Steel: Sections and Plates," Oct. 2018.
- [95] J. Sperle, L. Hallberg, J. Larsson, and H. Groth, "The Environmental Value of High Strength Steel Structures II The 'Steel Eco-Cycle', Scientific Report, 2004-2010, March 2011."
- [96] J.-O. Sperle, "Environmental advantages of using advanced high strength steel in steel constructions," in *Nordic Steel Construction Conference*, 2012.
- [97] L. Cederfeld and J. O. Sperle, "High strength steel in the roof of Swedbank Arena: Savings in weight, cost and environmental impact," in *Nordic Steel Construction Conf*, 2012, pp. 15–24.

-
- [98] J.-O. Sperle and L. Hallberg, "Environmental advantages of using high strength steel," in *The 2nd international conference on clean technologies in the steel industry*, 2011.
- [99] S. Shinde and M. May, "Recent developments in the use of quenched and self-tempered hot-rolled H-beams," in *COMAT2012 Recent trends in structural materials*, Plzeň, Czech Republic, Nov. 2012.
- [100] Veljkovic Milan and al, "High-strength tower in steel for wind turbines (HISTWIN): Final report," 2012. Accessed: Jul. 13, 2021. [Online]. Available: <https://op.europa.eu/en/publication-detail/-/publication/1081fa93-0319-4710-a16c-08692a5f5265/language-en/format-PDF/source-209815516>
- [101] Vayas Ioannis and al., "Innovative solutions for design and strengthening of telecommunications and transmission lattice towers using large angles from high strength steel and hybrid techniques of angles with FRP strips (ANGELHY): Final report," 2021.
- [102] Theofanous and al., "High strength long span structures (HILONG): Final report," 2017. Accessed: Jul. 13, 2021. [Online]. Available: <https://op.europa.eu/en/publication-detail/-/publication/dec2dad6-47a4-11e7-aea8-01aa75ed71a1>
- [103] Habraken Anne-Marie et al., "Optimal use of high strength steel grades within bridges (OPTIBRI): Final report.," 2019. Accessed: Jul. 13, 2021. [Online]. Available: <https://op.europa.eu/en/publication-detail/-/publication/d8bd0ac1-4479-11e9-a8ed-01aa75ed71a1/language-en>
- [104] CEN, "EN1993-1-1 ANB: 2010: Eurocode 3: Design of steel structures - Part 1-1 : General rules and rules for buildings - National Annex," Brussels, 2010.
- [105] D. Sfintesco, "Fondement expérimental des courbes européennes de flambement," *Construction métallique*, vol. 3, pp. 5–12, 1970.
- [106] H. Beer and G. Schulz, "Bases théoriques des courbes européennes de flambement," *Construction Métallique*, vol. 3, no. 485, pp. 37–57, 1970.
- [107] J. Strating and H. Vos, "Computer Simulation of the ECCS Buckling Curve using a Monte-Carlo Method," in *Construction Métallique*, vol. 2, 1973, pp. 23–39.
- [108] R. Maquoi and J. Rondal, "Mise en équation des nouvelles courbes européennes de flambement," 1978.
- [109] F. Jasiński, *Recherches sur la flexion des pièces comprimées*. Vve Ch. Dunod & P. Vicq, 1894.
- [110] ECCS, *Manual on stability of steel structures*. S. I: [s. n.], 1976.
- [111] T. Tankova, F. Rodrigues, C. Leitaó, C. Martins, and L. S. da Silva, "Lateral-torsional buckling of high strength steel beams: Experimental resistance," *Thin-Walled Structures*, vol. 164, p. 107913, 2021.
- [112] L. Schaper, T. Tankova, L. S. da Silva, and M. Knobloch, "Effects of state-of-the-art residual stress models on the member and local stability behaviour," *Steel Construction*, vol. 15, no. 4, pp. 244–254, 2022, doi: <https://doi.org/10.1002/stco.202200027>.
- [113] T. Tankova, L. Simões da Silva, and F. Rodrigues, "Buckling curve selection for HSS welded I-section members," *Thin-Walled Structures*, vol. 177, p. 109430, 2022, doi: <https://doi.org/10.1016/j.tws.2022.109430>.
-

- [114] G. L. Griffis, G. Axmann, B. V Patel, C. M. Waggoner, and J. Vinson, "High-strength steel in the long-span retractable roof of reliant stadium," *2003 NASCC Proc., Baltimore*, 2003.
- [115] O. Hechler, G. Axmann, and B. Donnay, "The right choice of steel—according to the Eurocode," *Economical Bridge Solutions based on innovative composite dowels and integrated abutments: Ecobridge*, pp. 21–43, 2015.
- [116] R. Stroetmann, "High strength steel for improvement of sustainability," in *Proceedings of the 6th European Conference on Steel and Composite Structures, Proceedings*, 2011, p. 31.
- [117] R. Stroetmann, "Nachhaltigkeit und ressourceneffizienter Einsatz höherfester Stähle," in *iforum Nachhaltigkeit an der TU Dresden*, Dresden, Oct. 2010.
- [118] T. V Galambos and R. L. Ketter, "Columns under combined bending and thrust," *Transactions of the American Society of Civil Engineers*, vol. 126, no. 1, pp. 1–23, 1961.
- [119] L. S. Beedle, "The influence of residual stress on column strength-A proposed pilot investigation," *Fritz Laboratory, Lehigh University, Bethlehem, PA, USA*, 1951.
- [120] R. L. Ketter, *The Influence of Residual Stress on the Strength of Structural Members*. Welding Research Council of the Engineering Foundation, 1958.
- [121] M. G. Lay and R. Ward, "Residual stresses in steel sections," *Journal of the Australian Institute of Steel Construction*, vol. 3, no. 3, pp. 2–21, 1969.
- [122] M. Clarin, "High strength steel: local buckling and residual stresses[PhD thesis]," Luleå Tekniska Universitet, 2004.
- [123] M. Abambres and W.-M. Quach, "Residual stresses in steel members: a review of available analytical expressions," *International Journal of Structural Integrity*, vol. 7, no. 1, pp. 70–94, 2016.
- [124] A. Skiadopoulou, A. de Castro e Sousa, and D. Lignos, "Database of Residual Stress Measurements on Hot-rolled Wide Flange Steel Cross Sections," 2023.
- [125] L. S. Beedle and L. Tall, "Basic Column Strength," *Journal of the Structural Division*, vol. 86, no. 7, Jul. 1960.
- [126] L. S. Beedle and A. W. Huber, "Residual stress and the compressive properties of steel—a summary report," *Fritz Laboratory Reports, paper*, vol. 46, 1957.
- [127] D. Feder and G. C. Lee, "Residual stress and the strength of members of high strength steel, Lehigh. University,(April 1959)," 1959.
- [128] A. W. Huber, *Residual stresses in wide-flange beams and columns*. Department of Civil Engineering and Mechanics, Lehigh Univ., 1956.
- [129] G. A. Alpsten, *Thermal residual stresses in hot-rolled steel members*. Fritz Engineering Laboratory, 1968.
- [130] C. Jez Gala, "Residual stresses in rolled I-sections," *Proceedings of the Institution of Civil Engineers*, vol. 23, no. 3, pp. 361–378, 1962.
- [131] J. Brozzetti, G. A. Alpsten, and L. Tall, "Residual stresses in a heavy rolled shape 14WF730," *Lehigh university, Fritz Lab. Report*, no. 337.10, 1970.

-
- [132] B. W. Young, *Residual stresses in hot-rolled sections*. University of Cambridge, 1971.
- [133] J. Szalai and F. Papp, "A new residual stress distribution for hot-rolled I-shaped sections," *J Constr Steel Res*, vol. 61, no. 6, pp. 845–861, 2005.
- [134] A. Skiadopoulos, A. de C. e Sousa, and D. G. Lignos, "Experiments and proposed model for residual stresses in hot-rolled wide flange shapes," *J Constr Steel Res*, vol. 210, p. 108069, 2023.
- [135] CEN, "FprEN1993-1-14: Eurocode 3: Design of steel structures — Part 1-14: Design assisted by finite element analysis," Brussels, Apr. 2024.
- [136] G. A. Alpsten and L. Tall, *Residual stresses in heavy welded shapes*. American Welding Society, 1970.
- [137] P. W. Key and G. J. Hancock, "A theoretical investigation of the column behaviour of cold-formed square hollow sections," *Thin-walled structures*, vol. 16, no. 1–4, pp. 31–64, 1993.
- [138] J.-L. Ma, T.-M. Chan, and B. Young, "Material properties and residual stresses of cold-formed high strength steel hollow sections," *J Constr Steel Res*, vol. 109, pp. 152–165, 2015.
- [139] W. F. Chen and D. A. Ross, "Tests of fabricated tubular columns," *Journal of the Structural Division*, vol. 103, no. 3, pp. 619–634, 1977.
- [140] J. Wang and L. Gardner, "Flexural buckling of hot-finished high-strength steel SHS and RHS columns," *Journal of Structural Engineering*, vol. 143, no. 6, p. 4017028, 2017.
- [141] J. Wang, S. Afshan, M. Gkantou, M. Theofanous, C. Baniotopoulos, and L. Gardner, "Flexural behaviour of hot-finished high strength steel square and rectangular hollow sections," *J Constr Steel Res*, vol. 121, pp. 97–109, Jun. 2016, doi: 10.1016/J.JCSR.2016.01.017.
- [142] J. Nseir, "Development of a new design method for the cross-section capacity of steel hollow sections," University of Liège, Liège, 2015.
- [143] Y. Fukumoto and Y. Itoh, "Evaluation of multiple column curves using the experimental database approach," *J Constr Steel Res*, vol. 3, no. 3, pp. 2–19, 1983.
- [144] C.-H. Lee, K.-H. Han, C.-M. Uang, D.-K. Kim, C.-H. Park, and J.-H. Kim, "Flexural strength and rotation capacity of I-shaped beams fabricated from 800-MPa steel," *Journal of Structural Engineering*, vol. 139, no. 6, pp. 1043–1058, 2013.
- [145] R. Maquoi, "Some improvements to the buckling design of centrally loaded columns," in *Structural Stability Research Council, Proceedings of the Annual Meeting*, 1982.
- [146] R. Maquoi and J.-P. Jaspart, "Quelques réflexions à propos des courbes de flambement et de l'amplitude relative d'imperfection géométrique équivalente," Liège, Dec. 2016.
- [147] G. Sedlacek, "Buckling behaviour of hot-formed SHS in high strength steel grade E-460. Comité international pour le développement et l'étude de la construction tubulaire," 1999.
- [148] X. Meng and L. Gardner, "Behavior and design of normal-and high-strength steel SHS and RHS columns," *Journal of Structural Engineering*, vol. 146, no. 11, p. 4020227, 2020.
- [149] K. J. R. Rasmussen and G. J. Hancock, "Tests of high strength steel columns," *J Constr Steel Res*, vol. 34, no. 1, pp. 27–52, 1995.
-

- [150] T.-Y. Ma, X. Liu, Y.-F. Hu, K.-F. Chung, and G.-Q. Li, "Structural behaviour of slender columns of high strength S690 steel welded H-sections under compression," *Eng Struct*, vol. 157, pp. 75–85, 2018.
- [151] T.-J. Li, G.-Q. Li, S.-L. Chan, and Y.-B. Wang, "Behavior of Q690 high-strength steel columns: Part 1: Experimental investigation," *J Constr Steel Res*, vol. 123, pp. 18–30, 2016.
- [152] G. Sabau, O. Lagerqvist, and N. Baddoo, "Statistical Analysis of Flexural-Buckling-Resistance Models for High-Strength Steel Columns," *Journal of Structural Engineering*, vol. 146, no. 2, p. 4019210, 2020.
- [153] G. Shi, H. Ban, and F. S. K. Bijlaard, "Tests and numerical study of ultra-high strength steel columns with end restraints," *J Constr Steel Res*, vol. 70, pp. 236–247, 2012.
- [154] H. Ban, G. Shi, Y. Shi, and Y. Wang, "Overall buckling behavior of 460 MPa high strength steel columns: Experimental investigation and design method," *J Constr Steel Res*, vol. 74, pp. 140–150, 2012.
- [155] J. Jönsson and T.-C. Stan, "European column buckling curves and finite element modelling including high strength steels," *J Constr Steel Res*, vol. 128, pp. 136–151, 2017.
- [156] B. Somodi and B. Kövesdi, "Flexural buckling resistance of cold-formed HSS hollow section members," *J Constr Steel Res*, vol. 128, pp. 179–192, 2017.
- [157] B. Somodi and B. Kövesdi, "Flexural buckling resistance of welded HSS box section members," *Thin-Walled Structures*, vol. 119, pp. 266–281, 2017.
- [158] X. Yun, Y. Zhu, X. Meng, and L. Gardner, "Welded steel I-section columns: Residual stresses, testing, simulation and design," *Eng Struct*, vol. 282, p. 115631, 2023, doi: <https://doi.org/10.1016/j.engstruct.2023.115631>.
- [159] F. Frey, "Effet du dressage à froid des profilés laminés en double té sur leur force portance," Zürich, 1969.
- [160] G. A. Alpsten, "Residual stresses, yield stress, and column strength of hot-rolled and roller-straightened steel shapes," *Rapports des commissions de travail AIPC = IVBH Berichte der Arbeitskommissionen = IABSE reports of the working commissions*, vol. 23, p. 39, 1975, doi: 10.5169/seals-19799.
- [161] T. V. Galambos, *Guide to stability design: criteria for metal structures*, 4th ed. in A Wiley-Interscience publication. New York, NY: Wiley-Interscience, 1988.
- [162] A. W. Huber, "The influence of residual stress on the instability of columns, Dissertation, Lehigh University,(May 1956)," 1956.
- [163] L. Tall, *Recent developments in the study of column behavior*. Fritz Engineering Laboratory, Department of Civil Engineering, Lehigh University, 1963.
- [164] G. Alpsten, "Residual stresses and strength of cold-straightened wide-flange shapes," *Jernkontorets Annaler*, vol. 154, pp. 1–9, 1970.
- [165] G. A. Alpsten, "Residual stresses, yield strength and column strength of hot-rolled and roller-straightened steel shapes," in *Proceedings of the Colloquium on Column Strength, Paris, France*, 1972, pp. 39–59.

-
- [166] X. Ge and J. A. Yura, "The strength of rotary-straightened steel columns," in *Proceedings of the Annual Stability Conference*, St. Louis, Missouri: Structural Stability Research Council (SSRC), Apr. 2019.
- [167] R. C. Spoorenberg, H. H. Snijder, and J. C. D. Hoenderkamp, "Experimental investigation of residual stresses in roller bent wide flange steel sections," *J Constr Steel Res*, vol. 66, no. 6, pp. 737–747, 2010.
- [168] R. C. Spoorenberg, H. H. Snijder, and J. C. D. Hoenderkamp, "Proposed residual stress model for roller bent steel wide flange sections," *J Constr Steel Res*, vol. 67, no. 6, pp. 992–1000, 2011.
- [169] B. T. Rosson, "Beam element material models for straightened hot rolled sections and welded HSS sections," in *Proceedings of the 2021 SSRC Annual Stability Conference*, 2021.
- [170] B. T. Rosson, "Beam Element Material Model for Rotary-Straightened Steel W-Shapes," *Journal of Civil Engineering and Architecture*, vol. 15, pp. 57–62, 2021.
- [171] H. Koh, B. T. Rosson, and H. B. Blum, "Stability analysis of stiffness reduction models on rotary- and non-rotary straightened W-shapes," *J Constr Steel Res*, vol. 208, p. 108024, 2023.
- [172] B. Guan, Y. Zang, D. Wu, and Q. Qin, "Stress-inheriting behavior of H-beam during roller straightening process," *J Mater Process Technol*, vol. 244, pp. 253–272, 2017, doi: 10.1016/j.jmatprotec.2017.01.026.
- [173] B. Charnish and S. Finnigan, "The Bay Adelaide Centre: Twenty-Five Years of Structural Innovation," in *Structures Congress*, 2015, pp. 742–754.
- [174] U. Klanšek and S. Kravanja, "Cost estimation, optimization and competitiveness of different composite floor systems—Part 1: Self-manufacturing cost estimation of composite and steel structures," *J Constr Steel Res*, vol. 62, no. 5, pp. 434–448, 2006, doi: 10.1016/j.jcsr.2005.08.005.
- [175] J. Haapio, "Feature-based costing method for skeletal steel structures based on the process approach," Tampere, 2012.
- [176] K. C. Sarma and H. Adeli, "Life-cycle cost optimization of steel structures," *Int J Numer Methods Eng*, vol. 55, no. 12, pp. 1451–1462, 2002, doi: 10.1002/nme.549.
- [177] L. Pavlovčič, A. Krajnc, and D. Beg, "Cost function analysis in the structural optimization of steel frames," *Structural and multidisciplinary optimization*, vol. 28, no. 4, pp. 286–295, 2004, doi: 10.1007/s00158-004-0430-z.
- [178] K. Jármai and J. Farkas, "Cost calculation and optimisation of welded steel structures," *J Constr Steel Res*, vol. 50, no. 2, pp. 115–135, 1999, doi: 10.1016/S0143-974X(98)00241-7.
- [179] CEN, "EN 15804: Sustainability of Construction Works - Environmental Product Declarations - Core Rules for the Product Category of Construction Products," Brussels, 2012.
- [180] MEPS Steel Prices & Indices (2023) Copyright © 2023 MEPS International Ltd. All Rights Reserved [online]. <https://mepsinternational.com/gb/en/products/europe-steel-prices>
- [181] SteelBenchmarker, "Price History: Tables and Charts," Oct. 2021. Accessed: Oct. 20, 2021. [Online]. Available: <http://steelbenchmarker.com/history.pdf>
- [182] CEN, "EN10204: Metallic products - Types of inspection documents," Brussels, 2004.
-

- [183] “Vosta Stahlhande GmbH: Mill price list,” <http://vosta.de/index.php/en/mill-price-list>.
- [184] US Steel Kosice, “Extra Price list: Hot rolled,” 2017.
- [185] TATA Steel, “Produits laminés à chaud: Liste des écarts de prix en Euro,” Apr. 2013.
- [186] TATA steel, “Hot-rolled strip products: Price extras in Euros,” Apr. 2015.
- [187] Salzgitter Flachstahl, “Price List for hot-rolled Products (Hot-rolled strip),” Oct. 2012.
- [188] Voestalpine, “Price list Hot-rolled steel strip,” Apr. 2013.
- [189] Acciaieria Arvedi, “Price list for Hot-rolled coil and strip.”
- [190] SSAB, “Tilläggspriser Varmvalsad bandplåt,” Jan. 2016.
- [191] United States Steel Corporation, “North American Flat Rolled Products,” Feb. 2021.
- [192] ArcelorMittal USA, “Products & prices,” Jan. 2019.
- [193] MathWorks, “MATLAB version R2019b,” 2019, *Natick, Massachusetts*: 2019b.
- [194] I. Sorsa, “Breakthrough of High Strength Steels in Construction,” Oct. 2014.
- [195] “Chemical elements by market price.” Accessed: Mar. 25, 2022. [Online]. Available: http://www.leonland.de/elements_by_price/en/
- [196] “Prices of Chemical Elements – \$/kg.” Accessed: Mar. 25, 2022. [Online]. Available: <https://material-properties.org/prices-of-chemical-elements-kg/>
- [197] Dillinger Hütte, “Price list for steel plates,” Apr. 2014.
- [198] IlsenBurger Grobblech, “Net Price List Heavy Plate Quarto Range,” Oct. 2011.
- [199] ArcelorMittal Europe - Long products, “Price-list: Sections, Channels and Merchant bars,” Esch-sur-Alzette (Luxembourg), Dec. 2017.
- [200] ArcelorMittal - Long products, “Price-list: Sections, Channels and Merchant bars,” Dec. 2017.
- [201] British steel, “Sections: Price extras pounds sterling,” 2020.
- [202] TATA steel, “Advance® sections Price extras Pounds Sterling,” Sep. 2013.
- [203] Corus Long Products, “Advance® sections price list 5,” May 2010.
- [204] M. Kierros and K. Mela, “SSAB High strength hollow sections: Handbook for steel structures 2017,” 2017.
- [205] International Energy Agency (IEA), “Achieving Net Zero Heavy Industry Sectors in G7 Members,” Paris, May 2022. Accessed: Jun. 23, 2022. [Online]. Available: <https://www.iea.org/reports/achieving-net-zero-heavy-industry-sectors-in-g7-members>
- [206] ArcelorMittal, “Brochure-XCarb™ Recycled and renewably produced-EN,” May 2021.
- [207] “ISO14025: Environmental labels and declarations — Type III environmental declarations — Principles and procedures,” 2006.

-
- [208] European standard committee (CEN), "EN 15804+A2 Sustainability of construction works - Environmental product declarations - Core rules for the product category of construction products -," 2012.
- [209] SSAB, "Download center - Environmental Product Declarations." Accessed: Jun. 19, 2022. [Online]. Available: [https://www.ssab.com/en/download-center#sort=%40customorder%20descending&f:document=\[3f0a0e364ca54f74a30faff866bd87ff\]](https://www.ssab.com/en/download-center#sort=%40customorder%20descending&f:document=[3f0a0e364ca54f74a30faff866bd87ff])
- [210] ArcelorMittal Europe, "Environmental Product Declarations." Accessed: Jun. 19, 2022. [Online]. Available: <https://constructalia.arcelormittal.com/en/tools/epd>
- [211] R. Stroetmann and P. Deepe, "Anwendung höherfester Stähle zur Steigerung der Ressourceneffizienz im Bauwesen," *VDI Ber*, vol. 2084, pp. 267–305.
- [212] P. Nuss and M. J. Eckelman, "Life cycle assessment of metals: a scientific synthesis," *PLoS One*, vol. 9, no. 7, p. e101298, 2014.
- [213] Sphera Solutions GmbH, "GaBi 10.0 LCA Software & LCI databases v2021.1."
- [214] H. S. Eggleston, L. Buenida, K. Miwa, T. Ngara, and K. Tanabe, "Industrial processes and product use," in *IPCC guidelines for National Greenhouse Gas Inventories*, vol. 3, Kanagawa, Japan, 2006, pp. 4.32-4.42.
- [215] American Institute of Steel Construction (AISC), "China, Global Warming and Hot-Rolled Structural Steel Sections," Apr. 2018. Accessed: Jun. 20, 2022. [Online]. Available: <https://www.aisc.org/globalassets/aisc/publications/white-papers/global-warming-potential-of-chinese-and-domestic-hot-rolled-structural-steel.pdf>
- [216] ArcelorMittal, "Steel building in Europe – Multi-storey Steel Buildings – Part 2: Concept design." [Online]. Available: https://constructalia.arcelormittal.com/en/news_center/articles/design_guides_steel_buildings_in_europe
- [217] K. Mela and M. Heinisuo, "Weight and cost optimization of welded high strength steel beams," *Eng Struct*, vol. 79, 2014, doi: 10.1016/j.engstruct.2014.08.028.
- [218] M. Veljkovic and B. Johansson, "Design of hybrid steel girders," *J Constr Steel Res*, vol. 60, no. 3–5, pp. 535–547, 2004.
- [219] V. L. Hoang, J-F. Demonceau, D. P. L. Ly, and B. Rossi, "Field of application of high strength steel circular tubes for steel and composite columns from an economic point of view," *J Constr Steel Res*, vol. 67, no. 6, 2011, doi: 10.1016/j.jcsr.2011.01.008.
- [220] ESDEP (European Steel Design Education Programme), "WG 7: Elements - Lecture 7.4.1: Tension Members I."
- [221] P. Langenberg, T. Nießen, and W. Dahl, "Bruch-und Verformungsverhalten von hochfesten Stählen mit Streckgrenzen von 690 bis 890 MPa," *Stahlbau*, vol. 69, no. 4, pp. 283–291, 2000.
- [222] CEN, "EN1993-1-5: Eurocode 3: Design of steel structures – Part 1-5: Plated structural elements," Brussels, 2005.

- [223] Saufnay Loris, "Interest of high strength steel rolled sections for steel structures (in French)," Master's Thesis, University of Liège, Liège, Belgium, 2019. Accessed: Jul. 13, 2021. [Online]. Available: <https://orbi.uliege.be/handle/2268/250358>
- [224] M. Sansom and R. M. Lawson, "STROnger Steels in the Built Environment (STROBE) - Deliverable 5.1: WP 5: Life cycle assessment of comparative conventional strength & HSS designs," 2021.
- [225] Greisch office and University of Liège, "FinelG: non-linear finite element analysis program: user's manual," Sep. 2018, *Liège*.
- [226] V. de Goyet, "L'analyse statique non linéaire par la méthode des éléments finis des structures spatiales formées de poutres à section non symétrique," *Université de Liège*, 1989.
- [227] N. Boissonnade, H. Degée, J. Naumes, and M. Oppe, "Experimental and numerical investigations for I-girders in bending and shear stiffened by trapezoidal stiffeners," *Advanced Steel Construction*, vol. 4, no. 1, pp. 1–12, 2008.
- [228] N. Boissonnade and H. Somja, "Influence of imperfections in FEM modelling of lateral torsional buckling," in *Proceedings of the Annual Stability Conference*, 2012, pp. 18–21.
- [229] M.-Z. Bezas, J.-F. Demonceau, I. Vayas, and J.-P. Jaspart, "Experimental and numerical investigations on large angle high strength steel columns," *Thin-Walled Structures*, vol. 159, p. 107287, 2021, doi: <https://doi.org/10.1016/j.tws.2020.107287>.
- [230] M.-Z. Bezas, J.-F. Demonceau, I. Vayas, and J.-P. Jaspart, "Design rules for equal-leg angle members subjected to compression and bending," *J Constr Steel Res*, vol. 189, p. 107092, 2022.
- [231] H. H. Snijder, L.-G. Cajot, N. Popa, and R. C. Spoorenberg, "Buckling curves for heavy wide flange steel columns," *Romanian Journal of Technical Science: Applied Mechanics*, vol. 59, no. 1/2, pp. 178–204, 2014.
- [232] L. S. da Silva, T. Tankova, L. Marques, and C. Rebelo, "Safety assessment of Eurocode 3 stability design rules for the flexural buckling of columns," *Advanced Steel Construction—an International Journal*, vol. 12, no. 3, pp. 328–358, 2016.
- [233] CEN, "EN 10210-2:2019 - Hot finished steel structural hollow sections - Part 2: Tolerances, dimensions and sectional properties," 2019.
- [234] B. W. Young, *Residual stresses in hot-rolled sections*. University of Cambridge, 1971.
- [235] T. Tankova, L. S. da Silva, and F. Rodrigues, "Buckling curve selection for HSS welded I-section members," *Thin-Walled Structures*, vol. 177, p. 109430, 2022.
- [236] G. A. Alpsten, "Variations in mechanical and cross-sectional properties of steel," in *Proceedings of the International Conference on the Planning and Design of Tall Buildings*, Lehigh University, Ed., ASCE-IABSE, 1972.
- [237] J. Lindner, U. Kuhlmann, and A. Just, "Verification of flexural buckling according to Eurocode 3 part 1-1 using bow imperfections," *Steel Construction*, vol. 9, no. 4, pp. 349–362, 2016.
- [238] K. H. Law and L. Gardner, "Lateral instability of elliptical hollow section beams," *Eng Struct*, vol. 37, pp. 152–166, Apr. 2012, doi: [10.1016/J.ENGSTRUCT.2011.12.008](https://doi.org/10.1016/J.ENGSTRUCT.2011.12.008).

-
- [239] J. Wang, S. Afshan, M. Gkantou, M. Theofanous, C. Baniotopoulos, and L. Gardner, "Flexural behaviour of hot-finished high strength steel square and rectangular hollow sections," *J Constr Steel Res*, vol. 121, pp. 97–109, 2016.
- [240] N. Tebedge, W. F. Chen, and L. Tall, "Experimental studies on column strength of European heavy shapes. Fritz Engineering Laboratory Report No. 351.7," Nov. 1972.
- [241] R. C. Spoorenberg, H. H. Snijder, and J. C. D. Hoenderkamp, "Experimental investigation of residual stresses in roller bent wide flange steel sections," *J Constr Steel Res*, vol. 66, no. 6, pp. 737–747, 2010.
- [242] A. A. Sousa and D. Lignos, "Residual stress measurements of European hot-rolled I-shaped steel profiles," 2017.
- [243] J. Lindner and L. da Silva, "Classification of rolled I-Profiles fabricated in steel grade S460 within Table 6.2 of EN 1993-1-1," 2015.
- [244] H. H. Snijder, "Recent developments regarding the next version of Eurocode 3 part 1-1 on steel structures.," *ce/papers*, vol. 1, no. 4, pp. 515–538, 2017.
- [245] A. Rusch and J. Lindner, "Überprüfung der grenz (b/t)-Werte für das Verfahren Elastisch-Plastisch," *Stahlbau*, vol. 70, no. 11, pp. 857–868, 2001.
- [246] A. Toffolon and A. Taras, "Proposal of a design curve for the overall resistance of cold formed RHS and SHS members," *ce/papers*, vol. 3, no. 3–4, pp. 517–522, 2019.
- [247] A. Müller, M. Vild, and A. Taras, "Decision tree for local+ global imperfection combinations in double-symmetric prismatic members—Practical recommendations in the framework of advanced analysis," *Steel Construction*, vol. 16, no. 1, pp. 2–15, 2023.
- [248] A. Taras, L. Gardner, D. Camotim, A. Bureau, G. Toquero, and V. Dehan, "HOLLOSSTAB project, Overall-Slenderness Based Direct Design for Strength and Stability of Innovative Hollow Sections," 2015. doi: Grant: RFCS-2015-709892.
- [249] J. Janss, "Essais de flambement sur profilés de classe 4 en acier à très haute résistance," Liège, Nov. 1993.
- [250] X. Meng and L. Gardner, "Testing of hot-finished high strength steel SHS and RHS under combined compression and bending," *Thin-Walled Structures*, vol. 148, p. 106262, Mar. 2020, doi: 10.1016/J.TWS.2019.106262.
- [251] CEN, "EN 10034:1994: Structural steel I and H sections - Tolerances on shape and dimensions," Brussels, 1994.
- [252] O. Ersvik and G. A. Alpsten, "Experimentell undersökning av knäckhållfastheten hos bredflänsprofiler HE 200 A riktade på olika sätt ('Experimental investigation of the column strength of wide-flange shapes HE 200 A rollerstraightened in different ways')," Stockholm, Dec. 1970.
- [253] CEN, "EN 15512: Steel static storage system: Adjustable pallet racking systems: Principles for structural design," Brussels, Mar. 2009.
- [254] C. A. Castiglioni and others, *Seismic behavior of steel storage pallet racking systems*. Springer, 2016.
-

- [255] “FEM 10.2.08: Recommendations for the design of static steel pallet racks under seismic conditions,” Oct. 2009.
- [256] V. Hua and K. J. R. Rasmussen, “Static Friction Coefficient Between Pallets and Beam Rail and Pallet Shear Stiffness Tests (No. R914),” 2011.
- [257] C. A. Castiglioni, A. Drei, P. Carydis, and H. Mouzakis, “Experimental assessment of static friction between pallet and beams in racking systems,” *Journal of Building Engineering*, vol. 6, pp. 203–214, 2016.
- [258] CEN, “EN 16681:2016: Steel static storage systems - Adjustable pallet racking systems - Principles for seismic design,” 2016.
- [259] B. P. Gilbert, L. H. Teh, R. X. Badet, and K. J. R. Rasmussen, “The influence of pallets on the behaviour and design of drive-in steel storage racks–Part I Behaviour,” in *Fifth International Conference on Structural Engineering, Mechanics and Computation, 2013a Cape Town, South Africa*, 2013.
- [260] B. P. Gilbert, L. H. Teh, R. X. Badet, and K. J. R. Rasmussen, “The influence of pallets on the behaviour and design of drive-in steel storage racks–Part II: Design,” in *Research and Applications in Structural Engineering, Mechanics and Computation*, CRC Press, 2013, pp. 491–492.
- [261] A. Longinow, M. A. Salmon, and R. E. Welch, “Analysis of Drive-in and Drive-thru Storage Racks,” 1973.
- [262] K. Adamakos, S. Sesana, and I. Vayas, “Interaction between pallets and pallet beams of steel storage racks in seismic areas,” *International Journal of Steel Structures*, vol. 18, pp. 1018–1034, 2018.
- [263] F. Dhanens and Van Impe R., “Experimentelle traglastermittlung an dünnwandigen, über drei feldern genenden, stahlernen balken mit C-formigen, offenem querschnitt,” Ghent, Jun. 1992.
- [264] D. Camotim, A. D. Martins, P. B. Dinis, B. Young, M.-T. Chen, and A. Landesmann, “Mode interaction in cold-formed steel members: state-of-art report: Part 1: Fundamentals and local-distortional coupling,” *Steel Construction*, vol. 13, no. 3, pp. 165–185, 2020.
- [265] D. Camotim, A. D. Martins, P. B. Dinis, B. Young, M.-T. Chen, and A. Landesmann, “Mode interaction in cold-formed steel members: state-of-art report: Part 2: Couplings involving global buckling,” *Steel Construction*, vol. 13, no. 3, pp. 186–207, 2020.
- [266] CEN, “EN1993-1-8: Design of steel structures - Part 1-8: Design of joints,” Brussels, 2005.
- [267] L. Saufnay and J.-F. Demonceau, “Stability behaviour of cold-formed elements for storage racks,” Jul. 2023. [Online]. Available: <https://orbi.uliege.be/handle/2268/307017>
- [268] T. Moreau, “Comportement tridimensionnel d’éléments porteurs de racks de stockage [Master’s thesis],” University of Liège, Liège, 1995.
- [269] CEN, “FprEN1993-1-3:2023: Eurocode 3 - Design of steel structures - Part 1-3: General rules - Supplementary rules for cold-formed members and sheeting,” Brussels, Oct. 2023.
- [270] CEN, “EN15620: Steel static storage systems - Adjustable pallet racking - Tolerances, deformations and clearances,” Brussels, Oct. 2008.

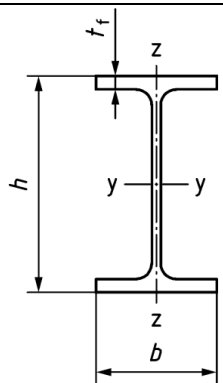
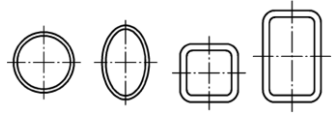
-
- [271] CEN, “EN10346: Continuously hot-dip coated steel flat products for cold forming — Technical delivery conditions,” Brussels, 2015.
- [272] L. Zhang and J. P. Jaspart, “Stability of members in compression made of large hot-rolled and welded angles,” *Université de Liège*, 2013.
- [273] ADEME - Agence de la transition écologique, “Impact CO2 - Le site de ressources qui vulgarise et valorise les données environnementales de l’ADEME.,” Calculer l’impact carbone des moyens de transport. Accessed: Aug. 21, 2024. [Online]. Available: <https://impactco2.fr/outils/transport>
- [274] T. Wansart, “Neo & Nea, agissons ensemble, maintenant,” Actions individuelles. Accessed: Aug. 21, 2024. [Online]. Available: <https://neonea.be/fr/agir/?type=individual>
- [275] Eurofer (The European Steel Association), “European Steel in Figures 2024,” Brussels, 2024. Accessed: Aug. 21, 2024. [Online]. Available: <https://www.eurofer.eu/assets/publications/brochures-booklets-and-factsheets/european-steel-in-figures-2024/European-Steel-In-Figures-2024-v2.pdf>

Appendices

Appendix A

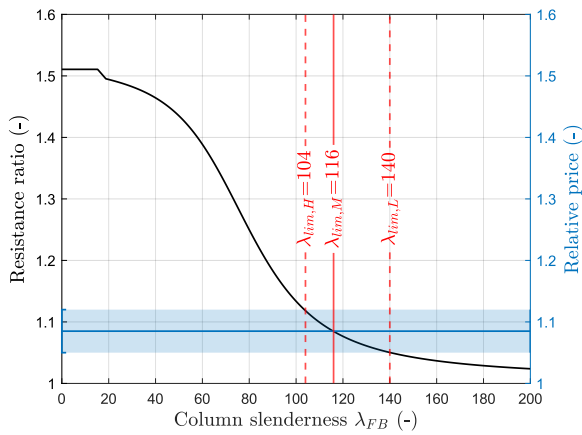
Slenderness limits for columns

Appendix A contains the various charts established in this thesis for columns, including the reference slenderness limits. These limits are set at a level below which a grade presents an economic benefit to be used in accordance with the standard FprEN1993-1-1:2022 [52]. The aforementioned limits are reported for all cases and grades covered in the thesis, with the tables below providing an explanation of the various captions and the relative prices between successive grades.

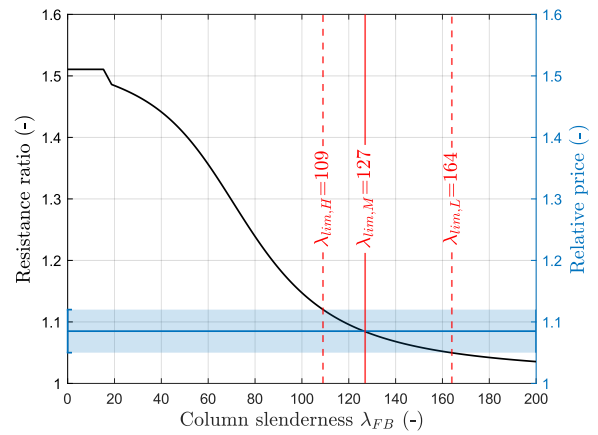
Cross-section		Limits	Buckling about axis	FprEN1993-1-1:2022		Caption letter	
				S235-S420	S460 up to S700 inclusive		
Rrolled I- or H-sections		$h/b > 1.2$	$t_f \leq 40 \text{ mm}$	y-y	a	a_0	(a)
				z-z	b	a	(b)
			$t_f > 40 \text{ mm}$	y-y	b	a	(b)
				z-z	c	b	(c)
		$h/b \leq 1.2$	$t_f \leq 100 \text{ mm}$	y-y	b	a	(b)
				z-z	c	b	(c)
			$t_f > 100 \text{ mm}$	y-y	d	c	(d)
				z-z	d	c	(d)
Hollow sections		Hot-finished	any	a	a_0	(a)	
		Cold-formed	any	c	c	(e)	

Price Level	Relative prices						
	S355/S235	S420/S355	S460/S420	S500/S460	S550/S500	S600/S550	S700/S600
Low	1.050	1.014	1.009	1.009	1.012	1.013	1.022
Med.	1.085	1.029	1.018	1.017	1.022	1.022	1.089
High	1.120	1.045	1.026	1.025	1.031	1.029	1.145

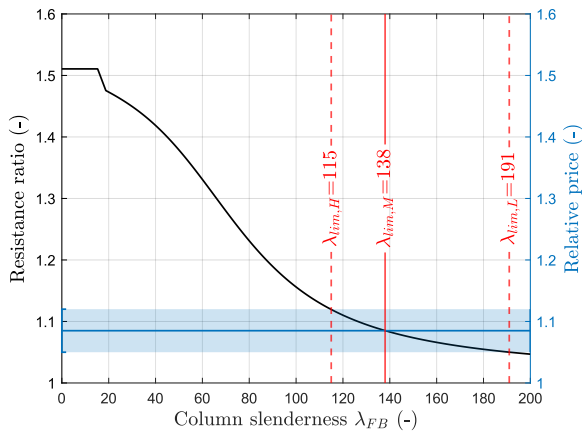
A.1. Grade S355 vs. S235



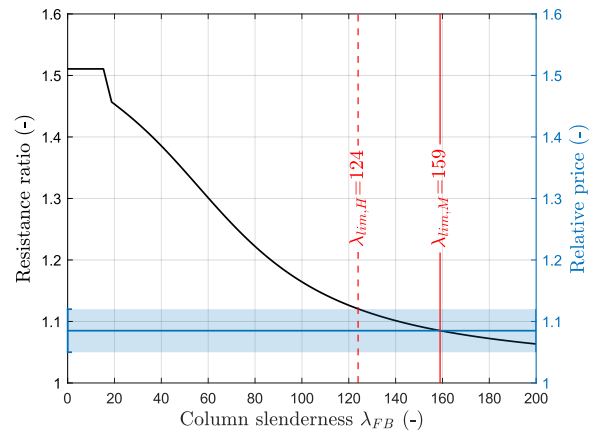
(a) Rolled: $h/b > 1.2 / t_f \leq 40$ mm / major axis & Hot-finished hollow sections



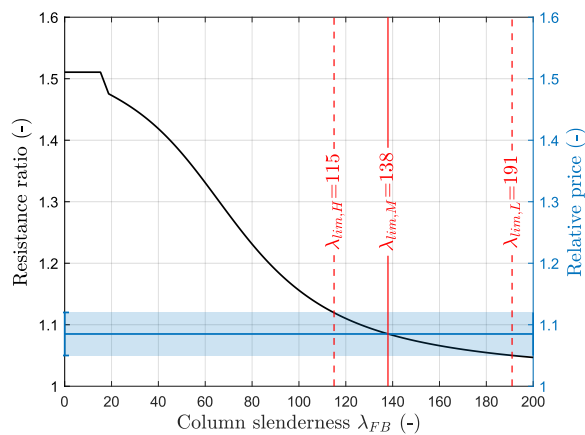
(b) Rolled: $h/b > 1.2 / t_f \leq 40$ mm / minor axis & Rolled: $h/b > 1.2 / t_f > 40$ mm / major axis & Rolled: $h/b \leq 1.2 / t_f \leq 100$ mm / major axis



(c) Rolled: $h/b > 1.2 / t_f > 40$ mm / minor axis & Rolled: $h/b \leq 1.2 / t_f \leq 100$ mm / minor axis

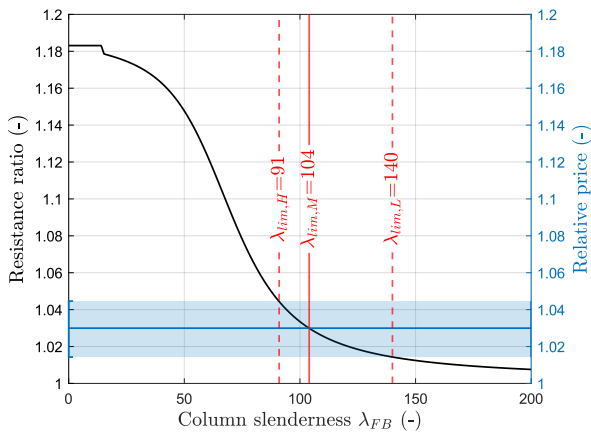


(d) Rolled: $h/b \leq 1.2 / t_f > 100$ mm / major axis & Rolled: $h/b \leq 1.2 / t_f > 100$ mm / minor axis

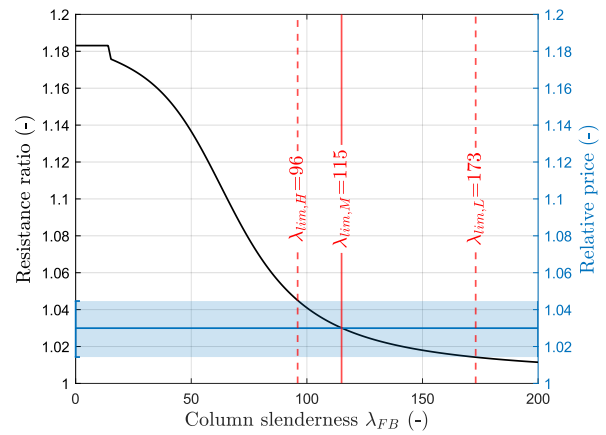


(e) Cold-formed hollow sections

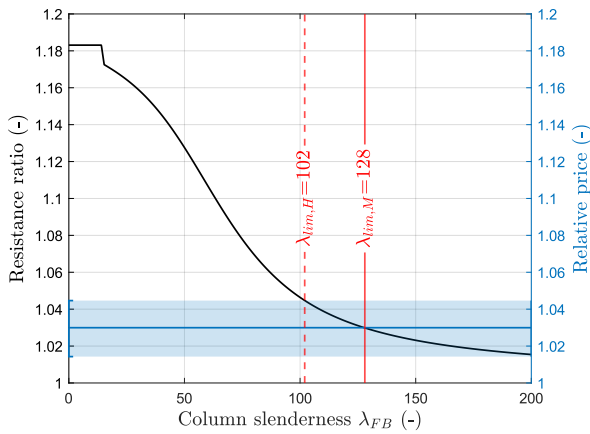
A.2. Grade S420 vs. S355



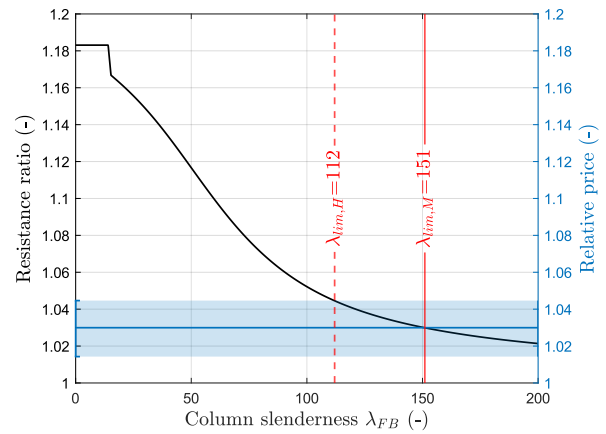
(a) Rolled: $h/b > 1.2 / t_f \leq 40$ mm / major axis & Hot-finished hollow sections



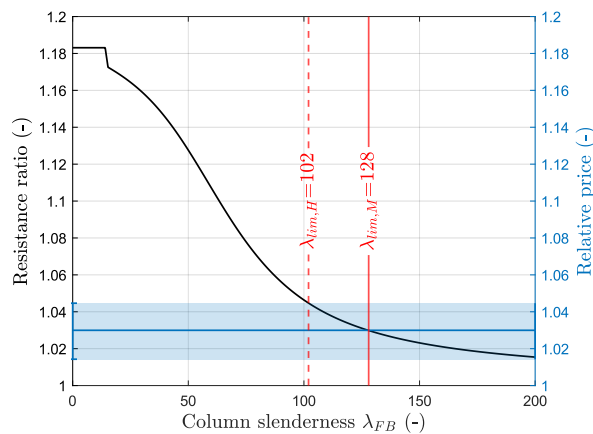
(b) Rolled: $h/b > 1.2 / t_f \leq 40$ mm / minor axis & Rolled: $h/b > 1.2 / t_f > 40$ mm / major axis & Rolled: $h/b \leq 1.2 / t_f \leq 100$ mm / major axis



(c) Rolled: $h/b > 1.2 / t_f > 40$ mm / minor axis & Rolled: $h/b \leq 1.2 / t_f \leq 100$ mm / minor axis

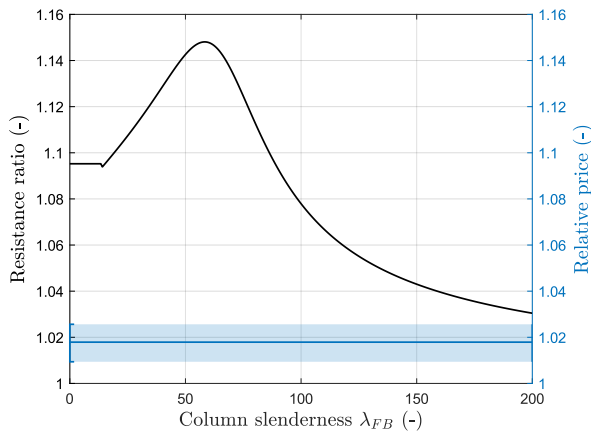


(d) Rolled: $h/b \leq 1.2 / t_f > 100$ mm / major axis & Rolled: $h/b \leq 1.2 / t_f > 100$ mm / minor axis

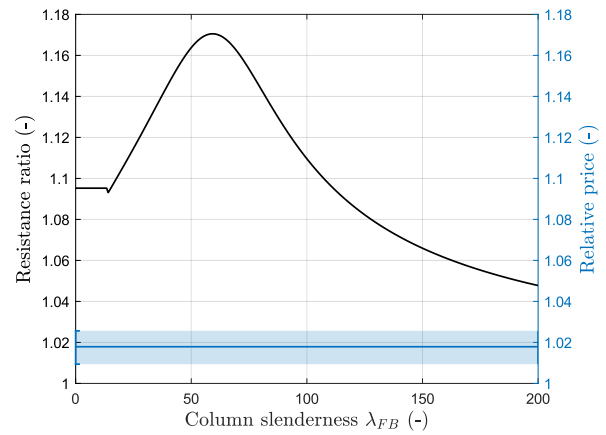


(e) Cold-formed hollow sections

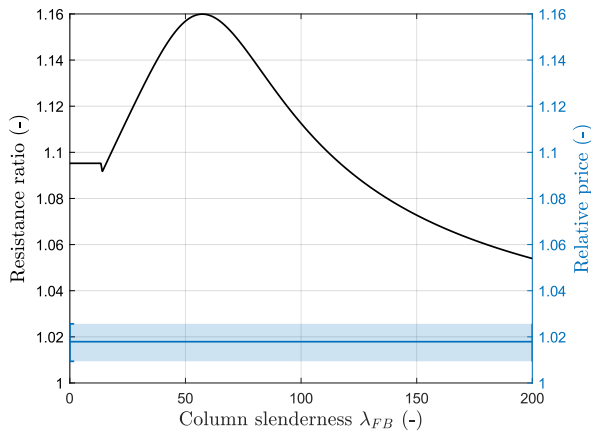
A.3. Grade S460 vs. S420



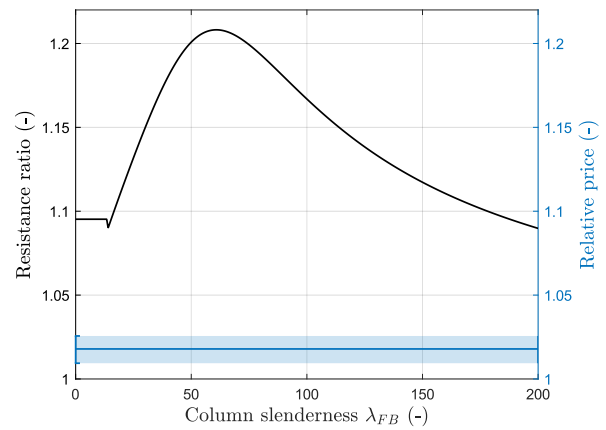
(a) Rolled: $h/b > 1.2 / t_f \leq 40$ mm / major axis & Hot-finished hollow sections



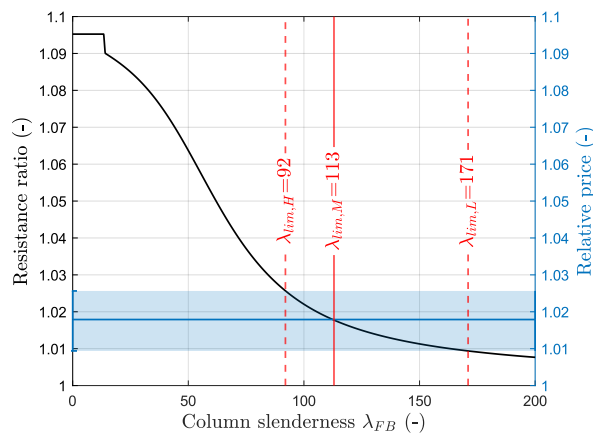
(b) Rolled: $h/b > 1.2 / t_f \leq 40$ mm / minor axis & Rolled: $h/b > 1.2 / t_f > 40$ mm / major axis & Rolled: $h/b \leq 1.2 / t_f \leq 100$ mm / major axis



(c) Rolled: $h/b > 1.2 / t_f > 40$ mm / minor axis & Rolled: $h/b \leq 1.2 / t_f \leq 100$ mm / minor axis



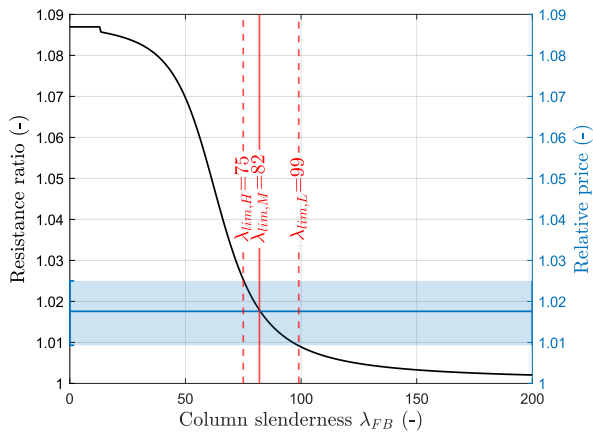
(d) Rolled: $h/b \leq 1.2 / t_f > 100$ mm / major axis & Rolled: $h/b \leq 1.2 / t_f > 100$ mm / minor axis



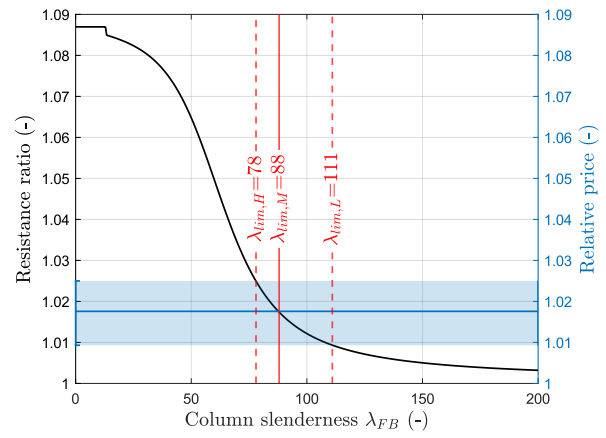
(e) Cold-formed hollow sections

Note: the resistance ratios above the yield strength ratio observed in this comparison can be attributed to the different buckling curves prescribed for the S420 and S460 grades. Indeed, the current stepwise evolution in FprEN1993-1-1:2022 [52] implies to have one buckling curve of gap between the S420 and S460 grades, which is highly beneficial to the S460 grade.

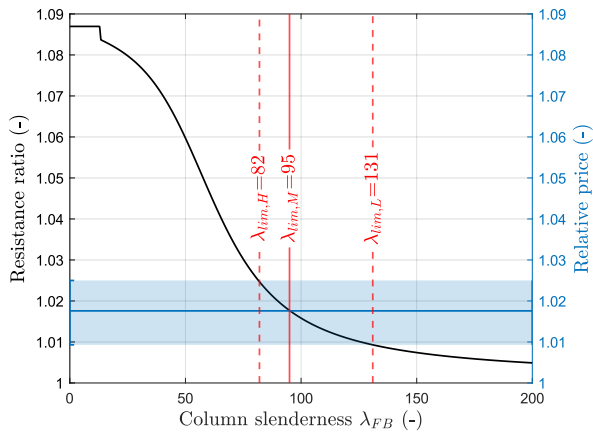
A.4. Grade S500 vs. S460



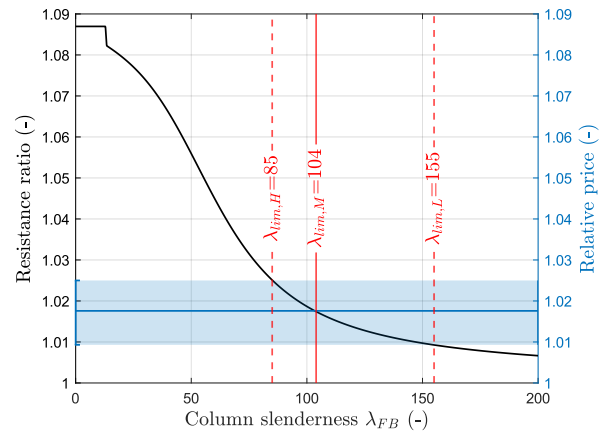
(a) Rolled: $h/b > 1.2 / t_f \leq 40$ mm / major axis & Hot-finished hollow sections



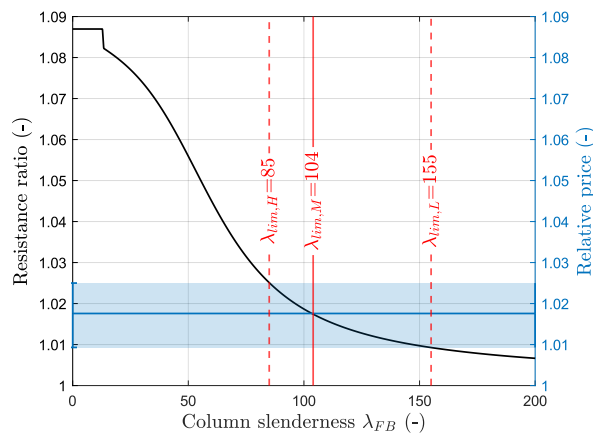
(b) Rolled: $h/b > 1.2 / t_f \leq 40$ mm / minor axis & Rolled: $h/b > 1.2 / t_f > 40$ mm / major axis & Rolled: $h/b \leq 1.2 / t_f \leq 100$ mm / major axis



(c) Rolled: $h/b > 1.2 / t_f > 40$ mm / minor axis & Rolled: $h/b \leq 1.2 / t_f \leq 100$ mm / minor axis

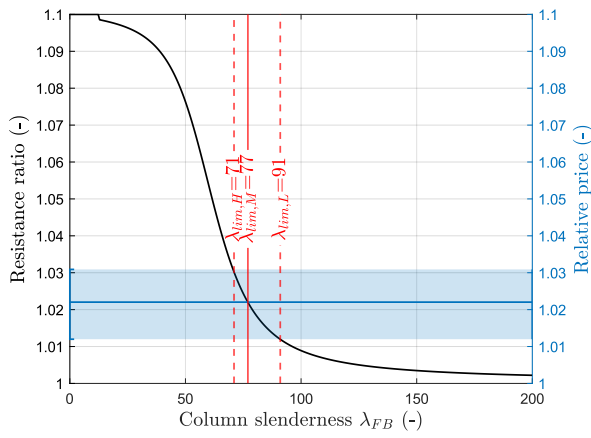


(d) Rolled: $h/b \leq 1.2 / t_f > 100$ mm / major axis & Rolled: $h/b \leq 1.2 / t_f > 100$ mm / minor axis

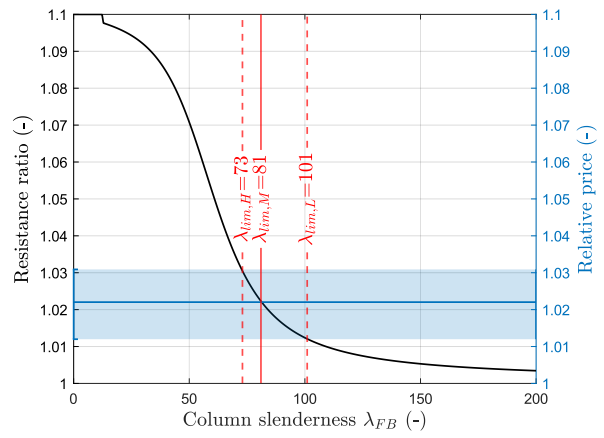


(e) Cold-formed hollow sections

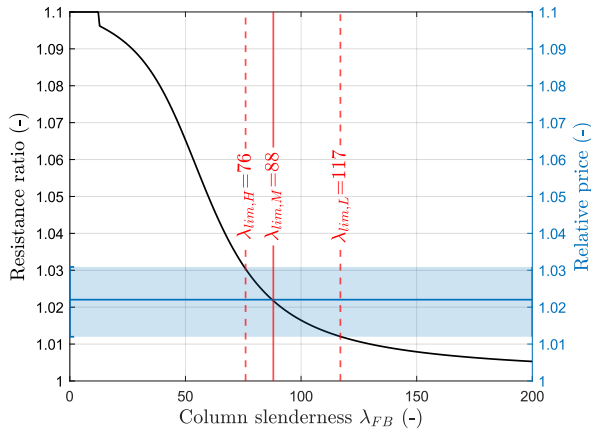
A.5. Grade S550 vs. S500



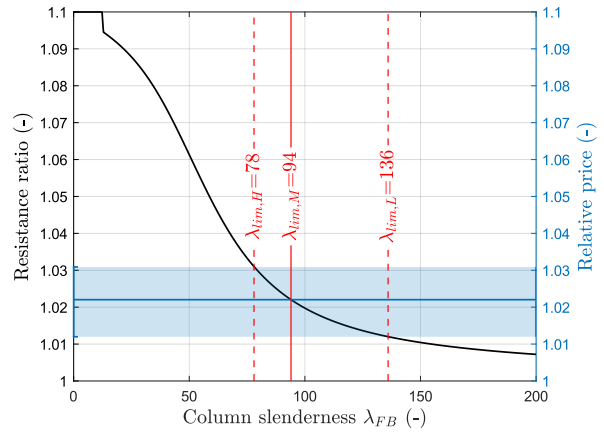
(a) Rolled: $h/b > 1.2 / t_f \leq 40$ mm / major axis & Hot-finished hollow sections



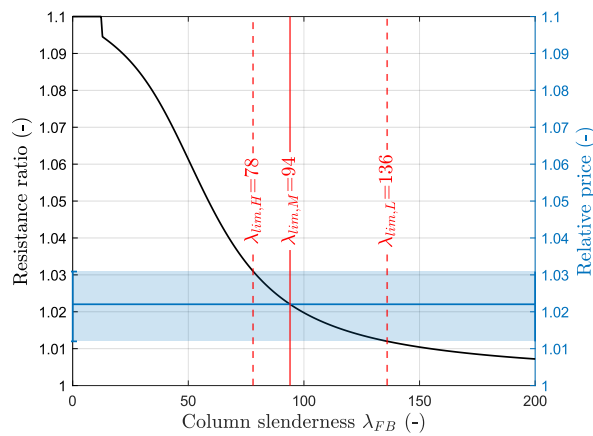
(b) Rolled: $h/b > 1.2 / t_f \leq 40$ mm / minor axis & Rolled: $h/b > 1.2 / t_f > 40$ mm / major axis & Rolled: $h/b \leq 1.2 / t_f \leq 100$ mm / major axis



(c) Rolled: $h/b > 1.2 / t_f > 40$ mm / minor axis & Rolled: $h/b \leq 1.2 / t_f \leq 100$ mm / minor axis

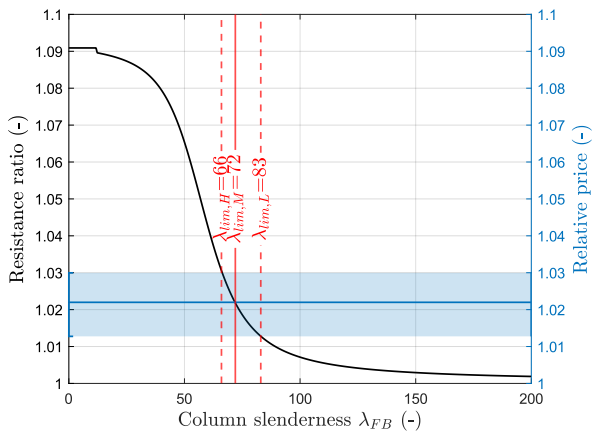


(d) Rolled: $h/b \leq 1.2 / t_f > 100$ mm / major axis & Rolled: $h/b \leq 1.2 / t_f > 100$ mm / minor axis

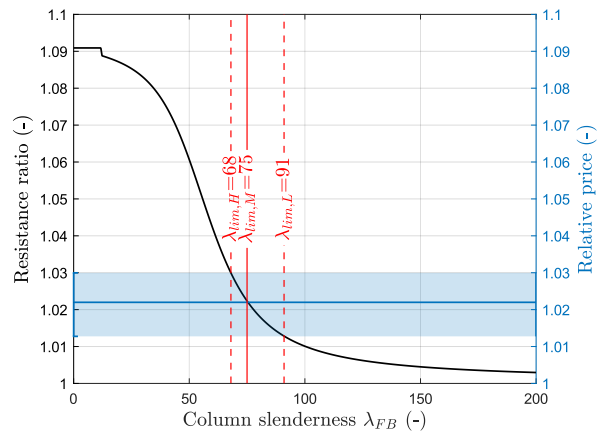


(e) Cold-formed hollow sections

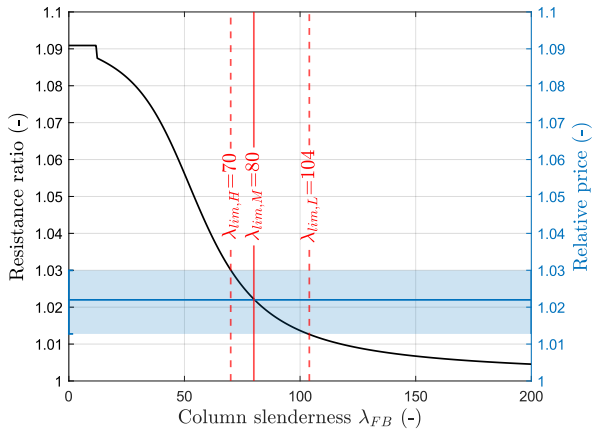
A.6. Grade S600 vs. S550



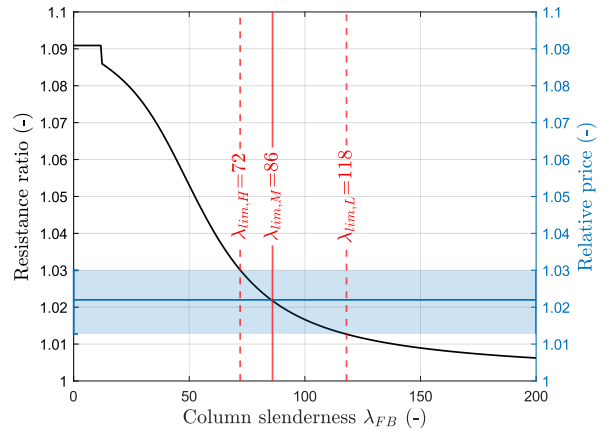
(a) Rolled: $h/b > 1.2 / t_f \leq 40$ mm / major axis & Hot-finished hollow sections



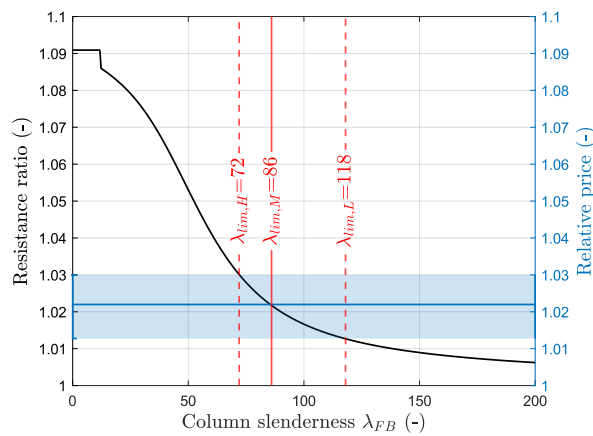
(b) Rolled: $h/b > 1.2 / t_f \leq 40$ mm / minor axis & Rolled: $h/b > 1.2 / t_f > 40$ mm / major axis & Rolled: $h/b \leq 1.2 / t_f \leq 100$ mm / major axis



(c) Rolled: $h/b > 1.2 / t_f > 40$ mm / minor axis & Rolled: $h/b \leq 1.2 / t_f \leq 100$ mm / minor axis

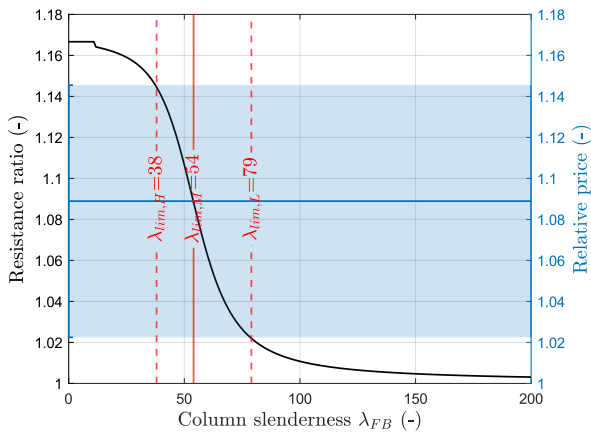


(d) Rolled: $h/b \leq 1.2 / t_f > 100$ mm / major axis & Rolled: $h/b \leq 1.2 / t_f > 100$ mm / minor axis

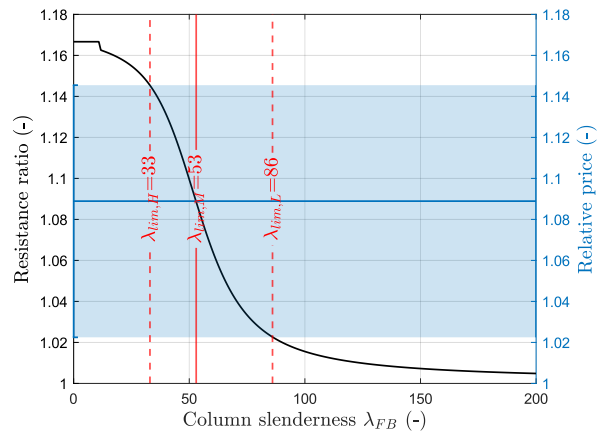


(e) Cold-formed hollow sections

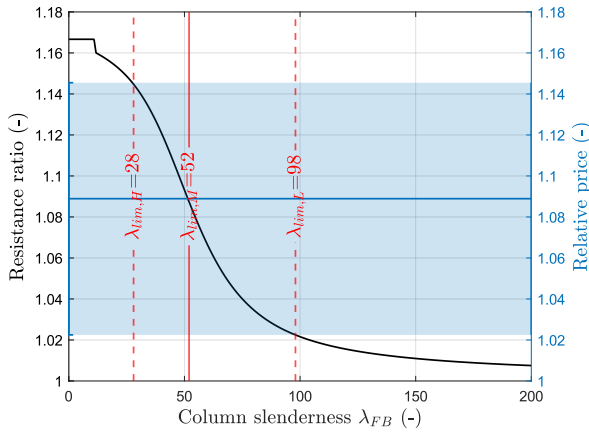
A.7. Grade S700 vs. S600



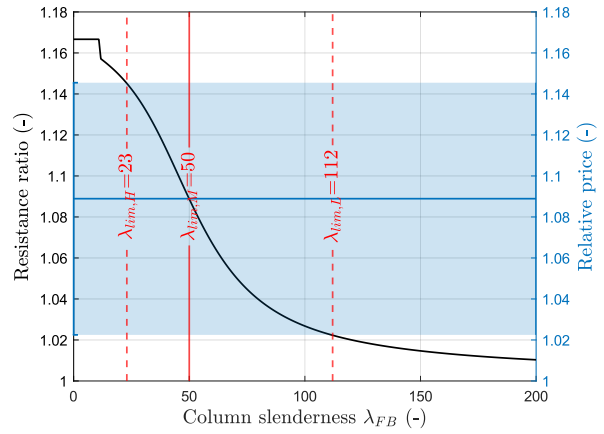
(a) Rolled: $h/b > 1.2 / t_f \leq 40$ mm / major axis & Hot-finished hollow sections



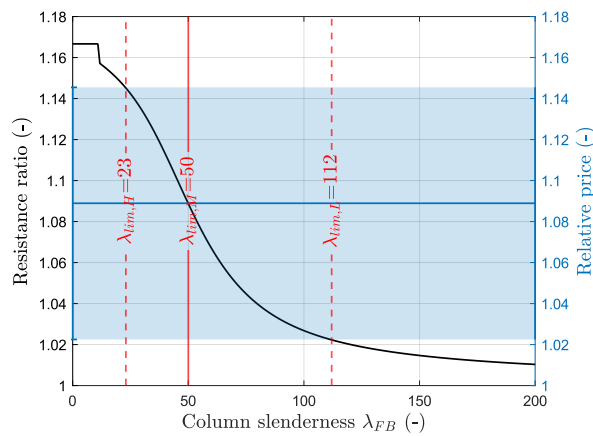
(b) Rolled: $h/b > 1.2 / t_f \leq 40$ mm / minor axis & Rolled: $h/b > 1.2 / t_f > 40$ mm / major axis & Rolled: $h/b \leq 1.2 / t_f \leq 100$ mm / major axis



(c) Rolled: $h/b > 1.2 / t_f > 40$ mm / minor axis & Rolled: $h/b \leq 1.2 / t_f \leq 100$ mm / minor axis

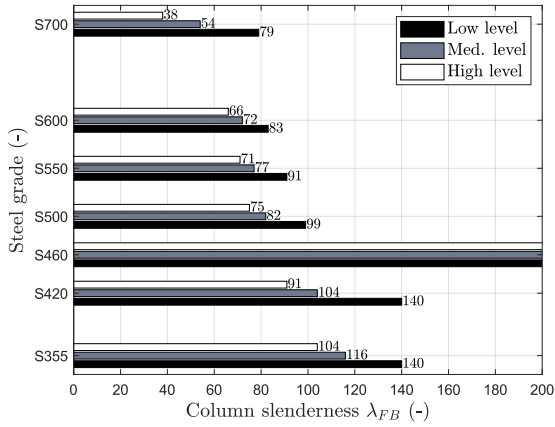


(d) Rolled: $h/b \leq 1.2 / t_f > 100$ mm / major axis & Rolled: $h/b \leq 1.2 / t_f > 100$ mm / minor axis

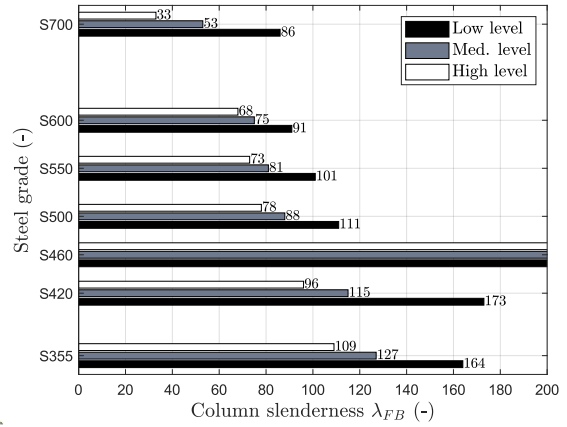


(e) Cold-formed hollow sections

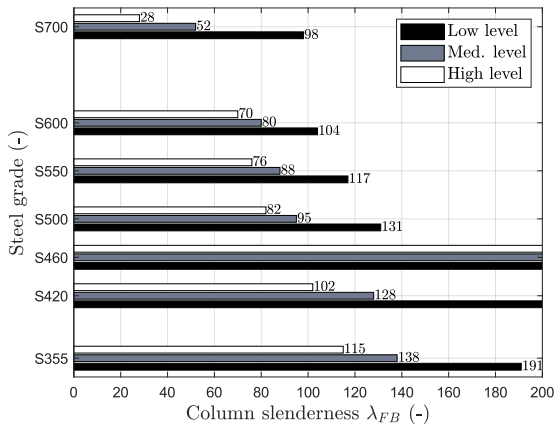
A.8. Summary of reference slenderness limits



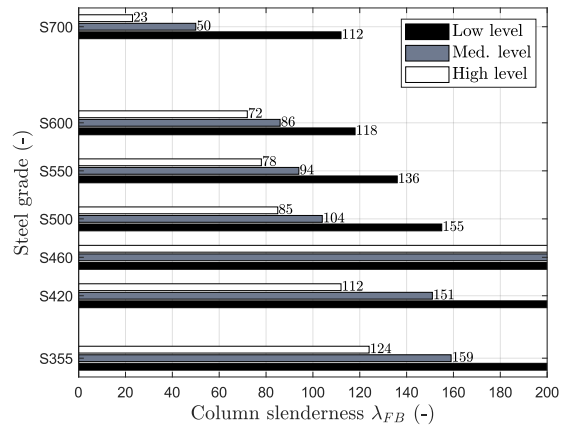
(a) Rolled: $h/b > 1.2 / t_f \leq 40$ mm / major axis & Hot-finished hollow sections



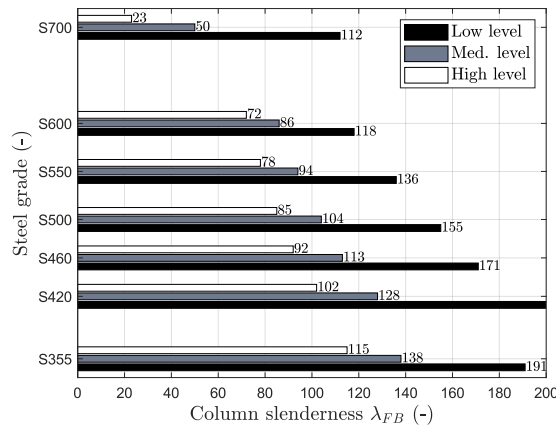
(b) Rolled: $h/b > 1.2 / t_f \leq 40$ mm / minor axis & Rolled: $h/b > 1.2 / t_f > 40$ mm / major axis & Rolled: $h/b \leq 1.2 / t_f \leq 100$ mm / major axis



(c) Rolled: $h/b > 1.2 / t_f > 40$ mm / minor axis & Rolled: $h/b \leq 1.2 / t_f \leq 100$ mm / minor axis



(d) Rolled: $h/b \leq 1.2 / t_f > 100$ mm / major axis & Rolled: $h/b \leq 1.2 / t_f > 100$ mm / minor axis

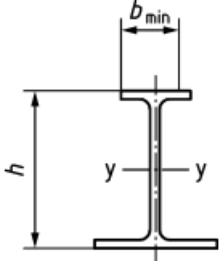


(e) Cold-formed hollow sections

Appendix B

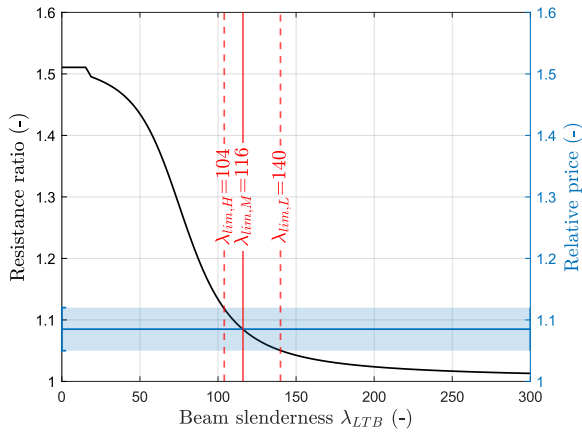
Slenderness limits for beams

Appendix B contains the various charts established in this thesis for beams, including the reference slenderness limits. These limits are set at a level below which a grade presents an economic benefit to be used in accordance with the standard FprEN1993-1-1:2022 [52]. The aforementioned limits are reported for all cases and grades covered in the thesis, with the tables below providing an explanation of the various captions and the relative prices between successive grades.

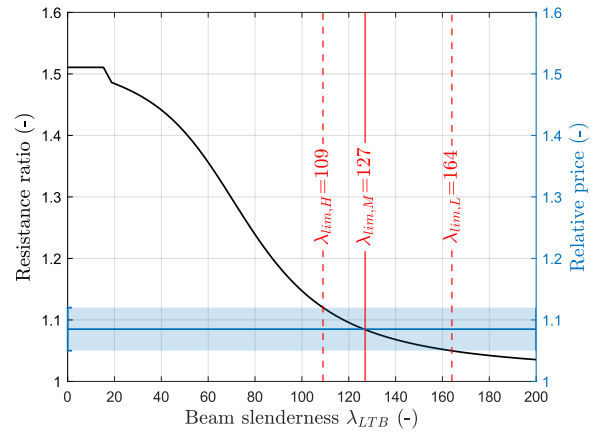
Cross-section		Limits	Buckling curve	Caption letter
Rolled I-sections		$h/b \leq 2.0$	a	(a)
		$h/b > 2.0$	b	(b)

Price Level	Relative prices						
	S355/S235	S420/S355	S460/S420	S500/S460	S550/S500	S600/S550	S700/S600
Low	1.050	1.014	1.009	1.009	1.012	1.013	1.022
Med.	1.085	1.029	1.018	1.017	1.022	1.022	1.089
High	1.120	1.045	1.026	1.025	1.031	1.029	1.145

B.1. Grade S355 vs. S235

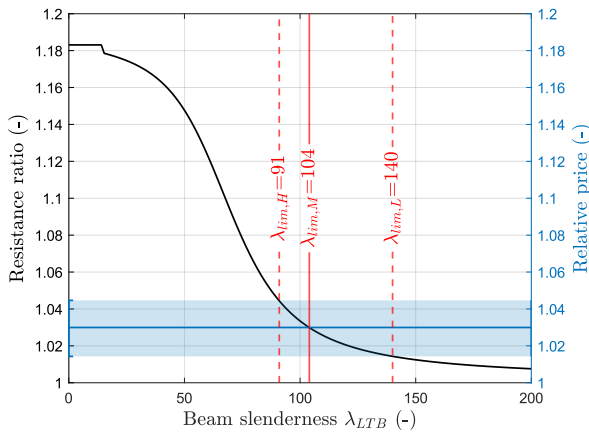


(a) $h/b \leq 1.2$

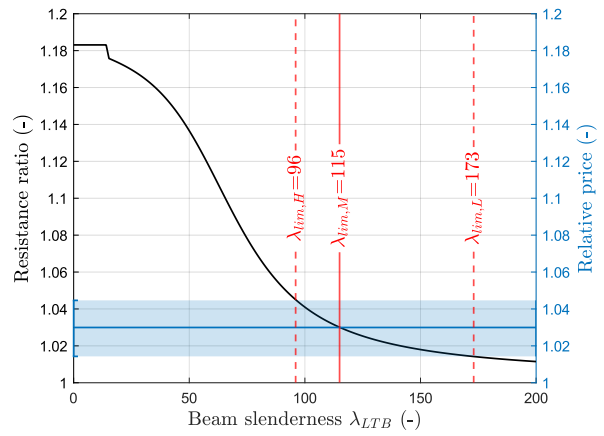


(b) $h/b > 1.2$

B.2. Grade S420 vs. S355

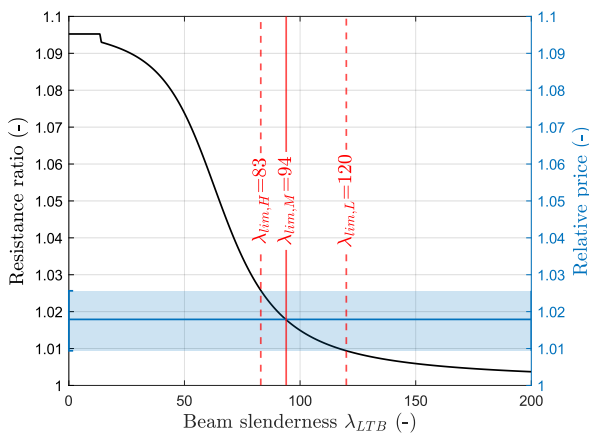


(a) $h/b \leq 1.2$

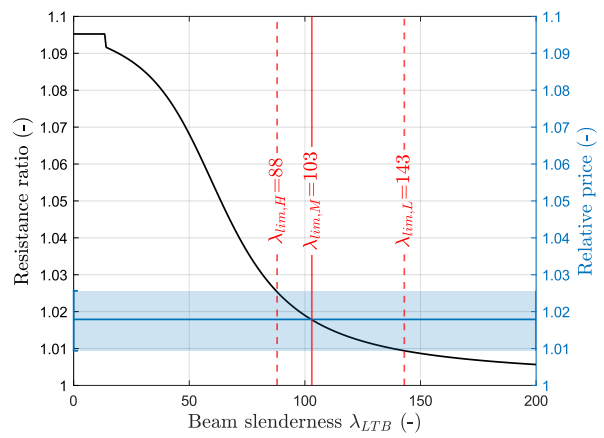


(b) $h/b > 1.2$

B.3. Grade S460 vs. S420

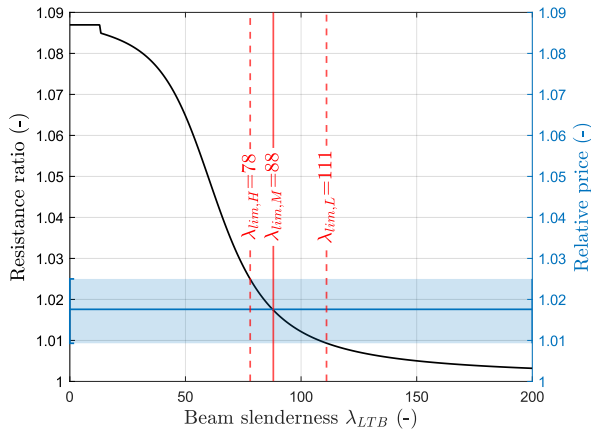


(a) $h/b \leq 1.2$

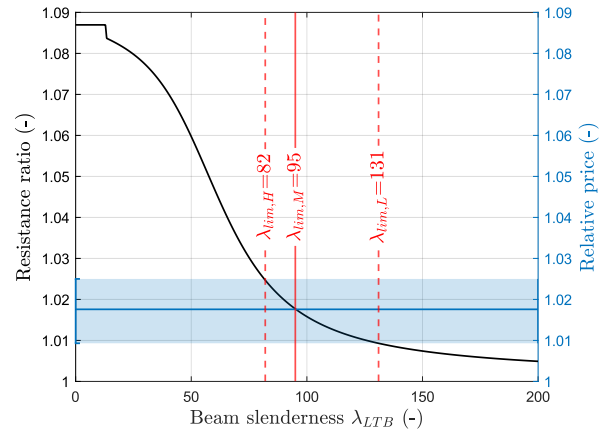


(b) $h/b > 1.2$

B.4. Grade S500 vs. S460

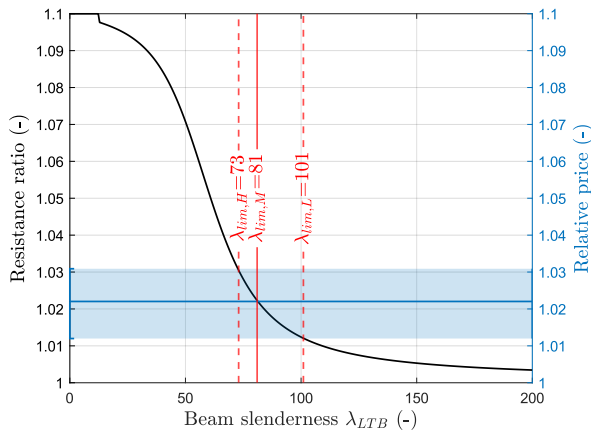


(a) $h/b \leq 1.2$

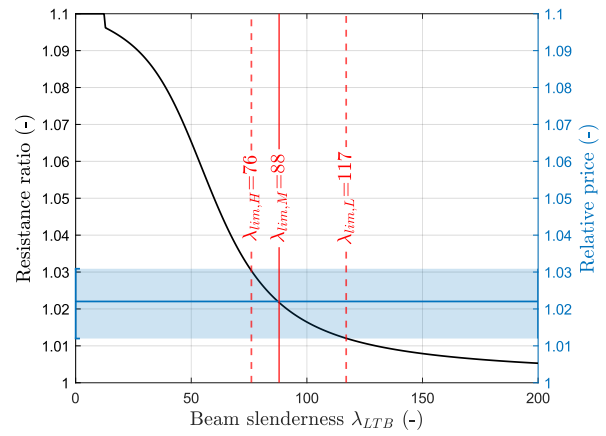


(b) $h/b > 1.2$

B.5. Grade S550 vs. S500

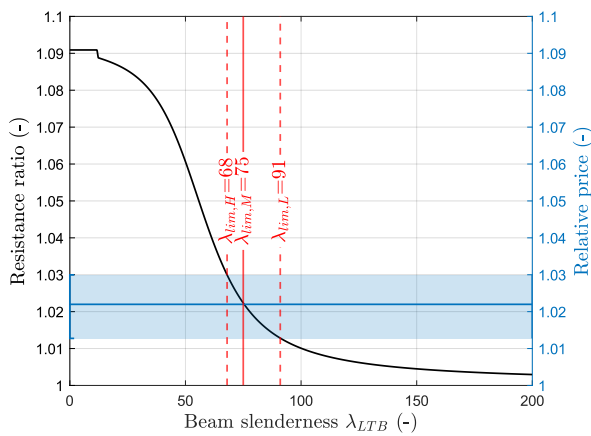


(a) $h/b \leq 1.2$

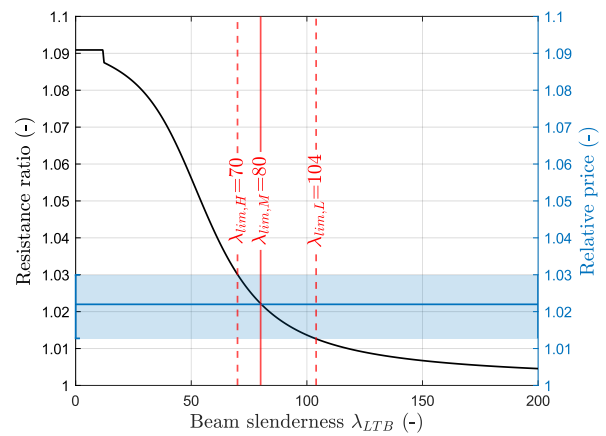


(b) $h/b > 1.2$

B.6. Grade S600 vs. S550

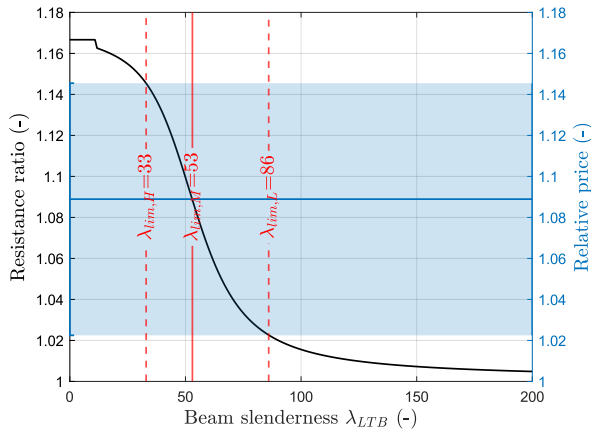


(a) $h/b \leq 1.2$

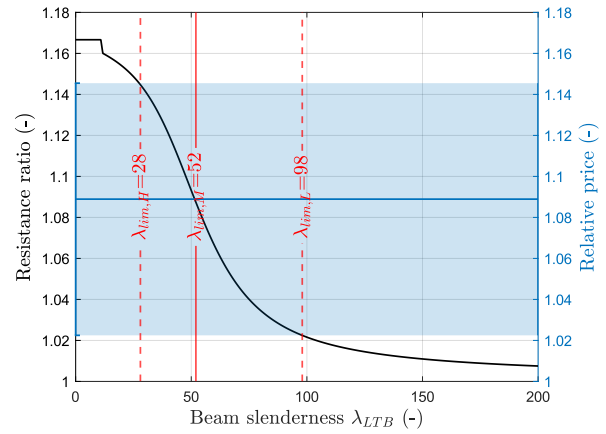


(b) $h/b > 1.2$

B.7. Grade S700 vs. S600

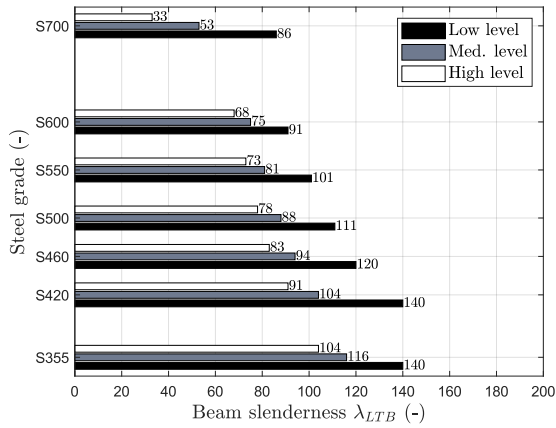


(a) $h/b \leq 1.2$

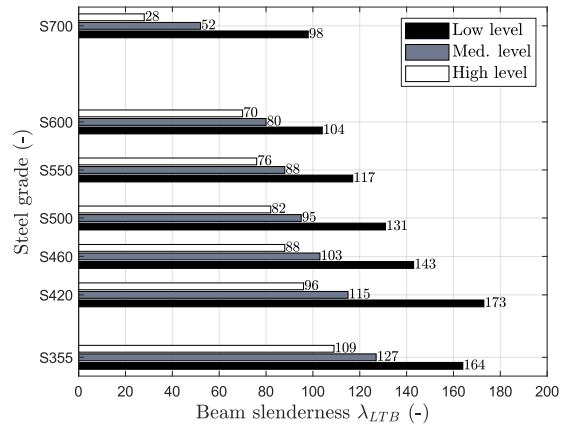


(b) $h/b > 1.2$

B.8. Summary of reference slenderness limits



(a) $h/b \leq 1.2$

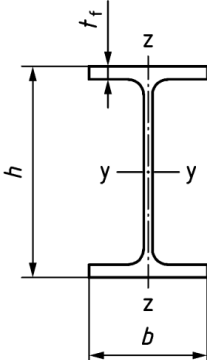
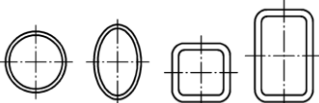


(b) $h/b > 1.2$

Appendix C

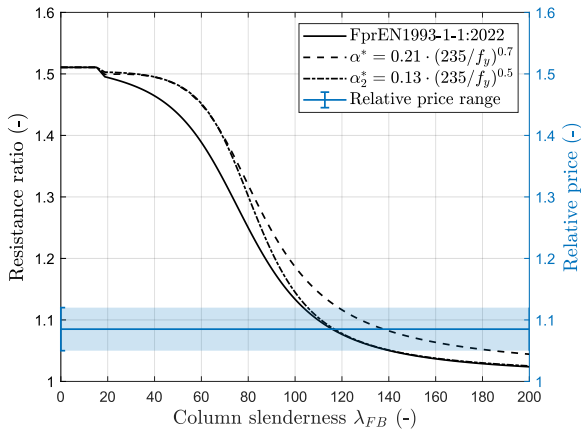
Impact of modified imperfection factors

Appendix C presents a comparison of the relative resistances between successive steel grades, as determined following the forthcoming version FprEN1993-1-1:2022 [52], and with the two modified imperfection factors established in Chapter 5. The following tables hereafter provide an explanation of the various captions and the relative prices.

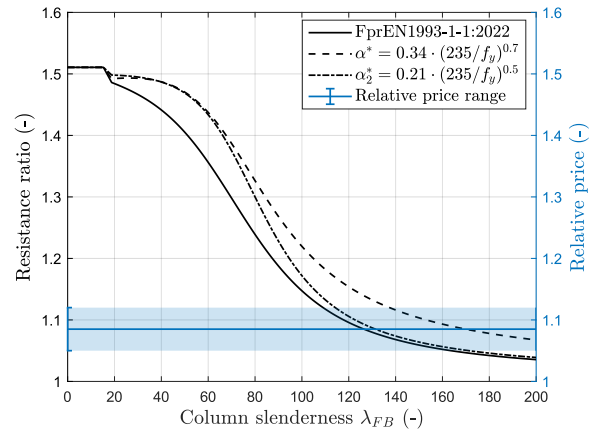
Cross-section		Limits		Buckling about axis	FprEN1993-1-1:2022		Caption letter
					S235-S420	S460 up to S700 inclusive	
Rolled I- or H-sections		$h/b \leq 1.2$	$t_f \leq 40 \text{ mm}$	y-y	a	a_0	(a)
				z-z	b	a	(b)
			$t_f > 40 \text{ mm}$	y-y	b	a	/
				z-z	c	b	/
		$h/b > 1.2$	$t_f \leq 100 \text{ mm}$	y-y	b	a	(c)
				z-z	c	b	(d)
$t_f > 100 \text{ mm}$	y-y	d	c	/			
	z-z	d	c	/			
Hollow sections		Hot-finished		any	a	a_0	(e)
		Cold-formed		any	c	c	/

Price Level	Relative prices						
	S355/S235	S420/S355	S460/S420	S500/S460	S550/S500	S600/S550	S700/S600
Low	1.050	1.014	1.009	1.009	1.012	1.013	1.022
Med.	1.085	1.029	1.018	1.017	1.022	1.022	1.089
High	1.120	1.045	1.026	1.025	1.031	1.029	1.145

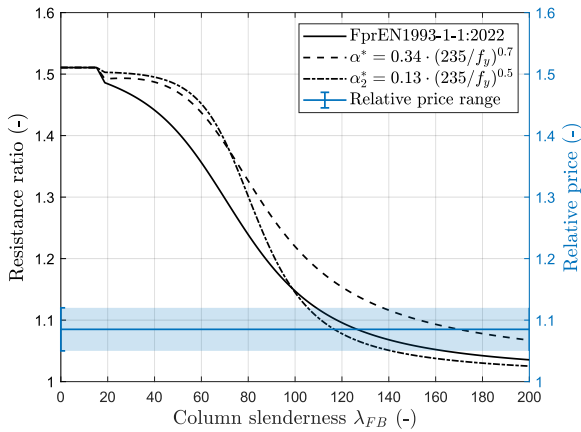
C.1. Grade S355 vs. S235



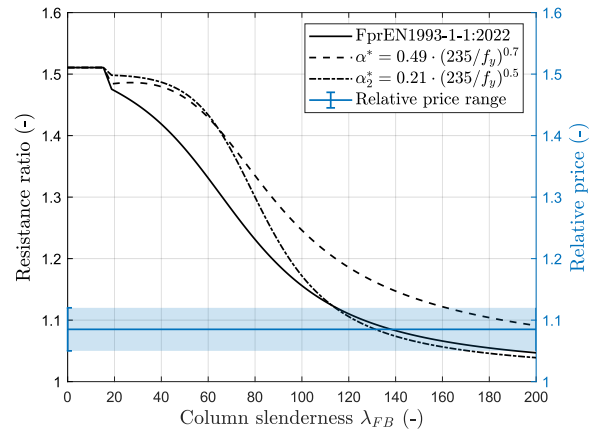
(a) Rolled: $h/b > 1.2$ / $t_f \leq 40$ mm / major axis



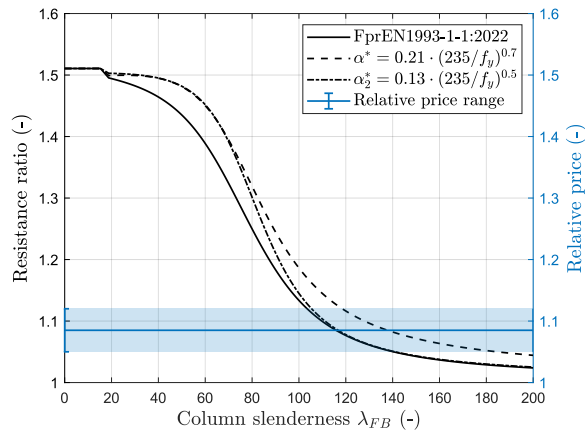
(b) Rolled: $h/b > 1.2$ / $t_f \leq 40$ mm / minor axis



(c) Rolled: $h/b \leq 1.2$ / $t_f \leq 100$ mm / major axis

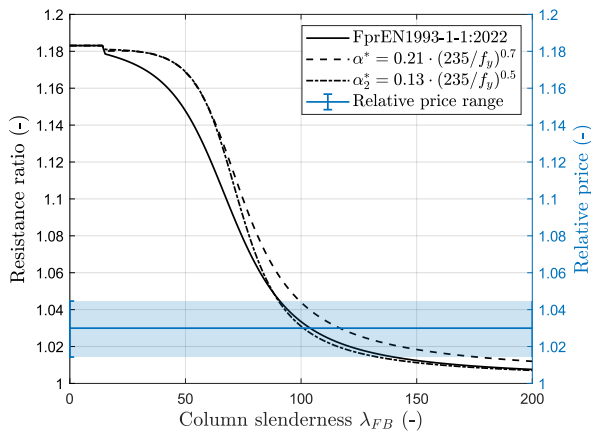
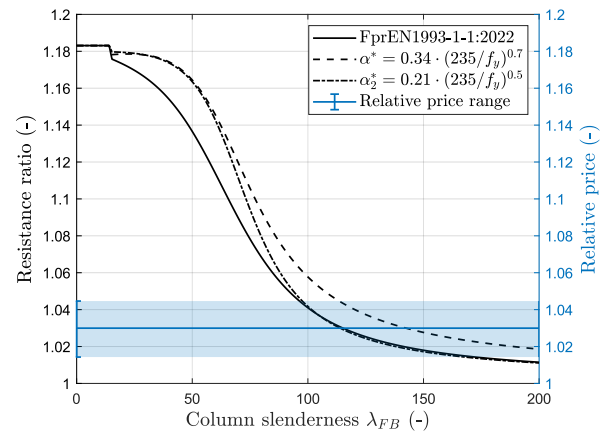
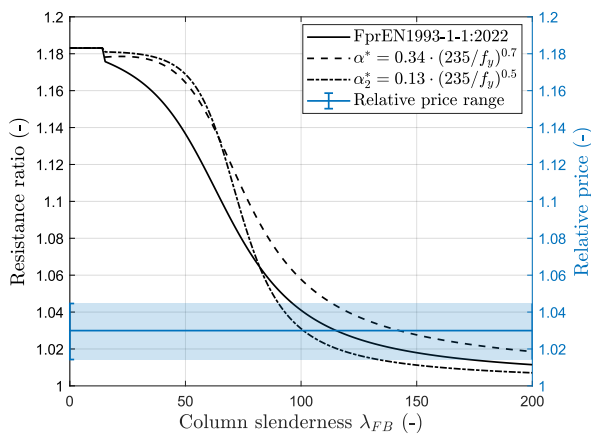
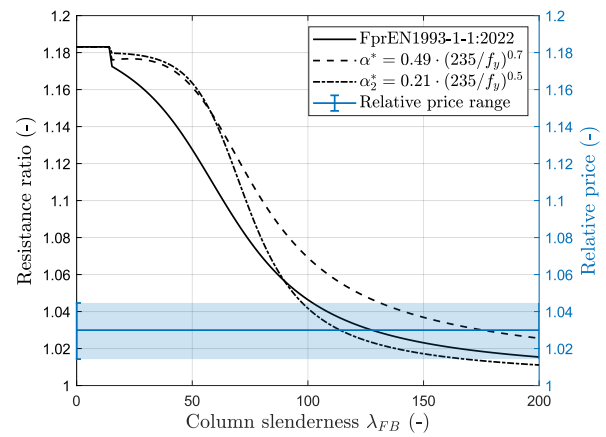
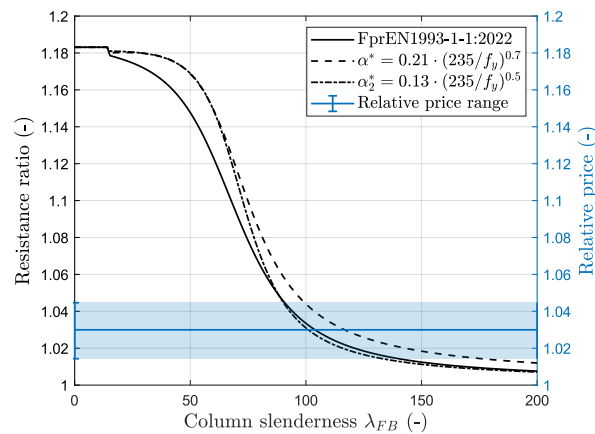


(d) Rolled: $h/b \leq 1.2$ / $t_f \leq 100$ mm / minor axis



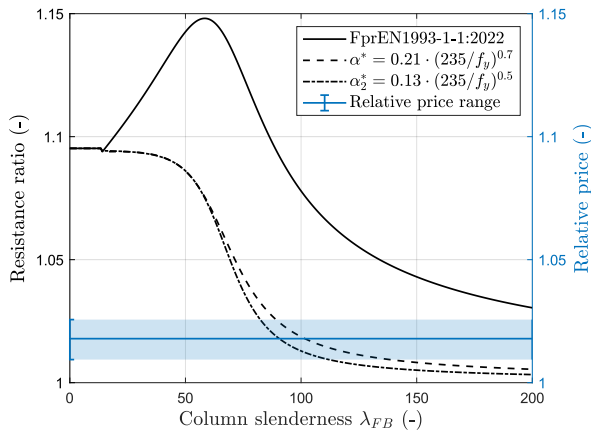
(e) Hot-finished hollow sections

C.2. Grade S420 vs. S355

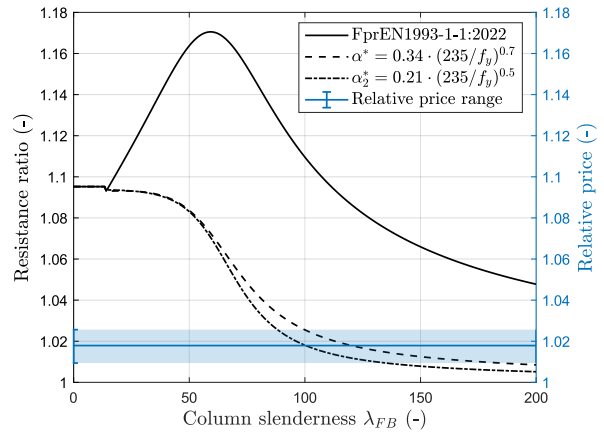
(a) Rolled: $h/b > 1.2 / t_f \leq 40$ mm / major axis(b) Rolled: $h/b > 1.2 / t_f \leq 40$ mm / minor axis(c) Rolled: $h/b \leq 1.2 / t_f \leq 100$ mm / major axis(d) Rolled: $h/b \leq 1.2 / t_f \leq 100$ mm / minor axis

(e) Hot-finished hollow sections

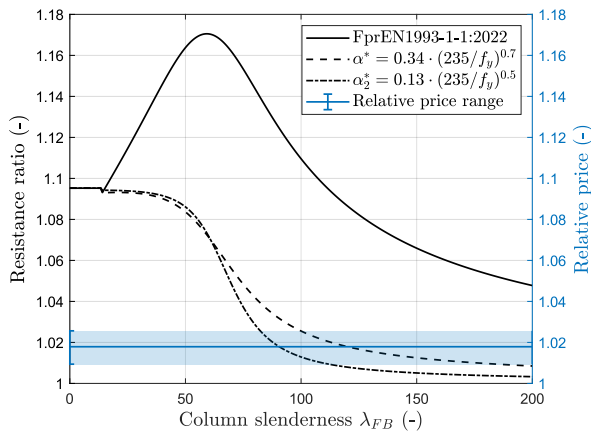
C.3. Grade S460 vs. S420



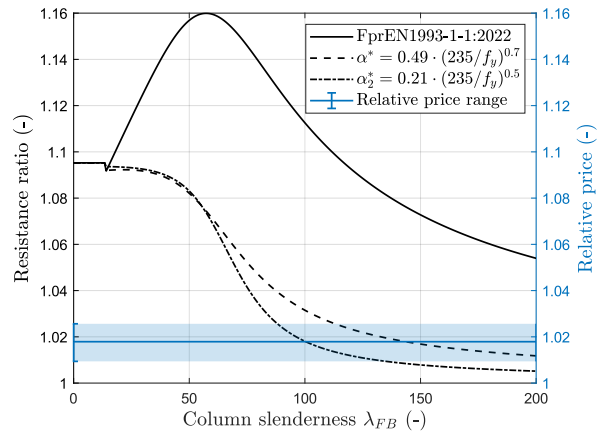
(a) Rolled: $h/b > 1.2 / t_f \leq 40$ mm / major axis



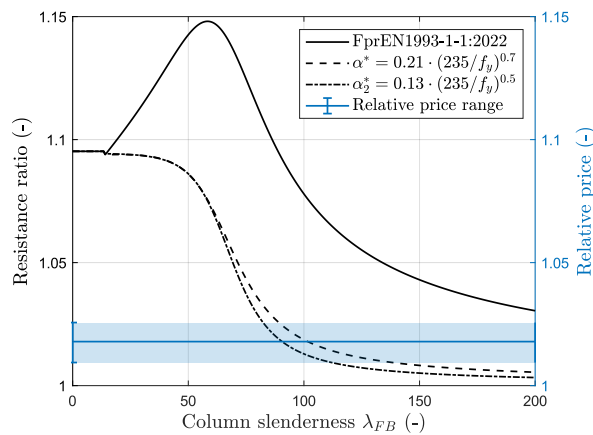
(b) Rolled: $h/b > 1.2 / t_f \leq 40$ mm / minor axis



(c) Rolled: $h/b \leq 1.2 / t_f \leq 100$ mm / major axis



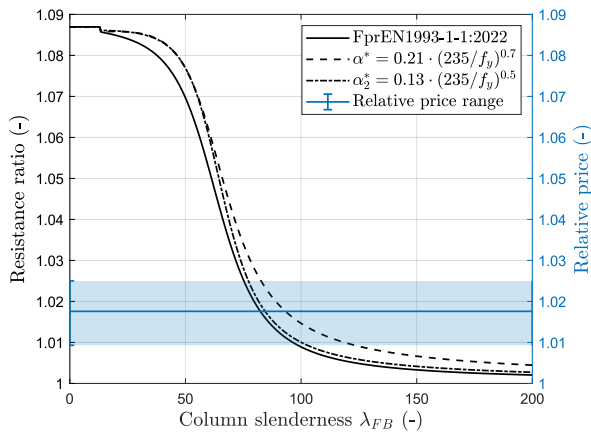
(d) Rolled: $h/b \leq 1.2 / t_f \leq 100$ mm / minor axis



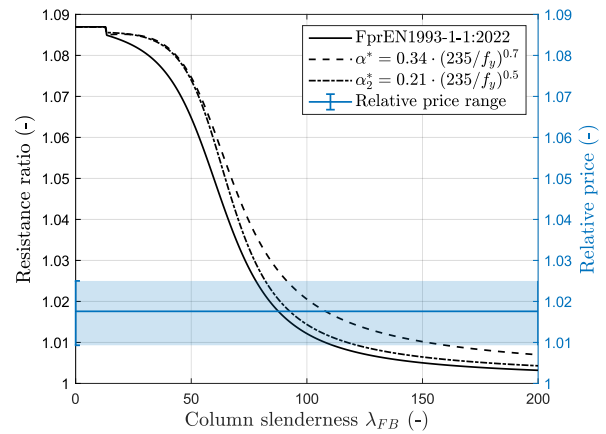
(e) Hot-finished hollow sections

Note: the resistance ratios above the yield strength ratio observed in this comparison can be attributed to the different buckling curves prescribed for the S420 and S460 grades. Indeed, the current stepwise evolution in FprEN1993-1-1:2022 [52] implies to have one buckling curve of gap between the S420 and S460 grades, which is highly beneficial to the S460 grade. Conversely, restoring continuity with modified imperfection factors eliminates this phenomenon.

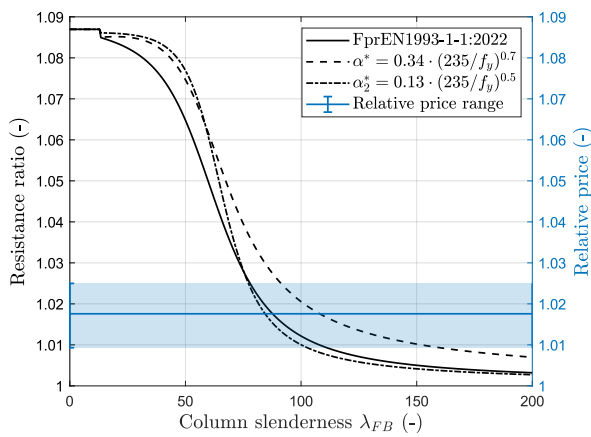
C.4. Grade S500 vs. S460



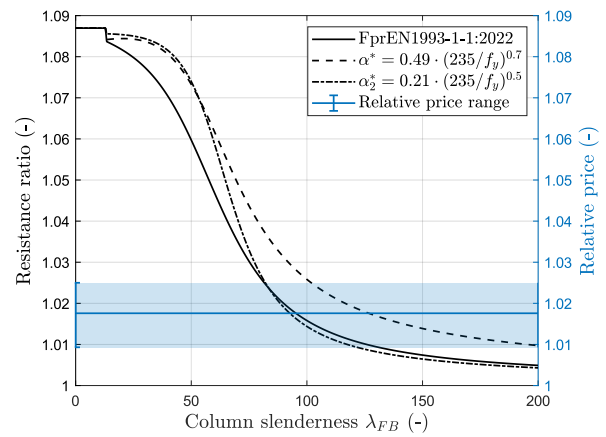
(a) Rolled: $h/b > 1.2 / t_f \leq 40$ mm / major axis



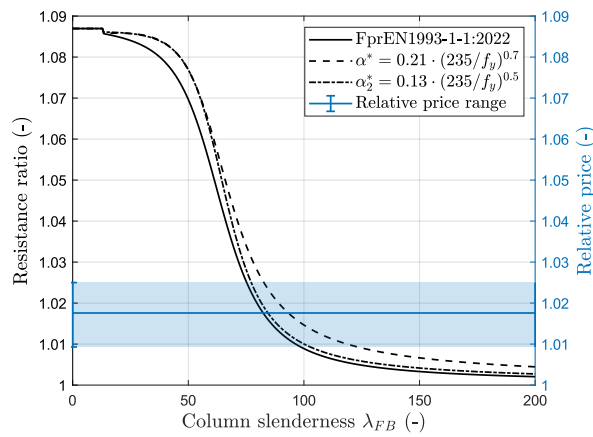
(b) Rolled: $h/b > 1.2 / t_f \leq 40$ mm / minor axis



(c) Rolled: $h/b \leq 1.2 / t_f \leq 100$ mm / major axis

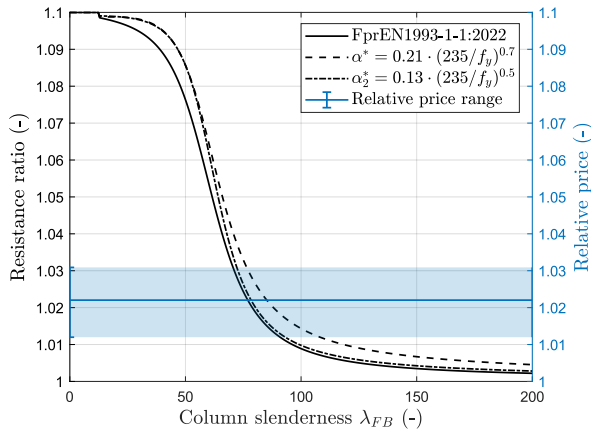


(d) Rolled: $h/b \leq 1.2 / t_f \leq 100$ mm / minor axis

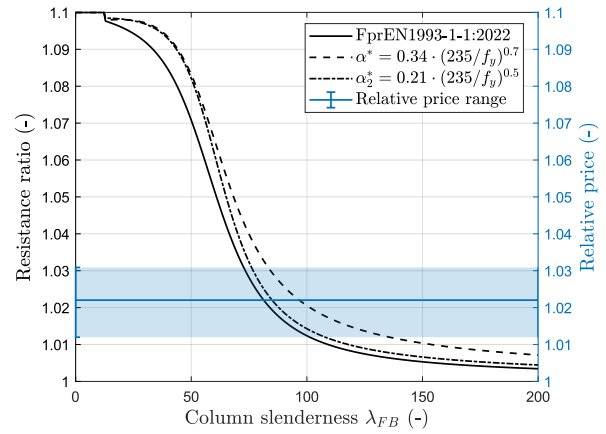


(e) Hot-finished hollow sections

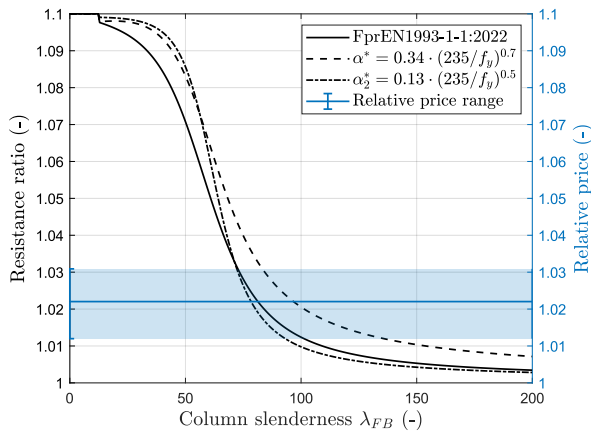
C.5. Grade S550 vs. S500



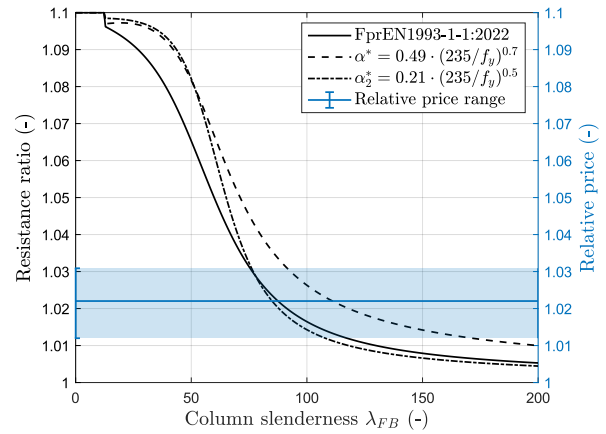
(a) Rolled: $h/b > 1.2$ / $t_f \leq 40$ mm / major axis



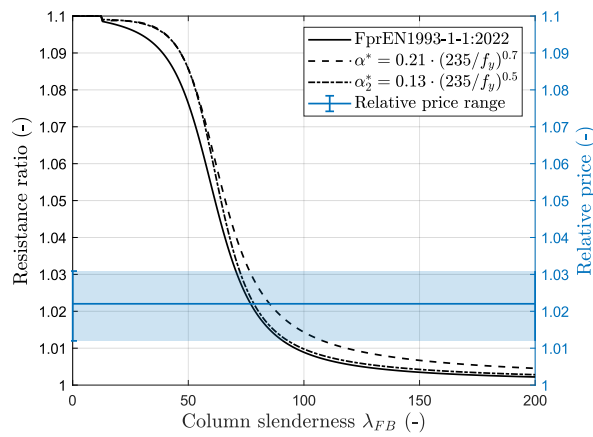
(b) Rolled: $h/b > 1.2$ / $t_f \leq 40$ mm / minor axis



(c) Rolled: $h/b \leq 1.2$ / $t_f \leq 100$ mm / major axis

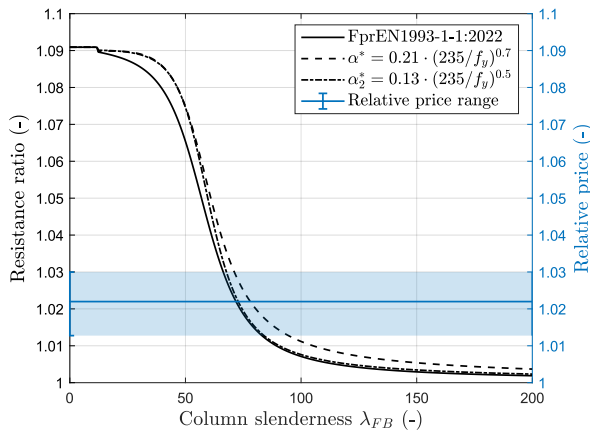


(d) Rolled: $h/b \leq 1.2$ / $t_f \leq 100$ mm / minor axis

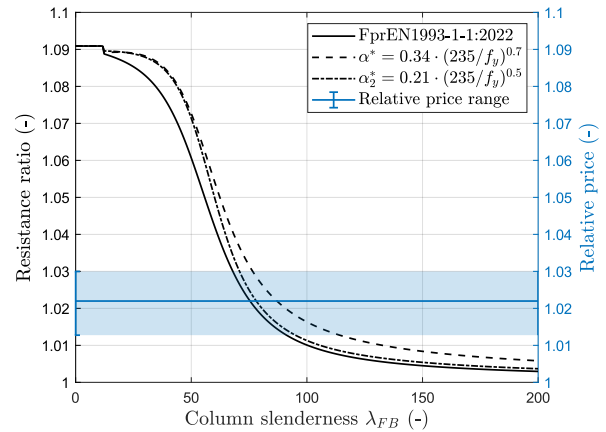


(e) Hot-finished hollow sections

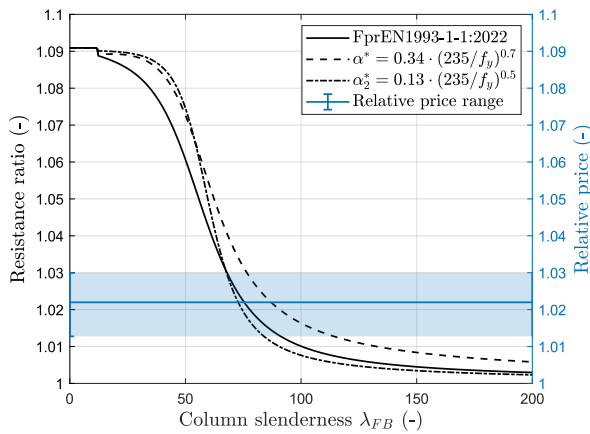
C.6. Grade S600 vs. S550



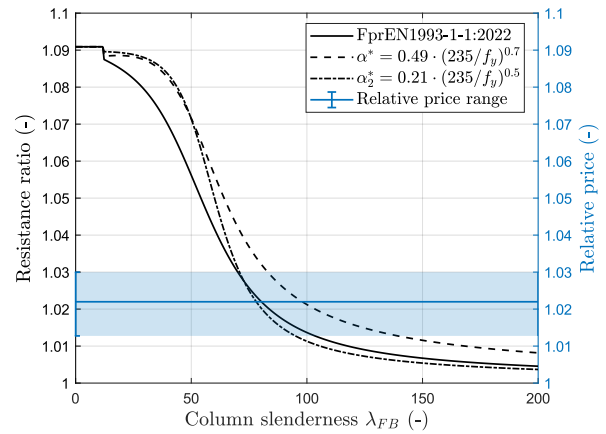
(a) Rolled: $h/b > 1.2 / t_f \leq 40$ mm / major axis



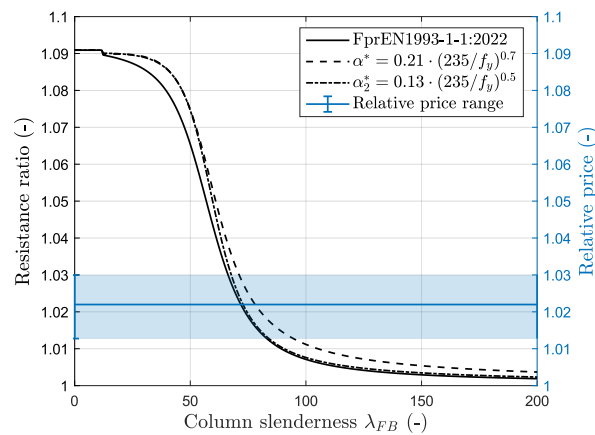
(b) Rolled: $h/b > 1.2 / t_f \leq 40$ mm / minor axis



(c) Rolled: $h/b \leq 1.2 / t_f \leq 100$ mm / major axis

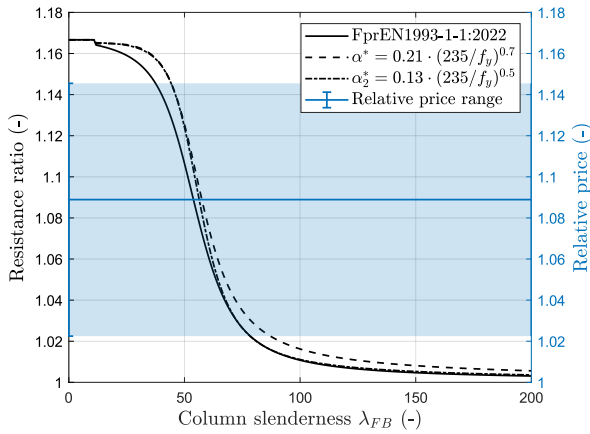


(d) Rolled: $h/b \leq 1.2 / t_f \leq 100$ mm / minor axis

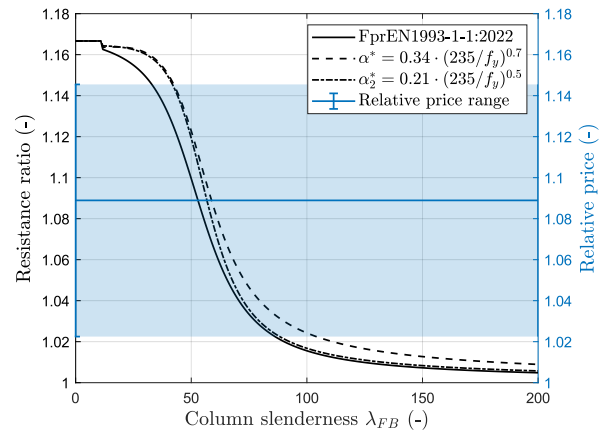


(e) Hot-finished hollow sections

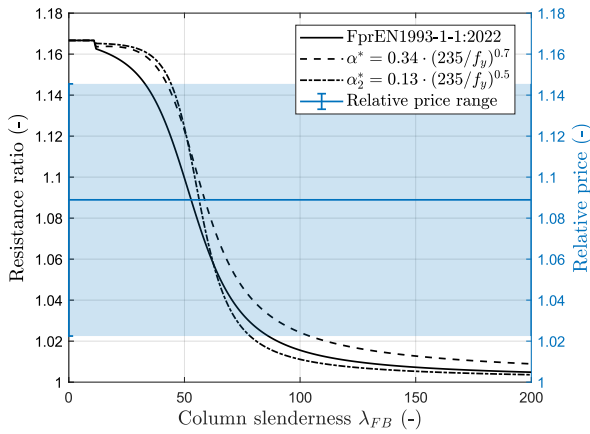
C.7. Grade S700 vs. S600



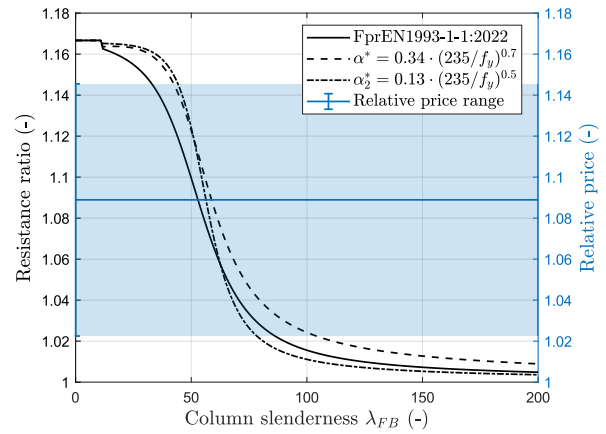
(a) Rolled: $h/b > 1.2 / t_f \leq 40$ mm / major axis



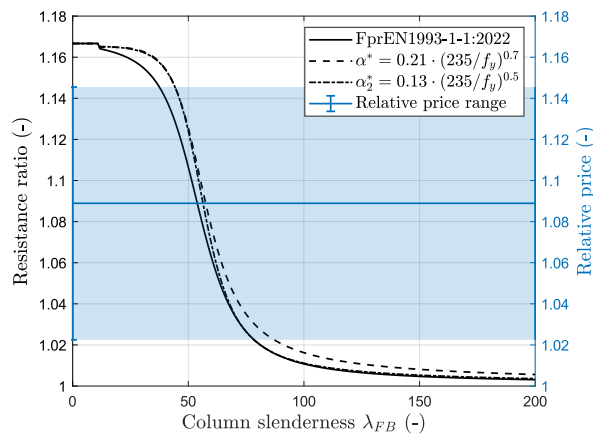
(b) Rolled: $h/b > 1.2 / t_f \leq 40$ mm / minor axis



(c) Rolled: $h/b \leq 1.2 / t_f \leq 100$ mm / major axis



(d) Rolled: $h/b \leq 1.2 / t_f \leq 100$ mm / minor axis

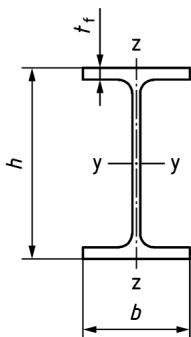
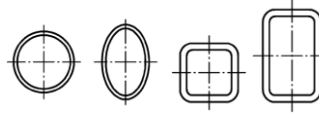


(e) Hot-finished hollow sections

Appendix D

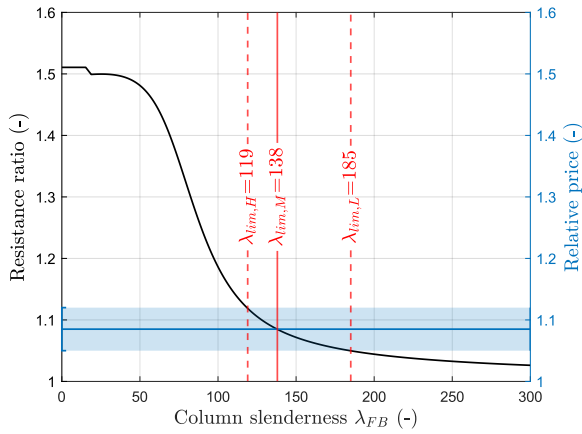
Modified slenderness limits for columns

Appendix D reports the same charts as Appendix A but considers the modified imperfection factor α^* for flexural buckling instead of the Eurocode recommendations of FprEN1993-1-1:2022 [52]. The tables hereafter provide the details about captions and the relative prices.

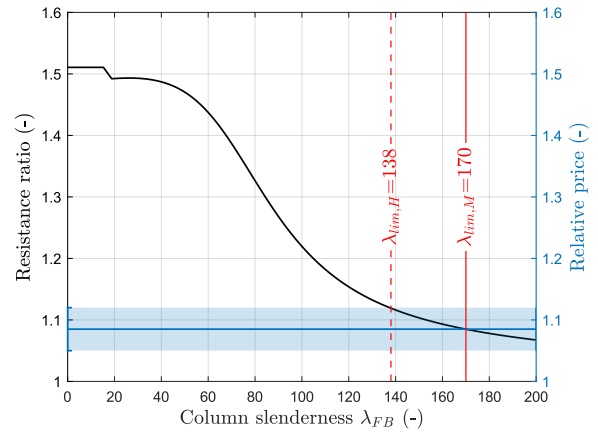
Cross-section		Limits		Buckling about axis	FprEN1993-1-1:2022		Caption letter
					S235-S420	S460 up to S700 inclusive	
Rolled I- or H-sections		$h/b \leq 1.2$	$t_f \leq 40 \text{ mm}$	y-y	a	a_0	(a)
				z-z	b	a	(b)
			$t_f > 40 \text{ mm}$	y-y	b	a	/
				z-z	c	b	/
		$h/b > 1.2$	$t_f \leq 100 \text{ mm}$	y-y	b	a	(c)
				z-z	c	b	(d)
			$t_f > 100 \text{ mm}$	y-y	d	c	/
				z-z	d	c	/
Hollow sections		Hot-finished		any	a	a_0	(e)
		Cold-formed		any	c	c	/

Price Level	Relative prices						
	S355/S235	S420/S355	S460/S420	S500/S460	S550/S500	S600/S550	S700/S600
Low	1.050	1.014	1.009	1.009	1.012	1.013	1.022
Med.	1.085	1.029	1.018	1.017	1.022	1.022	1.089
High	1.120	1.045	1.026	1.025	1.031	1.029	1.145

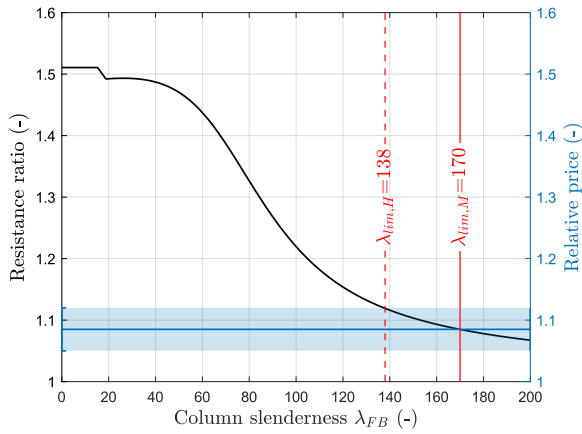
D.1. Grade S355 vs. S235



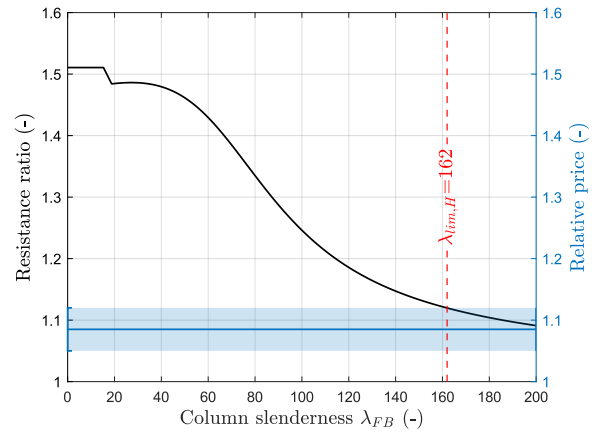
(a) Rolled: $h/b > 1.2 / t_f \leq 40$ mm / major axis



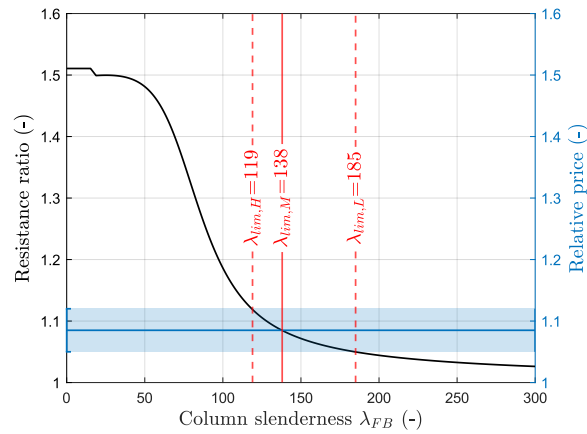
(b) Rolled: $h/b > 1.2 / t_f \leq 40$ mm / minor axis



(c) Rolled: $h/b \leq 1.2 / t_f \leq 100$ mm / major axis

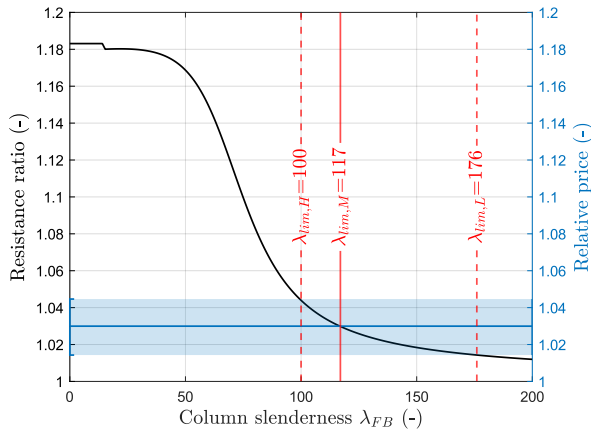


(d) Rolled: $h/b \leq 1.2 / t_f \leq 100$ mm / minor axis

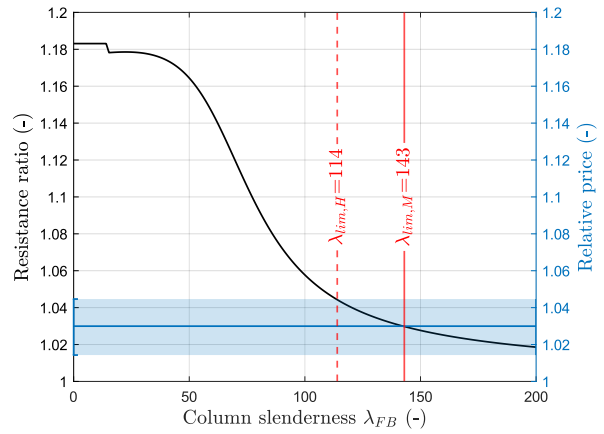


(e) Hot-finished hollow sections

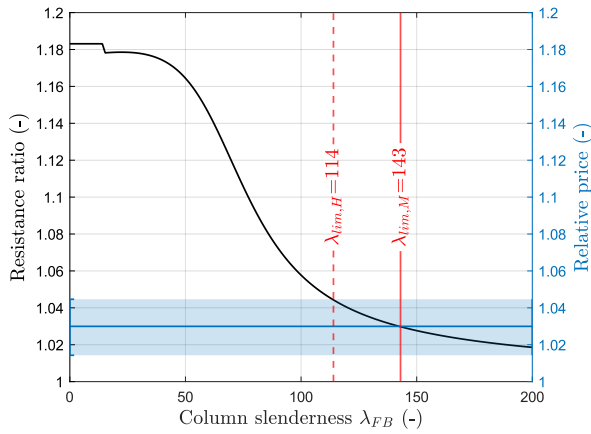
D.2. Grade S420 vs. S355



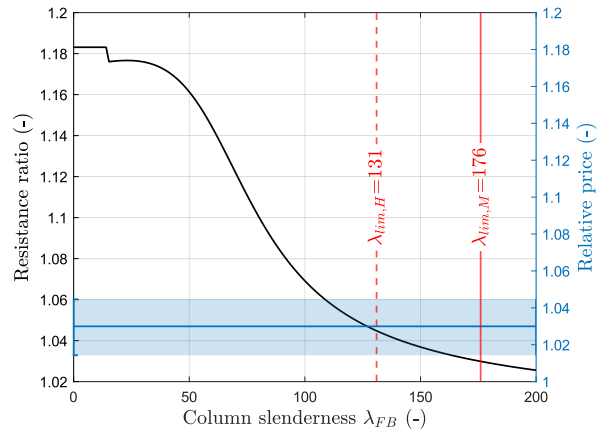
(a) Rolled: $h/b > 1.2 / t_f \leq 40$ mm / major axis



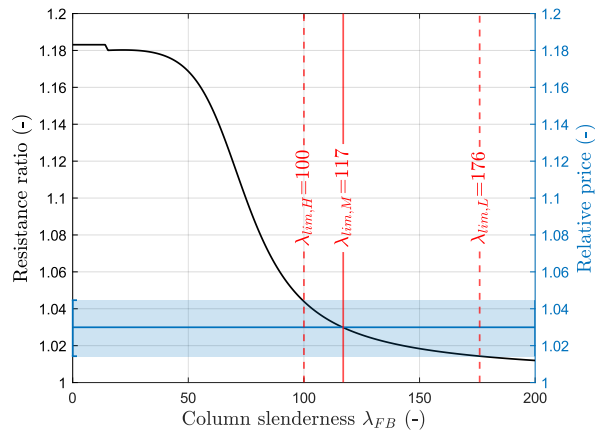
(b) Rolled: $h/b > 1.2 / t_f \leq 40$ mm / minor axis



(c) Rolled: $h/b \leq 1.2 / t_f \leq 100$ mm / major axis

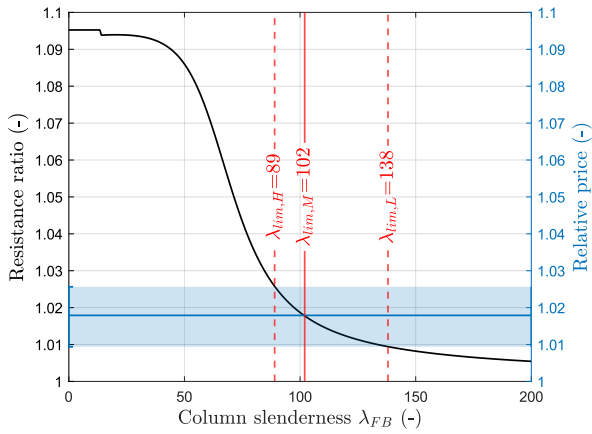


(d) Rolled: $h/b \leq 1.2 / t_f \leq 100$ mm / minor axis

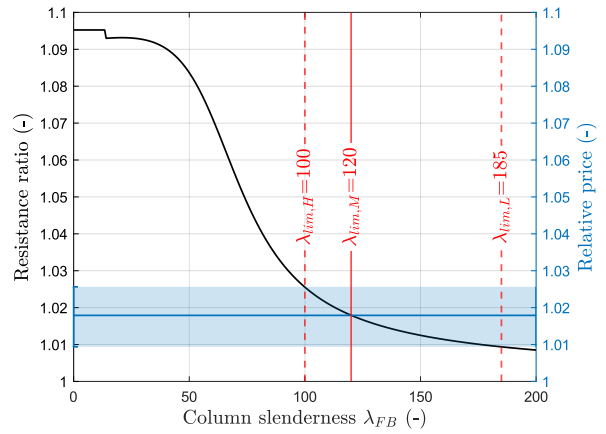


(e) Hot-finished hollow sections

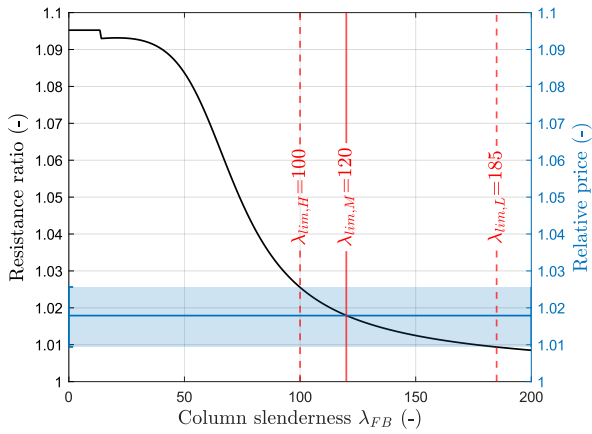
D.3. Grade S460 vs. S420



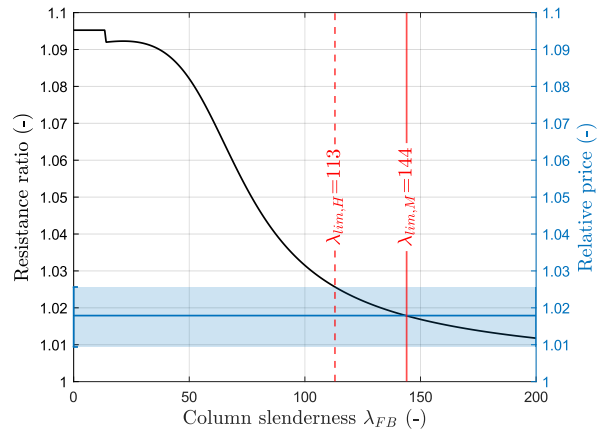
(a) Rolled: $h/b > 1.2 / t_f \leq 40$ mm / major axis



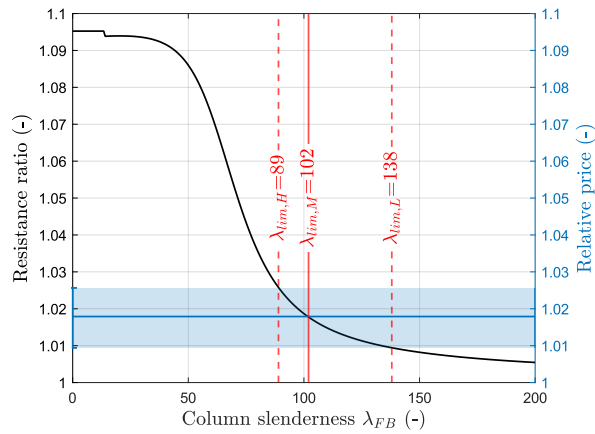
(b) Rolled: $h/b > 1.2 / t_f \leq 40$ mm / minor axis



(c) Rolled: $h/b \leq 1.2 / t_f \leq 100$ mm / major axis

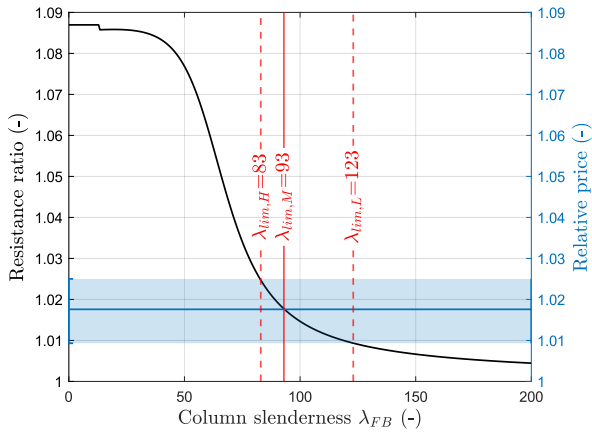


(d) Rolled: $h/b \leq 1.2 / t_f \leq 100$ mm / minor axis

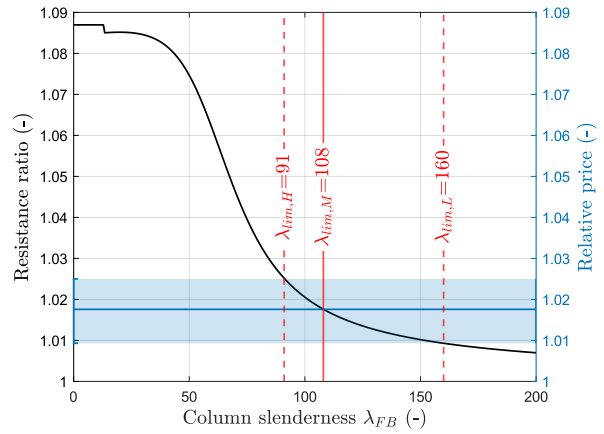


(e) Hot-finished hollow sections

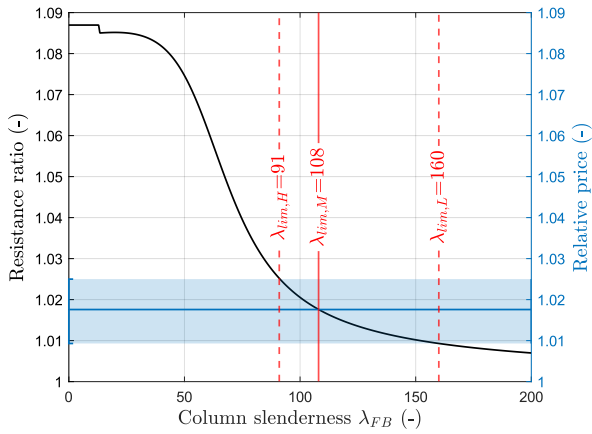
D.4. Grade S500 vs. S460



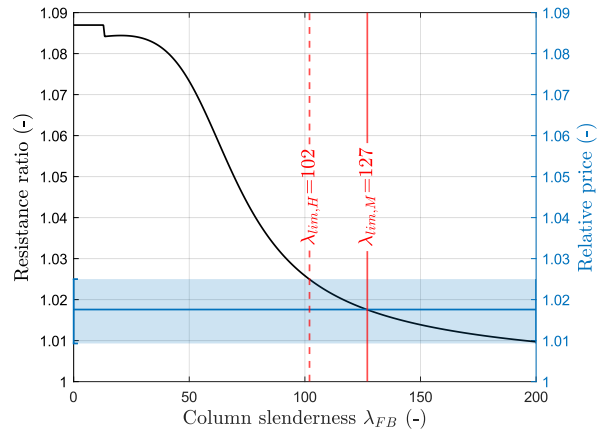
(a) Rolled: $h/b > 1.2 / t_f \leq 40$ mm / major axis



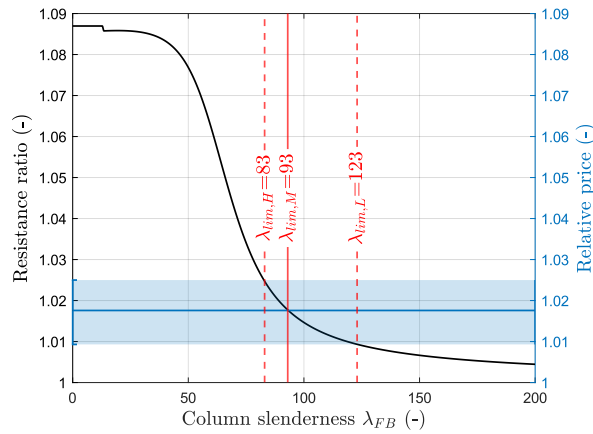
(b) Rolled: $h/b > 1.2 / t_f \leq 40$ mm / minor axis



(c) Rolled: $h/b \leq 1.2 / t_f \leq 100$ mm / major axis

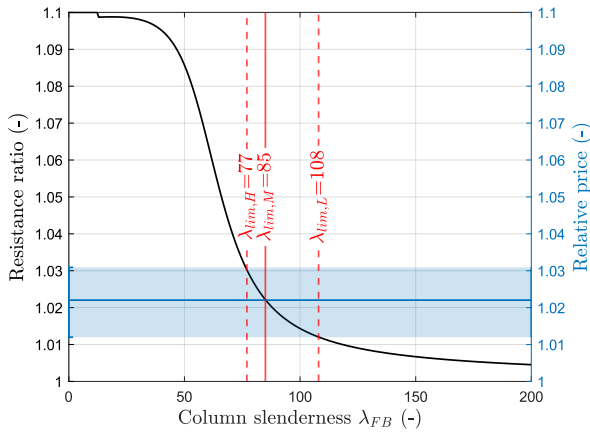


(d) Rolled: $h/b \leq 1.2 / t_f \leq 100$ mm / minor axis

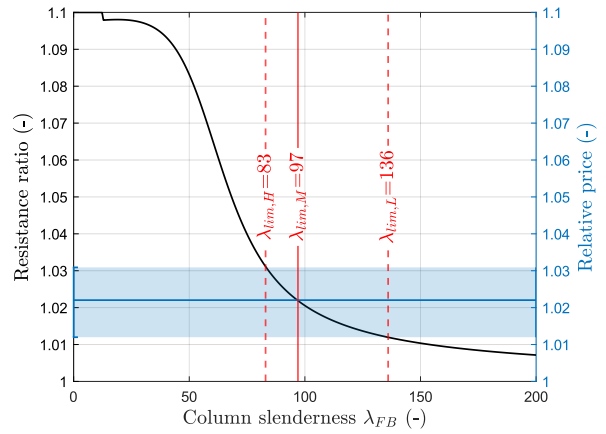


(e) Hot-finished hollow sections

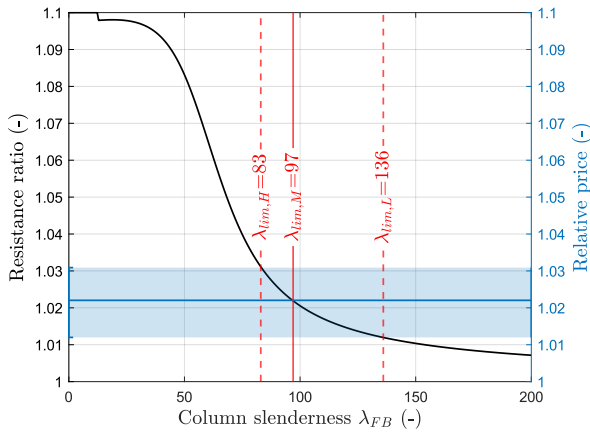
D.5. Grade S550 vs. S500



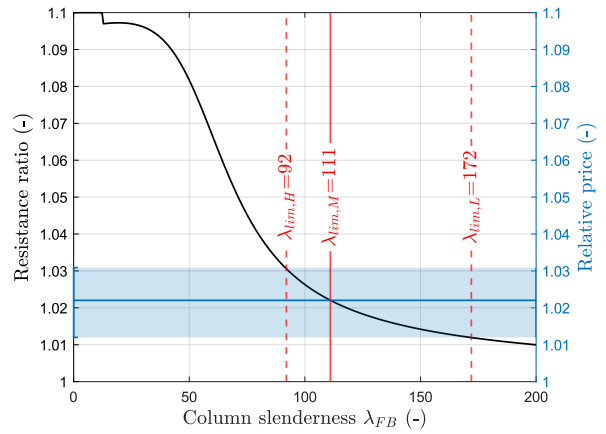
(a) Rolled: $h/b > 1.2 / t_f \leq 40$ mm / major axis



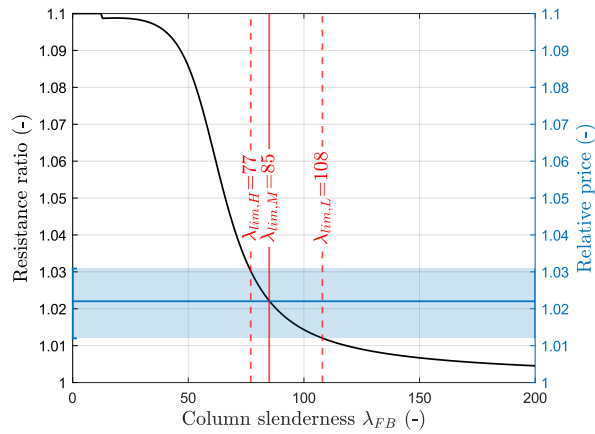
(b) Rolled: $h/b > 1.2 / t_f \leq 40$ mm / minor axis



(c) Rolled: $h/b \leq 1.2 / t_f \leq 100$ mm / major axis

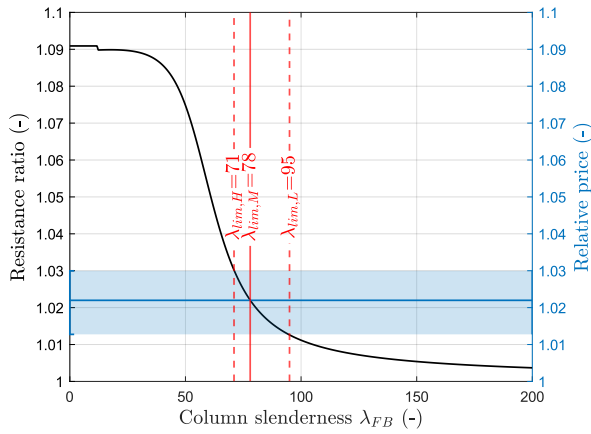


(d) Rolled: $h/b \leq 1.2 / t_f \leq 100$ mm / minor axis

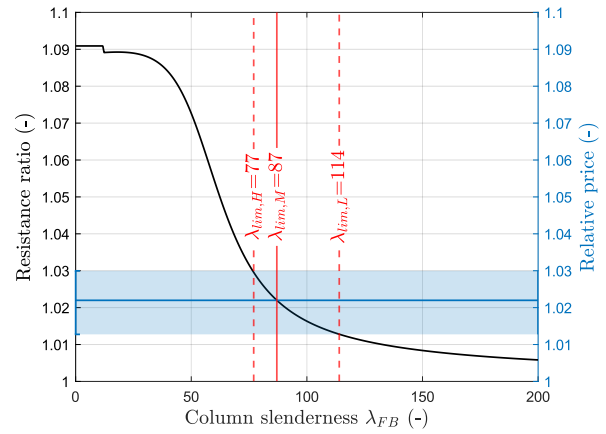


(e) Hot-finished hollow sections

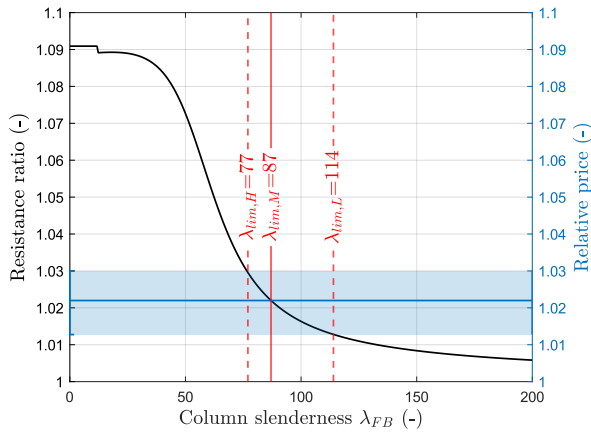
D.6. Grade S600 vs. S550



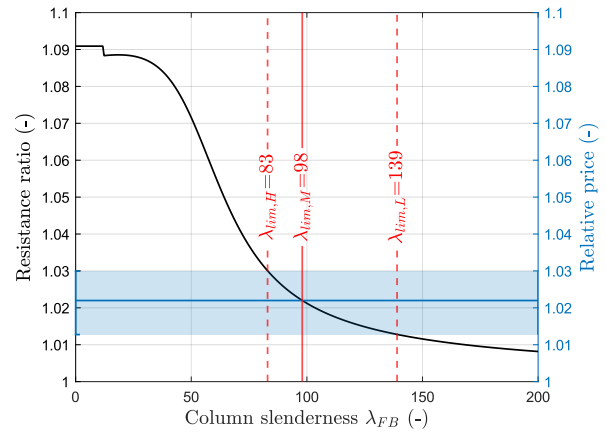
(a) Rolled: $h/b > 1.2 / t_f \leq 40$ mm / major axis



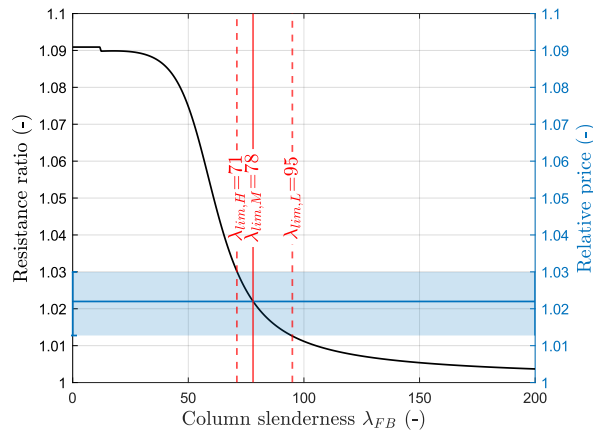
(b) Rolled: $h/b > 1.2 / t_f \leq 40$ mm / minor axis



(c) Rolled: $h/b \leq 1.2 / t_f \leq 100$ mm / major axis

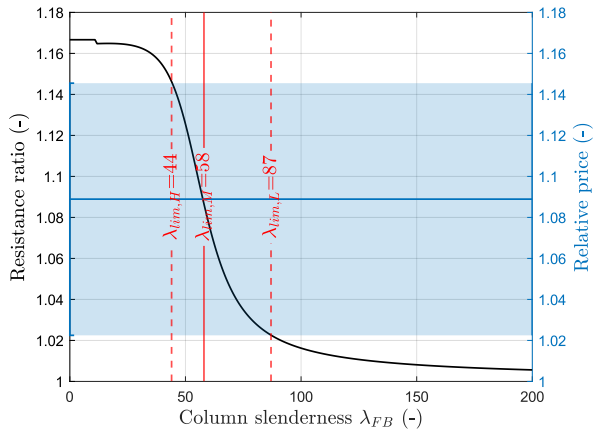


(d) Rolled: $h/b \leq 1.2 / t_f \leq 100$ mm / minor axis

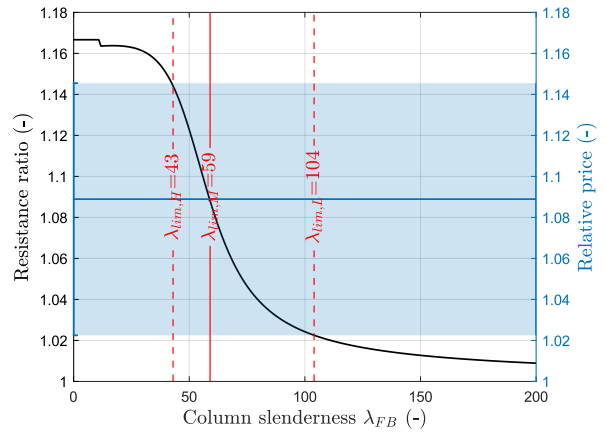


(e) Hot-finished hollow sections

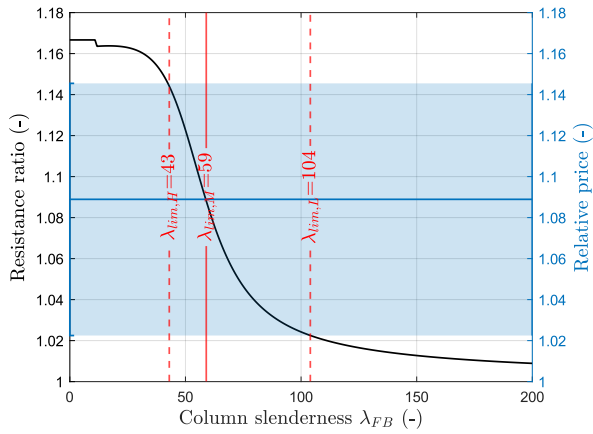
D.7. Grade S700 vs. S600



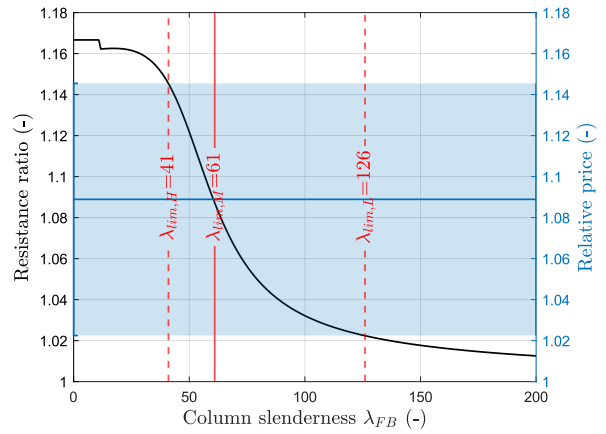
(a) Rolled: $h/b > 1.2 / t_f \leq 40$ mm / major axis



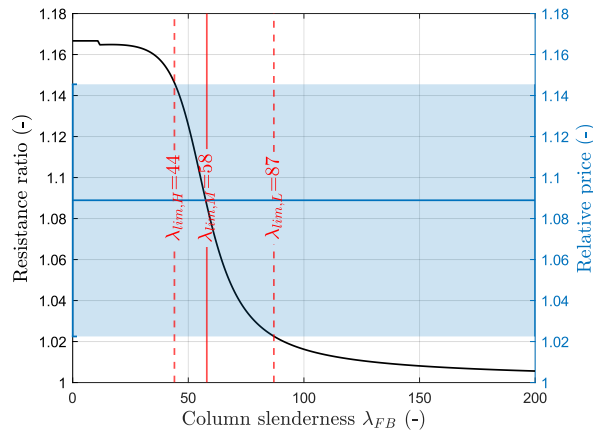
(b) Rolled: $h/b > 1.2 / t_f \leq 40$ mm / minor axis



(c) Rolled: $h/b \leq 1.2 / t_f \leq 100$ mm / major axis

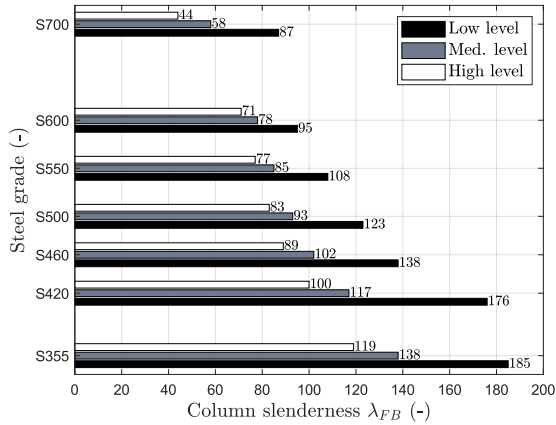


(d) Rolled: $h/b \leq 1.2 / t_f \leq 100$ mm / minor axis

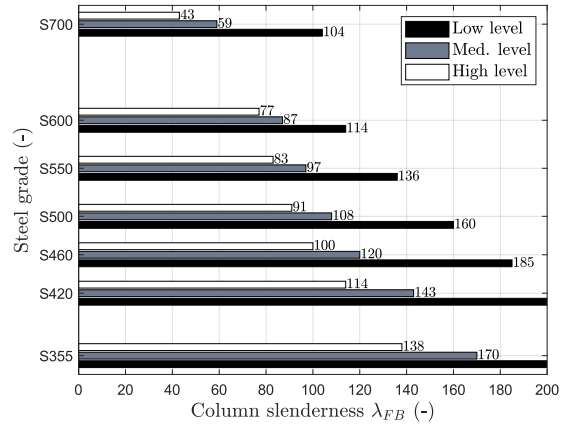


(e) Hot-finished hollow sections

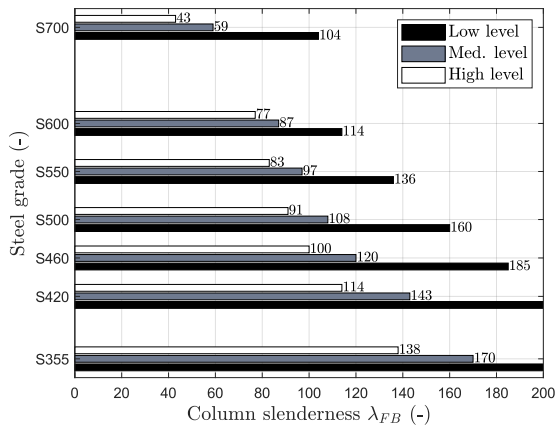
D.8. Summary of reference slenderness limits



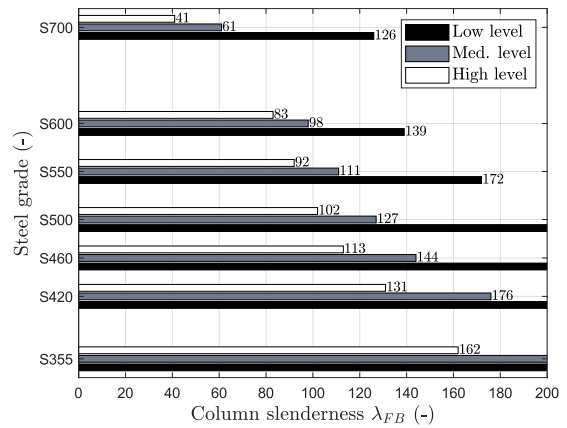
(a) Rolled: $h/b > 1.2 / t_f \leq 40$ mm / major axis



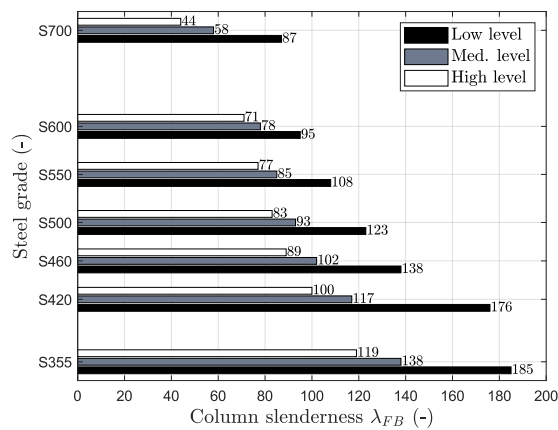
(b) Rolled: $h/b > 1.2 / t_f \leq 40$ mm / minor axis



(c) Rolled: $h/b \leq 1.2 / t_f \leq 100$ mm / major axis



(d) Rolled: $h/b \leq 1.2 / t_f \leq 100$ mm / minor axis



(e) Hot-finished hollow sections

List of Figures

Fig. 1-1. Global CO ₂ emissions and responsibility of the building sector.	1
Fig. 1-2. Toward net-zero emissions by 2050 – importance of the pathway (Adapted from istructe.org [24], [25], [26]).	4
Fig. 1-3. Tackle carbon early in the structure’s lifetime and hierarchy to net zero [24], [30], [31].	5
Fig. 1-4. Contextualising the potential impact of the researcher’s actions [adapted from [44]].	8
Fig. 2-1. Evolution of the yield strength depending on the thickness.....	15
Fig. 2-2. Strength-to-yield strength ratio for different steel grades from tensile tests.	16
Fig. 2-3. Weldability of high-strength steel grades.	18
Fig. 2-4. Characteristic fatigue resistance curves for non-welded details subject to nominal normal stress ranges.....	19
Fig. 2-5. Fatigue life as function of the yield strength.....	20
Fig. 2-6. Material relative prices as a function of yield strength according to literature references. ..	21
Fig. 2-7. GWP evolutions provided by Swedish researchers in the Steel Eco-Cycle project.	22
Fig. 2-8. Buckling curves in Eurocode provisions.....	24
Fig. 2-9. Relative material costs for tension members (a) and for compression members (b) considering a curve “a” and that the material can be fully utilised [86], [93].....	29
Fig. 2-10. Residual stress models for hot-rolled sections.....	32
Fig. 2-11. Residual stress models for hot-finished hollow sections.	32
Fig. 2-12. Residual stress distributions for straightened members in the literature.	36
Fig. 2-13. Existing residual stress models for straightened members in the literature.	37
Fig. 3-1. The three pillars of sustainability.	44
Fig. 3-2. Cost breakdowns of steel structures.	46
Fig. 3-3. European steel prices according to MEPS.	47
Fig. 3-4. Impact of the ordered quantity on the base price.	48
Fig. 3-5. Grade extras for TM steels for cold forming.	51
Fig. 3-6. European linear trend vs American grade extra values.	51
Fig. 3-7. Effect of a base price change on the relative prices.....	52
Fig. 3-8. Relative prices for TM steels for cold-forming (EN10149-2).	52
Fig. 3-9. Relative prices for QT steels (EN10025-6).	55
Fig. 3-10. Determination of realistic grade extras for future emerging hot-rolled section grades.....	58
Fig. 3-11. Establishment of reliable relative price intervals for steel grades up to S700.....	59
Fig. 3-12. Relative GWP of high-strength steels according to the literature.	63
Fig. 3-13. Validation of the exposed methodology for steels complying with EN10149-2.	65
Fig. 3-14. Validation of the exposed methodology for cold-formed hollow sections (acc. to EN10219-3 [60]).	66
Fig. 3-15. Evolution of GWP as a function of yield strength and steel quality [53], [54], [57], [59], [60], [66], [67], [68].....	68
Fig. 3-16. Comparison between established relative prices (blue ranges) and relative carbon emissions.	70
Fig. 4-1. Identification of aspects that govern the design of a steel structural member.	72
Fig. 4-2. Classical flooring system for an office building [216].	73
Fig. 4-3. Case studies covered in this research.....	74
Fig. 4-4. Flowchart of the developed optimisation routines.....	75

Fig. 4-5. Establishment of continuous geometrical properties for each section typologies.	77
Fig. 4-6. Area ratios obtained through the developed methodology compared to an existing algorithm developed within the ATTEL project.	79
Fig. 4-7. Introduction of the graphical representation for results based on ATTEL project assumptions.	80
Fig. 4-8. Relative material cost for tension members normalised with S235 and by assuming that the strength can be fully mobilised.	81
Fig. 4-9. Comparative study between S500 and S355 for tension members and the HEA profile series.	82
Fig. 4-10. Relative resistance to local buckling for hot-rolled sections under pure compression (S235 as reference).	84
Fig. 4-11. Relative material cost for a hot-rolled member prone to local buckling (S235 as reference).	85
Fig. 4-12. Relative resistance to flexural buckling for hot-rolled sections (curve “a” up to S420 and curve “a ₀ ” for S460 and above) considering grade S235 as reference.	86
Fig. 4-13. Relative material cost for hot-rolled columns under pure compression and taking S235 as reference (curve “a” up to S420 and curve “a ₀ ” for S460 and above).	87
Fig. 4-14. Slenderness limits to justify the benefit of a higher grade for hot-rolled sections respecting $h/b > 1.2 / t_f \leq 40$ mm / major axis.	88
Fig. 4-15. Column slenderness depending on the buckling length and the profile range.	89
Fig. 4-16. Optimisation results for continuous hot-rolled sections (HEA and HD profile series) under pure compression and medium cost level.	90
Fig. 4-17. Optimisation results for compression members considering the discrete HEA and HD profile series.	91
Fig. 4-18. Relative resistance to local buckling as a function of yield strength for hot-rolled sections under pure bending.	93
Fig. 4-19. Relative resistance to shear buckling as a function of yield strength and the web slenderness.	94
Fig. 4-20. Relative material cost and slenderness limits for members in simple bending.	95
Fig. 4-21. Limitations in terms of beam lengths for simply supported beams.	95
Fig. 4-22. Results of optimisation for simply supported beams and IPE profile series.	96
Fig. 4-23. Impact of intermediate lateral supports on the benefit of using high-strength steels for beams.	98
Fig. 4-24. Impact of the allowable deflection limit on the benefit of using high-strength steels for beams.	99
Fig. 4-25. Optimisation results for Cases 4 and 5 defined in Table 4-4.	100
Fig. 4-26. Case study for hot-rolled members subjected to combined compression and bending. ...	101
Fig. 4-27. Optimisation results for HD members subjected to combined compression and bending. ...	102
Fig. 4-28. Relative resistance to local buckling as a function of yield strength for hollow sections. ...	103
Fig. 4-29. Relative resistance and material cost for hollow sections under pure compression and considering S235 as reference.	104
Fig. 4-30. Slenderness limits for each steel grade and for hollow profiles.	105
Fig. 4-31. Optimisation results for CHS and SHS sections considering continuous quantities.	106
Fig. 4-32. Optimisation results by neglecting the reduction factor associated to local buckling.	106
Fig. 4-33. Optimisation results for hollow sections subjected to combined compression and bending.	108
Fig. 4-34. Validation of ArcelorMittal’s designs based on the optimisation routine.	110
Fig. 4-35. Benefit in increasing the material yield strength for columns in the Mapfre Tower.	110

Fig. 4-36. Optimum grades and slenderness limits depending on the optimisation criterion.....	111
Fig. 4-37. Benefit of high-strength steels for the retractable roof of the NRG stadium at Houston. .	112
Fig. 5-1. Description of model assumptions for beam finite element modelling.....	119
Fig. 5-2. Validation of the numerical model based on experimental results carried out in the Fritz Laboratory in 1972.	120
Fig. 5-3. Validation of the residual stress model used in the numerical simulations for high-strength steels.....	121
Fig. 5-4. Validation of the numerical model for hot-finished hollow sections.....	121
Fig. 5-5. Comparison between numerical simulations and Eurocode recommendations for grades S235 and S460.	123
Fig. 5-6. Impact of strain-hardening on numerical simulations for low-slenderness columns.	124
Fig. 5-7. Evaluation of the possibility of selecting one higher buckling curve for S355 and S420.	126
Fig. 5-8. Evolution of the imperfection factor α as function of the yield strength.	127
Fig. 5-9. Validation of the modified imperfection factor based on experimental tests for hot-finished hollow sections.....	128
Fig. 5-10. Description of model assumptions for shell finite element modelling.	130
Fig. 5-11. Impact of the element size on the local instability mode shape (represented for the HEB600 profile).	131
Fig. 5-12. Comparison between shell numerical simulations and the modified imperfection factor for slender cross-sections.	132
Fig. 5-13. Validity of the modified imperfection factor proposal for Class 4 cross-sections based on buckling tests.....	132
Fig. 5-14. Evolution of the mean values depending on the imperfection factor reference.....	134
Fig. 5-15. Comparison between the modified imperfection factor of Meng & Gardner and the new proposal for already covered grades.....	135
Fig. 5-16. Resulting gains from the use of the modified imperfection factor compared to forthcoming Eurocode recommendations [52].....	136
Fig. 5-17. Summary of the modification proposal.....	137
Fig. 5-18. The reference roller-straightening process.	138
Fig. 5-19. Free body diagram of the reference roller-straightening process.	139
Fig. 5-20. Vertical displacement and moment - curvature diagram at mid-length of the HEM500 profile during the roller-straightening process.....	141
Fig. 5-21. Machine setting for the roller-straightening process in the Alpsten's experimental campaign.	142
Fig. 5-22. Free body diagram of the roller-straightening process.....	142
Fig. 5-23. Material law for numerical simulations based on coupon test results.	143
Fig. 5-24. Residual stress measurements during the test campaign.....	143
Fig. 5-25. Comparison between residual stress from experiments and from numerical simulations.	143
Fig. 5-26. Impact of the shear deformations on the residual stress distribution for the tested profile (HEA200).....	145
Fig. 5-27. Impact of the shear deformations on the residual stress distribution for HEA240.	146
Fig. 5-28. Residual stress patterns for each selected profile and for the reference machine setting.	146
Fig. 5-29. Moment-curvature diagrams for HD400x262 (a) and HEA240 (b) considering the reference machine setting.	147
Fig. 5-30. Effect of each maximum bending moment on the residual stress distribution for the HEM500 profile.	147
Fig. 5-31. Residual stress distributions for the HEM500 profile depending on the first imposed displacement.	148

Fig. 5-32. Influence of the second imposed displacement on the residual stress distribution for the HEM500 profile.	149
Fig. 5-33. Influence of the yield strength on the residual stress distribution for the HEM500 profile.	149
Fig. 5-34. Effect of a second pass in the straightening machine.	150
Fig. 5-35. Residual stress patterns for evaluating the benefit of the roller-straightening process on the column bearing capacity.	151
Fig. 5-36. Effect of the sign of the initial geometrical imperfection on the column bearing capacity.	152
Fig. 5-37. Residual stress distributions for HEM500 before and after the stress adjustment into the software.	153
Fig. 5-38. Beneficial influence of the roller-straightening on the buckling resistances for grades S355 and S460.	153
Fig. 5-39. Resulting gains from the consideration of a higher buckling curve.	154
Fig. 5-40. Evolution of the imperfection factor with or without the consideration of residual stresses.	156
Fig. 5-41. Buckling resistance increase (%) as function of the imperfection factor reduction and the relative slenderness.	157
Fig. 5-42. Influence of a modified imperfection factor on relative buckling resistances and slenderness limits (Rolled: $h/b > 1.2 / t_f \leq 40$ mm / major axis or hot-rolled hollow sections considering a medium base cost).	158
Fig. 5-43. The impact of the proposed imperfection factors on the right choice of steel grade.	159
Fig. 5-44. Influence of the modified imperfection factors on the case studies discussed in Chapter 4.	159
Fig. 6-1. Experimental test set-up with geometrical properties of the test campaign realised in Ghent.	164
Fig. 6-2. Loading scenarios of the Ghent experimental campaign.	165
Fig. 6-3. Positions of the vertical displacement measurements performed during experimental tests.	166
Fig. 6-4. Torsion measurements performed during experimental tests.	166
Fig. 6-5. Vertical displacements and torsion angles in the first span for each tested specimen.	167
Fig. 6-6. Measuring device dismantling due to huge torsions during the experimental test.	168
Fig. 6-7. Pictures of test 2 during the Ghent campaign.	169
Fig. 6-8. Instability mode of Test 3a during the Ghent campaign.	169
Fig. 6-9. Numerical model for the mesh sensitivity study on C180x60x20*2.5.	170
Fig. 6-10. Impact of the mesh on first elastic buckling loads (comparison between beam and shell finite elements).	171
Fig. 6-11. Elastic second-order analyses – comparison between beam and shell finite elements.	171
Fig. 6-12. Loading distribution resulting from the rigid pallet assumption and the torsion induced by the load eccentricity.	172
Fig. 6-13. Compression springs to avoid any penetration of the supporting beams in uprights.	173
Fig. 6-14. Friction forces consideration in numerical models.	173
Fig. 6-15. Overestimation of the inclined stiffness at bolt nodes.	175
Fig. 6-16. Modelling of the midspan coupling elements.	175
Fig. 6-17. Numerical displacement computation to compare with experimental results.	175
Fig. 6-18. Consideration of loading symmetry to simplify the numerical models.	176
Fig. 6-19. Numerical models to validate Test 2 and Test 3a of the Ghent campaign.	176
Fig. 6-20. First instability mode of the LBA analysis for Test 2 (without coupling elements).	177
Fig. 6-21. Second instability mode of the LBA analysis for Test 3a (with coupling elements).	178

Fig. 6-22. Comparison between experimental and numerical results for Test 2 (without coupling elements).....	178
Fig. 6-23. Impact of the static friction coefficient on the results for Test 2 (without coupling elements).	179
Fig. 6-24. Verification of the sliding assumption for Test 2 (without coupling elements).	179
Fig. 6-25. Impact of the longitudinal restraint at bolt nodes for Test 2 (without coupling elements).	180
Fig. 6-26. Longitudinal displacements of the bolt nodes during loading for Test 2 (without coupling elements).....	180
Fig. 6-27. Effect of the pallet stiffness and the corresponding load distribution on results for Test 2 (without coupling elements).	181
Fig. 6-28. Comparison of failure loads for Test 2 (without coupling elements) for several steel grades.	182
Fig. 6-29. Comparison between experimental and numerical results for Test 3a (with coupling elements).....	182
Fig. 6-30. Impact of the static friction coefficient for Test 3a (with coupling elements).	183
Fig. 6-31. Verification of the sliding assumption for Test 3a (with coupling elements).....	183
Fig. 6-32. Impact of a longitudinal restraint at supports for Test 3a (with coupling elements).	184
Fig. 6-33. Longitudinal displacements at bolt nodes during loading for Test 3a (with coupling elements).	184
Fig. 6-34. Effect of the pallet stiffness on results for Test 3a (with coupling elements).....	185
Fig. 6-35. Necessity of the coupling elements for C-shaped supporting beams.	185
Fig. 6-36. Drawing of one span of the case study.	187
Fig. 6-37. Drawing of the midspan coupling element in the case study.	187
Fig. 6-38. Modelling of the support conditions in the case study.	188
Fig. 6-39. Numerical model for the mesh sensitivity study on SIG 160x60x20*1.8.	189
Fig. 6-40. First buckling loads obtained through LBA depending on the longitudinal mesh.	189
Fig. 6-41. First mode shape for the most refined shell mesh (longitudinal mesh=10 mm).	190
Fig. 6-42. Second-order elastic analyses for SIG 160x60x20 depending on the thickness.....	190
Fig. 6-43. Numerical model and first instability mode for model 1.	191
Fig. 6-44. Verification of the “no-sliding” assumption regarding model 1.....	192
Fig. 6-45. Unrealistic global instability mode which cannot occur with pallets.	192
Fig. 6-46. Numerical modelling of Euro pallets to account for their stabilising effect.....	193
Fig. 6-47. Numerical model and first instability mode for model 2.	193
Fig. 6-48. Verification of the “no-sliding” assumption regarding model 2.....	194
Fig. 6-49. Impact of the initial geometrical imperfections on results for model 2.	194
Fig. 6-50. Modelling of the coupling element for the case study.....	195
Fig. 6-51. Numerical model and first instability mode for model 3.	195
Fig. 6-52. Numerical model and first instability mode for model 4.	195
Fig. 6-53. Result comparison between the various developed models of the case study.	196
Fig. 6-54. Benefit of an increased yield stress for SIG 160x60x20x1.8 (model 1).	198
Fig. 7-1. Summary of the Chapter 3 to Chapter 5 contributions for members under pure compression.	204
Fig. 7-2. Closing the loop of these thesis contributions.	210
Fig. 7-3. Responsibility of each stakeholder for realising weight, cost and carbon savings.	211
Fig. 7-4. Collaboration between stakeholders for reducing carbon emissions.....	212

List of Tables

Table 1-1. CO ₂ intensity of steel production.	2
Table 2-1. Steel grade transitioning for hot-rolled sections: history and evolution outlook.....	11
Table 2-2. Steel categories according to FprEN1993-1-1:2022 (for a thickness below 80 mm).	12
Table 2-3. Product standards compatible with EN1993-1-1 and the related steel grades and qualities.	14
Table 2-4. Normative situation for hot-rolled sections depending on the region.	15
Table 2-5. Ductility requirements in design recommendations.....	16
Table 2-6. Selection of constructional details directly affected by an increased yield stress.....	20
Table 2-7. Normative situation in terms of covered steel grades.....	22
Table 2-8. Cross-sectional resistances depending on the section class.	23
Table 2-9. Comparison between reference slenderness for both global instability modes (FB and LTB).	25
Table 2-10. Buckling curve specification according to EN1993-1-1 [70].....	26
Table 2-11. Selection of buckling curve for flexural buckling according to the current and forthcoming version of EN1993-1-1.....	27
Table 2-12. Selection of buckling curve for lateral-torsional buckling in current and forthcoming version of EN1993-1-1.....	28
Table 2-13. Analytical formulations for residual stress models.	32
Table 2-14. Existing modified expressions of the imperfection parameter η in the literature.	34
Table 2-15. Reference high-rise buildings made of high-strength steels.....	40
Table 3-1. Life cycle stages according to EN15084.....	46
Table 3-2. Evolution of grade extras (€/t) in a period of high base price fluctuations.	48
Table 3-3. Adopted base price levels for relative price establishment.	49
Table 3-4. Grade extras for TM steels for cold forming (€/t).	50
Table 3-5. Chemical compositions of steels complying with EN10149-2.....	53
Table 3-6. Grade extras for heavy plates made of QT steels (EN10025-6).	54
Table 3-7. Grade extras for hot-rolled sections from recent ArcelorMittal pricelists (€/t).	57
Table 3-8. Grade extras for British sections (£/t).	57
Table 3-9. CO ₂ intensity of steel production depending on the production route.	61
Table 3-10. GWP for modules A1 to A3 depending on the typology and the producer (t CO ₂ eq/t)....	63
Table 3-11. Greenhouse gas emissions of alloying elements [kg CO ₂ eq/kg] according to [212], [213], [214].	64
Table 3-12. Relative reference values (-) for comparison studies considering S235 or S355 as the reference grade.	70
Table 4-1. Reference relative prices of Chapter 3 for comparative studies.....	76
Table 4-2. Optimum yield strength (MPa) depending on the prescribed buckling curve for S235, the column slenderness, and the reference relative cost level.....	87
Table 4-3. Allowable deflection limits considered in the framework of this research.	92
Table 4-4. Case studies for the impact evaluation of the joint stiffness.	100
Table 5-1. Geometrical properties and type of finite elements for each selected hot-rolled cross- section.	117
Table 5-2. Geometrical properties and type of finite elements for each selected hot-finished hollow section.	118

Table 5-3. Comparison between experimental and numerical results for hot-finished hollow sections.	122
Table 5-4. Eurocode selection of buckling curves for flexural buckling and hot-rolled sections.....	122
Table 5-5. Numerical sensitivity study of the longitudinal mesh and local imperfection magnitude influence.	131
Table 5-6. Numerical steps to simulate the roller-straightening process of a HEM500 profile.....	141
Table 5-7. Selected profiles to evaluate the potential benefit of the roller-straightening process. ..	145
Table 5-8. Optimised machine setting for each selected profile.	151
Table 6-1. Experimental test results of the Ghent campaign.....	167
Table 6-2. Coupon test results of the Ghent experimental campaign.	168
Table 6-3. Linear buckling analyses (LBA) for beam and shell finite elements.	170
Table 6-4. First mode shape of SIG 160x60x20*1.8 depending on the longitudinal mesh (beam vs shell finite elements).	189
Table 6-5. Selected steel grades to evaluate the resistance gain resulting from an increased yield stress.	197
Table 6-6. Grade extras for steels according to EN10346 (€/t).....	198
Table 7-1. Perspective works on the establishment of modified imperfection parameters for flexural buckling.	208
Table 7-2. Estimation of the market share of hot-rolled sections in building construction.	209



LIÈGE université

Sciences Appliquées

DOCTORAL COLLEGE IN ARCHITECTURE, ENGINEERING AND GEOLOGY

OCTOBER 2024